Inaugural dissertation

for

obtaining the doctoral degree

of the

Combined Faculty of Mathematics, Engineering and Natural Sciences

of the

Ruprecht-Karls-University Heidelberg

Presented by

Samantha Zottnick, M.Sc.

born in: Bietigheim-Bissingen, Germany

Oral examination: 11th August 2022

Assessment of methods to direct T cells toward a newly established HPV16 E6/E7-dependent orthotopic tumor model in A2.DR1 mice

Referees:

Prof. Dr. Martin Müller

PD Dr. Dr. Angelika Riemer

The work described in this thesis was performed from October 2017 to May 2022 under scientific supervision of PD Dr. Dr. Angelika Riemer in the Division of Immunotherapy and Immunoprevention at the German Cancer Research Center (DKFZ) in Heidelberg, Germany.

Peer-reviewed publication based on this work:

Zottnick, S., Voß, A. L., & Riemer, A. B. (2020). *Inducing Immunity Where It Matters: Orthotopic HPV Tumor Models and Therapeutic Vaccinations*. Frontiers in Immunology, 11.

Conference and workshop presentations based on this work:

Zottnick, S. *Analysis of factors that facilitate trafficking of vaccination-induced T cells to tumor sites.* (05/2018) Oral presentation at the Infection, Inflammation and Cancer (IIC) retreat 2018, Rastatt, Germany

Zottnick, S., Kruse, S., Bozza, M., Voß, A., Klevenz, A., Yang, R., Rösl, F., Harbottle, R.P., Riemer, A.B. *Establishment of an orthotopic HPV16 tumor model in MHC-humanized mice*. (05/2019) Poster presentation at the annual meeting of the association for cancer immunotherapy (CIMT) 2019, Mainz, Germany

Zottnick, S., Kruse, S., Bozza, M., Voß, A., Klevenz, A., Yang, R., Rösl, F., Harbottle, R.P., Riemer, A.B. *A vaginal HPV16 $E6^+/E7^+$ tumor model in MHC-humanized A2.DR1 mice.* (07/2019) Oral presentation at the DKFZ PhD retreat 2019, Weil der Stadt, Germany

Zottnick, S., Kruse, S., Bozza, M., Voß, A., Klevenz, A., Yang, R., Rösl, F., Harbottle, R.P., Riemer, A.B. *Establishment of a vaginal HPV16 $E6^+/E7^+$ tumor model in MHC-humanized A2.DR1 mice.* (09/2019) Poster presentation at the II Joint Meeting of the German Society for Immunology (DGfI) and the Italian Society of Immunology, Clinical Immunology and Allergology (SIICA), Munich, Germany

Zottnick, S. *Analysis of factors that facilitate trafficking of vaccination-induced T cells to tumor sites.* (11/2019) Oral presentation during the 2019 German-Japanese Junior Experts Exchange program (Cancer and Alzheimer's research), Tokyo, Japan

Zottnick, S., Kruse, S., Bozza, M., Voß, A., Klevenz, A., Yang, R., Rösl, F., Harbottle, R.P., Riemer, A.B. *Developing a therapeutic HPV16 vaccination strategy utilizing a vaginal tumor model in MHC-humanized mice.* (05/2021) eTalk at the annual meeting of the association for cancer immunotherapy (CIMT) 2021, Mainz, Germany

Zottnick, S., Kruse, S., Bozza, M., Henneberg, A.L., Klevenz, A., Förster, J.D., Yang, R., Rösl, F., Harbottle, R.P., Riemer, A.B. *A novel HPV16 E6/E7-dependent vaginal tumor model in MHC-humanized mice for development of therapeutic HPV16 vaccination strategies*. Poster presentation at the annual meeting of the association for cancer immunotherapy (CIMT) 2022, Mainz, Germany

I. Abstract

Human papillomaviruses (HPV) are responsible for formation of tumors in the anogenital and oropharyngeal mucosa. The most common malignancy among these cancers is cervical cancer, affecting about 570,000 women every year. Although prophylactic vaccines against several high-risk types of HPV, such as HPV16, have been existing for some time, vaccination rates remain low and cancer incidence rates high. In our group 'Immunotherapy and immunoprevention' we are therefore working on a therapeutic vaccine for treatment of HPV16-derived lesions and tumors. So far, no therapeutic vaccines against HPV-induced malignancies have been approved for clinical use even though there is a plethora of promising preclinical studies. These studies have mainly examined the impact of vaccinations with murine MHC-restricted epitopes on subcutaneous tumors. The tumors of patients, however, present human MHC (HLA)-restricted epitopes and are located in the patients' mucosae, which are restricted for the general circulation of T cells. Herein I present solutions to these problems by first establishing a novel orthotopic (vaginal) tumor model, consisting of a cell line immortalized by the viral oncogenes E6 and E7 and presenting HLA-A2:01-restricted epitopes on its surface for use in syngeneic MHC-humanized A2.DR1 mice. Second, I examined methods to facilitate migration of T cells into the cervicovaginal mucosa for eventual application in patients.

For the establishment of the tumor model I first successfully transfected $E6^{+}E7^{+}$ A2.DR1 lung cells with the activated oncoprotein $HRAS^{G12V}$ and firefly luciferase. These cells were specifically killed by HPV16-specific T cells, as well as being tumorigenic and detectable *in vivo*. This new cell line, E6/7-lucA2, depends on the HPV16 proteins E6 and E7 for its survival and was verified to present our lead epitope $E7_{11-19}$ on its MHC molecules. The cell line was then used to establish a novel orthotopic tumor model in the vaginal mucosa of A2.DR1 mice. This tumor model will ultimately be utilized for testing different therapeutic vaccination approaches. Therefore, I investigated methods to induce a robust vaccination-induced HPV16-specific $CD8^{+}$ T cell response in the vaginal mucosa. Different exclusively intravaginally delivered vaccine compounds did not elicit a detectable immune response while methods with prior induction of a systemic T cell response were more successful. However, it turned out that the level of mucosal $CD8^{+}$ T cells just correlates with the level of blood $CD8^{+}$ T cells and is not detectably influenced by application of immunomodulators such as chemokines or TLR agonists.

Taken together, the HPV16 E6/E7-dependent orthotopic, MHC-humanized tumor model E6/7-lucA2 in A2.DR1 mice constitutes a setting for exploration of therapeutic HPV vaccination approaches, which is mirroring the clinical situation much closer than previously available models.

II. Zusammenfassung

Humane Papillomviren (HPV) sind verantwortlich für Tumorwachstum in den anogenitalen und oropharyngealen Schleimhäuten. Die häufigste dieser Krebsarten ist Gebärmutterhalskrebs, welcher jedes Jahr ungefähr 570.000 Frauen neu betrifft. Obwohl es seit einiger Zeit prophylaktische Impfungen gegen HPV Hochrisikotypen, wie HPV16, gibt, bleiben die Impfraten niedrig und die Krebsraten hoch. In unserer Arbeitsgruppe „Immuntherapie und –prävention“ arbeiten wir an einem therapeutischen Impfstoff für die Behandlung von HPV16-induzierten Läsionen und Tumoren. Bis jetzt gibt es keine zugelassenen therapeutischen Impfungen gegen HPV-vermittelte Tumoren, auch wenn es eine Vielzahl von vielversprechenden präklinischen Studien gibt. Diese Studien haben zumeist den Einfluss von Impfungen mit murinen MHC-restringierten Epitopen auf subkutane Tumoren untersucht. Allerdings präsentieren die Tumoren von Patienten humane MHC (HLA)-restringierte Epitope und befinden sich außerdem in den Schleimhäuten, welche der T-Zell Zirkulation nur begrenzten Zugang ermöglichen. Hier beschreibe ich Lösungen für diese Probleme durch die Etablierung eines neuen orthotopen (vaginalen) Tumormodells, welches aus einer durch die viralen Onkoproteinen E6 und E7 immortalisierten Zelllinie besteht, die HLA-A2:01-restringierte Epitope auf ihrer Oberfläche präsentiert für die Nutzung in syngenen, MHC-humanisierten A2.DR1 Mäusen. Zudem habe ich Methoden zur Verbesserung der T-Zell Migration in die zervikovaginale Mukosa untersucht, welche später in Patienten Anwendung finden können.

Für die Etablierung des Tumormodells transfizierte ich zuerst $E6^{+}E7^{+}$ A2.DR1 Lungenzellen mit dem aktivierten Onkoprotein $HRAS^{G12V}$ und Luziferase aus dem Glühwürmchen. Die Zellen wurden spezifisch von HPV16-spezifischen T-Zellen getötet, waren tumorigen und konnten *in vivo* detektiert werden. Diese neue Zelllinie, E6/7-lucA2, ist für ihr Überleben auf die HPV16 Proteine E6 und E7 angewiesen und präsentiert nachgewiesenermaßen unser Hauptepitop $E7_{11-19}$ auf ihren MHC Molekülen. Die Zelllinie wurde dann verwendet um ein neues, orthotopes Tumormodell in der vaginalen Schleimhaut von A2.DR1 Mäusen zu etablieren. Das Tumormodell wird letztlich für die Testung verschiedener therapeutischer Impfmodalitäten genutzt werden. Daher untersuchte ich Methoden um eine robuste, impfinduzierte, HPV16-spezifische $CD8^{+}$ T-Zell Antwort in der vaginalen Schleimhaut zu induzieren. Verschiedene exklusiv intravaginal verabreichte Impfstoffe lösten keine messbare Immunantwort aus, während Methoden mit vorhergehender Induktion einer systemischen T-Zellantwort erfolgreicher waren. Allerdings zeigte sich, dass der Grad der mukosalen $CD8^{+}$ T-Zellantwort nur mit dem Grad der T-Zellantwort im Blut korrelierte und nicht erkennbar von der Verabreichung von Immunmodulatoren wie Chemokinen oder TLR Agonisten abhing.

Zusammengefasst bietet das HPV16 E6/E7-abhängige orthotope, MHC-humanisierte Tumormodell E6/7-lucA2 in A2.DR1 Mäusen eine Umgebung zur Erforschung von therapeutischen HPV Impfungen, welche die klinische Situation viel genauer widerspiegelt, als bereits verfügbare Modelle.

III. Danksagung

Hiermit möchte ich allen danken, die mich in den letzten Jahren während der Bearbeitung und des Schreibens meiner Doktorarbeit unterstützt haben.

Zuallererst möchte ich PD Dr. Dr. **Angelika Riemer** dafür danken, dass sie mir ermöglicht hat, in ihrer Arbeitsgruppe zu promovieren. Vielen Dank für Deine Unterstützung, Betreuung und Hilfe in allen wissenschaftlichen und nichtwissenschaftlichen Lebenslagen!

Außerdem vielen Dank an meinen Fakultätsgutachter und TAC-Mitglied Prof. Dr. **Martin Müller** für seine hilfreichen Ratschläge in den TAC-Meetings, die Übernahme der Erstbetreuung meiner Doktorarbeit, sowie das Teilen des E7 Antikörpers, der in dieser Arbeit verwendet wurde. Weiterhin möchte ich Prof. Dr. **Suat Özbek** und Dr. **Tim Waterboer** für ihre Teilnahme an meiner Disputation danken. Prof. Dr. **Magnus von Knebel Doeberitz** gebührt mein Dank für seine Hilfe und Anregungen als drittes Mitglied meines TACs.

Als nächstes möchte ich meinen Studenten, den unermüdlichen Minions, danken! Vielen Dank an **Alessa Henneberg**, **Patrick Wallisch**, **Lia Roth** und **Emilia Schmierer** für Eure hervorragende Arbeit, das Vorantreiben Eurer und meines Projekts, der lustigen Zeit im Labor und der Möglichkeit, mich als Betreuerin weiterzuentwickeln. An dieser Stelle für jeden von Euch ein extra Fleißbienchen!

Ein ganz großes Dankeschön an die gesamte **F130 Gruppe**, sowohl ehemalig als auch aktuell. Ihr seid der Grund, warum ich jeden Morgen gerne zur Arbeit komme. Danke an Dr. **Sebastian Kruse** für die tolle Einarbeitung am Anfang des Projekts, die Unterstützung in der Mitte des Projekts, das Setzen klarer Mittagessens-Regeln, viel Spaß im Büro und auf dem Weg zum Uni Shop, sowie hilfreiche Einblicke in die Finanzwelt. Dr. **Maria Bonsack** gebührt mein Dank für regelmäßige Kaffeepausen, fachliche, als auch persönliche Unterstützung und eine tolle Zeit im Büro. **Alexandra Klevenz** danke ich für ihre konstante Unterstützung bei meinen Experimenten (v.a. den Western Blots!), das Überbrücken von Wartezeiten im Tierhaus und unterhaltsamen Diskussionen im Labor. Auch an alle anderen Gruppenmitglieder ein herzliches Dankeschön für die schöne Zeit und den ganzen Spaß beim Zusammensitzen. Außerdem möchte ich **Jonas Förster** für seine Hilfe bei der MS-Analyse meiner Zellen danken, **Christoph Schifflers** für die stetige Versorgung mit belgischer Schokolade und hilfreichen Diskussionen über unsere Tierversuche, sowie **Kathrin Öhlenschläger** für das Korrekturlesen meiner Doktorarbeit.

Weiterhin danke an **Nika Vučković** für gute Gespräche, Sophia Föhr für gemeinsame Kaffeepausen, **Dr. Jonas Becker** für gute Laune im Büro sowie **Rebecca Köhler** für ihre technische Unterstützung. Ein ganz großes Dankeschön an **Monika Bock** für ihre administrative Hilfe, ihre gütige Art, das offene Ohr selbst zu fortgeschrittener Stunde und das Bestehen darauf, ihren Kollegen eine heiße Schokolade auszugeben, wenn sie nötig war. Du wirst vermisst. Außerdem danke an Dr. **Nitya Mohan**, **Nadine Steinhübel**, Dr. **Mine Özcan-Wahlbrink**, Dr. **Mogjib Salek,** sowie an **alle Studenten und Praktikanten** der Gruppe, die das Gruppenleben bereichert haben.

Am DKFZ möchte ich allen **Mitarbeitern der Flow Cytometry Core Facility** sowie dem **biostatistischen Consulting** für ihre Unterstützung danken, Dr. **Matthias Bozza** für seine Hilfe mit allen Vektor-Fragen, sowie den **Arbeitsgruppen Bund**, **Heikenwälder** und **Harbottle** für das Teilen ihrer Ressourcen. Im Tierhaus gebührt ein ganz großer Dank Dr. **Ramona Brecht** für ihre Unterstützung und Führung durch den Tierversuchsbürokratie-Dschungel. Außerdem vielen Dank an Dr. **Kerstin Dell** und all die **Tierpfleger** der ATV101, ATV108, ATV109 und Barriere C für die konstante Hilfe und das Kümmern um meine Mäuse. Ohne Euch hätte diese Arbeit so nicht funktioniert. Ebenso danke an **Kai Bates** für anregende Unterhaltungen.

Weiterhin vielen Dank an den PhD Council 2019 - **Sonja**, **Oguzhan**, **Michael**, **Khwab** und **Shub**, den **PhD Welcome Teams** und dem Organisationsteam des Career Day R&D 2021 – **Anne**, **Martha**, **Sabine**, **Julia**, **Ekaterina**, **Shiv**, **Jonas**, **Marion** und **Barbara** dafür, dass Ihr den PhD Alltag bunter gemacht habt. Außerdem einen herzlichen Dank an alle Mitarbeiter der **Helmholtz International Graduate School for Cancer Research** unter Dr. **Lindsay Murrells** für all die Unterstützung und Hilfe, die zum erfolgreichen Abschließen dieser Promotion geführt haben.

Außerhalb des DKFZs möchte ich **Armin Kübelbeck**, Dr. **Agnieszka Grabowska** und allen anderen Mitarbeitern von **Silvacx** für interessante Diskussionen und die Herstellung der Nanopartikel danken. Ein ganz großes Dankeschön an Dr. **Philipp Uhl** für die Produktion diverser Impfstoffe, allen voran von LPP-E7$_{11\text{-}19}$, um meine Versuche zu realisieren. Außerdem Danke an Dr. **Mikko Gynther** für die Herstellung der Liposomen, sowie allen anderen Mitgliedern von **MUNAVAC** für die gute Zusammenarbeit.

Zu guter Letzt möchte ich allen danken, die mich nicht unbedingt wissenschaftlich aber auf jeden Fall persönlich durch die Doktorarbeit getragen habe. So gilt mein Dank allen **Swing- und Steptänzern** Heidelbergs für die beschwingten Jahre.

Vielen lieben Dank an **Alessa** und **Marius**, meinen (Fast-)Mitbewohnern, sowie den Besitzern meines zweiten Zuhauses dafür, dass ich es unbeschadet durch diverse pandemiebedingte Lockdowns geschafft habe! Danke, dass Ihr für mich da seid!

Außerdem möchte ich all meinen Freunden dafür danken, dass sie mich stets in den verschiedenen Phasen meines PhD unterstützt haben und für mich da waren und sind. Danke **Johanna**, **Kathrin**, **Lilith**, **Vera**, **Teresa**, **Jojo**, **Julia**, **Sonja**, **Nina**, **Max**, **Jo** und **Wolfgang** für alles. Niemand könnte sich einen besseren Freundeskreis wünschen!

Abschließend möchte ich mich ganz herzlich bei meiner Familie bedanken – **Gudrun, Manfred** und **Alexander Zottnick**. Danke, dass Ihr mich auf diesem Weg begleitet habt, für die Unterstützung über all die Jahre und dafür, dass Ihr für mich da seid - komme was wolle. Ohne Euch wäre ich nie an diesem Punkt angelangt!

IV. Table of contents

V. Abbreviations

Abbreviation	Meaning
°C	degree Celsius
ACK	ammonium chloride potassium
AIN	anal intraepithelial lesion
AMP	adenosine monophosphate
APC	antigen-presenting cell
APC	allophycocyanin
ATP	adenosine triphosphate
ATRA	all-trans retinoic acid
BCR	B cell receptor
bp	base pairs
BSA	bovine serum albumin
BV	Brilliant Violet™
CAR	chimeric antigen receptor
CD	cluster of differentiation
CDK	cyclin-dependent kinase
CFFC	core facility flow cytometry
CFSE	carboxyfluorescein succinimidyl ester
CIN	cervical intraepithelial neoplasia
cm	centimeter
CMV	cytomegalovirus
COVID	**co**rona**vi**rus **d**isease
CPP	cell-penetrating peptide
CTL	cytotoxic T lymphocyte
CTLA	cytotoxic T-lymphocyte-associated protein
DC	dendritic cell
DC	detergent compatible
ddH_2O	double-distilled water
(d)dNTP	(di-)deoxynucleotide trisphosphate
DKFZ	*Deutsches Krebsforschungszentrum* (German Cancer Research Center)
DMEM	Dulbecco's Modified Eagle's medium
DMSO	dimethyl sulfoxide
DNA	deoxyribonucleic acid
dsDNA	double-stranded DNA
DTT	dithiothreitol
EDTA	ethylenediaminetetraacetic acid
EGFR	epidermal growth factor receptor
EMA	European Medicine Agency
ER	endoplasmic reticulum

Abbreviation	Meaning
ERA(A)P	endoplasmic reticulum aminopeptidase associated with antigen processing
FACS	fluorescence-activated cell sorting
Fc	fragment crystallizable
FCS	fetal calf serum
FDA	Food and Drug Administration
FITC	fluorescein isothiocyanate
FRT	female reproductive tract
FSC	forward scatter
g	gram
GP	GolgiPlug™
GS	GolgiStop™
GT	genital tract
GTP	guanosine triphosphate
Gy	Gray
h	hour
HEPES	4-(2-hydroxyethyl)-1-piperazineethanesulfonic acid
HIV	human immunodeficiency virus
HLA	human leukocyte antigen
HNSCC	head-and-neck squamous cell carcinoma
HPV	human papillomavirus
HSV	herpes simplex virus
i.m.	intramuscular
i.n.	intranasal
i.p.	intraperitoneal
ICS	intracellular cytokine staining
IFN	interferon
Ig	immunoglobulin
IL	interleukin
ILC	innate lymphoid cell
ITAM	immunoreceptor tyrosine-based activation motifs
IU	international unit
ivag.	intravaginal
IVC	individually ventilated cages
kg	kilogram
KO	knock-out
l	liter
LEEP	loop electrosurgical excision procedure
LP	lamina propria
LPP	lipoPEG peptide
LPS	lipopolysaccharide

Abbreviation	Meaning
M cell	Microfold cell
mA	milliampere
MACS	magnetic-activated cell sorting
MALT	mucosa-associated lymphoid tissue
MAPK	mitogen activated protein kinase
MCA	methylcholanthrene
MFI	mean fluorescence intensity
MHC	major histocompatibility complex
min	minute
µg	microgram
µl	microliter
µm	micrometer
ml	milliliter
mm	millimeter
MRI	magnetic resonance imaging
mRNA	messenger RNA
MS	mass spectrometry
MVA	modified vaccinia virus Ankara
N-9	nonoxynol-9
ng	nanogram
NK	natural killer
NLT	non-lymphoid tissue
nM	nanomolar (nmol/l)
ODN	oligodeoxynucleotide
ORF	open reading frame
P/S	penicillin-streptomycin
PAMP	pathogen-associated molecular pattern
PBS	phosphate-buffered saline
PC	plasma cell
PCR	polymerase chain reaction
PD	programmed cell death protein
PD-L	programmed cell death protein ligand
PE	phycoerythrin
PEG	polyethylene glycol
PerCP-Cy	peridinin chlorophyll protein-cyanine
PIN	penile intraepithelial lesion
PKC	protein kinase C
PLC	peptide-loading complex
PMA	phorbol 12-myristate 13-acetate
PML	promyelocyctic leukemia
PMSF	phenylmethylsulfonyl fluoride

Abbreviation	Meaning
poly(I:C)	polyinosinic:polycytidylic acid
PP_i	inorganic pyrophosphate
PRR	pattern recognition receptor
PVDF	polyvinylidene difluoride
RAS	Rat sarcoma virus
Rb	Retinoblastoma
RNA	ribonucleic acid
ROI	region of interest
ROS	reactive oxygen species
rpm	revolutions per minute
RPMI	Roswell Park Memorial Institute medium
RT	room temperature
s	second
s.c.	subcutaneous
S/MAR	scaffold/matrix attachment region
S1P	sphingosine-1-phosphate
S1PR	sphingosine-1-phosphate receptor
SD	standard deviation
SDS-PAGE	sodium dodecyl sulfate–polyacrylamide gel electrophoresis
SIN	squamous intraepithelial lesion
SiNP	silica nanoparticle
SiO_2	silica
SLO	secondary lymphoid tissue
SLP	synthetic long peptide
SSC	side scatter
SV40	simian virus 40
TAE	tris-acetate-EDTA
TAP	transporter associated with antigen processing
Taq	Taq polymerase
T_{CM}	central memory T cell
TCR	T cell receptor
TCZ	T cell zone
T_{EM}	effector memory T cell
TERT	telomerase reverse transcriptase
T_{FH}	follicular helper T cells
TGF	transforming growth factor
T_H	helper T cell
TIL	tumor-infiltrating lymphocytes
TLR	toll-like receptor
TNF	tumor necrosis factor
T_{reg}	regulatory T cell
T_{RM}	tissue-resident T cell

Abbreviation	Meaning
UbC	ubiquitin C
URR	upstream regulatory region
US	United States
UV	ultraviolet
V	Volt
VAIN	vaginal intraepithelial lesion
VIN	vulval intraepithelial lesion
VLP	virus-like particle
WHO	World Health Organization
xg	times gravity
ZPF	*Zentrum für präklinische Forschung* (Center for preclinical research)
β_2m	β2 microglobulin

VI. List of figures

VII. List of tables

1 Introduction

1.1 Immune system

1.1.1 Overview

A multitude of pathogens threatens the health of the human body every day. These bacteria, viruses, parasites or fungi, along with intrinsic threats such as mutated cells, are cleared in most cases by the immune system. The human immune system consists of two branches that work interconnectedly. Those are the innate immune system that an individual is born with and the adaptive immune system that is acquired over one's lifetime. This work addresses in most parts the adaptive immune response, which is why the focus of this introduction will be on the acquired immune system.

1.1.1.1 Innate immune system

The innate immune system incorporates the mechanical, 'outer' barriers of the body, the complement system and the innate immune cells such as macrophages, granulocytes, dendritic cells (DCs) and natural killer (NK) cells. Upon encounter with a pathogen, the first line of defense are the anatomical barriers such as the skin or the mucosae of the oropharyngeal and anogenital cavities as well as of the intestinal tract. These barriers contain antimicrobial peptides whose different classes have specialized effects on different classes of pathogens. For example, they can lyse and digest bacterial walls and membranes. If the pathogens have managed to overcome the first obstacle, they might be eliminated by the complement system, which is comprised of different plasma proteins. Once these are activated by the antigen, a variety of signaling cascades are triggered that lead to promotion of inflammatory processes and the eventual phagocytosis of the pathogen. If the complement system also fails to clear the threat, innate immune cells take over (Murphy & Weaver, 2017). These cells express pattern recognition receptors (PRRs) on their surfaces that are able to recognize pathogen-associated molecular patterns (PAMPs), which are foreign molecules derived from the pathogen. Among those PRRs are the so-called Toll-like receptors (TLRs) that recognize a range of different molecules such as lipopolysaccharides (LPS) from the surface of gram negative bacteria (recognized by TLR4), flagellin (TLR5) or double-stranded ribonucleic acid (RNA)(TLR3) (Medzhitov, 2001). Activation of these PRRs in turn activates the innate immune cells the receptors are expressed on and leads to the cells' corresponding effector functions. These

include phagocytosis and production of inflammatory proteins such as cytokines and chemokines (Murphy & Weaver, 2017).

1.1.1.2 Adaptive immune system

While the innate immune system is triggered immediately after the infection with a pathogen, the adaptive response is delayed in its activation. The adaptive part of the immune system is highly specific in recognizing antigens, which stands in contrast to the more general activity of the innate part. The adaptive immune response also forms the immunological memory after an infection has passed. This allows for a faster response upon reinfection.

The most important cells of the adaptive immune system are the lymphocytes that can be distinguished into B and T cells, which are characterized by their different receptors – the B cell receptor (BCR) and the T cell receptor (TCR). Lymphocytes circulate in blood and lymph and can stay in lymphoid organs of the lymphatic system. This system includes lymph nodes and immunologically important organs such as the thymus, the bone marrow or the spleen. Initially, lymphocyte progenitor cells are given rise to in the bone marrow. B cells, so called because of their place of discovery – the poultry bursa of Fabricius – stay in the bone marrow while T cells migrate to the thymus, which also gave these cells their name. After maturation, both cell populations enter the blood circulation (Murphy & Weaver, 2017).

The receptors of B and T cells both have constant, conserved regions, as well as regions that are highly specific and bind antigens. The BCR is a surface immunoglobulin (Ig) and is comprised of two heavy chains and two light chains. It is Y-shaped and has two antigen-binding sites. In contrast, the TCR has a single antigen-binding site. The receptor specificity derives from the so-called somatic recombination where the deoxyribonucleic acid (DNA) for the antigen receptors is rearranged from different segments (V, D and J), which results in a diversity of billions of different specificities.

Innate immune cells present antigenic peptides (‘epitopes’) on their surface after taking up the pathogen. In most parts, this is accomplished by DCs that represent the link between the innate and the adaptive immune system and belong to the professional antigen-presenting cells (pAPC). The DCs accumulate in lymph nodes where the presented antigen is recognized by an antigen-specific lymphocyte. Thus, the lymphocyte gets activated and starts to proliferate. The cells can then differentiate into effector cells: plasma cells for B lymphocytes and helper or

cytotoxic effector cells for T lymphocytes. Plasma cells produce antibodies that are secreted into the bloodstream and bind the pathogen, which neutralizes it or leads to opsonization, where the pathogen, e.g. a bacterium is coated with antibodies and then gets phagocytosed. The antibody-mediated immune response in the blood belongs to the humoral immunity found in bodily fluids. In contrast to the B cell-mediated humoral part of the adaptive immune response stands cellular immunity, mediated by T cells. Roughly, activated cytotoxic, or cluster of differentiation (CD)8^+, T cells can detect infected cells, or in case of cancer, mutated cells and eliminate them by releasing proteins that induce the death of the target cell. Additionally, the helper, or $CD4^+$, T cells help the immune response by producing cytokines and activating B and T cells. The T cell response will be discussed in more detail in the following sections. After the immune response has subsided and the pathogens have been cleared, only memory cells that resulted from the early proliferation and from the effector cells remain. These memory cells are specific for the encountered pathogen and react faster upon reinfection (Murphy & Weaver, 2017).

1.2 T cell immunology

As described above, T cells represent the cellular part of adaptive immunity. They recognize foreign epitopes presented to them on major histocompatibility complex (MHC) proteins. Those transmembrane proteins are expressed on most body cells and can be categorized into two classes (Murphy & Weaver, 2017).

1.2.1.1 Antigen processing and presentation on MHC

MHC class I (MHC I) molecules are expressed on all nucleated cells and present epitopes to $CD8^+$ T cells, which can detect a presented pathogen or mutation-derived peptide and subsequently eliminate the presenting cell. MHC II molecules on the other hand are expressed only on pAPCs. They interact with $CD4^+$ T cells and activate them. In humans, the MHC is located on chromosome 6 and is called human leukocyte antigen (HLA), while the murine MHC on chromosome 17 is called H-2. The MHC is a polygenic gene complex, meaning it contains different genes for the two MHC classes. Additionally, it is highly polymorphic, i.e. there exist many different alleles of the MHC genes in the population (Murphy & Weaver, 2017). For HLA I there are three genes: HLA-A, HLA-B and HLA-C; as well as for HLA II: HLA-DR, HLA-DP and HLA-DQ (Rock et al., 2016). MHC I molecules are comprised of four domains:

three α domains and β_2-microglobulin (β_2m) (Figure 1, left). The α_3 domain anchors the molecule in the cell membrane and interacts with the T cell CD8 co-receptor as well as β_2m, while the α_1 and α_2 domains form the peptide-binding cleft (Bjorkman et al., 1987; Murphy & Weaver, 2017). MHC II molecules are a complex of one β and one α chain with two domains each. The β_1 and α_1 domains form the peptide-binding cleft while the β_2 and α_2 domains contain the transmembrane domains (Figure 1, right) and interact with the T cell CD4 co-receptor (Jardetzky et al., 1994; Murphy & Weaver, 2017).

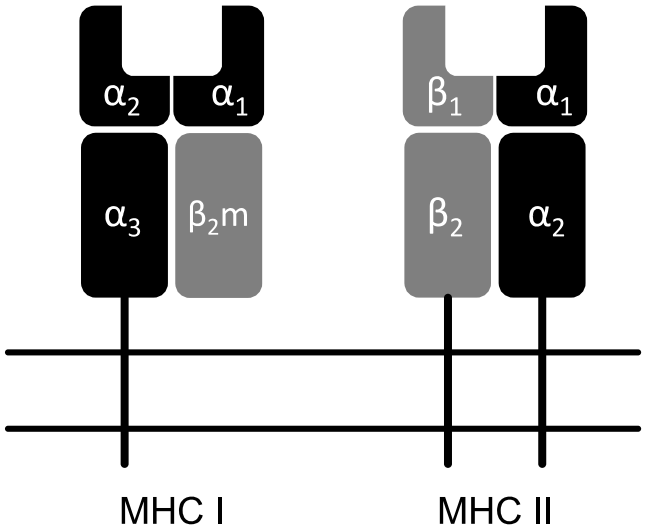

Figure 1. Structure of MHC molecules expressed on the cell surface. The MHC I molecule is comprised of one α chain with three domains and β2m (left), while the MHC II molecule is made up of one α and one β chain with two domains each (right).

The MHC allelic variants mostly differ in the composition of their peptide-binding cleft, which results in the binding and presentation of different peptides. A given MHC molecule binds peptides that have the same or similar amino acid in so-called anchor positions that determine the binding capacity of the epitope. MHC I proteins have a closed binding groove that binds 8 – 10 amino acid long peptides (Falk et al., 1991; Wieczorek et al., 2017), whereas the peptide groove of MHC II is open and the presented peptides are 13 – 25 amino acids long (Rudensky et al., 1991; Wieczorek et al., 2017).

Cell surface MHC I molecules present peptides derived from intracellularly found self and non-self proteins (Rock et al., 2016). The proteins are degraded by the proteasome into smaller peptides. Through the transporters associated with antigen processing (TAP) the peptides are

transported into the lumen of the endoplasmic reticulum (ER). There they bind free MHC I molecules or get trimmed even further by the endoplasmic reticulum aminopeptidase associated with antigen processing (ERAAP in mice/ERAP in humans) so they fit on MHC I. The binding is facilitated by the peptide-loading complex (PLC). Afterwards the MHC I:peptide complex is transported to the cell surface (Hammer et al., 2007; Rock et al., 2016; Murphy & Weaver, 2017). Although MHC I mostly presents intracellular peptides on the surface of cells, MHC I molecules of DCs can also present exogenous peptides (that have been phagocytosed before) to $CD8^+$ T cells in a process termed cross-presentation (Joffre et al., 2012). Exogenous peptides can also be presented on MHC II molecules of pAPCs such as DCs, macrophages or B cells.

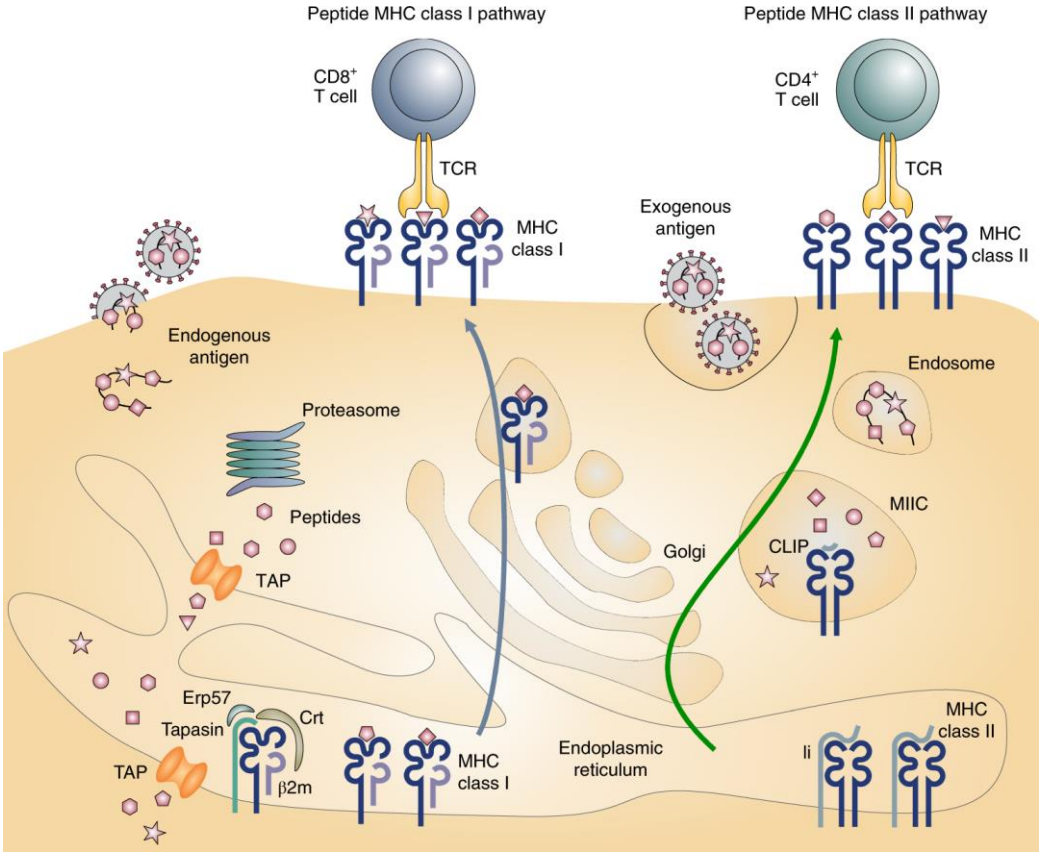

Figure 2. Antigen processing machinery and MHC presentation. Endogenous antigen gets degraded by the proteasome and is loaded onto MHC I molecules in the ER (left). Exogenous antigens get taken up, the endosomes are fused with MHC II-containing vesicles and loaded MHC II are transported to the surface (right). Figure from Purcell et al. (2019).

For this, the foreign antigen is taken up by the cell through endocytosis, phagocytosis or pinocytosis and is encapsulated by an endosome. MHC II molecules are assembled in the ER and then get transported to the cytosol in vesicles that fuse with the antigen-containing

endosomes. Meanwhile, the antigen has been degraded into peptides through proteases contained in the endosome. Upon fusion, the peptide binds the MHC II molecule and the MHC:peptide complex is transported to the cell surface where the epitope is presented to $CD4^+$ T cells (Figure 2)(Murphy & Weaver, 2017).

1.2.1.2 T cell development and subsets

T cells are characterized by their expression of the TCR that is mostly formed by an α and a β chain that form a heterodimer responsible for antigen recognition. There are also T cells with TCRs made of γ and δ chains. If not mentioned otherwise, T cells covered in this work belong to the α:β T cell family. The fully functional TCR complex is completed by the ε, δ, and γ chains, forming the CD3 complex, and by a homodimer of two ζ chains (Figure 3, left).

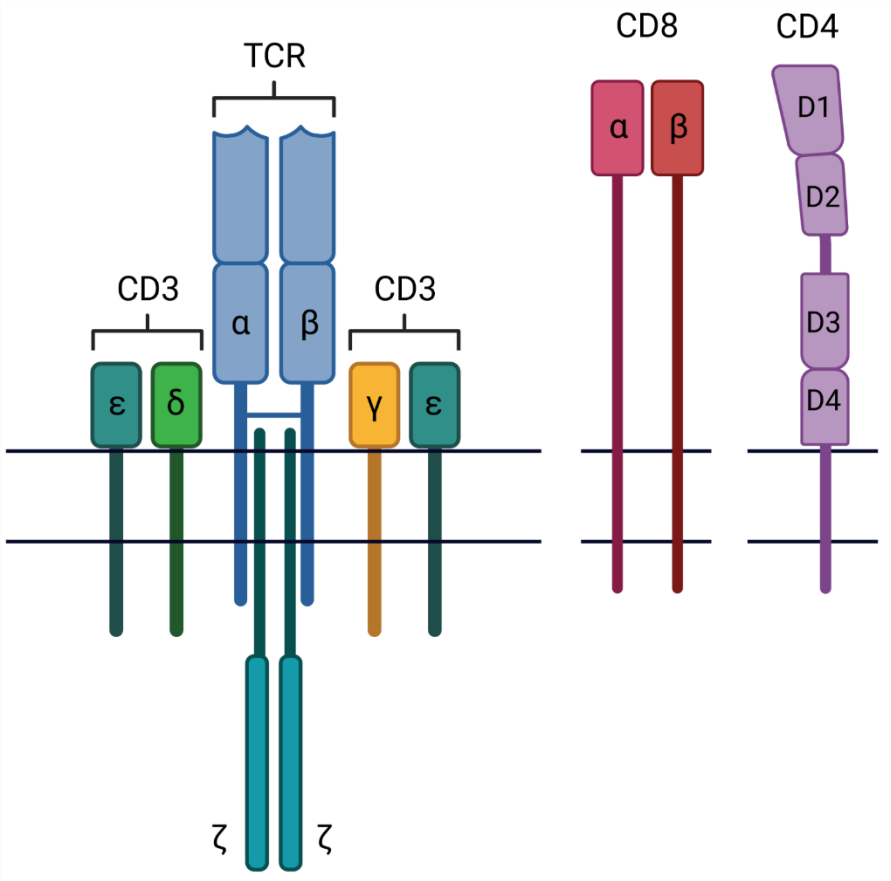

Figure 3. TCR complex and T cell co-receptors. The TCR complex is comprised of the TCR, the CD3 heterodimer and the ζ chains holding ITAM motifs for signaling (left). The CD8 co-receptor consists of an α:β heterodimer (middle) while CD4 contains four Ig-like domains (D1-D4, right). Figure created with BioRender.com.

The CD3 complex and the ζ chains contain ten immunoreceptor tyrosine-based activation motifs (ITAMs) in total. These ITAMs become phosphorylated upon TCR activation and induce an intracellular signaling cascade (Alcover et al., 2018). In the following the term 'TCR' will be used for the full TCR-CD3-ITAM complex. The two major subsets of T cells are $CD4^+$ and $CD8^+$ T cells that are named after the co-receptor they are expressing. The CD8 co-receptor is a heterodimer of an α and a β chain. CD4 in contrast is a single chain with four Ig-like domains. Additionally to $CD4^+$ and $CD8^+$ T cells many more smaller T cell subsets exist, which will not be addressed here (Murphy & Weaver, 2017).

As mentioned before, T cells develop from the lymphatic line in the bone marrow and mature in the thymus. There the so-called thymocytes are tested for their ability to exert their specific functions. Early T cells do neither express the characteristic CD3 molecules nor CD4 or CD8, leading to the term double-negative thymocytes. Throughout differentiation, the thymocytes start to express the TCR, as well as the co-receptors CD4 and CD8, becoming double-positive thymocytes. Before they differentiate into single-positive thymocytes, the early T cells have to undergo a rigorous selection process to ensure they bind to MHC but do not react when presented with a self-peptide. In positive selection, all thymocytes binding self MHC:peptide complexes in the thymus receive a survival signal . Depending on which kind of MHC:peptide complex (I or II) the TCR of the double-positive cells interact with, the co-receptor specificity is determined (CD4 – MHC II; CD8 – MHC I), leading to abrogation of expression of the other co-receptor. The fact that T cells interact with a target only when their cognate peptide is presented on an MHC molecule is called MHC restriction. After positive selection, the single-positive thymocytes in the thymus are presented with a selection of self-peptides from the whole body. If the cells strongly react to self-antigens they are sorted out and die by apoptosis (negative selection). After the selection processes the cells leave the thymus as mature, naïve T cells into the blood stream (Murphy & Weaver, 2017). While $CD8^+$ T cells act as cytotoxic cells that lead to the destruction of target cells, $CD4^+$ T cells differentiate into a variety of subsets upon activation:

T_H1 cells help with the defense against intracellular pathogens such as viruses or microbes. They are characterized by the secretion of the cytokine interferon γ (IFNγ) and have a role in activation of macrophages. T_H2 cells on the other side help with defeating extracellular parasites and promote immune responses by eosinophil and basophil granulocytes and mast cells by their

release of interleukin-4 (IL-4), IL-5 and IL-13. T_H17 cells received their name because of the secretion of IL-17. They help with the response against extracellular bacteria and fungi by activating neutrophil granulocytes among others. Finally, follicular helper T cells, T_{FH}, support the B cell response against a range of different pathogens. While the aforementioned T helper cell subsets activate and sustain the immune response, the regulatory T cells, T_{reg}, suppress T cell responses and prevent autoimmunity (Jiang & Dong, 2013).

1.2.1.3 T cell response

Naïve T cells leave the thymus after maturation and patrol the blood stream while passing lymphoid tissue and lymph nodes. Thereby they pass DCs on their way and check the MHC:peptide complexes on the DC surfaces. If a T cell detects its specific epitope on a DC, it stops patrolling, gets activated and subsequently starts proliferating. This process is called priming of naïve T cells. The activation of T cells includes three signals (Figure 4): First, the MHC:peptide complex interacts with the TCR specific for the epitope presented on the MHC protein. This induces the initial activation of the T cell. Second, co-stimulatory molecules bind and start signaling. Most prominent are the CD28 molecules on T cells that bind CD80/CD86 (B7.1/B7.2)(Murphy & Weaver, 2017). Another co-stimulatory molecule is CD40L, which is upregulated by T cells upon antigen recognition. This molecule also provides a costimulatory signal by binding CD40 on DCs (Bevan, 2004). Third, cytokines are released that determine the fate of the naïve T cell: T_H1 through IFNγ and IL-12; IL-4 for T_H2; transforming growth factor β (TGFβ), IL-6 and IL-23 for T_H17; IL-6 for T_{FH} as well as TGFβ and IL-2 for T_{reg}. IL-2, which binds its receptor CD25 that is upregulated on activated T cells is also crucial for $CD8^+$ cytotoxic T lymphocyte (CTL) differentiation (Murphy & Weaver, 2017). In principle, the three steps of T cell activation apply to both, $CD4^+$ and $CD8^+$ T cells. However, $CD8^+$ T cells require more co-stimulation than $CD4^+$ T cells to acquire their effector function. Either the $CD8^+$ T cells have to produce enough IL-2 upon their activation by DCs, which drives them to differentiate into CTLs or they have to receive $CD4^+$ T cell help. For this, DCs first have to activate the $CD4^+$ T cells that start to express IL-2 and CD40L. CD40L then binds to CD40 on the DCs, which in turn increase their expression of co-stimulatory molecules. The enhanced co-stimulation in addition to IL-2 secretion by $CD4^+$ T cells helps in activation of $CD8^+$ T cells (Murphy & Weaver, 2017).

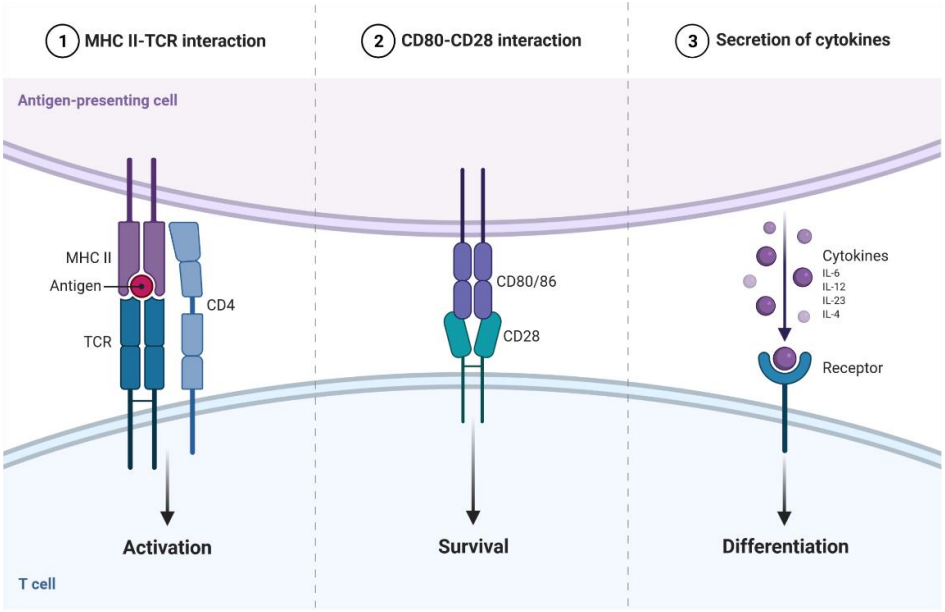

Figure 4. The three signals of T cell activation. Exemplarily shown with CD4 activation. Figure adapted from "Three Signals Required for T cell Activation" by BioRender.com (2022).

Primed CTLs egress from lymphoid tissue to the blood stream and migrate to the target tissue in a chemotactic way (Halle et al., 2017). One of the chemokine receptors on activated T cells is CXCR3 that binds IFNγ-inducible chemokines such as CXCL9 (MIG), CXCL10 (IP-10) and CXCL11 (IP-9) (Kuo et al., 2018). The chemokine signaling leads the CTLs towards the inflamed site. Once arrived at the effector site, an activated CTL forms an immunological synapse through its TCR with the target cell's MHC I, which presents the foreign epitope. Subsequently, the effector molecules perforin and different granzymes are transported towards the target cell in cytotoxic granules inside of the CTL (Halle et al., 2017). The vesicles are set free and perforins form pores in the target cell membrane. Other than damaging the target, perforin-induced pores also enable granzymes to enter the infected cell (Lopez et al., 2013). The two most abundant granzymes are granzyme A and granzyme B, which both activate caspase-dependent apoptosis of affected cells. CTLs additionally release cytokines such as IFNγ and tumor necrosis factor α (TNFα) that activate macrophages and also induce apoptosis (Murphy & Weaver, 2017).

1.2.1.4 T cell memory

Immune cell memory is the basis for vaccination and the origin of modern immunology in 1798. Edward Jenner then discovered that inoculation with cowpox could prevent small pox infection, although variolation i.e. the inoculation with dried smallpox pustules can be traced back to 10th

century China (Jenner, 1798; Gourley et al., 2004). The idea of vaccination is to induce an immune response whereupon memory cells form, which protect from a real infection with the same pathogen. While prophylactic vaccines available against infectious diseases were developed to induce durable B cell antibody responses, cancer vaccines employ the T cell memory response needed for control and killing of mutated cells (Sigrist, 2018; Blass & Ott, 2021).

While innate immune memory can even be found in plants and invertebrate animals, adaptive immune responses are limited to vertebrates and can specifically identify and protect from pathogens encountered earlier (Netea et al., 2019). It is not entirely resolved how memory T cells form, most likely they result from the 5 – 10 % of effector cells that do not die after the effector phase but rather differentiate into memory cells with their previous specificity (Omilusik & Goldrath, 2017). Throughout this process they change the expression of their homing molecules (Mueller et al., 2013). These memory T cells are maintained long-term by IL-7 and IL-15 (Laidlaw et al., 2016). Some memory T cells may also arise from the initial differentiation after priming of naïve T cells (Omilusik & Goldrath, 2017). Although most research on memory formation has been conducted in murine model systems, it can be assumed that human T cell memory is formed comparably (Ahmed & Akondy, 2011).

As taken advantage of in vaccination approaches, memory T cells recognize a previously encountered antigen. In contrast to the primary immune response, the secondary response occurs much quicker as memory cell proliferation and execution of effector function do not require fresh priming and therefore need less time than before (Schenkel & Masopust, 2014). Memory T cells express distinct surface markers they require for homing to particular tissues. The most characteristic surface marker is CD44, a receptor for hyaluronic acid expressed in peripheral tissues, which is expressed on all memory T cells (Murphy & Weaver, 2017). As for non-memory T cells, memory T cells can be distinguished into different subsets with different duties that are reflected in their respective names:

Central memory T cells (T_{CM}) are characterized by their expression of CD62L (‘L-selectin’), a homing receptor directing T cells into secondary lymphoid tissue. They also express the chemokine receptor CCR7, which allows them to recirculate in blood similar to naïve T cells. T_{CM} migrate from blood into secondary lymphoid organs into the lymphatic system and back

into the blood (Figure 5A). They are slower in acquiring an effector function compared to other memory T cells. However, once they are activated they proliferate extensively and produce large quantities of IL-2 (Mueller et al., 2013; Murphy & Weaver, 2017).

Effector memory T cells (T_{EM}) neither express CD62L nor CCR7. Instead, they express integrins and receptors for inflammatory cytokines and can therefore enter inflamed tissue. T_{EM} migrate from the blood into peripheral, non-lymphoid tissues, through the lymphatic system back to the blood stream (Figure 5A). Upon restimulation by their cognate antigen, they can rapidly mature into effector T cells and secrete IFNγ, IL-4 and IL-5. In contrast to T_{CM}, T_{EM} display a more limited proliferative capacity (Mueller et al., 2013; Murphy & Weaver, 2017).

The third memory T cell subset are tissue-resident memory T cells (T_{RM}). Similar to T_{EM}, they do not or express only low levels of CD62L (Mueller et al., 2013). The most reported upon markers for this cell subset are CD69 and CD103. CD69 is an early activation surface marker of T cells and leads to the downregulation of sphingosine-1-phosphate receptors (S1PR) on the activated cells. As Sphingosine-1-phosphate (S1P) is highly expressed in blood and lymph, the downregulation of S1PR on T cells leads to their retention in tissue (Murphy & Weaver, 2017; Jameson & Masopust, 2018). In effector T cells, the expression of CD69 is high after initial antigen recognition in the lymph node. This prevents T cells from sensing the S1P gradient in blood and enables them to stay in the lymph node for further differentiation signaling. Once CD69 expression wanes, the effector T cells can egress into blood (Hunter et al., 2016). They chemotactically travel to the inflammation site and downregulate S1PR again after extravasation (Aoki et al., 2016). T_{RM} maintain their CD69 expression and the associated downregulation of S1PR. CD103 ('α_E') on the other hand is an integrin that forms a heterodimer with β_7, resulting in α_E:β_7. This integrin complex binds E-cadherin, which is expressed by the epithelium (Murphy & Weaver, 2017). CD103 is only marginally expressed in other memory T cells and was found so far on T_{RM} in the gut, kidney, brain, skin, female reproductive tract (FRT), and thymus (Carbone, 2015). It was also found to be expressed more dominantly on $CD8^+$ than $CD4^+$ T cells, which is why $CD8^+$ T_{RM} are better examined (Schenkel & Masopust, 2014; Park & Kupper, 2015). TGFβ signaling is a key mediator of CD103 expression (Shin & Iwasaki, 2013). Although CD69 and CD103 are the most used markers for T_{RM}, they are not necessarily expressed on all T_{RM} (Mueller & Mackay, 2016). Other surface markers are CD49a

('VLA-1') and CXCR3 as well as CCR9, which enable migration to peripheral tissues (Murphy & Weaver, 2017; Mami-Chouaib et al., 2018).

T_{RM} represent the adaptive immune system's first line of defense in barrier regions such as the skin or the mucosal linings of the respiratory tract, gut and genital tract (GT) (Shin & Iwasaki, 2013). As each tissue has to deal with different pathogens, the T_{RM} repertoire in the various tissues is mostly non-overlapping (Park & Kupper, 2015). Although T_{RM} stay in their dedicated barrier region and do not recirculate in blood, they can migrate within their tissue (Figure 5A) (Shin & Iwasaki, 2013; Mueller & Mackay, 2016). There are different ways for T_{RM} to form.

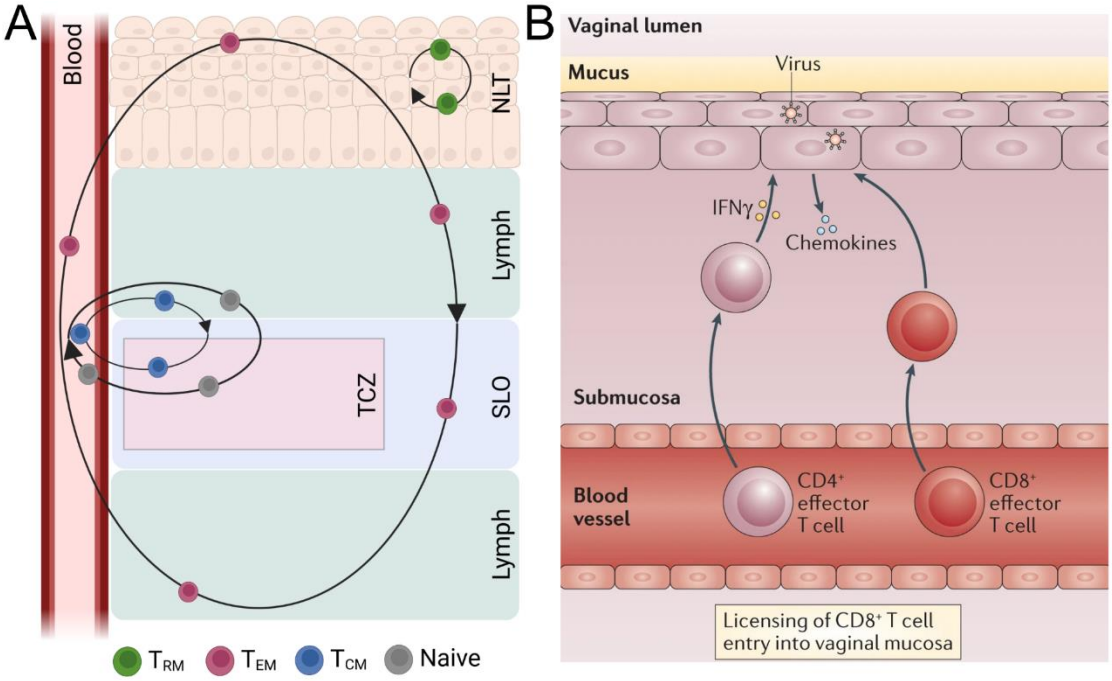

Figure 5. Migration of memory and effector T cells. A) Different subsets of memory T cells migrate through different tissues. NLT = non-lymphoid tissue, SLO = secondary lymphoid tissue, TCZ = T cell zone. Adapted from Schenkel and Masopust (2014), created with BioRender.com. B) $CD8^+$ effector T cells migrate into the vaginal mucosa after $CD4^+$ effector cells induce secretion of chemokines via IFNγ signaling. Adapted from Laidlaw et al. (2016).

The local way is that T cells upon infection of a T_{RM}-containing area travel to the draining lymph node where the residing, tissue-derived DCs program the T cells for tissue tropism, guiding them back to the site of infection and induce tissue-residency. The global approach involves T cells, which migrate from somewhere else in the body towards the inflamed tissue when their homing receptors get upregulated. Therefore, prospective T_{RM} do not have to be anatomically nearby. However, both $CD4^+$ and $CD8^+$ T cells can only enter restrictive tissues

such as the vaginal mucosa upon inflammation as the tissues lack tissue-tropic chemokines or adhesion molecules. It is important to note that T_{RM} probably do not derive from T_{EM} and that their lineage is possibly determined shortly after naïve T cell activation (Shin & Iwasaki, 2013; Amsen et al., 2018). When residing in peripheral tissues, T_{RM} can be maintained in absence of cognate antigen. They just require an inflammatory cue to be attracted to the mucosa and then persist there (Mueller et al., 2013). However, this might be tissue-dependent as $CD4^+$ T_{RM} may require antigen for maintenance in the genital mucosa (Schenkel & Masopust, 2014; Mueller & Mackay, 2016). Interestingly, the $CD8^+$ T_{RM} response can be recalled also in absence of $CD4^+$ T cell help, although $CD4^+$ T cells can support the formation of T_{RM} by directing effector $CD8^+$ T cells to the mucosa by IFNγ signaling (Figure 5B)(Mueller et al., 2013; Laidlaw et al., 2016). Upon restimulation, T_{RM} induce a tissue-wide state of alert by releasing IFNγ and the expression of innate immune genes throughout the impacted tissue. Therefore, T_{RM} act as a bridge between the innate and adaptive immune response (Mueller & Mackay, 2016).

1.2.1.5 Immune system of the female reproductive tract

The FRT of mammals has to fulfill a variety of immunological functions. Not only does it need to protect from infections with mucosal pathogens, but at the same time it needs to be tolerant to sperm and to a growing fetus, enabling its reproductive function (Zhou et al., 2018). The anatomy of human and murine FRT can be seen in the upper part of Figure 6. Both tracts start on the outside with the vagina, followed by the cervix, which can be separated into ecto- and endocervix in humans, leading to the uterus. While most parts of the so-called Müllerian ducts have fused during embryonal development in humans, forming the vaginal canal, cervix and uterine body, the fallopian tubes represent the unfused parts. In mice, the Müllerian ducts remain separated for the most part, resulting in bilateral uterine horns and oviducts (Cunha et al., 2019). The uterus and endocervix of human females are lined with columnar epithelial cells (‘type I mucosa’), while ectocervix and vagina are lined with non-keratinized stratified squamous epithelial cells, making it type II mucosa (Iwasaki, 2010; Zhou et al., 2018; VanBenschoten & Woodrow, 2021). In mice on the other hand the whole cervical and vaginal mucosae are lined with stratified squamous epithelium (Cunha et al., 2019). As for humans, the murine uteri are also lined by a singular columnar epithelium (Böttinger et al., 2020). The uterine type I mucosa is part of the organized mucosa-associated lymphoid tissue (MALT) (Iwasaki, 2010). The findings described below are merged from human and mouse studies. The

cervicovaginal mucosa contains at least four kinds of myeloid-derived pAPC subsets: Langerhans cells (tissue-resident macrophages) in epithelium, $CD14^+$ and $CD14^-$ DCs, as well as $CD14^+$ macrophages in lamina propria (LP). Although these were found in human tissue, mouse studies imply similar distinct pAPC populations in murine vaginal epithelium, which contain at least three DC subsets. The cell populations also change during the estrus cycle, implying an influence of hormones on the cell populations. Additional lymphocytes found in the vaginal epithelium are NK cells, innate lymphoid cells (ILCs) and B cells. The production of IgG and IgA by vaginal plasma cells is also hormonally regulated. It is known for human cervical mucosa that one third of the residing $CD45^+$ cells are T cells, of which about 60 % are $CD8^+$, most of them displaying an effector phenotype. They are more abundant in the ecto- than the endocervix, which reflects the likelihood of pathogen exposure in the respective area. Human endometrial cells have also been found to contain lymphoid aggregates consisting of B cells, $CD8^+$ T cells and macrophages when in a non-pregnant state. The function of these aggregates is not clear but they may play a role during menstrual shedding of endometrial tissue (Zhou et al., 2018). Hormonal changes during the female reproductive cycle in general influence the immune response and cell composition in the genital mucosa. The reproductive cycle in humans is the menstrual, in rodents the estrus cycle. As this work is focused on mice, only the estrus cycle is discussed in the following. The estrus cycle consists of four phases: proestrus (comparable to follicular phase in humans), estrus, metestrus and diestrus. Metestrus and diestrus are comparable to the secretory phase of the menstrual cycle. The whole estrus cycle lasts for four to five days (Ajayi & Akhigbe, 2020). During metestrus and diestrus the number of leukocyctes was found to be elevated, as well as the level of antigen-presentation by vaginal cells in diestrus (Wira et al., 2015; De Gregorio et al., 2018). During this phase, bacteria are also more readily taken up by the mucosa as shown in infections of mice with *Neisseria gonorrhoae* (Islam et al., 2016).

An important part of cervicovaginal immunity are $CD4^+$ and $CD8^+$ T_{RM}, which were introduced in 1.2.1.4. Upon infection, $CD4^+$ T cells enter the vaginal mucosa via IFNγ-dependent mechanisms and secrete even more IFNγ. This induces the production of CXCL9 and CXCL10 by keratinocytes and immune cells, leading to chemotactic attraction of $CD8^+$ $CXCR3^+$ T cells into the tissue (see also Figure 5B)(Nakanishi et al., 2009; Metzemaekers et al., 2018).

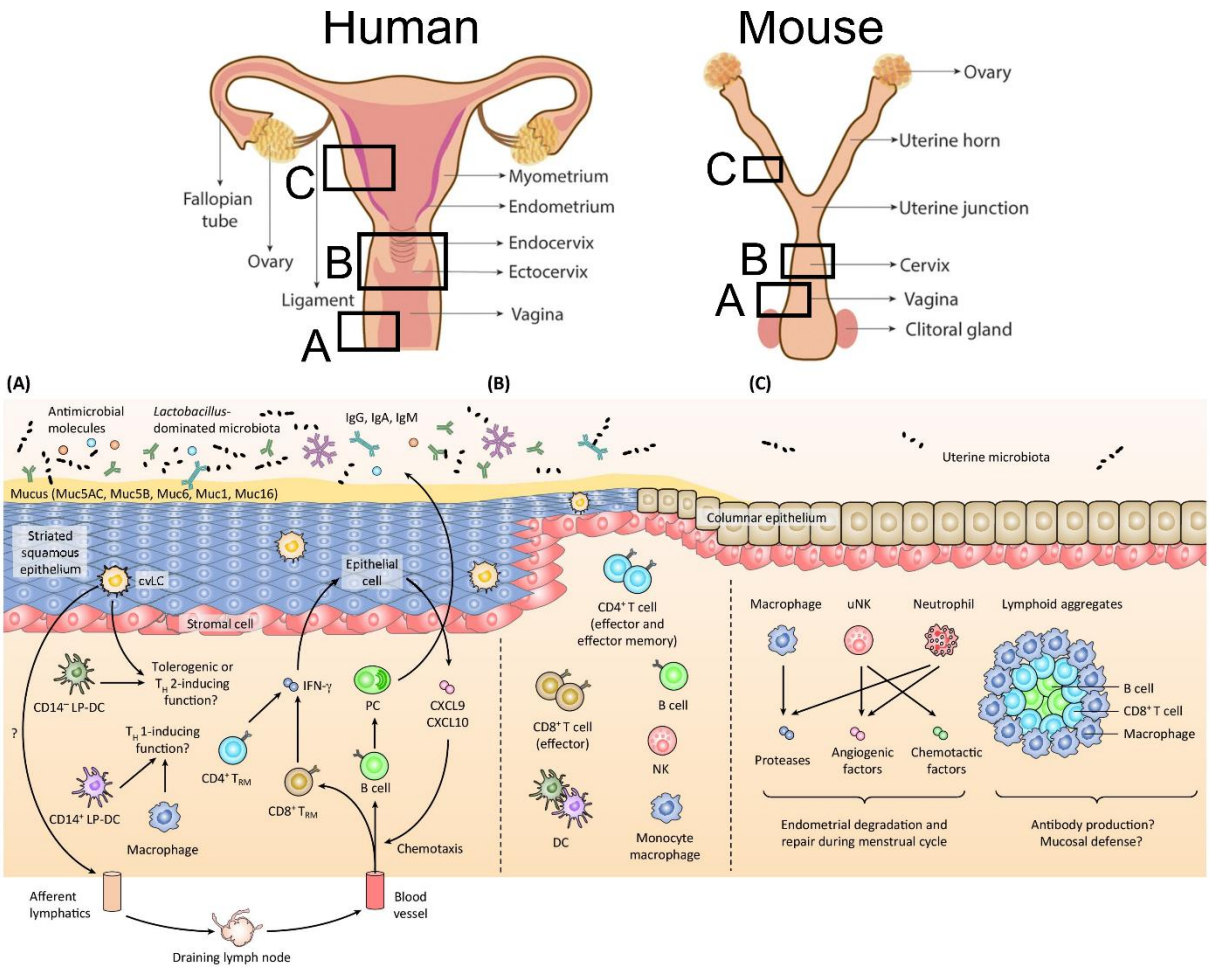

Figure 6. Immunology of the female reproductive tract. The FRT in women and mice roughly consists of the ovaries, which are connected to the oviducts leading to the uteri. The connection to the outside is made through the cervix and vagina. While the caudal parts are lined with stratified squamous epithelium topped by a mucous layer, the cranial parts are lined with columnar epithelium. The squamous epithelium contains tissue-resident macrophages - Langerhans cells (LC) and lamina propria DCs (LP-DC) that both present antigen to the tissue-resident T cells and to B cells, which differentiate into plasma cells (PC). The vaginal epithelium also harbors NK cells (not depicted). The immune cells present in the uterine tissue are involved in facilitating changes during the reproductive ('estrus' in mice, 'menstrual' in humans) cycle. Additionally, they form lymphoid aggregates that are probably involved in antigen scavenging. Figure merged and adapted from Chumduri and Turco (2021) and Zhou et al. (2018).

These $CD8^+$ T cells have the potential to remain resident in the mucosa as T_{RM}. Vaginal $CD8^+$ T_{RM} release IFNγ upon reactivation by their cognate antigen and thereby induce a state of inflammation, which activates local innate, cellular and humoral immune responses. The coordinated actions of T_{RM} are vital to uphold vaginal immunity to pathogens. Therefore, the induction of mucosal T_{RM} and local immunity has become a focus of vaccination studies against mucosal pathogens (Zhou et al., 2018).

1.2.1.6 Induction of vaginal immunity

Vaccination with the goal of inducing systemic immunity always leads to migration of some T cells into the cervicovaginal mucosa (Decrausaz et al., 2010; Shin & Iwasaki, 2013). However, it is desirable to increase the level of T_{RM} by either directly vaccinating at the mucosal site or by attracting T cells to the mucosa (Shin & Iwasaki, 2013). Therefore, T_{RM}-based vaccines show promise as many pathogens display specific tissue tropisms (Park & Kupper, 2015).

For vaginal immunization, the focus lies on protection from sexually transmitted pathogens. Examples for such are the three most common viruses infecting the cervicovaginal mucosa - human immunodeficiency virus (HIV), human papillomavirus (HPV; described further in 1.3) and herpes simplex virus (HSV) or bacteria such as *Chlamydia trachomatis* or *N. gonorrhoae* (VanBenschoten & Woodrow, 2021). Intravaginal (ivag.) delivery of attenuated *Salmonella enterica* expressing HPV16 L1, for example, has been shown to induce vaginal inflammation, systemic and mucosal immunity, as well as subcutaneous (s.c.) anti-tumor properties (Echchannaoui et al., 2008). However, the ivag. delivery of L1 virus-like particles (VLP) did only work when combined with previous treatment of the mucosa with nonoxynol-9 (N-9), a surfactant disrupting the vaginal epithelium (Fraillery et al., 2009). A vaginal prime/boost regimen with HPV pseudovirions expressing a model antigen was also shown to induce more cervicovaginal antigen-specific $CD8^+$ T cells expressing CD103 than with only an ivag. prime. The prime/boost approach did also provide long-lasting immunity from infection with a virus expressing the model antigen. In contrast, an exclusively intramuscular (i.m.) vaccination approach did not protect against the viral challenge, underlining the need for vaginal vaccines (Çuburu et al., 2012). The efficacy of the HPV pseudovirion approach was also shown for vaccination against HSV-2 (Çuburu et al., 2015). Even more effective than the ivag. immunization proved to be an i.m. prime, followed by an ivag. boost with adenoviruses encoding the HPV16 proteins E6 and E7. This increased the amount of antigen-specific $CD8^+$ T cells compared to an ivag. only vaccination. The application of immunomodulators such as imiquimod increased the amount of $CD8^+$ T cells even more (Çuburu et al., 2019). Ivag. administration of Fragment crystallizable (Fc)-fused IL-7 led to immune cell recruitment in the GT (Choi et al., 2016) while an ivag. HPV DNA vaccine induced more specific $CD8^+$ T cells in the mucosa than i.m. vaccination. This DNA vaccine even led to tumor control in the mucosa of mice (Sun et al., 2016). Another approach was a vaccine made by fusing an HPV epitope to

another peptide to form nanofibers. These induced a specific $CD8^+$ T cell response upon ivag. vaccination and suppressed orthotopic tumor growth (Li et al., 2020).

Vaginal immunity can also be induced by vaccinating systemically and afterwards employing methods to direct the immune cells towards the mucosa. One of these methods is the addition of all-trans retinoic acid (ATRA) to a systemic vaccination, which induces the upregulation of the integrin complex α_E:β_7 on T cells, which were then to be found in mucosal tissues (Tan et al., 2011). The trafficking of T cells can also be influenced by topical application of chemokines. Systemic vaccination with an attenuated HSV strain, followed by topical application of CXCL9 and CXCL10 to the vaginal mucosa of mice resulted in the recruitment of activated, specific $CD8^+$ T cells to the cervicovaginal mucosa. Afterwards, memory cells were found to stay in the mucosa and were able to protect against an HSV challenge. This method was termed 'prime and pull' (Shin & Iwasaki, 2012). In this context also the antibiotic neomycin had the capacity to pull $CD8^+$ T cells into the vaginal mucosa and protected from HSV challenge (Gopinath et al., 2020). Other studies showed that the prime and pull method only had a modest effect on B cell recruitment (Tregoning et al., 2013). Ivag. application of CpG-oligodeoxynucleotides (ODN) or of polyinosinic:polycytidylic acid (poly(I:C)) was also able to induce an influx of specific $CD8^+$ T cells to vaginal tissue, even leading to regression of genital tumors in a large fraction of mice (Domingos-Pereira et al., 2013). I.m. vaccination with a DNA vaccine coding for HPV16 E7, followed by topical application of the TLR7 agonist imiquimod led to accumulation of E7-specific $CD8^+$ T cells in the cervicovaginal mucosa by the upregulation of CXCL9 and CXCL10 expression (Soong et al., 2014). This imiquimod pull was also replicated in guinea pigs (Bernstein et al., 2019). Interestingly, a vaccination at a mucosal site can induce a local immune response in another mucosal tissue. When women were immunized ivag. with a cholera vaccine, corresponding IgG was found in the blood and saliva additionally to IgA and IgG in the cervicovaginal tract (Kozlowski et al., 1997). Vice versa, an intranasal (i.n.) vaccination with cholera toxin induced higher IgA levels in vaginal secretions (Johansson et al., 2001). In mice i.n. vaccination with an HPV16 polypeptide led to a higher frequency of antigen-specific T cells within the genital mucosa, even higher than via an ivag. vaccination route. The i.n. immunization was also able to protect from genital $HPV16^+$ tumors (Decrausaz, Domingos-Pereira, et al., 2011). In another study an i.n. HPV peptide vaccine did also confer protective immunity against vaginal tumors (Sierra et al., 2020). An HIV C envelope

peptide vaccination led to the highest IgG response in the vaginal mucosa when administered i.n. compared to sublingual and s.c. approaches. Vaccinating ivag. on the other site did not induce a vaginal or systemic immune response to the epitope (Buffa et al., 2012). However, in a study by Çuburu et al. (2012) an ivag. immunization with HPV pseudovirions induced more specific T cells in the vagina than after the i.n. inoculation (Çuburu et al., 2012). Finally, the ivag. boost of an i.n. primed immune response with a recombinant influenza HIV vector shifted HIV-specific $CD8^+$ T cell populations into the vaginal submucosa (Tan et al., 2017).

Taken together these studies illustrate the requirement to induce a mucosal immune response directly or indirectly to establish cervicovaginal immunity.

1.3 Human papillomavirus

1.3.1 Epidemiology

The sexually transmitted HPV is a DNA virus that has been around since at least the Classical antiquity when genital warts were already described by Hippocrates (Karamanou et al., 2010). Papillomaviruses can be found in many species and display a very distinct host specificity (Egawa et al., 2015). HPVs infect basal keratinocytes in skin and mucosal tissue and can cause warts, mucosal lesions and cancer (Lowy et al., 2008; Gheit, 2019). It is estimated that at least 80 % of all sexually active adults over 45 years of age in the US have been infected with HPV at least once (Chesson et al., 2014). However, over 90 % of infections are cleared by the immune system within two years, mostly by a combination of innate and adaptive immune responses, with T cells being responsible for clearance of infected cells (Plummer et al., 2007; Roden & Stern, 2018). If the infection is not cleared, there is a risk of cancer development at affected sites. In 2018, HPVs accounted for 690,000 new cancer cases worldwide, making up 12 % of all human cancers (Araldi et al., 2018; de Martel et al., 2020). The viruses can cause oropharyngeal, as well as anogenital cancers, most prominently cervical cancers, which accounted for 570,000 (80 %) of worldwide HPV cancer cases in 2018 (Figure 7).

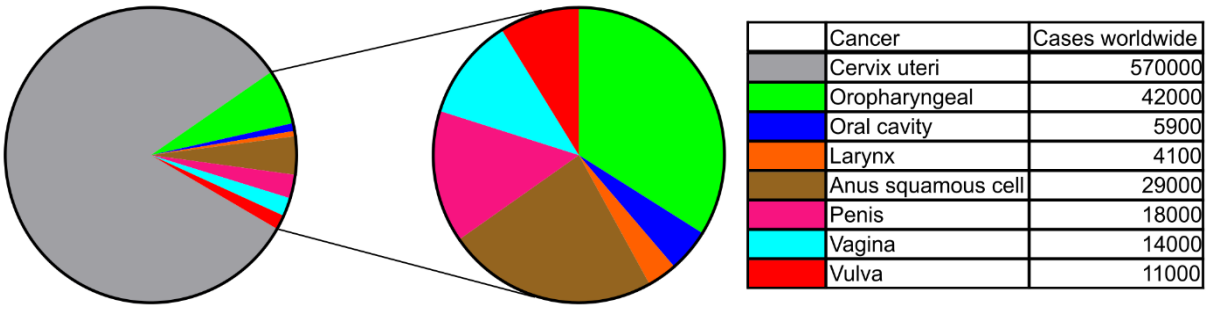

Cancer	Cases worldwide
Cervix uteri	570000
Oropharyngeal	42000
Oral cavity	5900
Larynx	4100
Anus squamous cell	29000
Penis	18000
Vagina	14000
Vulva	11000

Figure 7. HPV-associated cancer cases in 2018. The left chart depicts all cancer cases attributed to HPV infection worldwide (with cervical cancer cases making up the majority of cases) while the right chart depicts all non-cervical cancer cases. Numbers taken from de Martel et al. (2020).

About 70,000 cases of HPV-associated cancers were recorded for men (de Martel et al., 2020). In women, cervical cancer was the fourth common cancer in 2018 and the leading cause of cancer-related death in Sub-Saharan women (Arbyn et al., 2020). In general, cervical cancer is more common in low-income countries while other HPV-related cancers such as head-and-neck squamous cell carcinomas (HNSCC) are more prevalent in high-income countries, as these regions offer widely available preventive screenings for cervical cancer (Schiffman et al., 2016; de Martel et al., 2020).

There are currently over 200 different known genotypes ('types') of HPV in five phylogenetic genera. The five genera are named α, β, γ, μ, and ν. Most of the papillomaviruses infect cutaneous epithelium but some members of the α genus infect mucosal epithelium. Common warts are caused by members of μ, ν and some α HPVs (McBride, 2022). Fourteen types have so far been identified as being carcinogenic (HPV16, 18, 31, 33, 35, 39, 45, 51, 52, 56, 58, 59, 66 and 68) and ten more types are probably or potentially carcinogenic, all belonging to the α genus (Lechner et al., 2022; McBride, 2022). Virtually all HPV cancer cases in men, and 72 % of all HPV cancer cases in total are caused by the high-risk types HPV16 and HPV18, which belong to the α genus (Schiffman et al., 2016; de Martel et al., 2020). The most frequently detected HPV is HPV16, causing 60 % of cervical cancers and about 85 % of all HPV-related non-cervical cancers (Schiffman et al., 2016).

The development from an HPV infection to cancer depends mainly on three factors: the genetic composition of the infecting HPV, the host's immune response and the host's behavior such as smoking or hormonal contraceptive use (Schiffman et al., 2016). If a cervical infection with a high-risk HPV is not cleared by the immune system, it becomes persistent and can transform

the infected cells to dysplasia, so-called cervical intraepithelial neoplasia (CIN). After progressing through three CIN stages, cancer will develop from the infected cells (Schiffman et al., 2016). High-grade CINs or cancers will develop 5 – 14 years after initial infection (de Sanjosé et al., 2018).

1.3.2 Virus structure and genome

HPV is a dsDNA virus with an icosahedral capsid that is composed of 72 pentamers of the L1 capsid protein in addition to L2 proteins and has a diameter of 50 – 60 nm (Conway & Meyers, 2009; Doorbar et al., 2015). The genome consists of about 8,000 bp and incorporates eight to nine open reading frames (ORFs), depending on the genotype (Doorbar et al., 2015). Although there are not many genes, several more proteins can be synthesized due to alternative splicing and use of many promotors (Doorbar et al., 2015). HPVs contain at least six early genes and two late genes (Figure 8)(de Villiers, 2013). The early genes are denoted E1 – E7 with E3 missing. This is a result of an initial mis-sequencing of the bovine papillomavirus 1 genome (Doorbar et al., 2015). While the early genes E1 and E2 are involved in viral replication and transcription of early proteins, E4 additionally plays a role in the release of freshly produced viral particles from cells. E5, E6 and E7 are implicated in oncogenesis by promoting the cell cycle and helping in immune evasion (Doorbar, 2013; Doorbar et al., 2015; Pal & Kundu, 2019). The two late genes L1 and L2 encode for the viral capsid proteins, needed for viral packaging (Doorbar et al., 2015). Lastly, the upstream regulatory region (URR) contains the origin of DNA replication (ori) as well as transcription factor binding sites (Scarth et al., 2021).

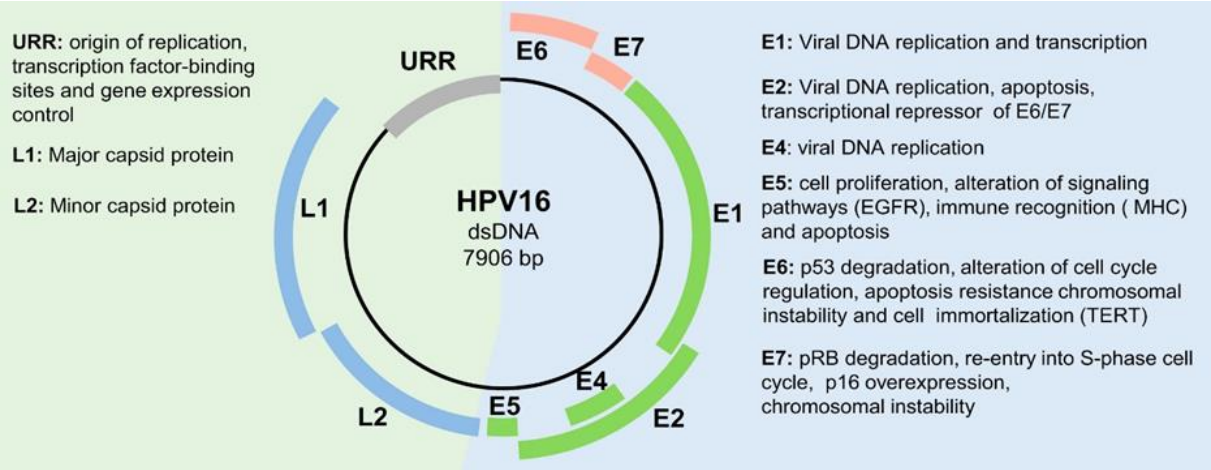

Figure 8. Genome of HPV16. The genome consists of eight ORFs coding for six early and two late proteins. Functions are stated in the Figure. Figure adapted from de Sanjosé et al. (2018).

1.3.3 Infectious cycle, malignant transformation and immune evasion

The HPV life cycle has been best described for α papillomaviruses but it can be applied to viruses of all genera (Doorbar et al., 2015). HPV is transmitted through direct physical, mostly sexual, contact and infects the basal layer of stratified epithelia (Schiffman et al., 2016). This layer consists of self-renewing cells, which divide symmetrically for replenishment of the basal layer, as well as asymmetrically to generate daughter cells that form the cell layers above (McBride, 2022). Infection with HPV occurs at a site of epithelial abrasion, where the virus infects the constantly dividing basal layer of keratinocytes close to the wound. After mitosis of these epithelial cells, one daughter cell remains attached to the basal layer while the other cell migrates through the suprabasal layers. During this migration, the cell terminally differentiates (Figure 9)(Roden & Stern, 2018). A particularly susceptible site for HPV infection and carcinogenesis is the transformation or transition zone of the cervix where the columnar epithelium of the endocervix meets stratified epithelial layers of the ectocervix (McBride, 2022). For infection, the L1 protein of the virion binds heparan sulfate proteoglycans on the basement membrane. The resulting induction of a conformational change of the virion capsid loosens the binding to the proteoglycans but allows for subsequent engagement of a secondary receptor (Day & Schelhaas, 2014). Then the virion is internalized by the host cell through an endocytosis mechanism, which is similar to micropinocytosis (Graham, 2017). While trafficking through the endosomal system of the host cell, the virion is partially uncoated of its capsid proteins in the endosome. The viral particle travels to the nucleus and enters through the nuclear pores or during mitosis when the nuclear envelope is dissolved (Day & Schelhaas, 2014; Graham, 2017). During mitosis the virions associate with the free chromosomes and thus get enclosed in the nuclear envelope (McBride, 2022). The viral capsid is disassembled and L2 and the viral genome attach to promyelocyctic leukemia (PML) bodies in the nucleus (Graham, 2017). Expression of viral genes at the PML bodies starts with E1 and E2, which initiate the first rounds of viral DNA replication. The resulting plasmids remain extrachromosomal and are passed on to daughter cells (McBride, 2022). In general, the viral copy numbers in the host cells remain low, which is supported by E2 transcriptionally repressing the promotor P97. This strategy is an important component of viral immune evasion. Apart from E1 and E2, E6 and E7 are also important in the early phase of viral replication: E6 is needed for episomal genome maintenance while E7 activates the cell cycle checkpoint promoting G_1 to S-phase progression.

Thus, keratinocytes do not terminally differentiate but keep on producing viral DNA (Graham, 2017). Due to their functions, E6 and E7 are considered oncoproteins in high-risk HPV types (Conway & Meyers, 2009). E7 binds members of the retinoblastoma (Rb) protein family (p105 (Rb), p107, p130) and can target them for proteasomal degradation (Moody & Laimins, 2010). The resulting freeing of the transcription factor E2F in turn activates cell-cycle promoting genes such as the cyclins A and E, which stimulates G_1 to S-phase transition. E7 also influences other transcription factors, leading to transcriptional changes in the host cell (Graham, 2017). Moreover, E7 has an effect on the tumor suppressor $p16^{INK4a}$. Epigenetically silenced in uninfected cells, this protein inhibits cyclin-dependent kinases (CDKs) 4 and 6 upon activation. The following accumulation of hypophosphorylated pRb leads to a cell cycle arrest. If a cell is infected with HPV, E7 induces an overexpression of $p16^{INK4a}$, which would normally lead to senescence of the cell. However, as E7 also degrades pRb, this is not the case and the cell is able to proliferate continuously. The overexpression of $p16^{INK4a}$ through E7 provides an excellent biomarker for high-risk HPV-associated lesions (Munger et al., 2013).

While sustained cell proliferation usually results in apoptosis through a p53-regulated pathway, the HPV E6 protein targets p53 for proteasomal degradation. E6 can also change p53's conformation. This either inhibits p53's transcriptional transactivation properties or sequesters the protein in the cytoplasm, preventing it from fulfilling its nuclear functions. Together with the degradation of pRb by E7, the degradation or inhibition of p53 promotes the uncontrolled proliferation of HPV-infected cells. Additionally, E6 activates the transcription of telomerase reverse transcriptase (TERT), which replicates telomeric DNA and is vital for immortalization (Moody & Laimins, 2010; Graham, 2017). In the late phase of viral replication, the proteins E1, E2, E4 and E5 are still expressed. E4 enhances the amplification of the viral genome by activating kinases and regulating cell cyle arrest, thereby counteracting the function of E7. The E5 protein controls cell division by influencing essential signaling pathways such as the epidermal growth factor receptor (EGFR) or mitogen activated protein kinase (MAPK) pathways. In the end of the infectious cycle, L2 and L1 are synthesized and afterwards imported to the nucleus, putting them into proximity of the newly amplified viral episomes (Graham, 2017). Subsequent to genome amplification and synthesis of capsid proteins, new virions are assembled in the nucleus. They are released from the cornified cell layer by the collapse of the cellular keratin networks, which is caused by E4 (Conway & Meyers, 2009). In uninfected

epithelia, the cells arrest their cell cycle when detaching from the basal layer (Conway & Meyers, 2009). The continuing differentiation leads to keratinization and finally, desquamation of the cells (Alberts et al., 2002; Sanclemente & Gill, 2002). When infected, HPV wanders within the cell to the cornified layer. Meanwhile its genome amplification occurs in mid-epithelial layers while virus assembly and release happens close or at the epithelial surface (Schiffman et al., 2016).

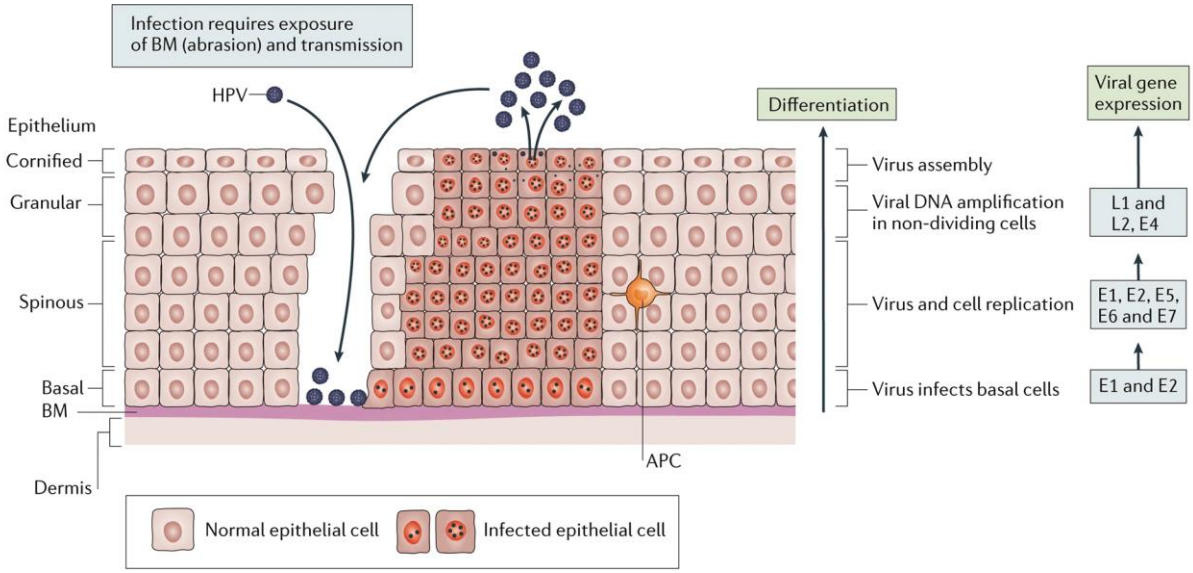

Figure 9. HPV infectious cycle and gene expression. HP virions infect the basal layer of an epithelium. During migration of the infected cells through the cell layers, the HPV genome is replicated and proteins synthesized, resulting in the assembly of new virions in the topmost layers of the epithelium with subsequent release of virions. BM = basal membrane. Adapted from Roden and Stern (2018).

The primary cause of cancer are HPV infections that persist over a period of time and are not cleared by the immune system (Graham, 2017). In high-grade lesions, HPV DNA is mostly integrated into the host genome at sites of genomic instability while the viral DNA persists episomally in earlier, precancerous lesions. Genomic integration may therefore contribute to malignant progression (Moody & Laimins, 2010). As mentioned above, the main proteins responsible for malignant transformation of infected cells are the proteins E6 and E7 of high-risk HPV types. Integration into the host cell genome commonly leads to disruption of E2 and thus to an unregulated expression of these oncoproteins and drives unchecked cell cycle progression (Moody & Laimins, 2010). Both proteins together are highly efficient in immortalizing keratinocytes even though E7 alone is sufficient (Halbert et al., 1991; Moody & Laimins, 2010). Although the oncoproteins are necessary for malignant progression, their expression is not the only factor, as most people with HPV infections do not develop cancer. It

was observed that mouse cells, artificially engineered to express E6 and E7, are not tumorigenic and additionally require an activated oncoprotein such as a member of the *RAS* gene family (Moody & Laimins, 2010). The accumulation of DNA damage throughout sustained cell proliferation and avoidance of apoptosis elicited by HPV leads over time to development of mucosal carcinomas (Moody & Laimins, 2010). Before cancer develops, the epithelium passes through different stages of squamous intraepithelial lesions (SIN). Depending on their location they are termed cervical (CIN), vaginal (VAIN), vulval (VIN), anal (AIN) or penile (PIN) intraepithelial neoplasia (Stanley, 2003). There are no such precursor lesions known for HNSCC (Johnson et al., 2020). Throughout the three SIN stages E6 and E7 activity increases and the genome of host cell changes. Over time, this leads to invasive cancer development.

To avoid clearance by the immune system, HPV has evolved different methods for immune evasion. One of those is that the virus does not induce inflammation, viremia or host cell death, which could alarm the immune system. Staying above the basement membrane also enables the virus to stay undetected from immune cells residing in lower tissues. When new virions are assembled they are shed from the surface of the outermost epithelial layer, preventing detection by the immune system (Steinbach & Riemer, 2017). There are also a number of changes in antigen processing induced by HPV, as well as in the immune cell function (reviewed in Steinbach and Riemer (2017)). Additionally, virions are cloaked by the L2 protein from detection and immunogenic capsid proteins are expressed only in the uppermost layers of the epithelium to evade recognition (Graham, 2017; McBride, 2022). More strategies are the dysregulation of host gene expression, protein functions or cytoplasmic trafficking (reviewed in Westrich et al. (2017)).

1.3.4 Anti-HPV strategies

1.3.4.1 Prophylactic vaccination

Infection with HPV and thus the increased chance to develop a mucosal cancer can be effectively prevented by prophylactic vaccination inducing HPV-specific antibodies. In 2006, the American Food and Drug Administration (FDA) approved the first prophylactic vaccine targeted at HPV. Gardasil® by Merck & Co. is inducing immunity against infection with HPV types 16, 18, 6 and 11. One year later, Cervarix® (GlaxoSmithKline) against HPV16 and 18 was first approved by the European Medicine Agency (EMA). The third vaccine, Gardasil9® (Merck & Co.) was approved by the FDA in 2014, protecting from HPV types HPV6, 11, 16,

18, 31, 33, 45, 53, and 58, having the potential to protect from 90 % of cervical cancers (Cheng et al., 2020). All of the approved vaccines are based on virus-like particles (VLPs) that consist of 360 copies of the L1 capsid protein, which self-assemble into an empty capsid-like structure without the help of L2 or other HPV proteins. The lack of viral DNA renders them non-infectious (Kirnbauer et al., 1992; Roden & Stern, 2018; Schiller & Lowy, 2018). These VLPs efficiently induce long-lived plasma cells in the vaccinated individual while also serving as danger signals to the humoral immune system (Schiller & Lowy, 2018). As HPVs are not internalized by keratinocytes for several hours, the antibodies have enough time to exude at the site of epithelial abrasion, bind L1 and dispose of the threat (Schiller & Lowy, 2012; VanBenschoten & Woodrow, 2021). However, the protection provided is mostly HPV type-specific with only some cross-protectional properties. The available, multivalent vaccines are able to induce much higher antibody titers than a natural infection with HPV does (Roden & Stern, 2018). Furthermore, the titers for the bivalent, quadrivalent and nonavalent vaccine after three doses remain stable for at least 10, 9.9 and 5 years, respectively (World Health Organization, 2017). However, the year of approval for the respective vaccine has to be taken into account and there are no longer-term data available so far. It has been shown in different studies for different countries that prophylactic HPV vaccination substantially reduced risk of cervical cancer development in 10 - 30 year old females (Lei et al., 2020; Falcaro et al., 2021; Kjaer et al., 2021). Additionally, HPV vaccines have induced a decline in occurrence of genital warts in vaccinated females as well as in unvaccinated males since their introduction (Brotherton, 2019). Moreover, the likelihood of developing oropharyngeal malignancies is lower in vaccinated than unvaccinated individuals (Lechner et al., 2022). Even though the VLP HPV vaccines induce strong antibody and robust L1-specific $CD8^+$ T cell responses, they do not work in already infected individuals. This is due to L1 only being expressed in the outer epithelial cell layers and thereby hiding the HPV-infected basal cells from the vaccination-induced immune response (Roden & Stern, 2018). Hence, HPV vaccination is recommended for girls and boys from 9 – 14 years, preferably before sexual debut, excluding the possibility of a previous HPV infection (World Health Organization, 2017; Rieck et al., 2021). While the vaccines are highly effective in prevention of HPV infection, worldwide coverage remains low. In total, 107 of the 194 world health organization (WHO) member states had introduced HPV vaccination in 2020, most of them in the Americas and Europe. Thirty-three of the countries had introduced gender-neutral vaccination programs by 2019. About 15 % of girls and 4 % of

boys worldwide were fully vaccinated against HPV in 2019, with highest coverages in Australia (77 %), Latin America (61 %) and North America, as well as Europe (35 %). The vaccination coverage in low-income countries lies at 23% (Bruni et al., 2021). In Germany only 47.2 % of 18 year old female and 2.5% of male adolescents were completely vaccinated in 2019 (Rieck et al., 2021). It is to expect that the COVID-19 pandemic has further impeded HPV vaccination efforts around the globe (Toh et al., 2021). Therefore, therapeutic options need to be as efficacious as possible.

1.3.4.2 Conventional therapies

If an HPV infection is not prevented by vaccination, screening for cervical cell alterations is paramount. Vaccinated or not, it is recommended for women to get regular Papanicolaou (Pap) tests where a cervical smear is taken and stained to detect cellular abnormalities (Papanicolaou & Traut, 1941; Szymonowicz & Chen, 2020). HPV-induced cellular changes at other locations are not as closely monitored but it is possible to take anal Pap smears or test the oral cavity for overexpression of $p16^{INK4A}$ (Szymonowicz & Chen, 2020). If HPV infections progress to precancerous lesions they can be removed by loop electrosurgical excision procedure (LEEP), laser therapy, cryotherapy or cold knife conization. Genital warts, as well as anal or penile lesions can be treated by topical application of imiquimod, for example (Roberts et al., 2017; Szymonowicz & Chen, 2020; Issa et al., 2021). HNSCCs are not preceded by known precancerous lesions and can only be treated by surgery, chemotherapy, targeted therapy and/or radiotherapy, with HPV^+ HNSCC being much more susceptible to irradiation than HPV^- ones (Gottgens et al., 2019; Szymonowicz & Chen, 2020). Untreated cervical lesions can eventually progress to cervical cancer if they do not regress spontaneously (Schiffman et al., 2016; Hu & Ma, 2018). This is treated by surgical removal of the tumor and surrounding tissue or radical hysterectomy, pelvic radiotherapy, brachytherapy (radiation source in uterus and vagina), chemotherapy or combination therapies (Cohen et al., 2019). Drawbacks to all these methods are radiation-induced damages to surrounding tissues such as bladder, bowel or rectum, as well as fertility problems arising from cervical or uterine surgery. Treatments can also negatively affect sexual functions. Additionally, elaborate and expensive treatment solutions are hard to implement in low-income countries, which have high incidences of cervical cancers (Cohen et al., 2019; Rafael et al., 2022). Therefore, other treatment options ought to be examined. In recent years, immunotherapy has gained importance concerning HPV-associated diseases.

1.3.4.3 Immunotherapeutic approaches

The concept of cancer immunotherapy is to employ the body's own immune system as a tool to treat cancer. The idea has existed for more than a century when Wilhelm Busch, Friedrich Fehleisen and William Coley found out that tumors can regress if patients develop the skin rash erysipelas. In 2018, cancer immunotherapy was recognized in form of a Nobel prize for James P. Allison and Tasuku Honjo (Waldman et al., 2020). HPV-associated malignancies are prime targets for immunotherapy as they have to constantly express viral proteins for their maintenance. The oncoproteins can be utilized as targets for immunotherapeutic approaches. They are most suitable as the viral proteins are on one hand expressed only by tumor cells and on the other hand are neoantigens. Hence, they are exempt from central tolerance and can be targeted by immune cells (Lee et al., 2016; Chabeda et al., 2018). The main goal of HPV immunotherapy is the induction of HPV-specific cytotoxic $CD8^+$ T cells to promote the anti-tumor response (Gulley, 2013; Frazer & Chandra, 2019).

One method of immunotherapy is the so-called immune checkpoint blockade. The most famous immune checkpoint receptors are programmed cell death protein 1 (PD-1) and cytotoxic T-lymphocyte-associated protein 4 (CTLA-4). They are expressed on T cells and serve as negative regulators of the T cell response when they are bound by their ligands, PD-L1 and CD80/CD86, respectively. This can be inhibited by usage of specific antibodies that prevent the receptors from binding their ligands (Postow et al., 2015). This checkpoint blockade does not work in an antigen-specific way but rather influences the specific T cell response (Pardoll, 2012). Nowadays, at least five commercially available monoclonal antibodies for checkpoint blockade are licensed for HPV^+ oropharyngeal cancers (Frazer & Chandra, 2019). Checkpoint blockade antibodies were and currently are in clinical studies for cervical cancer. So far, PD-1 blockade has been successful, leading to FDA approval of at least one antibody for treatment of $PD\text{-}L1^+$ cervical cancer (Duranti et al., 2021). Monotherapy with CTLA-4 blockade has not been successful in first clinical trials for cervical cancer but results from combination therapies with other checkpoint blockade antibodies are encouraging (Lheureux et al., 2018; Duranti et al., 2021).

In contrast to immune checkpoint blockade, there are also antigen-specific immunotherapeutic approaches of either passive administration of effectors or active immunizations. One of those methods is T cell receptor therapy where patients receive T cells genetically engineered to carry

a tumor antigen-specific chimeric antigen receptor (CAR) or TCR. Jin et al. introduced a TCR specific for the HPV16 HLA-A2:01 epitope YMLDLQPET ($E7_{11-19}$) that is presented on cervical cancers (Riemer et al., 2010; Jin et al., 2018). These T cells were able to kill cervical and oropharyngeal cancer cell lines *in vitro*, as well as established tumors in a mouse model (Jin et al., 2018). Application of the T cell therapy in a clinical trial led to regression of tumors in half of the enrolled patients (Nagarsheth et al., 2021). In another cell-based study, tumor-infiltrating lymphocytes from HPV^+ tumors were injected into HPV cancer patients, which resulted in tumor responses in a small number of probands (Stevanović et al., 2019).

Many studies have examined the potential of therapeutic vaccinations against HPV-associated malignancies with the goal of inducing a $CD8^+$ T cell response against HPV-derived epitopes. So far, no therapeutic vaccine against HPV has been approved for human use (Chabeda et al., 2018; Messa & Loregian, 2022). Therapeutic vaccination strategies to induce HPV-specific T cell responses that are currently under investigation include vaccinations with vectors such as bacteria or viruses, protein and peptide-based vaccines as well as nucleic acid vaccinations (Chabeda et al., 2018). Vector vaccinations are either bacteria or viruses that have been rendered harmless to harness their capability of stimulating the immune system and promoting presentation of antigen to the host immune system. There have been several clinical trials involving bacteria such as *Lactobacilli* or *Listeria* expressing HPV16 that had only limited success in CIN and cervical cancer treatment, respectively (Maciag et al., 2009; Kawana et al., 2014). Viral vector vaccinations tested so far in clinical trials have for example been with modified vaccinia virus Ankara (MVA) expressing the HPV proteins E6 and E7, which led to reduction of intraepithelial lesions (Baldwin et al., 2003; Rosales et al., 2014). However, the problems arising with vector vaccines are first the anti-vector immune response that can superimpose the HPV-specific response and second, the possible previous immunity of a patient to the used vector (Chabeda et al., 2018). As E6 and E7 are popular targets for immunotherapeutic approaches, there have been many tests of protein or peptide-based vaccinations. Proteins and peptides by themselves are not very immunogenic and therefore require the addition of adjuvants stimulating the innate immune response. Short peptide vaccines are MHC-restricted while long peptides or whole protein formulations already incorporate epitopes for different MHCs. However, the presenting cells must have the chance to process the proteins or long peptides (Chabeda et al., 2018). Although synthetic long peptide

(SLP) vaccinations can achieve the regression of intraepithelial lesions, they fail to promote control of cervical cancers so far (Kenter et al., 2009; van Poelgeest et al., 2013). Examples for short peptide-based vaccinations are PDS0101, containing six HPV16 peptides, or DPX-E7, containing the HPV16 epitope $E7_{11-19}$. PDS0101 was able to induce regression of CIN lesions in clinical trials (Karkada et al., 2013; Smalley Rumfield, Pellom, et al., 2020; Smalley Rumfield, Roller, et al., 2020). TA-CIN, an HPV16 L2, E7, E6 fusion protein vaccine was proven to be well tolerated and induced regression of intraepithelial lesions in some patients. It is currently tested as a cervical cancer vaccine in clinical trials (de Jong et al., 2002; Davidson et al., 2004; Chabeda et al., 2018). Preclinical data also indicate a benefit of using TA-CIN in combination with PD-1 blockade (Peng et al., 2021). Nucleic acid vaccinations with DNA and RNA have a high safety profile, are easy to produce and do not induce any anti-vector immune responses (Chabeda et al., 2018). One of the most promising ones is the DNA vaccine VGX-3100 based on E6 and E7 from both HPV16 and HPV18 that managed to induce regression of CIN stages 2/3 with a treatment effect of up to 1.5 years (Bagarazzi et al., 2012; Trimble et al., 2015; Bhuyan et al., 2021). VGX-3100 also showed encouraging results in first clinical trials with cervical cancer after chemoradiation, and HNSCC patients (Hasan et al., 2018; Aggarwal et al., 2019). RNA vaccines have been so far successful in preclinical testing against HPV^+ cancers but can be expected to become a bigger focus of therapeutic vaccine research due to the success of mRNA vaccinations in the COVID-19 pandemic (Grunwitz et al., 2019; Miao et al., 2021; Salomon et al., 2021). Additional to these exemplary clinical trials there has been a plethora of preclinical studies of therapeutic HPV vaccines. Some of these induced promising results in mouse models. However, these successes have not translated well into the clinics, which might be due to the fact that even though some vaccines induced high levels of HPV-specific T cells in the blood of patients, these cells do not readily migrate into the mucosa where the tumors are located (Shin & Iwasaki, 2013). Therefore, it is necessary to either influence the migration of T cells by induction of an inflammation at the tumor site or directly vaccinate there with the goal of establishing T_{RM} (Figure 10)(Nizard et al., 2016).

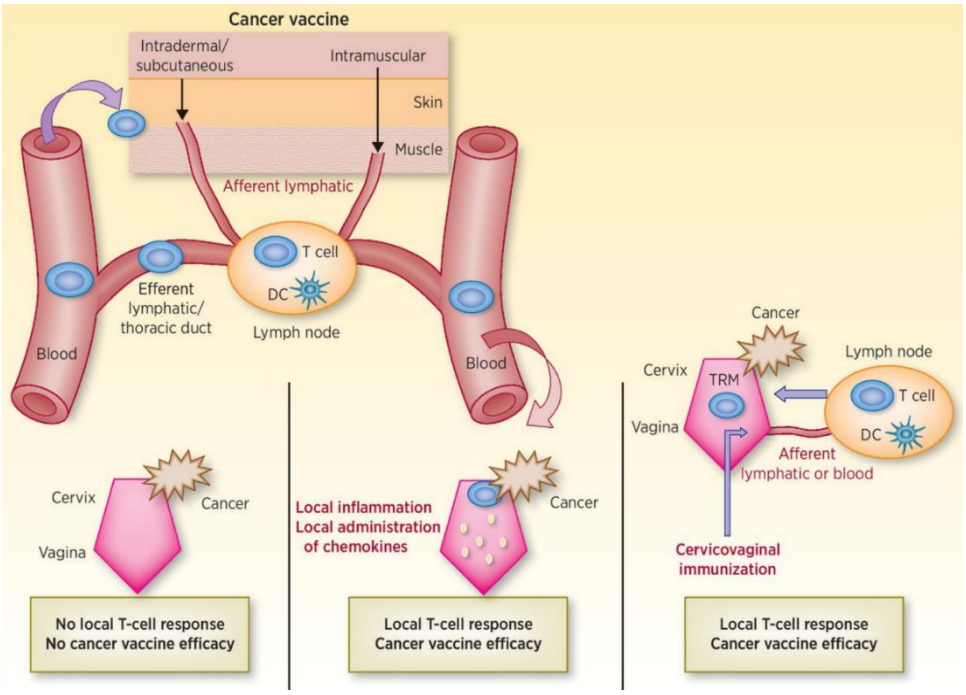

Figure 10. Enhancing the efficacy of a therapeutic vaccine against HPV-induced cancers. Systemically induced HPV-specific T cells do not migrate into the mucosa where the tumor is located. They are in need of an inflammatory stimulus to cross into the tumor site. A durable T_{RM} response can also be induced by direct vaccination at the mucosal site. Figure adapted from (Nizard et al., 2016).

1.4 Model systems

1.4.1 Mouse and tumor models in HPV research

Newly developed therapeutic approaches to HPV-associated diseases need to be tested in *in vivo* models prior to clinical trials to assess efficacy as well as safety. Unfortunately, productive papillomavirus infections are species-restrictive, which means that the common experimental animal in biomedical research, the laboratory mouse (*mus musculus)*, cannot be infected with human papillomavirus (Christensen et al., 2017; Hickman et al., 2017). A variety of species such as cattle, dogs or rabbits are used in papillomavirus research by infecting the animals with their species-specific papillomavirus strain (Christensen et al., 2017). The murine papillomavirus MmuPV1 was discovered in 2011 and may provide a model for human β and γ papillomavirus infections, as well as the mouse models *Mastomys natalensis* or *M. coucha* infected with MnPV (Doorbar, 2016). When studies employ common laboratory mice the animals either receive transplanted HPV^+ tumors or are genetically modified to express HPV proteins or to develop a tumor. Genetic modifications include engineering of mice that express the HPV proteins E5, E6 and E7 under the control of the cytokeratin 14 promoter and thereby

expressing the proteins only in basal keratinocytes. However, the translatability of these models is limited as there are no L proteins expressed and the genes are under the control of a host cell promoter (Santos et al., 2017). Furthermore, the immune system develops a tolerance for the HPV proteins in the mice as the proteins are expressed during the immune system's development (Trimble & Frazer, 2009). Other genetically altered mouse strains express oncogenes in their ocular lenses for the examination of the biological activity of E6 and E7 in epithelial cells (Griep et al., 1993; Santos et al., 2017). For studying the development of cervical lesions into cancer, mice with conditional expression of E6, E7 and mutant K-RAS in the vaginal mucosa were created (Böttinger et al., 2020). Another possibility of inducing tumor growth in the cervicovaginal tract is electroporation of mucosal cells of C57BL/6 mice with HPV16 E6/E7-Luciferase, AKT, c-Myc and sleeping beauty transposase, which results in formation of intraepithelial lesions that progress to cancer (Henkle et al., 2021). Transplantable tumor models include the cell line AT-84 E7 in C3H mice that serves as a model for oral squamous cell carcinomas and expresses HPV16 E7, as well as its luciferase-expressing descendant cell line AT-84 E7-Luc (Paolini et al., 2014). Numerous transplantable HPV tumor models have also been generated for use in C57BL/6 mice. The cell line mEERL95 for example serves as a model for HNSCC and was generated by transformation of tonsillar epithelial cells with HPV16 E6, E7 and oncogenic HRAS that were passaged *in vivo* (Hoover et al., 2007; Mermod et al., 2018). In another cell line, EL4 thymoma cells were transfected with HPV16 E7 and the resulting EL4-E7/C2 cells were used for s.c. tumor injection to examine vaccination successes (Tindle et al., 1995; Fernando et al., 1998). The C3 cell line was generated from C57BL/6 embryonic cells by transfection with the complete HPV16 genome including the L proteins, as well as activated RAS to receive a transformed phenotype (Feltkamp et al., 1993). Later the cells were also transfected with luciferase to induce bioluminescence (Li et al., 2016). In contrast to most other murine HPV protein-expressing cell lines the U14/LV-HPV18 E6E7 and U14/LV-HPV58 E6E7 cell lines are derived from an induced mouse cervical cancer (Yuan et al., 1995). These cells were transfected with the proteins indicated in their names (Wan et al., 2022). By far the most used cell line to study HPV16 therapeutic vaccinations are however TC-1 cells. They were generated in 1996 by transducing C57BL/6 lung cells with HPV16 E6 and E7, as well as activated HRAS (Lin et al., 1996). They have been used as a transplantable s.c. tumor model for a multitude of preclinical vaccination studies such as with bacterial vectors

(Gunn et al., 2001), viral vectors (Ji et al., 1998), SLP (Decrausaz et al., 2010), peptides (Barrios & Celis, 2012), DNA (Soong et al., 2014) or mRNA (Grunwitz et al., 2019).

As described in 1.2.1.4, mucosal tissues where HPV tumors are located in patients are difficult to access for $CD8^+$ T cells. However, the TC-1 cells are mostly used as an s.c. tumor model, which does not accurately model the environment found in patients. Therefore Decrausaz et al. set out to develop an orthotopic version of TC-1, i.e. the tumors are located at the anatomical correct location, in the case of cervical cancer in the cervicovaginal mucosa of mice. To make these cells visible in the vaginal cavity the cells were transduced with firefly luciferase for detection via bioluminescent imaging later on (Decrausaz, Goncalves, et al., 2011). This orthotopic tumor model has since been used to examine vaccinations with peptides (Decrausaz, Domingos-Pereira, et al., 2011), DNA (Sun et al., 2015), mRNA (Bialkowski et al., 2016) or peptides in nanofibers (Li et al., 2020). The tested vaccination approaches were not only used to induce systemic immunity to HPV but also for ivag. (Decrausaz, Domingos-Pereira, et al., 2011; Domingos-Pereira et al., 2013) or i.n. (Decrausaz, Domingos-Pereira, et al., 2011; Sierra et al., 2020) vaccination. Interestingly, an intralymphatic vaccine managed to protect better from s.c. tumors than from genital ones, which underlines why the orthotopic model is needed for more accurate assessment of vaccination successes (Bialkowski et al., 2016).

A big drawback of TC-1 and TC-1-luc cells is the usage of C57BL/6 mice, which present the $H\text{-}2D^b$ restricted HPV16 $E7_{49\text{-}57}$ epitope RAHYNIVTF (Feltkamp et al., 1993). This highly immunodominant epitope induces high frequencies of specific $CD8^+$ T cells leading to tumor control. However, HLA-restricted epitopes, which cannot be examined in wild-type mouse models, might be much less immunogenic, resulting in worse vaccination results in human studies than found in murine tests (Kruse, 2019). Therefore, an MHC-humanized mouse model might be beneficial to improve translatability to the clinics.

1.4.2 A2.DR1 mice

The MHC-humanized A2.DR1 mice used for this work were generated on a C57BL/6 background, lack all C57BL/6 (murine) MHC molecules on their cells and instead express HLA-DR1 on their pAPCs and a chimeric, HLA-A2:01 epitope-presenting HHD molecule as MHC I (Figure 11).

C57BL/6 mice, on which A2.DR1 are based, express the MHC molecules H-2D^b, H-2K^b and the MHC II molecule IA^b. Additionally, they also produce a non-functional IEβ^b chain, as H-2IEα is a pseudogene (affymetrix eBioscience; Pajot et al., 2004). Mice expressing the HHD molecule with β$_2$m and H-2D^b being knocked-out were generated by Pascolo et al. (1997).

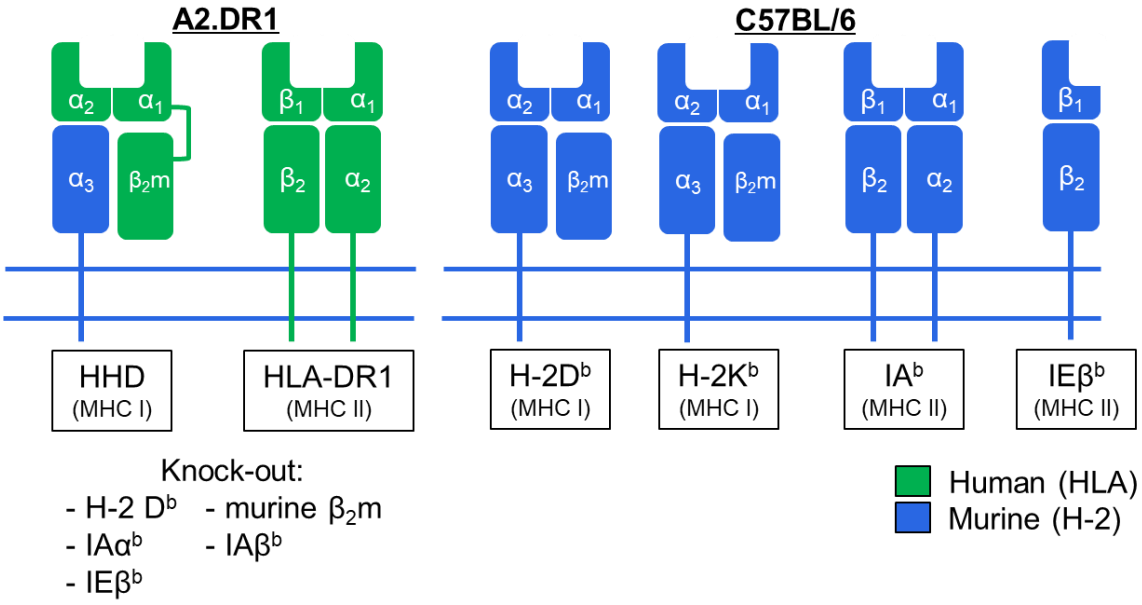

Figure 11. MHC composition of A2.DR1 mice compared to C57BL/6 mice. The expression of all C57BL/6 murine MHC molecules was knocked out and the HHD and HLA-DR1 genes were introduced into the genome of A2.DR1 mice. HHD consists of the human α_1 and α_2 domains of HLA-A2:01, forming the peptide-binding groove, covalently linked to human β_2m and anchored in the cell membrane by the murine H-2D^b α_3-domain.

The HHD molecule consists of the α_1 and α_2 domains of human HLA-A2:01, linked covalently to human β_2m through a 15 amino acid-long peptide linker to the NH_2 terminus of the heavy chain. The α_3 domain is from murine H-2D^b and anchors the molecule in the cell membrane of nucleated cells as well as improves the interaction with the murine CD8$^+$ T cells that bind through their co-receptor. C57BL/6 mice having received the construct were crossed with previously produced H-2D$^{b\,-/-}$ β_2m$^{-/-}$ mice, resulting in mice expressing HHD but not H-2D^b or β_2m (Koller & Smithies, 1989; Koller et al., 1990; Pascolo et al., 1997). The HHD$^{+/+}$ H-2D$^{b\,-/-}$ β_2m$^{-/-}$ mice were then crossed with HLA-DR1-transgenic, H-2 class II-knock-out (KO) mice. These were previously generated by crossing HLA-DR1 transgenic mice (HLA-DRA1*0101 and HLA-DRB1*0101) with H-2IA^b KO mice (Cosgrove et al., 1991; Altmann et al., 1995; Pajot et al., 2004). The resulting mice expressed HHD and HLA-DR1 and were knocked-out for H-2D^b, murine β_2m (preventing H-2K^b expression) as well as IA^b. However, reports indicate

the formation of HLA-DRα/H-2IEβ^{b} hybrid complexes in HLA-transgenic mice (Lawrance et al., 1989). Therefore, the strain was further crossed with mice lacking all MHC class II genes to prevent this (Madsen et al., 1999; Pajot et al., 2004). The final mouse strain was then called A2.DR1 and was used in this work. Cells of these mice present HLA-A2:01 and HLA-DR1-restricted epitopes to their immune system. HLA-A2:01 can be found expressed in about 50 % of European individuals while DR1 is present in about 20 % of Europeans (Gonzalez-Galarza et al., 2020). Hence, the A2.DR1 mouse model's MHC configuration covers a large proportion of the European population. Another mouse line, which is also called A2.DR1, exists but these animals lack the IEβ^{b} KO (Kruse, 2019) and were not used in this thesis. Only their derivative cell line 2277-NS, which was the basis for development of PAP-A2 cells, was utilized.

1.4.2.1 Existing HPV tumor models in MHC-humanized mice

Several MHC-humanized HPV mouse tumor models exist. One of those are TC-1/A2 cells which are based on TC-1 cells but also express the AAD molecule. This chimeric MHC molecule is similar to HHD but contains murine β_2m instead of human β_2m (Newberg et al., 1996; Peng et al., 2006). TC-1/A2 cells have been used to examine a DNA vaccine, which resulted in a strong immune response against the immunodominant H-2D^{b} E7$_{49-56}$ epitope. When the sequence of the epitope was mutated in the vaccine, an HLA-A2-restricted immune response against E7$_{11-20}$ emerged (Peng et al., 2006). This result highlights the importance of using fully MHC-humanized animals for HPV vaccination studies. It was also shown that AAD-expressing mice transfected with E6(R55K)(delK75)/E7(R53S) (removing the immunodominant epitope) and NRAS^{G12V} develop sarcomas. This means that mutated E6 and E7 can also immortalize cells. These mice developing sarcomas were used as a model for head-and-neck cancers (Peng et al., 2022).

The only A2.DR1 HPV tumor model so far is the transplantable PAP-A2 cell line (Kruse et al., 2018). This cell line is based on the 3-methylcholandrene (MCA)-induced A2.DR1 sarcoma cell line 2277-NS (Quandt, 2014). 2277-NS cells were transduced with a lentiviral construct containing 3x flag (E6) and 2x strep (E7)-tagged versions of the full-length HPV16 E6 and E7. The cells were shown to be killed by CD8^{+} T cells specific for E7$_{7-15}$, E7$_{11-19}$, E7$_{82-90}$ as well as E6$_{25-33}$ (Kruse et al., 2018). Importantly, this cell line is tumorigenic in itself because of its sarcoma origin. Therefore, it can be assumed that the loss of E6 and E7 does not lead to senescence of the cells but rather has little to no impact. Anti-tumor vaccination approaches

may thus fail due to missing antigen expression on the target cells instead of weak immunogenicity of the vaccine. Hence, the development of a truly HPV-dependent, MHC-humanized tumor cell line is desirable.

2 Aims

The overall aim of this thesis was to develop an HPV16-dependent A2.DR1-derived tumor cell line and an orthotopic tumor model to eventually examine the success of methods to direct HPV16-specific $CD8^+$ T cells towards the mucosally located tumors.

2.1 Generation of an HPV16-dependent tumor cell line for A2.DR1 mice

Previous HPV16 tumor cell lines have been mostly immunologically murine or did not depend on the HPV oncoproteins for sustained proliferation. The independence of E6 and E7 can result in unnoticed loss of the vaccination targets and might limit the informative value of vaccination studies. In this study, I set out to generate a truly HPV16 E6 and E7-dependent tumor cell line for use as an orthotopic tumor model in HPV16 vaccination studies involving A2.DR1 mice. The two chosen paths to pursue were the further development of the PAP-A2 cell line as well as the establishment of the aforementioned HPV16 E6 and E7-dependent tumor cell line.

2.2 Orthotopic tumor model

Subcutaneous tumor models are often used in preclinical validation of HPV16 vaccination strategies. Often the results are very promising with many tumors regressing. However, when the treatments are tested in the clinic, many fail to induce such a meaningful effect as seen in mice. One major reason for limited translatability is that HPV16 tumors are located in the mucosa of patients instead of their subcutis. This elicits the obvious need for an orthotopic tumor model, which more closely mirrors the environment found in human tumors. Therefore, my goal was to establish a robust method for induction of tumor formation in the vaginal mucosa of A2.DR1 mice.

2.3 Vaccination and T cell trafficking

Systemically circulating T cells do not readily enter the mucosal tissue. When vaccinating against HPV16-induced lesions and tumors a strong $CD8^+$ T cell response at the tumor site is a requirement for treatment success. Therefore, I aimed to examine different ways to induce HPV16-specific T cells in the vaginal mucosa of A2.DR1 mice as well as to study how to manipulate the trafficking of vaccination-induced specific T cells towards the mucosa.

3 Materials and Methods

3.1 Materials

3.1.1 Antibodies

3.1.1.1 Flow cytometry

Antigen	Fluophore	Clone	Catalog No.	Company
CD3ε	APC-Vio®770	REA606	130-117-676	Miltenyi Biotec, Bergisch Gladbach, Germany
CD4	PerCP-Vio®700	REA604	130-118-794	Miltenyi Biotec, Bergisch Gladbach, Germany
CD4	FITC	RM4-5	553047	BD, Franklin Lakes, NJ, USA
CD8a	PE	REA601	130-109-247 /130-123-781	Miltenyi Biotec, Bergisch Gladbach, Germany
CD19	PE/Cyanine5.5®	6D5	ab25548	abcam, Cambridge, UK
CD44	BV711™	IM7	103057	Biolegend, San Diego, CA, USA
CD62L	PE/Cyanine5	MEL-14	104410	Biolegend, San Diego, CA, USA
CD69	PerCP/Cyanine5.5	H1.2F3	104522	Biolegend, San Diego, CA, USA
CD69	FITC	REA937	130-115-459	Miltenyi Biotec, Bergisch Gladbach, Germany
CD103	VioBlue®	REA789	130-111-845	Miltenyi Biotec, Bergisch Gladbach, Germany
HLA-A2	FITC	BB7.2	551285	BD, Franklin Lakes, NJ, USA
IFNγ	APC	XMG1.2	554413	BD, Franklin Lakes, NJ, USA
IgG2b, κ	FITC	MG2b-57	401206	Biolegend, San Diego, CA, USA
TNFα	PE/Cyanine7	MP6-XT22	506324	Biolegend, San Diego, CA, USA
TNFα	eFluor450	MP6-XT22	48-7321-82	Invitrogen, Waltham, MA, USA

3.1.1.2 Western blot

Antigen	Clone	Catalog No.	Dilution	Raised in	Company
CDKN2A/p16^{INK4a}	EPR20418	ab211542	1:1,500	Rabbit	abcam, Cambridge, UK
E6 (HPV16)	E6-6F4	E6-6F4	1:1,000	Mouse	Euromedex, Souffelweyersheim, France
E7 (HPV16)	NM2	-	1:1,000	Mouse	kindly given by Prof. Dr. Martin Müller, DKFZ
IgG anti-Mouse IgG (H+L)-HRPO	polyclonal	115-035-003	1:10,000	Goat	Dianova, Hamburg, Germany
IgG anti-rabbit IgG (H&L)-HRPO	polyclonal	611-1302	1:5,000	Goat	Rockland Immunochemicals, Limerick, PA, USA
Ras (G12V Mutant Specific)	D2H12	14412	1:500	Rabbit	Cell Signaling Technologies, Danvers, MA, USA

Antigen	Clone	Catalog No.	Dilution	Raised in	Company
α-tubulin	B-5-1-2	T5168	1:5,000	Mouse	Sigma-Aldrich, St. Louis, MO, USA
β-actin	AC-74	A2228	1:50,000	Mouse	Sigma-Aldrich, St. Louis, MO, USA

3.1.2 Buffers & solutions

Buffer	Ingredients
Ammonium chloride potassium (ACK) lysis buffer	150 mM NH_4Cl 10 mM $KHCO_3$ 0.1 mM Na_2EDTA
Blocking buffer	5 % (w/v) non-fat milk powder 1 % (w/v) BSA in 0.2 % PBST
Coomassie brilliant blue staining solution	25 ml CH_3COOH 125 ml methanol 100 ml H_2O 0.25 g Coomassie Brilliant blue G
Staining buffer for flow cytometry	1x PBS 0.1 % (w/v) BSA 0.1 % (v/v) NaN_3
Fixation buffer for flow cytometry	1x PBS 1 % (v/v) FCS 2.5 % (v/v) formaldehyde
Giemsa stock solution	1 g Giemsa powder 66 ml glycerol 66 ml methanol
MACS buffer	1x PBS 0.5 % (w/v) BSA 2 mM EDTA
10x PBS	1.37 M NaCl 27 mM KCl 100 mM $Na_2HPO_4 \cdot 2H_2O$ 20 mM KH_2PO_4 pH 7.3
PBS Tween (PBST) buffer	1x PBS 0.2 % (v/v) Tween20

Buffer	Ingredients
Protein lysis buffer (complete)	10 mM tris-HCl pH 7.5 50 mM KCl 2 mM $MgCl_2$ 1 % (v/v) Triton® X-100 1 mM DTT 1 mM PMSF 2x protease inhibitor cocktail (1 tablet in 750 µl ddH_2O)
10x SDS-PAGE electrophoresis buffer	30.3 g tris 144 g glycine 10 g SDS in 1 l ddH_2O pH 8.3
50x TAE	484 g tris 41 g $C_2H_3NaO_2$ 37 g EDTA in 2 l ddH_2O pH 7.8
Transfer buffer	25 mM tris 192 mM glycine in 1 l ddH_2O 20 % methanol pH 8.3
Washing buffer	ddH_2O 10 % (v/v) 10x BD Perm/Wash™ Buffer

3.1.3 Cell lines

Cell line	Description	Medium	Source
2277-NS	MCA-induced A2.DR1 sarcoma cell line.	2277-NS medium	Quandt (2014)
CaSki	Cell line derived from an epidermoid carcinoma of the cervix from a 40-year-old female previously undergone irradiation and surgical treatment.	CaSki medium	Pattillo et al. (1977)
$E6^+E7^+$ lung cells	A2.DR1 lung cells expressing HPV16 E6 and E7.	$E6^+E7^+$ lung cell medium	generated by Dr. Sebastian Kruse and Dr. Ruwen Yang, DKFZ
E6/7H-luc; E6/7-lucA2	A2.DR1 $E6^+E7^+$ lung cells additionally expressing $HRAS^{G12V}$, firefly luciferase and blasticidin resistance.	E6/7-lucA2 medium	self-generated
HeLa-CaG-luc	Firefly luciferase expressing HeLa cells (cervical cancer cells taken from a woman in 1951 (Masters, 2002)).	HeLa medium	kindly given by Dr. Matthias Bozza. DKFZ

PAP-A2	A2.DR1 sarcoma cell line 2277-NS expressing HPV16 E6 and E7 as well as puromycin resistance.	PAP-A2 medium	Kruse et al. (2018)
PAP-A2-luc	A2.DR1 PAP-A2 cells additionally expressing firefly luciferase and blasticidin resistance.	PAP-A2 -luc medium	self-generated
TC-1/A2-luc	C57BL/6 lung cells expressing HPV16 E6 and E7, $HRAS^{G12V}$ and AAD as well as luciferase.	TC-1 medium	TC-1/A2 from Peng et al. (2006), transduced with luciferase by Dr. Rainer Will, DKFZ

3.1.4 Chemicals

Name	Formula	Catalog No.	Company
6x DNA Loading Dye		R0611	Thermo Fisher Scientific, Waltham, MA, USA
Agarose		A8963	AppliChem GmbH, Darmstadt, Germany
Ammonium chloride	NH_4Cl	P726.1	Roth, Karlsruhe, Germany
Bovine serum albumin (BSA)		A9418	Sigma-Aldrich, St. Louis, MO, USA
Dimethyl sulfoxide (DMSO)		D8418	Sigma-Aldrich, St. Louis, MO, USA
Distilled water DNase/RNase free		821932	MP Biomedicals, Illkirch, France
Dithiothreitol (DTT)		43819	Sigma-Aldrich, St. Louis, MO, USA
Double-distilled water (ddH_2O)			
Ethanol (absolute)			Sigma-Aldrich, St. Louis, MO, USA
Ethylenediaminetetraacetic acid (EDTA)		E6758	Sigma-Aldrich, St. Louis, MO, USA
Formaldehyde			PanReac AppliChem, Darmstadt, Germany
GelRed® Nucleic Acid Gel Stain in water		41003	Biotium, Fremont, CA, USA
Giemsa stain		G5637	Sigma-Aldrich, St. Louis, MO, USA
Glycerol		15523	Sigma-Aldrich, St. Louis, MO, USA
Hydrogen chloride	HCl	30024.29	VWR International, Fontenay-sous-Bois, France
Isoflurane CP®		1214	Cp-pharma, Burgdorf, Germany
Isopropanol	C_3H_8O	33539	Sigma-Aldrich, St. Louis, MO, USA
Methanol	CH_3OH	32213	Sigma-Aldrich, St. Louis, MO, USA
Nonoxynol-9 (N-9)		ab143672	abcam, Cambridge, UK

Name	Formula	Catalog No.	Company
Potassium bicarbonate	$KHCO_3$	X887.1	Roth, Karlsruhe, Germany
Potassium chloride	KCl	6781.1	Roth, Karlsruhe, Germany
Potassium dihydrogen phosphate	KH_2PO_4	3904.1	Roth, Karlsruhe, Germany
ROTI® Histofix 4 %		P087.1	Roth, Karlsruhe, Germany
Sodium acetate	$C_2H_3NaO_2$	6773.2	Roth, Karlsruhe, Germany
Sodium azide	NaN_3	A1430,0100	AppliChem, Darmstadt, Germany
Sodium chloride	NaCl	10428420	Thermo Fisher Scientific, Waltham, MA, USA
Sodium hydroxide	NaOH	P031.2	Roth, Karlsruhe, Germany
Sodium phosphate dibasic dihydrate	$Na_2HPO_4 \cdot 2H_2O$	12694947	Acros organics, Thermo Fisher Scientific, Geel, Belgium
Tris(hydroxymethyl)aminomethane (tris)		167620010	Acros organics, Thermo Fisher Scientific, Geel, Belgium
Triton® X-100		142314.1611	AppliChem, Darmstadt, Germany
Trypan blue stain (0.4 %)		T10282	Thermo Fisher Scientific, Waltham, MA, USA
Trypsin/EDTA (0.04 %/0.03 %)		C-41000	PromoCell, Heidelberg, Germany
Tween20 (polysorbate 20)		Tween201	MP Biomedicals, Illkirch, France

3.1.5 Consumables

Name	Company
Aluminium foil	CeDo GmbH, Mönchengladbach, Germany
Cell culture flask (25 cm^2, 75 cm^2, 125 cm^2)	TPP, Trasadingen, Switzerland
Cell culture dish (100 mm x 20 mm)	TPP, Trasadingen, Switzerland
Cell culture plate (12-, 24-, 48-well)	Corning, Corning, NY, USA
Cell culture plate (96-well), flat-bottom	BD, Franklin Lakes, NJ, USA
Cell culture plate (96-well), U-bottom	TPP, Trasadingen, Switzerland
Cell culture plate (96-well), V-bottom	Greiner Bio-One, Frickenhausen, Germany
Cell culture plate 'CytoOne' (6-well)	Starlab, Hamburg, Germany
Cell strainer 40 µm	Corning, Corning, NY, USA
Cell strainer 70 µm	Sarstedt, Nümbrecht, Germany
Cling film	CeDo GmbH, Mönchengladbach, Germany
Countess® cell counting chamber slides	Life Technologies, Carlsbad, CA, USA
Cryogenic tubes Greiner Bio-One™ Cryo.s™	Thermo Fisher Scientific, Waltham, MA, USA
Cryogenic tubes Nalgene™	Thermo Fisher Scientific, Waltham, MA, USA
FACS™ tubes (5 ml Polystrene round-bottom tube)	BD, Franklin Lakes, NJ, USA

Name	Company
Falcon® cell strainer 70 µm	NeoLab, Heidelberg, Germany
FINE-Ject® 26G needle	Henke-Sass, Wolf, Tuttlingen, Germany
gentleMACS™ C Tubes	Miltenyi Biotec, Bergisch Gladbach, Germany
MACS® Separation Column LS	Miltenyi Biotec, Bergisch Gladbach, Germany
Microscope slides 'Menzel Gläser'	Thermo Fisher Scientific, Waltham, MA, USA
Mini-PROTEAN® TGX Precast Gels	Bio-Rad Laboratories, Hercules, CA, USA
Nucleo Counter Via1-Cassettes™	ChemoMetec, Allerod, Denmark
Parafilm	Bemis, Neeah, WI, USA
Pasteur capillary pipettes short size 150 mm WU Mainz®	Wilhelm Ulbrich, Bamberg, Germany
PCR reaction tube CapStrips	Biozym Scientific, Oldendorf, Germany
PCR reaction tube SoftStrips	Biozym Scientific, Oldendorf, Germany
PCR reaction tubes, single	Biozym Scientific, Oldendorf, Germany
Pipette tips, with and without filter	Starlab, Hamburg, Germany
PVDF Transfer membrane	Thermo Fisher Scientific, Waltham, MA, USA
Reaction tubes (0.2 ml, 0.5 ml, 1.5 ml, 2 ml)	Starlab, Hamburg, Germany
Reaction tubes (5 ml)	Eppendorf, Hamburg, Germany
Reaction tubes, black, flip cap (1.5 ml)	NeoLab, Heidelberg, Germany
Scalpel No. 20	Feather, Osaka, Japan
StarGuard® Comfort Gloves M	Microflex, Reno, NV, USA
Syringe (20ml, 50ml BD Plastipak Luer-Lok™)	BD, Drogheda, Ireland
Syringe filter (pore size 0.22 µm)	TPP, Trasadingen, Switzerland
Syringe Injekt® Luer Lock Solo (1 ml, 2 ml)	B Braun, Melsungen, Germany
Test tube (15 ml and 50 ml)	nerbe plus, Winsen/Luhe, Germany
Vacuum Filter (bottle top, pore size 0.22 µm)	TPP, Trasadingen, Switzerland
Western Blotting filter paper	Thermo Fisher Scientific, Waltham, MA, USA

3.1.6 Kits

Name	Catalog No.	Company
Fixation/Permeabilization Solution Kit with BD GolgiStop™	554715	BD, Franklin Lakes, NJ, USA
$CD8a^+$ T Cell Isolation Kit, mouse	130-104-075	Miltenyi Biotec, Bergisch Gladbach, Germany
Gel Extraction Kit, peqGOLD	12-2501	VWR Peqlab, Erlangen, Germany
REDTaq® ReadyMix™ PCR Reaction Mix	R2523	Sigma-Aldrich, St. Louis, MO, USA
CloneAmp™ HiFi PCR Premix	639298	Takara, Kusatsu, Japan
Tumor dissociation kit, mouse	130-096-730	Miltenyi Biotec, Bergisch Gladbach, Germany
Zombie Aqua™ Fixable Viability Kit	423101	Biolegend, San Diego, CA, USA
Zombie Yellow™ Fixable Viability Kit	423103	Biolegend, San Diego, CA, USA

Name	Catalog No.	Company
CellTrace™ Far Red Cell Proliferation Kit	C34564	Life Technologies, Carlsbad, CA, USA
CellTrace™ CFSE Cell Proliferation Kit	C34554	Life Technologies, Carlsbad, CA, USA

3.1.7 Laboratory Appliances

Appliance	Description	Company
Analytical balance	Entris®	Sartorius, Göttingen, Germany
Automated cell counter	Countess™	Thermo Fisher Scientific, Waltham, MA, USA
Automated cell counter	NucleoCounter® NC-200™	ChemoMetec, Allerod, Denmark
Cell freezing container	Nalgene® Mr. Frosty® Cryo 1°C Freezing Container	Thermo Fisher Scientific, Waltham, MA, USA
Centrifuge	Centrifuge 5417 R, 5418	Eppendorf, Hamburg, Germany
Centrifuge	Biofuge™ pico, fresco	Heraeus, Hanau, Germany
Centrifuge	Megafuge™ 16 R	Heraeus, Hanau, Germany
Centrifuge	Sunlab® Minizentrifuge SU1550	Labdiscount GmbH, Mannheim, Germany
Centrifuge rotor for microcentrifuge	F45-30-11	Eppendorf, Hamburg, Germany
Centrifuge rotor for plates	M-20, 75003624	Thermo Fisher Scientific, Waltham, MA, USA
Centrifuge rotor for swinging buckets	TX-400, 75003629	Thermo Fisher Scientific, Waltham, MA, USA
Digital calipers 0-150mm		Aerospace, Hunan, China
Electrophoresis chamber	Mini-PROTEAN® Tetra Cell	Bio-Rad Laboratories, Hercules, CA, USA
Electrophoresis chamber for agarose gels	Owl™ Easycast™ B2	Thermo Fisher Scientific, Waltham, MA, USA
Electrophoresis chamber for agarose gels	PerfectBlue™ gel system, Mini L	VWR Peqlab, Erlangen, Germany
Flow cytometer	BD FACSAria™ II	BD, Franklin Lakes, NJ, USA
Flow cytometer	FACS Canto II™	BD, Franklin Lakes, NJ, USA
Flow cytometer	LSRFortessa™	BD, Franklin Lakes, NJ, USA
Freezer (-20°C)	Mediline	Liebherr, Biberach an der Riß, Germany
Freezer (-20°C)		Bosch, Stuttgart, Germany
Freezer (-80°C)	U725 Innova	New Brunswick, Nürtingen, Germany
Gel documentation system	Molecular Imager® Gel Doc™ XR System	Bio-Rad Laboratories, Hercules, CA, USA
Glassware	Duran®	Schott, Mainz, Germany

Appliance	Description	Company
Glassware	Fisherbrand™	Thermo Fisher Scientific, Waltham, MA, USA
Heating pad		Beurer, Ulm, Germany
Ice buckets		NeoLab, Heidelberg, Germany
Ice machine	FM 120 KE-50-HC	Hoshizaki, Tokyo, Japan
Imaging system	ChemiDoc™ Touch Imaging System	Bio-Rad Laboratories, Hercules, CA, USA
In vivo Imaging system	IVIS® Lumina III	PerkinElmer, Waltham, MA, USA
Incubator (37°C, 5% CO_2, cell culture)	Heracell™ 150i	Thermo Fisher Scientific, Waltham, MA, USA
Incubator (37°C, 5% CO_2, cell culture)	C200	Labotec, Göttingen, Germany
Irradiation device	Gammacell® 1000 D	Best Theratronics, Ottawa, Canada
Isoflurane dispenser		Drägerwerk, Lübeck, Germany
Laminar flow hood	SterilGard® Class II laminar flow hood	The Baker Company, Sanford, USA
Laminar flow hood	Maxisafe 2020	Thermo Fisher Scientific, Waltham, MA, USA
Light microscope	Wilovert Standard 30 microscope	Hund Wetzlar, Wetzlar, Germany
Light microscope	Axiovert 25	Carl Zeiss Microscopy, Jena, Germany
Light microscope	Zeiss Primovert	Carl Zeiss Microscopy, Jena, Germany
Liquid nitrogen tank	Locator™ 8 plus	Barnstead/Thermolyne, Dubuque, IA, USA
Liquid nitrogen tank	ARPEGE110 NU	Cryopal, Bussy-Saint-Georges, France
Live cell imager	Incucyte®	Sartorius, Göttingen, Germany
Luminescence reader	Mithras^2 LB 943	Berthold Technologies, Bad Wildbad, Germany
Luminescence reader	GloMax® Explorer Multimode Microplate Reader	Promega, Madison, WI, USA
Magnet for MACS	QuadroMACS™	Miltenyi Biotech, Bergisch Gladbach, Germany
Magnetic stirrer	RSM-01S	Phoenix Instrument, Garbsen, Germany
Magnetic stirrer, heatable	MR-Hel Standard	Heidolph Instruments, Schwabach, Germany
Microplate reader	Multiskan™ FC Microplate Photometer	Thermo Fisher Scientific, Waltham, MA, USA
Microwave		Sharp, Osaka, Japan
Multichannel pipette	300µl Finnpipette™ F2	Thermo Fisher Scientific, Waltham, MA, USA
Multichannel pipetting reservoir	Multi-channel pipettor Trifill reservoir	Roth, Karlsruhe, Germany

Appliance	Description	Company
Spectrophotometer	NanoDrop™ 1000	Thermo Fisher Scientific, Waltham, MA, USA
Spectrophotometer	NanoDrop™ 8000	Thermo Fisher Scientific, Waltham, MA, USA
pH Meter	SevenCompact™ pH/Ionmeters S220 with pH Electrode InLab Ultra-Micro-ISM	Mettler Toledo, Glostrup, Denmark
Pipette	PIPETBOY acu 2	Integra Biosciences, Biebertal, Germany
Pipette	PIPETGIRL acu 2	Integra Biosciences, Biebertal, Germany
Pipette	Pipetman® Gilson 100 µl	Gilson, Middleton, WI, USA
Pipettes	ErgoOne® Single-Channel pipettes 2 µl, 20 µl, 200 µl, 1 000 µl	Starlab, Hamburg, Germany
Pipettes, glass		Hirschmann Labortechnik, Eberstadt, Germany
Power supply	EPS3500	Pharmacia, Uppsala, Sweden
Power supply	MP 250V	MS Major Science, Saratoga, CA, USA
Refrigerator (4°C)	Mediline	Liebherr, Biberach an der Riß, Germany
Refrigerator (4°C)		Bosch, Stuttgart, Germany
Scale	Kern EG 4200-2NM	Kern & Sohn, Balingen, Germany
Shaver	Aesculap Isis GT420 & GT421	Aesculap Schermaschinen, Suhl, Germany
Surgical tweezer and scissors		Dimeda, Tuttlingen, Germany
Thermal cycler	Bioer GeneTouch Thermal Cycler	Biozym Scientific, Oldendorf, Germany
Thermomixer	Thermomixer compact	Eppendorf, Hamburg, Germany
Timer	Neolab 2-2002	NeoLab, Heidelberg, Germany
Tissue dissociator	gentleMACS™ Octo Dissociator with Heaters	Miltenyi Biotec, Bergisch Gladbach, Germany
Transport box	Fisherbrand™ transport box	Fisher Scientific, Schwerte, Germany
UV table		Konrad Benda, Wiesloch, Germany
Vacuum pump	N86KT.18	KNF Neuberger, Freiburg, Germany
Vortexer	Vortex-Genie™ 2	Scientific Industries, Bohemia, USA
Water bath		GFL, Burgwedel, Germany

3.1.8 Media

Media	Ingredients
2277-NS	DMEM 10 % (v/v) FCS 1 % (v/v) HEPES 0.1 % (v/v) β-mercaptoethanol (50 mM) 1 % (v/v) gentamicin 2 % (v/v) L-glutamine 1 % (v/v) sodium pyruvate (100 mM)
CaSki	RPMI 10 % (v/v) FCS 1 % (v/v) P/S 1 % (v/v) L-glutamine
E6/7-lucA2	RPMI 10 % (v/v) FCS 1 % (v/v) P/S 1 % (v/v) L-glutamine 2 µg/ml puromycin 1 µg blasticidin
$E6^+E7^+$ lung cell	RPMI 10 % (v/v) FCS 1 % (v/v) P/S 1 % (v/v) L-glutamine 2 µg/ml puromycin
GolgiStop™/GolgiPlug™ (GS/GP) medium	RPMI 10 % (v/v) FCS 3 µl GolgiStop™/ml 2 µl GolgiPlug™/ml
HeLa	DMEM 10 % (v/v) FCS 1 % (v/v) P/S 1 % (v/v) L-glutamine
PAP-A2	DMEM 10 % (v/v) FCS 1 % (v/v) HEPES 0.1 % (v/v) β-mercaptoethanol (50 mM) 1 % (v/v) gentamicin 2 % (v/v) L-glutamine 1 % (v/v) sodium pyruvate (100 mM) 2 µg/ml puromycin

Media	Ingredients
PAP-A2-luc	DMEM 10 % (v/v) FCS 1 % (v/v) HEPES 0.1 % (v/v) β-mercaptoethanol (50 mM) 1 % (v/v) gentamicin 2 % (v/v) L-glutamine 1 % (v/v) sodium pyruvate (100 mM) 2 µg/ml puromycin 2 µg/ml blasticidin
TC-1	RPMI 10 % (v/v) FCS 1 % P/S 1 % L-glutamine
T cell	αMEM 10 % (v/v) FCS 0.1 % (v/v) β-mercaptoethanol (50 mM) 1 % (v/v) L-glutamine 1 % P/S 100 nM of respective peptide (20 IU/ml IL-2)

3.1.9 Mice

All experimental procedures were approved by Regierungspräsidium Karlsruhe, Germany prior to experimental procedures (permit numbers DKFZ279, G82-13, G143-18, G189-18, G241-18 and G6-19). The animals were kept in the ZPF animal facility in individually ventilated cages (IVC). Mice used for experiments were female and 6 – 20 weeks old at the beginning of experiments.

Strain	Description	Source
A2.DR1	Mice generated on a C57BL/6 background, knocked-out for murine MHCs, knocked-in HLA-DR1 and HHD (MHC I presenting HLA-A2:01 epitopes, see 1.4.2 (Pajot et al., 2004))	In-house bred at ZPF, DKFZ. Originally from Institut Pasteur, Paris, France

3.1.10 Proteins and peptides

Name	Sequence N - C	Description	Source
HPV16 $E7_{11-19}$	YMLDLQPET	HLA-A*02:01-restricted epitope	Mario Koch, DKFZ
Human $Survivin_{96-104}$	LMLGEFLKL	HLA-A*02:01-restricted epitope	Mario Koch, DKFZ
Recombinant murine MIG (CXCL9)		murine chemokine	PeproTech, Hamburg, Germany

Name	Sequence N - C	Description	Source
Recombinant murine IP-10 (CXCL10)		murine chemokine	PeproTech, Hamburg, Germany

3.1.11 Oligonucleotides/primers

Name	Sequence 5' - 3'	Source
hrasLucSeq1Fwd	AGCCGCTAGCATGGAAG	Sigma-Aldrich, St. Louis, MO, USA
hrasLucSeq2Rev	GTGAAATGGCACCACGC	Sigma-Aldrich, St. Louis, MO, USA
hrasLucSeq3Fwd	TTGCACGAGATCGCCAG	Sigma-Aldrich, St. Louis, MO, USA
hrasLucSeq4Fwd	CCCATGGCCAAGCCTTT	Sigma-Aldrich, St. Louis, MO, USA
hrasLucSeq5Fwd	GGTCTCCTCCCATGCAT	Sigma-Aldrich, St. Louis, MO, USA
SRBLF1Fwd	TACCGAAGCCGCTAGCACCATGACGGAATATA AGCTGGT	Sigma-Aldrich, St. Louis, MO, USA
SRBLF1Rev	CCGCTGCCGGAGAGCACACACTTGCAGC	Sigma-Aldrich, St. Louis, MO, USA

3.1.12 Reagents

Reagent	Catalog No.	Company
β-estradiol	E8875	Sigma-Aldrich, St. Louis, MO, USA
β-mercaptoethanol	31350-010	Life Technologies Europe BV, Bleiswijk, Netherlands
4x Laemmli buffer	1610747	Bio-Rad Laboratories, Hercules, CA, USA
Albumin, from bovine serum albumin (BSA)	A9418	Sigma-Aldrich, St. Louis, MO, USA
Amersham™ ECL Prime Western Blotting Detection Reagent	12316992	GE Healthcare, Chicago, IL, USA
Blasticidin S hydrochloride	10658203	Fisher Scientific, Schwerte, Germany
DC protein assay reagent A	5000113	Bio-Rad Laboratories, Hercules, CA, USA
DC protein assay reagent B	5000114	Bio-Rad Laboratories, Hercules, CA, USA
DC protein assay reagent S	5000115	Bio-Rad Laboratories, Hercules, CA, USA
Depo-Clinovir® and Depo-Provera® (Medroxyprogesterone acetate)		Pfizer, New York, NY, USA
D-luciferin potassium salt	14681	Cayman Chemical, Ann Arbor, MI, USA
Dulbecco's Modified Eagle Medium (DMEM), high glucose (-hi)	D5671	Sigma-Aldrich, St. Louis, MO, USA
FastDigest Green Buffer (10x)	B72	Thermo Fisher Scientific, Waltham, MA, USA

Reagent	Catalog No.	Company
Fetal Calf Serum (FCS)	10270	Thermo Fisher Scientific, Waltham, MA, USA
FuGENE 6® Transfection Reagent	E2691	Promega, Madison, WI, USA
GeneRuler™ 50 bp DNA Ladder	SM0371	Thermo Fisher Scientific, Waltham, MA, USA
GeneRuler™ Ladder Mix, 100 bp - 10000 bp	SM0333	Thermo Fisher Scientific, Waltham, MA, USA
Gentamicin	15750060	Thermo Fisher Scientific, Waltham, MA, USA
GolgiPlug™	555029	BD, Franklin Lakes, NJ, USA
HEPES	11560496	Life Technologies Europe BV, Bleiswijk, Netherlands
IL-2, recombinant human	200-02	PeproTech, Rocky Hill, NJ, USA
Imiquimod	14956	Cayman Chemical, Ann Arbor, MI, USA
Ionomycin	10634	Sigma-Aldrich, St. Louis, MO, USA
Precision Plus Protein™ Kaleidoscope	1610375	Bio-Rad Laboratories, Hercules, CA, USA
L-glutamine	25030024	Thermo Fisher Scientific, Waltham, MA, USA
Luciferase assay system	E4550	Promega, Madison, WI, USA
Matrigel® Matrix basement membrane	354234	Corning, Corning, NY, USA
Minimum Essential Medium Eagle, α modification (αMEM)	M4526	Sigma-Aldrich, St. Louis, MO, USA
NEBuffer™ 2	B7002S	New England Biolabs, Ipswich, MA, USA
Peanut oil	sc-215683	Santa Cruz Biotechnology, Dallas, TX, USA
Phorbol 12-myristate 13-acetate (PMA)	P8139	Sigma-Aldrich, St. Louis, MO, USA
Phosphate buffered saline (PBS)	10010015	Life Technologies Europe BV, Bleiswijk, Netherlands
Penicillin/Streptomycin solution (P/S) 10,000 U penicillin and 10 mg streptomycin per ml (100x)	P0781	Sigma-Aldrich, St. Louis, MO, USA
Polyinosinic-polycytidylic acid (poly(I:C)), high molecular weight, VacciGrade™	vac-pic	InvivoGen, San Diego, CA, USA
Protease inhibitor cocktail, cOmplete™	11873580001	Roche, Basel, Switzerland
Puromycin-dihydrochlorid	P9620	Sigma-Aldrich, St. Louis, MO, USA
Resiquimod	SML0196	Sigma-Aldrich, St. Louis, MO, USA
Rosswell Park Memorial Institute medium 1640 (RPMI)	R0883	Sigma-Aldrich, St. Louis, MO, USA
Sodium pyruvate	25-000-CIR	Corning, Kaiserslautern, Germany
Vidisic® Eye gel EDO®	117021	Dr. Gerhard Mann chem.-pharm. Fabrik, Berlin, Germany

3.1.13 Restriction enzymes

Name	Restriction site 5' - 3'	Source
FastDigest NheI	GCTAGC	Thermo Fisher Scientific, Waltham, MA, USA
FastDigest XhoI	CTCGAG	Thermo Fisher Scientific, Waltham, MA, USA
AseI	ATTAAT	New England Biolabs, Ipswich, MA, USA
EcoRV	GATATC	New England Biolabs, Ipswich, MA, USA

3.1.14 Software

Software	Description	Company
BD FACSDiva™ Software 8	Analysis of flow cytometry data	BD, Franklin Lakes, NJ, USA
Endnote™ 20	Reference management tool	Clarivate, London, UK
FlowJo™ V10	Analysis of flow cytometry data	BD Life Sciences, Ashland, USA
GIMP V2	Image editing software	The GIMP team
Graphpad Prism®7	Data visualization and statistical analysis	Graphpad Software, San Diego, USA
Image Lab software	Image acquisition and analysis software for gel documentation images	Bio-Rad Laboratories, Hercules, CA, USA
Incucyte® Software 2020B	Operating and analysis software for Incucyte®	Sartorius, Göttingen, Germany
Inkscape V1	Vector graphics editing software	The Inkscape team
Living Image® V4	Operating and analysis software for IVIS® Lumina III imaging	PerkinElmer, Waltham, MA, USA
Microsoft Office Standard 2016	Office suite software	Microsoft Corporation, Redmond, WA, USA
NanoDrop 1000 and 8000 software	Operating software for ND™-1000 and ND™-8000	Thermo Fisher Scientific, Waltham, MA, USA
NucleoView™	Operating software for NucleoCounter® NC-200™	ChemoMetec, Allerod, Denmark
Quantity One 1-D Analysis Software V4	Operating software for gel documentation	Bio-Rad Laboratories, Hercules, CA, USA
SnapGene® V4	Cloning software	Insightful Science, San Diego, CA, USA

3.1.15 Vaccine compounds

Vaccine compound	Description	Source
Liposomes	Tetraether liposomal formulations with cell-penetrating peptides (CPP). For details see Uhl et al. (2019) and Uhl et al. (2021)	Produced by Dr. Philipp Uhl, Heidelberg University Hospital and Dr. Mikko Gynther, Heidelberg University Hospital, Germany

Vaccine compound	Description	Source
LPP-E7$_{11-19}$	Amphiphilic peptide construct consisting of (1,2-distearoyl-3-sn-phosphatidylethanolamine)-PEG-maleimide coupled N-terminally to YMLDLQPET via a cysteine residue. For details see Kruse et al. (2018).	Produced by peptides & elephants, Henningsdorf, Germany; the Eichmüller group, DKFZ and Dr. Philipp Uhl, Heidelberg University Hospital, Germany
SiO_2-Arg (SiNP)	SiO_2 nanoparticles with a diameter of 25 nm consisting of an amorphous silica core adsorptively linked to an epitope via a KKK-W-citrullin linker.	Produced by Silvacx

3.2 Methods

If not indicated otherwise, everything described below was performed by myself.

3.2.1 *In vitro* methods

3.2.1.1 Vector production

The S/MAR-UbC-Hras-Luc vector (Appendix Figure 1) was designed prior to my work by Dr. Matthias Bozza and Dr. Sebastian Kruse and was subsequently produced by Alexandra Klevenz and Dr. Sebastian Kruse. Episomal vectors containing a scaffold/matrix attachment region (S/MAR) element bind the chromosomal scaffold and are replicated in mitosis, which ensures sustained gene expression (Bozza et al., 2020). They provide a safer method of transforming a cell than viral transduction (Wong et al., 2011). The first of the encoded proteins on the vector is a mutated form of HRAS. This gene is also known as p21 and belongs to one of the most frequently mutated gene families in cancer, *RAS* (Moore et al., 2020). The point-mutated HRAS^{G12V} used here renders the GTPase constitutively active and leads to tumorigenic transformation of cells (Gibbs et al., 1984; Matlashewski et al., 1987; Lin et al., 1996). Firefly luciferase, the second encoded protein, is required for intracorporeal detection of tumors formed by the newly generated cell line. Luciferase is the enzyme responsible for the glowing of *Photinus pyralis* and is commonly used as a marker protein in biotechnology. Cells expressing the luciferase gene can emit light upon addition of their substrate luciferin:

$$Luciferin + O_2 + ATP \xrightarrow[Luciferase]{} Oxyluciferin + CO_2 + AMP + PP_i + \boldsymbol{Light}$$

(ATP = Adenosine triphosphate; AMP = Adenosine monophosphate; PP_i = inorganic pyrophosphate)(Gates & DeLuca, 1975).

3.2.1.1.1 Primer design and restriction digest

Restriction digest is a method to verify the presence of inserted fragments in a newly generated vector. There, restriction enzymes bind and cut DNA at a specific nucleotide sequence, their restriction site (Loenen et al., 2014). The resulting fragments will result in characteristic bands of a certain length when applied to an agarose gel, allowing the confirmation of the vector identity.

For the restriction digests in this work, I prepared two different reaction mixtures to check the S/MAR-UbC-Hras-Luc vector for the UbC-Hras and for the Luciferase-blasticidin resistance fragments, respectively:

UbC-Hras		**Luciferase-blasticidin resistance**	
Component	**Plasmid DNA**	**Component**	**Plasmid DNA**
Water, nuclease-free	20.5 µl	Water, nuclease-free	7 µl
NEBuffer™ 2	2.5 µl	10x FastDigest® Green buffer	1 µl
Vector DNA	1 µl (~500 ng)	Vector DNA	1 µl (~500 ng)
Enzymes AseI + EcoRV	0.5 µl + 0.5 µl	FastDigest Enzymes NheI & XhoI	0.5 µl + 0.5 µl
Total volume	25 µl	Total volume	10 µl

After a short centrifugation, the mixtures were incubated for 1 h at 37°C and the resulting DNA fragments were analyzed by gel electrophoresis.

3.2.1.1.2 Agarose gel electrophoresis

Agarose gel electrophoresis is used to separate nucleotide fragments by their length (Peacock & Dingman, 1968). The nucleic acids are mixed with a DNA-intercalating, fluorescent dye. Historically, mostly ethidium bromide was used for this (Waring, 1965), however I used the less toxic GelRed® Nucleic Acid Gel Stain for my gels. After the DNA fragments are loaded onto the agarose gel, a current is applied, which leads to migration of the negatively charged molecules towards the anode. Meanwhile they are separated by their size by the pores of the gel and can be made visible in the end by UV light (Aaij & Borst, 1972). The gel was cast by mixing 1 g of agarose with 100 ml of 1x TAE buffer for an 1 % gel. The mixture was boiled, cooled down and 10 µl of GelRed were added. After the gel hardened in its casting form, the comb was removed and DNA from the restriction digest, as well as DNA ladder were pipetted into the pockets of the gel. Subsequently, the electrophoresis chamber was filled with 1x TAE

buffer, covering the gel and a current of 100 V was applied. After the bands were separated, the gel was analyzed with the Molecular Imager® Gel Doc™ XR System.

3.2.1.1.3 Sanger sequencing

Sanger sequencing is used to verify the assumed nucleotide sequence of a DNA fragment. For this, the DNA is amplified by a polymerase, which adds deoxynucleotide trisphosphates (dNTPs) equivalent to a polymerase chain reaction (PCR). However, the reaction mix also includes di-deoxynucleotide trisphosphates (ddNTPs), which cause the amplification to abort. These ddNTPs are fluorescently labeled and can therefore be excited by lasers. The detected light indicates the order of nucleotides and analysis of the different lengths of amplified fragments allow determination of the original nucleotide sequence (Sanger et al., 1977). The DNA fragments in this thesis were sent along with the primers listed in 3.1.11 to Microsynth Seqlab, Göttingen, Germany for analysis by Sanger sequencing.

3.2.1.2 Cell culture

All cultured cells were treated in a sterile laminar flow hood and were incubated at 37°C, 5 % CO_2 and 95 % relative humidity. Centrifugations were conducted at room temperature (RT) if not indicated otherwise.

3.2.1.2.1 Culturing and passaging of adherent cells

Adherent cell lines (2277-NS, CaSki, $E6^+E7^+$ lung cells, E6/7H-luc, E6/7-lucA2, HeLa-CaG-luc, PAP-A2, PAP-A2-luc and TC-1/A2-luc) were cultured in cell culture-specific vessels such as multi-well plates or cell culture flasks of different sizes according to cell amount and cell growth. When the cells reached a confluency between 40 – 90 % I passaged, i.e. subcultured them. For passaging, the old medium was removed and the cells were washed with PBS to remove excess medium. Afterwards, I added trypsin/EDTA and incubated the cells until they were fully detached. The protease trypsin detaches the cells from the surface they are adhering to by digesting the adhesion proteins. EDTA on the other hand acts as a chelator that binds Ca^{2+}, which reduces cell-cell interactions (Vogel, 1978). After the incubation, fresh medium was added to stop the enzymatic degradation of adhesion proteins as the fetal calf serum (FCS) in the medium contains protease inhibitors. The cells were then centrifuged at 1,300 rpm for 4 min, and were resuspended in fresh medium. Counting was done by either taking up 60 µl with a Via1-Cassette™ and analyzing it with the NC-200™ cell counter or by mixing 10 µl of

the cell suspension with 10 µl of trypan blue for counting with the Countess™ cell counter. In the end, the cells were either resuspended in an appropriate amount of medium and subcultured, frozen down or used for experiments.

3.2.1.2.2 Culturing and passaging of murine T cells

Either T cells were taken into culture after extraction from murine tissue (see 3.2.1.2.5) or after thawing the cells according to 3.2.1.2.3. After freshly isolating T cells I took 30 x 10^6 cells up in 10 ml of T cell medium containing no interleukin 2 (IL-2) but 100 nM of their cognate peptide, mostly $E7_{11-19}$. The cell suspension was then put into T25 cell culture flasks and was incubated for one week. If the cells were not frozen down afterwards, they needed to be passaged and mixed with syngeneic, irradiated primary murine splenocytes as feeder cells presenting cognate peptide to the T cells for their maintenance. For this, 30 x 10^6 primary splenocytes per T cell line were taken up into PBS and were subsequently irradiated in the Gammacell® 1000 D device with 33 Gy. Then the feeder cells were centrifuged at 1,500 rpm for 4 min, the supernatant discarded and the cells taken up in 6 ml of T cell medium supplemented with 100 nM peptide and 20 IU/ml of IL-2. After I plated the irradiated feeder cells at 1 ml/well into a 24-well cell culture plate, 1 ml of the epitope-specific T cells was added to each feeder cell well. This process was repeated every week until freezing or the start of an experiment. Frozen T cells were mixed with feeder cells immediately after thawing.

3.2.1.2.3 Thawing and freezing

Frozen cells from the liquid nitrogen (N_2) tank were thawed rapidly in a 37°C water bath, immediately added to 10 ml of warm, cell-appropriate medium, and afterwards centrifuged at 1,300 rpm for 4 min. For freezing, cells were centrifuged at 1,300 rpm for 4 minutes and resuspended in an appropriate amount of freezing medium, consisting of 50 % (v/v) FCS, 40 % (v/v) of cell-specific medium and 10 % (v/v) dimethyl sulfoxide (DMSO). The DMSO prevents formation of ice crystals during the freezing process. When the cell suspension had been transferred into a cryo vial, I put them into a Mr. Frosty® freezing container filled with isopropanol and placed it into the -80°C freezer. The container ensures a constant cooling rate of 1°C/min to protect the cells. One day after freezing, the vials were transferred to liquid N_2.

3.2.1.2.4 Transfection and antibiotic selection

Transfection is a method of introducing nucleic acids into cells with the goal of genetic alteration (Kim & Eberwine, 2010). In this work I transfected immortalized A2.DR1 mouse cells with an S/MAR vector construct with the transfection reagent FuGene 6® (FuGene). The reagent was proven to transfect many eukaryotic cell lines efficiently and without major cytotoxic side effects (Nagy & Watzele, 2006). To be able to distinguish transfected from non-transfected cells the S/MAR vector contained a blasticidin i.e. antibiotic resistance gene as marker. Cells surviving in the antibiotic-containing medium are therefore the successfully transfected ones.

One day before transfection, I seeded the cells in a number according to their growth rate i.e. a doubling time of 24 h, in 2 ml medium/well into a 12-well plate. The transfection was performed at a cell density of 50 – 80%. At this density, the cultured cells were in the exponential growth phase, which is required for successful transfection. The reaction mixture contained 2 µg of DNA, a variable volume of FuGene, depending on the FuGene:DNA ratio and serum-free growth medium to a total volume of 100 µl/well. Before use, the FuGene transfection reagent was brought to RT and then was vortexed briefly. Afterwards, FuGene was mixed with serum-free growth medium. After an incubation of 5 min at RT the DNA was added and everything incubated for 15 min at RT. The old medium on the target cells was removed, fresh pre-warmed medium added and 50 µl of the FuGene/DNA/Medium mix were dropped onto the cells. Subsequent to an overnight incubation at 37°C in an incubator, the transfected cells were harvested and were either frozen down or used for further culturing or experiments.

For antibiotic testing I seeded untransfected cells at 3.6×10^4 cells in 2 ml/well in a 6-well plate and added different concentrations of blasticidin between 0 µg/ml – 10 µg/ml. The plate was then checked every day for how many cells had died. The optimal dose of antibiotic to be used for selection of transfected cells was defined as the lowest concentration at which all cells were dead after one week.

3.2.1.2.5 Dissociation of murine tissue

For analysis of immune cells in murine tissues and tumors or culturing of murine T cells, the tissues had to be dissociated and processed into a single-cell suspension. Mice were killed by

CO_2 asphyxia, followed by cervical dislocation. Their organs and tumors were removed under sterile conditions.

3.2.1.2.5.1 Spleen

The spleen represents an important part of the lymphatic system and contains high amounts of lymphocytes (Mebius & Kraal, 2005). Therefore, the cells contained in the spleen were used in this work as a proxy for the systemic T cell response to vaccination. After removal of the spleen from a mouse, I transferred the organ into a reaction tube containing 1 ml of ice-cold PBS. Then, the spleen was put onto a 70 µm cell strainer on top of a 50 ml centrifuge tube and was mashed with a syringe plunger. Subsequently, the cell strainer was washed with 2x 5 ml of ice-cold PBS and the cell suspension was centrifuged at 1,500 rpm at 4°C for 4 min. The supernatant was removed, the cell pellet resuspended and 4 ml of cold ACK lysis buffer were added. This hypotonic buffer causes the osmotic rupture of erythrocytes. After 50 s the tube was filled up with cold PBS to 50 ml and then centrifuged at 1,500 rpm at 4°C for 4 min. When the supernatant had been discarded, the cells were taken up in 50 ml of cold PBS and were counted according to 3.2.1.2.1. The cell suspension was again centrifuged at 1,500 rpm at 4°C for 4 min and then adjusted to the desired concentration after removal of the supernatant. Finally, the cells were either cultured or used for antibody staining.

3.2.1.2.5.2 Genital tracts

For GT dissociation, I first prepared the proprietary enzyme mixture consisting of 2.35 ml RPMI, 100 µl enzyme D, 50 µl enzyme R and 12.5 µl enzyme A from the mouse tumor dissociation kit (Miltenyi Biotec, 2021). Then the murine GT was removed from oviduct to vaginal opening while as much adipose tissue as possible was discarded. After transferring the whole organ to a reaction tube containing 1 ml of the enzyme solution, it was cut into very small pieces with fine scissors. When the enzyme-tissue mixture had been added to the rest of the enzyme solution in a centrifuge tube, it was incubated at 37°C on a shaker for 45 min. The resulting sample was applied to a 70 µm cell strainer on top of a 50 ml centrifuge tube and was mashed with a syringe plunger. Throughout, the cell strainer was washed with 2x 5 ml of RPMI. After centrifuging the cell suspension at 300x g for 7 min, the supernatant was discarded and the cells were resuspended in 10 ml of RPMI. The cells were counted according to 3.2.1.2.1, centrifuged at 1,500 rpm for 4 min and then adjusted to the desired concentration after removal of the supernatant. Finally, the cells were either cultured or used for antibody staining.

3.2.1.2.5.3 Tumors

To take tumors into culture, they were dissociated according to the manufacturer's protocol of the mouse tumor dissociation kit (Miltenyi Biotec, 2021). Prior to tumor removal I prepared the proprietary enzyme mixture consisting of 2.35 ml RPMI, 100 µl enzyme D, 50 µl enzyme R and 12.5 µl enzyme A and filled it into a C tube. Then, the tumor was removed from the mouse and minced into fine pieces in a petri dish. After transferring the tissue to the prepared C tube, it was attached to the gentleMACS™ Octo Dissociator and the program 37C_m_TDK2 was started. The resulting sample was resuspended, applied to a 70 µm cell strainer on top of a 50 ml centrifuge tube and rinsed with 10 ml RPMI. After a centrifugation at 300 x g for 7 min the cells were resuspended in an appropriate amount of medium and counted according to 3.2.1.2.1. Finally, the cells were transferred to a cell culture flask to keep them at 37°C in the incubator.

3.2.1.3 Western blot

Western blotting, also called immunoblotting, is used to examine specific proteins in a protein mixture. First, the protein lysate, e.g. of a cell line of interest, is separated by molecular mass by a sodium dodecyl sulfate–polyacrylamide gel electrophoresis (SDS page)(Laemmli, 1970). In this kind of electrophoresis, the proteins are mixed with SDS that binds and denatures the proteins as well as giving them a negative charge (Manns, 2011). Once a current is applied to the gel, the proteins migrate towards the anode. The speed is mostly determined by their size and therefore their mass, as the proteins have to pass through the pores of the gel. After gel electrophoresis, the proteins are transferred to a membrane or paper by laying the gel onto the membrane and applying a current with the anode on the side of the membrane. Thereupon the proteins will be pulled into the membrane. This membrane can then be treated with antibodies against the protein of interest that bind their targets on the membrane. The antibodies can be made visible by a secondary antibody coupled to an enzyme, in this case horseradish peroxidase, which converts added substrate to a chemiluminescent signal, which can be detected and quantified. All Western blots and their preceding procedures described in this thesis were done by Alexandra Klevenz with occasional help from Marie-Luise Koch.

3.2.1.3.1 Protein extract production and DC assay

To obtain the necessary protein lysate for Western blotting, the cells of the examined cell lines were first lysed and their concentration was determined by a detergent compatible (DC) assay, which is based on the Lowry assay (Lowry et al., 1951).

All steps of the protein extraction were conducted on ice. First, the adherent cells were detached from their cell culture vessel and counted as described in 3.2.1.2.1. The cells were washed 2x with 50 ml PBS, centrifuged at 1,300 rpm for 4 min and then all residual liquid was removed. The resulting cell pellet was resuspended with 80 µl complete protein lysis buffer/10^6 cells and subsequently incubated on ice for 20 min with intermittent mixing every minute. After centrifugation at 14,000 x g for 10 min at 4°C, the supernatant was transferred to another tube and the protein concentration was determined with the DC Protein Assay by Bio-Rad. For this, 20 µl of the protein assay solution S was added to 1 ml of solution A. Of this mixture, 20 µl were added to 2 µl of the previously generated cell lysate. After addition of 200 µl solution B the sample was incubated for 15 min and the absorbance was measured at 750 nm in a photometer. The measured absorbance of the lysate was compared to a bovine serum albumin (BSA) standard curve and the respective concentration was determined. Subsequently, the cell lysate was mixed with 4x Laemmli buffer containing β-mercaptoethanol, heated to 95°C for 5 min for denaturation and then stored at -80°C.

3.2.1.3.2 SDS page

For this study, 10 - 30 µg of protein were pipetted into the pockets of the precast SDS page gel located in an electrophoresis chamber that was filled with 1x SDS buffer. After loading the protein and Precision Plus Protein™ Kaleidoscope™ Prestained Protein Standards, the chamber was connected to a power supply and the gel ran at 150 V for 1 h.

3.2.1.3.3 Immunoblotting

The separated proteins were transferred from the gel to a polyvinylidene difluoride (PVDF) membrane. Before, the membrane had been immersed for activation in 100 % methanol for 30 s and then was equilibrated in transfer buffer containing 20 % methanol. Additionally, Western blot filter papers were prepared by immersing them in transfer buffer with methanol. For assembly of the Western blot sandwich in the transfer chamber, the gel was laid on two filter

papers and then covered by the PVDF membrane and two more sheets of filter paper. Finally, a current of 150 mA was applied to the chamber for 45 min, which allowed the proteins to be transferred to the membrane. After transfer, the membrane was incubated for 1 h at RT with blocking buffer with constant agitation. Then, the primary antibody diluted in blocking buffer was added and the membrane incubated either overnight at 4°C or for 1 h at RT. Subsequent to removal of the primary antibody after incubation, the membrane was washed three times with PBST for 10 min and then the secondary antibody diluted in blocking buffer was added. The incubation lasted for 1 h at RT with constant agitation and was followed by three more PBST washing steps. For detection of the secondary antibody on the membrane, the solutions of the Amersham™ ECL™ Prime Western Blotting Detection Reagent were prepared according to the manufacturer's instruction. The detection reagent was then poured onto the membrane and the chemiluminescent signals measured with the ChemiDoc™ Touch Imaging System. Analysis of captured pictures was performed with the Bio-Rad Image Lab software.

3.2.1.4 Live cell imaging

For analysis of cell lines using live cell imaging, 10,000 cells/well in 200 µl of the respective growing medium were plated into an F-bottom 96-well plate. Afterwards the plate was placed into the Incucyte® live cell imager in an incubator. After one week, the collected data were analyzed and plotted by Christoph Schifflers with the Incucyte® Software 2020B.

3.2.1.5 Flow cytometry

Flow cytometry is a high-throughput method to analyze a single-cell suspension for the cells' expressed markers of interest. Cells meant for flow cytometric analysis are first labeled with fluorophore-coupled antibodies against surface or – after membrane permeabilization - intracellular markers of interest. These cells are then analyzed by being passed through differently colored lasers in a laminar stream inside the flow cytometer. The pattern of light scattering conveys information about size (forward scatter (FSC)) and granularity (side scatter (SSC)) of the analyzed cells. The emission of light from the excited fluorophore on the antibody is detected by the optical system of the cytometer and is processed by the associated software, generating plots depicting fluorescence intensity (Jahan-Tigh et al., 2012). Unspecific staining can be detected by utilizing so-called isotype controls, where cells are stained with antibodies of the same IgG that are not binding to the antigen of interest but are coupled to the same fluorophore as the antibody used to detect the antigen.

3.2.1.5.1 Staining for HLA-A2/HHD

For detection of HLA-A2 or HHD levels on human and A2.DR1 cells, respectively, I performed staining with an HLA-A2 antibody, which binds both molecules. The cells were detached from their cell culture vessel as described in 3.2.1.2.1 and centrifuged at 2,000 rpm for 3 min. Afterwards, the cells were resuspended in 50 µl staining buffer containing 0.5 µl of the HLA-A2 FITC antibody or IgG2b, κ (isotype control), respectively. They were incubated at 4°C for 30 min and then washed three times with staining buffer. In the end, 100 µl of fixation buffer were added and the samples stored in the dark at 4°C until measurement at the FACS Canto II™.

3.2.1.5.2 Intracellular cytokine staining

Analysis of vaccination-induced HPV16 $E7_{11-19}$-specific T cells was performed via intracellular cytokine staining (ICS). After dissociation of murine tissues the cells extracted from spleen and GTs were restimulated with either the cognate $E7_{11-19}$ epitope or the non-cognate $Surv_{96-104}$, which is a known HLA-A2 binder and immunogenic epitope (Wobser et al., 2006). Upon restimulation, vaccination-induced, specific T cells produce the cytokines IFNγ and TNFα. The cells were first stained for their surface molecules and were then permeabilized to enable IFNγ and TNFα-specific antibodies to bind their respective antigens inside the cell. As positive control for the ICS served the unspecific activators of T cells, phorbol 12-myristate 13-acetate (PMA) and ionomycin. PMA can diffuse into the T cell and activates the protein kinase C (PKC) (Ai et al., 2013) while the ionophore ionomycin activates Ca^{2+} signaling and PKC, too (Chatila et al., 1989). Together, PMA and Ionomycin unspecifically stimulate T cell activation by bypassing the TCR complex and its signaling cascade.

In detail, the murine splenocytes and GT cells were acquired by dissociation of the respective tissue as described in 3.2.1.2.5. In the end of this process, I resuspended the cells to a concentration of 2 x 10^6 (splenocytes) or 0.75 x 10^6 (GT cells)/100 µl in RPMI supplemented with 10 % (v/v) FCS, respectively. For each condition ($E7_{11-19}$-stimulated, $Surv_{96-104}$-stimulated and PMA/Ionomycin-stimulated) 100 µl of the cell suspension were pipetted into respective wells of a 96-well plate. To prevent intracellular trafficking of cytokine-containing vesicles, 96 µl of GS/GP medium were added to each well. GolgiStop™ (GS) containing monensin and GolgiPlug™ (GP) containing brefeldin A both impair transport within and from the Golgi

apparatus and therefore retain vesicles inside the cell instead of allowing them to secrete their cargo (Pohlmann et al., 1984; Lippincott-Schwartz et al., 1991). Finally, peptide-stimulated wells received 4 µl of a 500 µM dilution of peptide in GS/GP medium, resulting in an end concentration of 10 µM of peptide in the well. PMA/Ionomycin-stimulated wells received 2 µl of a 1 µg/ml PMA dilution and 2 µl of a 100 µg/ml ionomycin dilution in GS/GP medium, resulting in an end concentration of 10 ng/ml PMA and 1 µg/ml ionomycin, respectively. After an incubation at 37°C for 5 h, the cells were centrifuged at 2,000 rpm for 3 min at 4°C, which were also the parameters for subsequent centrifugations. Subsequently, the antibodies against the surface markers of interest were added in 50 µl staining buffer/well in their respective dilutions (Table 1). Zombie Aqua™ and Zombie Yellow™ served as dead cell exclusion dyes. For cells in experiments where only splenocytes were analyzed, the antibody panel for the FACS Canto II™ was used while the LSRFortessa™ panel was used in experiments examining both GT and splenocytes. Once the antibody incubation of 30 min at 4°C in the dark had passed, 150 µl of staining buffer/well were added and the cells were centrifuged. Then they were washed two more times with 200 µl staining buffer/well, meaning addition of staining buffer, centrifugation and discarding of supernatant. When the last supernatant had been discarded, the cells were resuspended in 100 µl of fixation/permeabilization solution/well. This solution fixes the surface antibodies on the cell as well as the membrane integrity while permeabilizing the membrane and thus enabling entry for intracellular antibodies later. After the incubation of 10 min at 4°C in the dark, 100 µl of wash buffer were added and the cells again centrifuged and washed two times with 200 µl wash buffer/well. Next, the antibodies against intracellular cytokines were added, diluted in 50 µl staining buffer/well.

Table 1. Antibody panels for FACS Canto II™ and LSR Fortessa™.

FACS Canto II™			**LSRFortessa™**		
Antigen	Fluorophore	Dilution	Antigen	Fluorophore	Dilution
CD3ε	APC-Vio®770	1:25	CD3ε	APC-Vio®770	1:25
CD4	FITC	1:200	CD4	PerCP-Vio®700	1:50
CD8a	PE	1:50	CD8a	PE	1:50
CD19	PE/Cy5.5®	1:100	CD44	BV711™	1:25
Zombie Aqua™		1:200	CD62L	PE/Cyanine5	1:100
			CD69	FITC	1:10
			CD103	VioBlue®	1:100
			Zombie Yellow™		1:100

IFNγ APC antibody was used for both panels in a 1:200 dilution while TNFα antibody was used in a 1:100 dilution for the FACS Canto II™ (eFluor450) and in a 1:50 dilution for the LSRFortessa™ (PE/Cyanine7) panel, respectively.

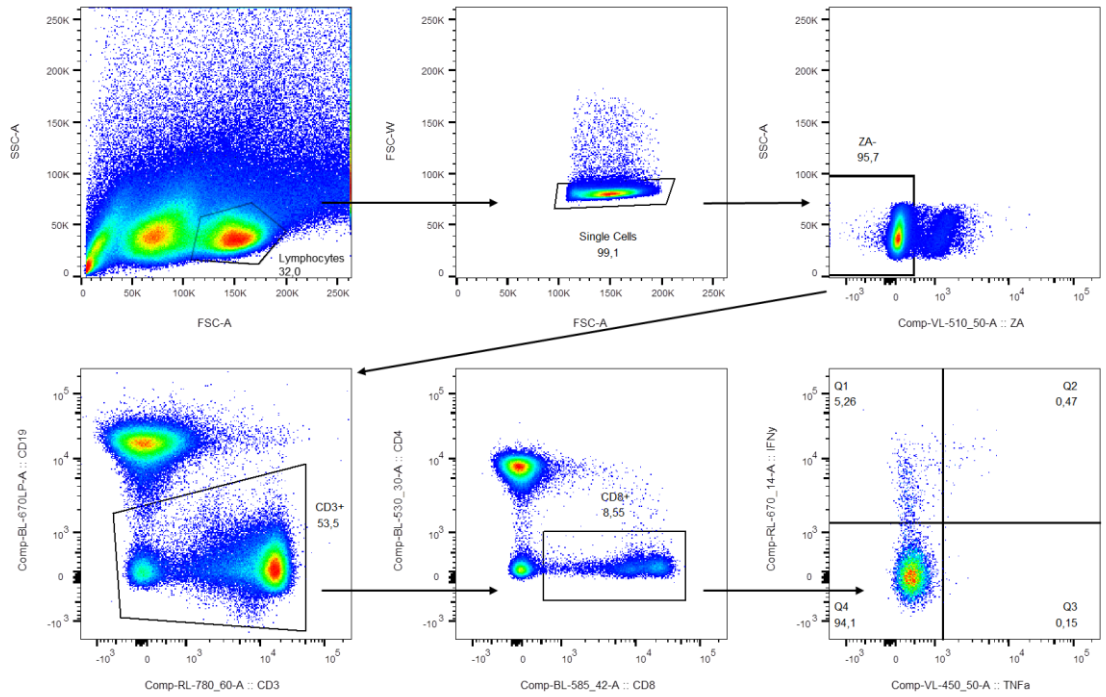

Figure 12. Gating strategy for FACS Canto II™-derived flow cytometry data. First, lymphocytes were gated on, followed by the exclusion of doublets and dead cells. Then, $CD3^+$ cells and $CD8^+$ cells were focused upon. Finally, the percentage of IFNγ and TNFα was assessed.

After another incubation at 4°C for 30 min in the dark, 150 µl of wash buffer were added, the cells washed two more times and then resuspended in an appropriate amount of fixation buffer, preserving the stained cells in the refrigerator until measurement.

The cell suspensions were analyzed at either the three-laser BD FACS CantoII™ or five-laser BD LSRFortessa™ with the BD Diva Software™ in the flow cytometry core facility (CFFC) of DKFZ. For final analysis, I used the FlowJo™ software. Exemplary gating strategies for both panels can be seen in Figure 12 and Figure 13, respectively. For gating $CD3^+$ cells mostly all cells from the parental gate were used as activated A2.DR1 $CD8^+$ T cells considerably downregulate $CD3^+$ expression (own observations). Therefore, only proceeding with the distinct $CD3^+$ cell population, one would lose many specific $CD8^+$ T cells in the analysis.

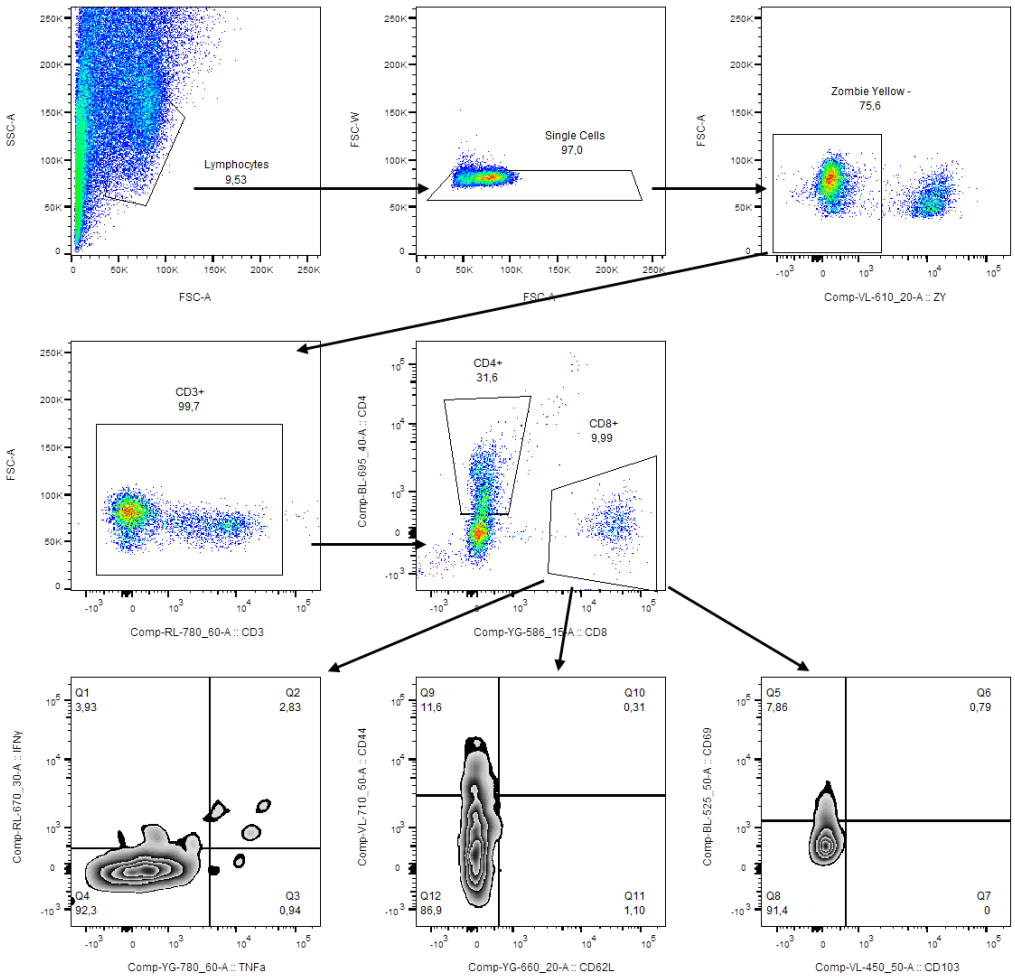

Figure 13. Gating strategy for LSRFortessa™-derived flow cytometry data. First, lymphocytes were gated on, followed by the exclusion of doublets and dead cells. Then, $CD3^+$ cells and $CD8^+$ cells were focused upon. The CD8+ cells were examined for their expression of IFNγ and TNFα, CD44 and CD62L and CD69 and CD103, respectively.

3.2.1.5.3 Cell sorting

Flow cytometry can also be used to single-cell sort cell suspensions. In this work, tumor cell line suspensions were single-cell sorted into 96-well plates (1 cell/well) based upon their HHD molecule expression. The cells were detached from their cell culture vessel as described in 3.2.1.2 and centrifuged at 2,000 rpm for 3 min. After discarding the supernatant, I added the HLA-A2 FITC antibody in a dilution of 1:100 in 150 µl staining buffer to the cells. They were incubated for 30 min at 4°C in the dark and afterwards washed three times with 1 ml staining buffer, meaning addition of staining buffer, centrifugation at 2,000 rpm for 3 min and discarding of supernatant. Afterwards, 500 µl staining buffer were added and the cell suspension was

filtered through a 40 µm cell strainer. The cells were subsequently single-cell sorted into a 96-well plate with the BD FACS Aria II™ by a member of the DKFZ CFFC.

3.2.1.6 Cellular assays

3.2.1.6.1 VITAL-FR cytotoxicity assay

The VITAL-FR cytotoxicity assay can be used to assess the specificity or cytotoxicity of T cells or - as is the case in this work - to find out if a given target cell line can be killed by specific T cells. In principle, target cells of interest (here: newly established HPV16 E7-positive cell lines) are co-cultured with a cell line that does not present the epitope of interest on its surface. Here, the $HPV16^-$ A2.DR1 sarcoma cell line 2277-NS (Quandt, 2014) was used. Both cell lines are labeled with different fluorescent marker molecules (Stanke et al., 2010). Then, CTLs specific for the HPV16 epitope $E7_{11-19}$ were added in increasing numbers to the co-cultured cells. After 48 h, the cell suspensions were analyzed by flow cytometry on the BD FACS CantoII™ to examine the ratio of labeled target cells with T cells in comparison to those without.

First, I harvested both the $HPV16^+$, as well as the $HPV16^-$ target cells as described in 3.2.1.2.1 and centrifuged them at 1,500 rpm for 4 min, which were also the parameters for subsequent centrifugations. The cell lines were diluted in PBS to a concentration of 1 x 10^6 cells/ml and then stained with the fluorescent dyes. HPV^+ cells were stained with 20 µl/1 x 10^6 cells of a 100 µM CFSE/PBS solution while HPV^- cells were stained with 2.5 µl/1 x 10^6 cells of a 100 µM Far Red/PBS solution. After an incubation of 15 min at 37°C, the cells were centrifuged, washed two times with 1 ml RPMI/10 % FCS per 1 x 10^6 cells and centrifuged again. Then, they were resuspended in RPMI/10 % FCS and transferred to a 6-well plate at 1 x 10^6 cells in 3 ml/well. The next day the cells were harvested by trypsinization, counted and 250,000 Far Red-labeled cells were mixed with 250,000 CFSE-labeled cells. If the target cell line had to be pulsed with either cognate $E7_{11-19}$ or non-cognate $Surv_{96-104}$ peptide prior to mixing, the cells were incubated for 90 min at 37°C with 1 ml/1 x 10^6 cells of a 10µM peptide dilution in RPMI/10% FCS. After a centrifugation, the cell mixture was washed three times with 1 ml RPMI/10 % FCS and was resuspended after the last centrifugation to a concentration of 1,000 cells/50 µl. Finally, the cells were transferred into a flat-bottomed 96-well plate by pipetting 100 µl into each well, resulting in 1,000 CFSE and 1,000 Far Red-labeled cells in each well, respectively.

After setting up the co-culture, peptide-specific T cells had to be added. These derived from vaccination experiments and were obtained and cultured as stated in 3.2.1.2.2. Prior to adding $CD8^+$ T cells, they first needed to be isolated as a splenocyte mixture contains many different cell subsets. For this, I used the mouse $CD8^+$ T Cell Isolation Kit from Miltenyi Biotec according to the manufacturer's instruction. In brief, the splenocytes were resuspended in 40 µl of magnetic-activated cell sorting (MACS®) buffer per 1 x 10^7 cells and 10 µl of the biotin-labeled antibody cocktail were added. These antibodies bound various $CD8^-$ cells in the mixture. After a 5 min incubation at 4°C, 30 µl of MACS buffer and then 20 µl of anti-biotin microbeads were added. The suspension was incubated for 10 min at 4°C and then applied to an LS column. This column was previously placed into the magnetic field of a MACS separator. While flowing through the LS-column all $CD8^-$ cells bind to magnetic microbeads via the antibodies were removed from the cell suspension. The column was washed with 3 ml to collect all of the flow through and the resulting $CD8^+$ T cell-enriched suspension was centrifuged in preparation for the next steps. The effector cells were then adjusted to increasing concentrations in IL-2 medium (RPMI/10 % FCS supplemented with 20 IU IL-2/ml) and then 10 µl of the respective effector cell suspension was added to the prepared plate with the target cells. After addition of 90 µl IL-2 to each well, the plate was incubated for 48 h at 37°C. In the end, the experimental plate contained 1,000 CFSE-labeled HPV^+ cells, 1,000 Far Red-labeled HPV^- cells and 0, 333, 1,000, 3,333, 10,000, 20,000 or 40,000 CTLs in 200 µl medium with 10 IU/ml IL-2/well.

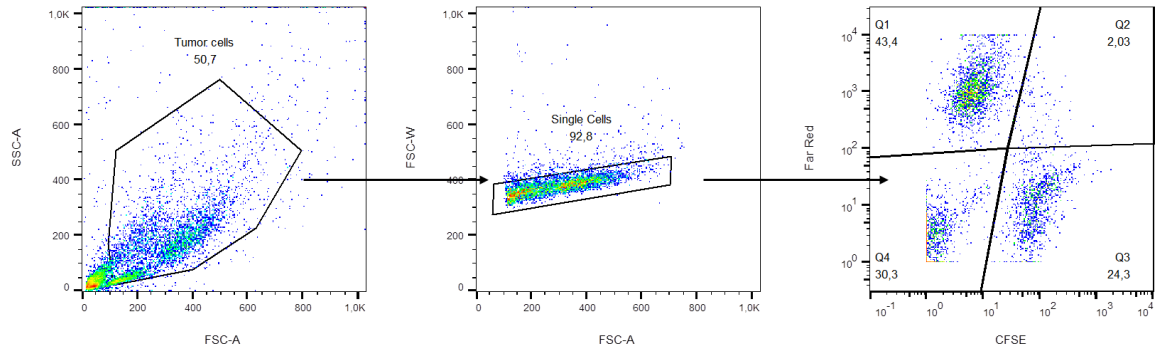

Figure 14. Gating strategy for VITAL-FR assay data. After gating for the cells in the suspension, single cells were examined for Far Red^+ (Q1) and $CFSE^+$ (Q3) cells. T cells were found in Q4.

After the incubation, the cells were trypsinized and transferred to a new 96-well plate with intermittent centrifugations of the plates at 1,500 rpm for 4 min, as well as the contents of each

well's supernatant to ensure a high cell yield. Finally, the cells were resuspended in 95 µl staining buffer and measured at the BD FACS CantoII™. For final analysis I used the FlowJo™ software, the gating strategy for VITAL-FR data can be seen in Figure 14. The specific killing was then calculated using the following formula:

Equation 1. Calculation of specific killing in VITAL-FR assays according to Stanke et al. (2010).

$$Specific\ killing\ [\%] = 100 - \frac{\left(\frac{\%\ CFSE^{+} specific\ target\ cells\ (with\ T\ cells)}{\%\ Far\ Red^{+}\ unspecific\ target\ cells\ (with\ T\ cells)}\right)}{\left(\frac{\%\ CFSE^{+} specific\ target\ cells\ (without\ T\ cells)}{\%\ Far\ Red^{+}\ unspecific\ target\ cells\ (without\ T\ cells)}\right)}\ x100$$

3.2.1.6.2 Luminescence measurements

The luciferase enzyme was used in this work as an *in vivo* marker for tumor cell detection. For detection of bioluminescence *in vitro*, a microplate assay was used. For this, I put 10,000 cells of the respective cell line in replicates into wells of a 96-well plate, or pipetted only medium as a control into the wells. After addition of 100 µl Promega luciferase assay solution/well, luminescence was measured in either the Mithras^2 LB 943 or GloMax® Explorer Multimode Microplate Reader.

3.2.1.7 Mass spectrometry and immunopeptidomics

The immunopeptidomics results derived from mass spectrometry (MS) measurements shown in this thesis were completely prepared, generated and analyzed by Jonas Förster with help from Rebecca Köhler.

In brief, HLA immunoprecipitation (IP) and peptide isolation were performed according to published protocols (Bassani-Sternberg et al., 2016; Chong et al., 2018). For the targeted LC-MS analysis, liquid chromatography (UltiMate 3000, Thermo Fisher Scientific) was coupled to an Orbitrap Exploris™ 480 mass spectrometer (Thermo Fisher Scientific) and parallel reaction monitoring (PRM) was used to generate chromatograms for the peptides of interest (Peterson et al., 2012). Afterwards, MS2 data was analyzed using the Skyline software (MacLean et al., 2010) and data was visualized with R with the 'tidyverse' suite of packages (RC Team, 2013; Wickham et al., 2019). To assess peptide detection, acquired chromatograms were compared to reference chromatograms acquired from synthetic peptides. To ensure optimal assessment of co-elution, the retention time axis of the reference chromatogram was transformed linearly according to adjacent anchor peptides that were captured in both assays.

3.2.2 *In vivo* methods

All *in vivo* experiments were performed with A2.DR1 mice kept in IVC in the DKFZ 'Center for preclinical research' (ZPF) where they were checked every day by animal caretakers. For experiments, 6 - 20 week old female mice were arranged into age-matched groups and pooled at least one week prior to experimental start. The mice were anesthetized with 1 – 4 % isoflurane in O_2 for all interventions, except for weighing and s.c. tumor measurements. If the mice were kept in anesthesia for a longer time, they were lain onto a warming pad and their eyes were treated with Vidisic® Eye gel EDO® to prevent drying and blindness.

3.2.2.1 Vaginal applications

All ivag. vaccinations and applications were preceded by synchronization of the mice' estrus cycles with the female sex hormones β-estradiol and medroxyprogesterone acetate according to Domingos-Pereira et al. (2013). B-estradiol is a steroidal sex hormone belonging to the estrogens, peaking prior to ovulation in the estrus stage of mice (Gruber et al., 2002; Caligioni, 2009). Medroxyprogesterone acetate on the other side is a commercially available form of progesterone that is used as a contraceptive in humans (Schindler et al., 2008). In mice, progesterone has its highest levels at the metestrus and diestrus stages (Ajayi & Akhigbe, 2020). The medroxyprogesterone acetate treatment induces a diestrus-like state with many leukocytes in the GT as found in vaginal washes (De Gregorio et al., 2018).

Six days prior to experiments including vaginal treatments, I injected mice s.c. with 0.1 µg of β-estradiol in 100 µl of peanut oil into the flank. One day later, the animals received 2 mg of medroxyprogesterone acetate (Depo-Clinovir®/Depo-Provera®) s.c. in 100 µl PBS into the flank. After four more days, i.e. one day before experimental start, a vaginal swab was taken from each mouse to check its stage of the estrus cycle as experiments had to start in the diestrus state, which facilitates uptake of cells and compounds. For this, 40 µl of PBS were pipetted into the mouse vagina and taken up again. The PBS was mixed with 40 µl of FCS and the mixture dropped onto a glass slide. The vaginal smears were then stained with a Giemsa staining solution (5 ml ddH_2O + 150 µl methanol + 125 µl Giemsa stock solution) for 15 min and dried for 15 min. Afterwards, the estrus stage was microscopically assessed. The assessment of the stage was abandoned after some experiments as all swabbed mice were in metestrus or diestrus upon examination.

All ivag. applications were preceded by a treatment with N-9, which is a commercially available surfactant used as a spermicide in contraception (Iyer & Poddar, 2008). It disrupts the vaginal mucosa and facilitates accessibility of the vaginal basement membrane (Çuburu et al., 2019). Six h before an ivag. application mice were instilled ivag. with 20 µl of 4 % N-9 in ddH_2O (v/v). Afterwards their bottoms were kept in an elevated position for 15 min to prevent discharge of the N-9 solution. After the 6 h waiting period, the vagina was washed 5x with 50 µl PBS before treatment to remove residual N-9.

3.2.2.2 Tumor inoculation

Before preparation for tumor challenge, I harvested the tumor cells for tumor inoculation according to 3.2.1.2.1, counted them and washed them twice with PBS.

3.2.2.2.1 Subcutaneous

The tumor cells were resuspended in a 1:2 Matrigel/PBS dilution and were kept on ice until injection into mice. Before injection, the flank of the animals was shaved to enable easy access to the forming tumor. Then, the cell suspension was rigorously inverted and 100 µl were injected s.c. into the shaved flank of the mice. While the animal caretakers checked the mice every day for signs of distress, I weighed the mice regularly and measured the size of their tumors with digital calipers. Mice were killed upon signs of distress, at least 20 % weight loss or if the tumor size was ≥ 1,000 mm³. The volume was calculated as follows:

Equation 2. Calculation of s.c. tumor volume. l = length, w=width.

$$V = \frac{4}{3}\pi((0.5\ l)(0.5w)^2)$$

3.2.2.2.2 Intravaginal

Vaginal tumors were instilled after the pretreatment as described in 3.2.2.1 and 6 h after N-9 treatment. The N-9 causes mucosal disruptions and allows tumor cells to enter the emerging wounds. Once they heal, the tumor cells are trapped in the epithelium and form a tumor there (Decrausaz, Goncalves, et al., 2011). The tumor cells were checked before every ivag. instillation for their continued expression of luciferase as described in 3.2.1.6.2. After the N-9 had been washed out of the murine vagina (see above), 20 µl of a tumor cell suspension (5 x 10^4 – 1 x 10^6 cells) in PBS was carefully pipetted into the vaginal cavity. Then the bottoms of the mice were put into an elevated position and kept there for 1 h to prevent discharge of the

tumor cells. During the waiting, the animals' lower bellies were shaved to facilitate bioluminescent imaging later. The animal caretakers checked the mice every day for signs of distress while I weighed the animals regularly and monitored tumor growth with the IVIS® Lumina III imaging machine. Mice were killed upon signs of distress, at least 20 % weight loss or vaginal bleeding.

3.2.2.3 IVIS® Lumina III measurements

For bioluminescent imaging of ivag. tumors, I injected mice intraperitoneally (i.p.) with 150 mg sterile D-luciferin in PBS per kg body weight. They were then put into the IVIS® Lumina III imaging machine and the tumors' bioluminescent signals were acquired every 2 min for 20 min in total with the automatic settings of the Living Image® operating software in place. For analysis with the software, a region of interest (ROI) was placed on the torso of each mouse and the measured photons/s were recorded. The highest photon flux value for each mouse on each day of imaging was used for final analysis.

3.2.2.4 MRI measurements

Magnetic resonance imaging (MRI) was carried out by the DKFZ small animal imaging core facility using a Bruker BioSpec 3Tesla device (Ettlingen, Germany). For imaging, the mice were anesthetized with 3.5 % sevoflurane in air. For lesion detection, T2 weighted imaging was performed using a T2_TurboRARE sequence: TE = 48 ms, TR = 2000 ms, FOV 30x30 mm, slice thickness 1 mm, averages = 8, Scan Time 6 m 24 s, echo spacing 12 ms, rare factor 8, slices 9, image size 192 x 192 (Zottnick et al., 2020).

3.2.2.5 Vaccination

3.2.2.5.1 Subcutaneous

Amphiphilic peptide constructs i.e. lipopeptides (LPP) were produced by peptides & elephants, the Eichmüller group of DKFZ or Dr. Philipp Uhl. If not stated otherwise I vaccinated mice s.c. into the flank with 50 nmol LPP-$E7_{11-19}$ and 50 µg poly(I:C) in 100 µl PBS.

SiO_2 nanoparticles (SiNP) were produced by Armin Kübelbeck and Dr. Eva Feidt of Silvacx. KKK-W-Cit-$E7_{11-19}$ @SiO_2-Arg (25 nmol peptide) and 50 µg poly(I:C) in 100 µl PBS were injected s.c. into the flank of the mice. Alternatively, they received 'empty' SiNP, i.e. without KKK-W-Cit-$E7_{11-19}$.

3.2.2.5.2 Intravaginal

For ivag. vaccinations I pretreated the mice according to 3.2.2.1 and instilled N-9 6 h prior to instillation of vaccine compounds if not stated otherwise. After washing the vagina 5x with 50 µl PBS, 20 µl of the vaccines were instilled. Afterwards the mice' bottoms were kept in an elevated position for 20 min to prevent discharge.

If not stated otherwise, for LPP vaccination, 50 nmol LPP-$E7_{11-19}$ and 50 µg poly(I:C) in 20 µl PBS were instilled ivag.

Of SiNPs, KKK-W-Cit-$E7_{11-19}$@SiO_2-Arg (25 nmol peptide) and 50 µg poly(I:C) in 20 µl PBS were instilled. Alternatively, the mice received 'empty' SiNP, i.e. without KKK-W-Cit-$E7_{11-19}$.

Liposomes covered by cell-penetrating peptides were produced by Dr. Philipp Uhl or Dr. Mikko Gynther. Liposomes containing different cargos as stated in the respective figure legends were instilled in 20 µl PBS.

3.2.3 Statistics

Statistical analysis was performed with the Graphpad Prism®7 software. The individual statistical testing method is stated in the respective figure legend.

4 Results

4.1 Establishment of an orthotopic tumor model

For establishing a syngeneic A2.DR1 HPV16 $E6^+$ and $E7^+$ cell line for orthotopic tumor formation, which can be used as a model for immunotherapeutic approaches against HPV16 malignancies, I tested different approaches for cell line generation. The first one was the further development of the already established A2.DR1 HPV16 $E6^+$ and $E7^+$ cell line PAP-A2 (Kruse et al., 2018). As this cell line was already tumorigenic due to its sarcoma origin it needed to be made bioluminescent for *in vivo* use. Alternatively and more suitable to the purpose was the second approach: an A2.DR1 cell line dependent on the HPV16 oncoproteins for survival. Such cells will become senescent upon HPV protein loss and therefore cannot form tumors anymore. This resembles the clinical situation more closely than the PAP-A2 cell line. The HPV16-dependent cell line needed to be transfected with the two HPV oncoproteins and vaccination targets E6 and E7, an additional activated oncogene for tumorigenicity, as well as luciferase for *in vivo* detection of tumors.

4.1.1 PAP-A2

PAP-A2 cells are A2.DR1 2277-NS sarcoma cells that were previously transduced with E6 and E7 (Kruse et al., 2018). The goal was to transfect PAP-A2 cells with an S/MAR vector containing firefly luciferase and $HRAS^{G12V}$. Although the oncogene was not necessary for tumorigenic transformation of PAP-A2 cells, the vector was designed by our group to be a versatile tool for transfection of various cell lines.

4.1.1.1 Generation and verification of S/MAR-UbC-Hras-CMV-Luc vector

The S/MAR vector 'S/MAR-UbC-Hras-CMV-Luc' containing $HRAS^{G12V}$, an activated form of the oncogene, as well as luciferase and a blasticidin resistance gene with ubiquitin C (UbC) and cytomegalovirus (CMV) promoters, respectively, was conceptualized by Dr. Matthias Bozza and Dr. Sebastian Kruse. It was then generated by Dr. Sebastian Kruse and Alexandra Klevenz prior to this work (Appendix Figure 1). After the vector was synthesized, I verified if the necessary genes were in place by a restriction digest utilizing restriction sites for the enzymes NheI, XhoI, AseI and EcoRV. The restriction digest was analyzed with an agarose gel (Figure 15A, left) and compared to the outcome predicted by the software SnapGene® (Figure 15A, right). As the bands were found to be on the predicted height, I sent the vector DNA for further

verification by Sanger sequencing to Microsynth Seqlab. Sanger sequencing also confirmed the identity of the plasmid (Figure 15B).

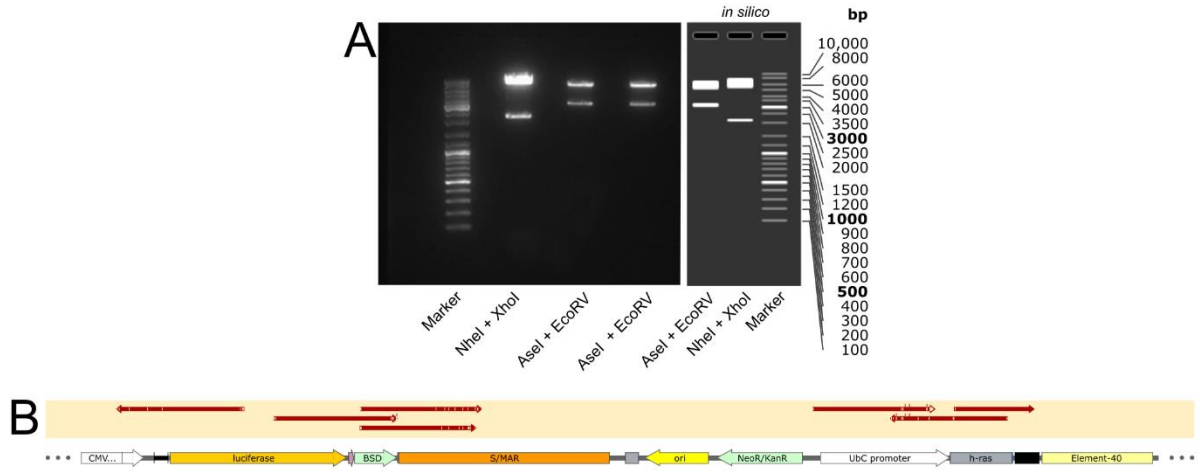

Figure 15. Verification of successful synthesis of S/MAR-UbC-Hras-CMV-Luc vector. (A) Restriction digest and subsequent gel electrophoresis (left) were performed with the completed vector and indicated restriction enzymes. The right side depicts the *in silico* predicted gel. (B) Alignment of sequenced parts of the vector. Sequencing was done by Microsynth Seqlab GmbH, Göttingen with self-designed primers for the inserted luciferase and resistance against blasticidin genes. Sequencing results were aligned to the vector map with SnapGene®.

4.1.1.2 Transfection and selection

After vector identity had been confirmed, I transfected PAP-A2 cells in a 1:3 ratio of 2 µg vector DNA to 6 µl FuGene transfectant reagent. As the amount of time needed for successful transfection differs with different cell lines, both 24 h and 48 h were tested as incubation times. Subsequent luminescence measurements confirmed uptake of the plasmid and production of luciferase protein by detection of light from the cells in comparison to control conditions (Figure 2A). As the cells transfected for 48 h were more luminescent, they were chosen for further use. The expression of the previously and newly introduced proteins, HPV16 E6/E7 and $HRAS^{G12V}$, respectively, was checked by Western blotting. It showed that HPV16 E6 and E7 were still expressed by the cells. However, presence of $HRAS^{G12V}$ could not be detected in transfected PAP-A2 cells (Figure 2B). Fortunately, this protein is not necessary for the sarcoma cell line PAP-A2 to be tumorigenic. An antibiotic titration of untransfected PAP-A2 cells resulted in an ideal blasticidin concentration of 1 µg/ml for the selection medium (data not shown). The new, luciferase-expressing PAP-A2 cell line was named ‘PAP-A2-luc’.

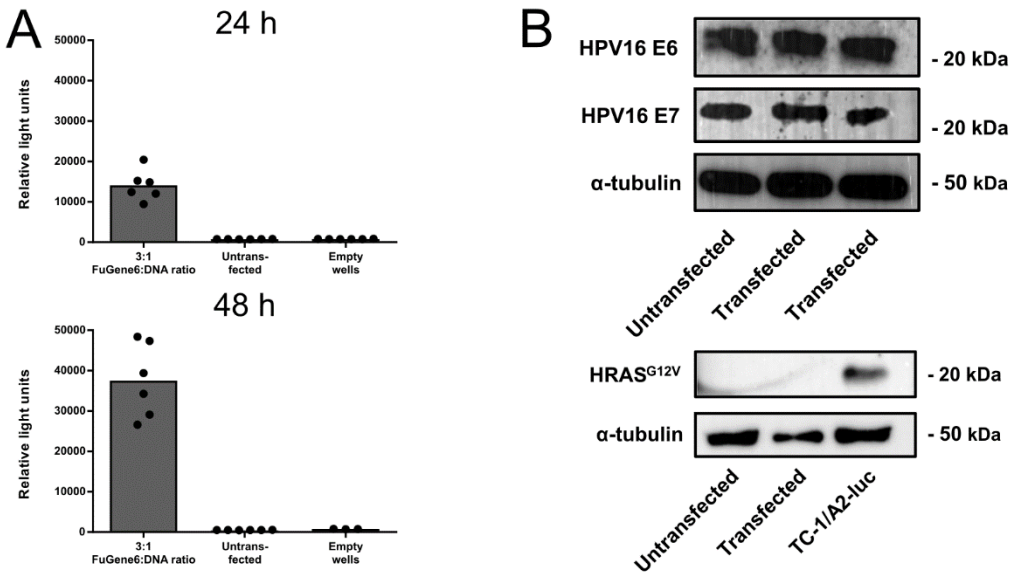

Figure 16. Characterization of PAP-A2 cells transfected with S/MAR-UbC-Hras-CMV-Luc. PAP-A2 cells were transfected with the S/MAR-UbC-Hras-CMV-Luc vector in a FuGene6:DNA ratio of 3:1. (A) Luminescence measurement of transfected PAP-A2 cells after addition of D-luciferin after 24 h (top) and 48 h (bottom) of incubation with transfection reagent in comparison to untransfected PAP-A2 cells and empty wells. (B) Western blots for detection of HPV16 proteins E6 and E7 (top) and $HRAS^{G12V}$ (bottom) in transfected PAP-A2 cells. HPV16 E6 and E7 expression was assessed in two batches of transfected PAP-A2 cells in comparison to untransfected ones. Expression of $HRAS^{G12V}$ was assessed in transfected as well as untransfected PAP-A2 cells and TC-1/A2-luc cells, which are known to express $HRAS^{G12V}$.

4.1.1.3 Test of subcutaneous tumorigenicity and reisolation of resulting tumors

To test if the PAP-A2-luc cells were still sufficiently tumorigenic, I injected 1.5 x 10^6 of the transfected cell pool s.c. into three mice in a matrigel-PBS-solution. All of the mice developed tumors and had to be euthanized due to the tumor size (Figure 17A).

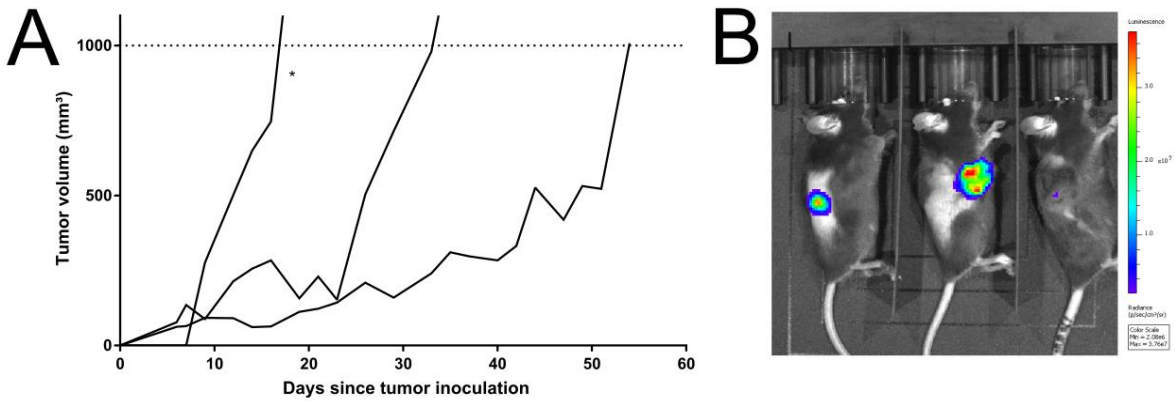

Figure 17. S.c. tumor growth of PAP-A2-luc cells in A2.DR1 mice. 1.5 x 10^6 PAP-A2-luc cells were injected s.c. in 100 µl of a 1:2 matrigel:PBS mixture into the flank of three A2.DR1 mice. Subsequently, the tumor volumes were measured and luminescence imaging after i.p. injection of 200 µl 15 mg/ml D-luciferin in PBS was performed. Mice were killed upon tumors reaching a volume of 1 cm^3. (A) Tumor growth curve of s.c. PAP-A2-luc cells over time in three mice. The asterisk indicates the mouse whose tumor was resected for further development of the cell line. (B) Luminescence measurement of mice in A) on day 14 after tumor inoculation.

Additionally, it was checked via luminescent imaging if bioluminescence could also be detected *in vivo*, which was the case (Figure 17B). All three tumors were reisolated and the cell suspension of one of them (marked with an asterisk in Figure 17A) was single-cell sorted based on high expression of the HHD molecule on the cells' surface. The single-cell sorted clonal PAP-A2-luc cell lines were used for further development of the cell line.

4.1.1.4 Characterization of single-cell sorted clonal cell lines

Twelve stably growing clonal cell lines were obtained from single-cell sorting, which all displayed different levels of luminescence (Figure 18). Afterwards, I handed the development of the PAP-A2-luc cell line over to a master's student, Alessa Henneberg (née Voß) who was supervised by me.

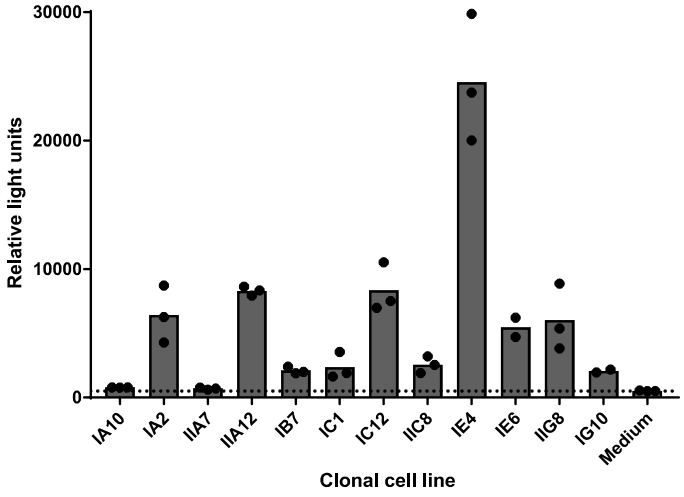

Figure 18. Luminescence of PAP-A2-luc clonal cell lines. 1 x 10^4 cells per cell line were plated in triplicates into a 96 well plate. After addition of D-Luciferin, luminescence was measured over 10 s/well. Shown are the means of triplicate samples.

4.1.1.5 Development of PAP-A2-luc cell line (as done by Alessa Henneberg)

The tumorigenicity of the PAP-A2-luc clonal cell lines was tested again s.c.. The tumors were reisolated and dissociated, which was followed by a check for vaginal tumor formation by the new, now twice reisolated cell lines (Figure 19A). It was also checked in a VITAL-FR cytotoxicity assay if the chosen PAP-A2-luc cell lines could be killed by $E7_{11-19}$ specific CTLs. However, this was only possible when the cells were previously pulsed with the cognate peptide (Figure 19B). The development of the PAP-A2-luc cell lines can be read up in the resulting M.Sc. thesis (Voß, 2020). As the PAP-A2-luc cells could not be killed by specific T cells, the

cell lines were unsuited for use in therapeutic vaccination experiments. Therefore, further development of PAP-A2-luc was abandoned.

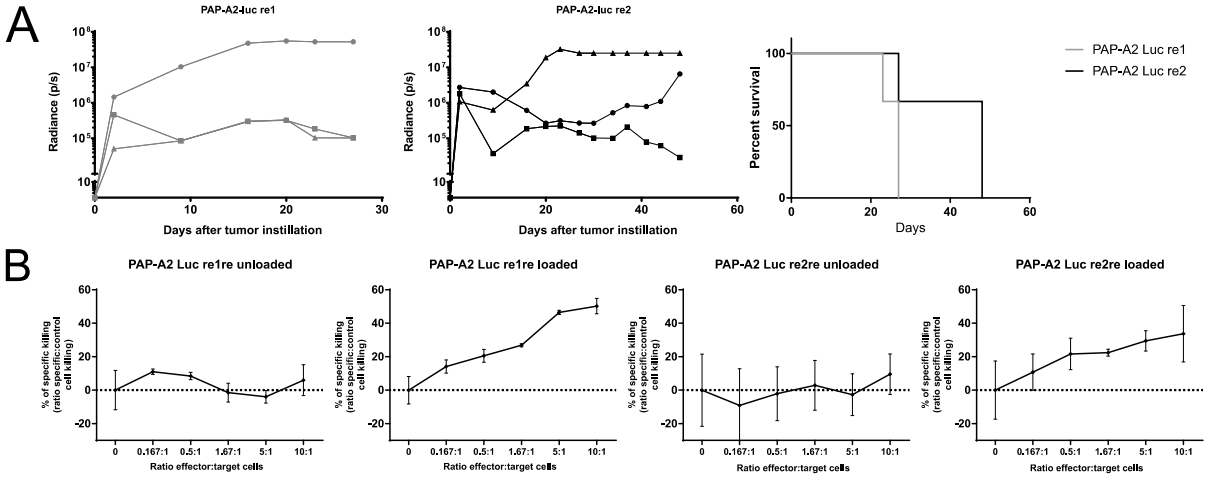

Figure 19. Establishment of the PAP-A2-luc cell line. (A) Tumor growth and survival curves of three mice per PAP-A2-luc cell line as assessed by luminescence measurements. The two cell lines (PAP-A2-luc re1 and PAP-A2-luc re2) derived from PAP-A2-luc s.c. tumors that were reisolated. Mice were killed upon visible signs of distress or vaginal bleeding. (B) Specific killing of PAP-A2-luc cell lines either unpulsed (‚unloaded') or pulsed (‚loaded') with $E7_{11-19}$ as assessed by a VITAL-FR cytotoxicity assay. CFSE-labeled PAP-A2-luc cells ('target') were co-cultured with Far Red-labeled 2277-NS cells, mixed with $E7_{11-19}$-specific T cells (‚effector') in different ratios and analyzed 48 h hours later via flow cytometry. Specific killing was calculated according to Equation 1. Shown are the means of three replicates. Experiments performed by Alessa Henneberg; figures adapted from Voß (2020).

4.1.2 HPV16 E6 and E7-dependent cell line E6/7-lucA2

The first choice of source material for a newly generated, HPV16-dependent cell line were primary, neonatal A2.DR1 keratinocytes. However, keratinocytes are notoriously difficult to transfect or to transduce, which was also the case with HPV16 E6 and E7, and they did not grow *in vivo* (data not shown). Therefore, the template used for the new cell line to be generated was the TC-1 cell line from C57BL/6 mice (Lin et al., 1996), which are lung cells expressing HPV16 E6 and E7 as well as $HRAS^{G12V}$. A2.DR1 lung cells expressing HPV16 E6 and E7 were previously generated by Dr. Sebastian Kruse and Dr. Ruwen Yang (vector map see Appendix Figure 2). These cells ('$E6^+E7^+$ lung cells') were then used by me as a basis for the establishment of the new cell line.

4.1.2.1 Transfection and selection

The $E6^+E7^+$ lung cells were transfected in different FuGene:DNA ratios with the same vector as used for PAP-A2 (see 4.1.1.1). Luminescence was detected after addition of the substrate after 24 h as well as after 48 h of incubation with transfectant reagent (Figure 20A). Western

blots then confirmed that, the transfected $E6^+E7^+$ lung cells still expressed the previously introduced proteins HPV16 E6 and E7 (Figure 20B, top). In contrast to PAP-A2-luc cells, they indeed expressed $HRAS^{G12V}$ (Figure 20B, bottom).

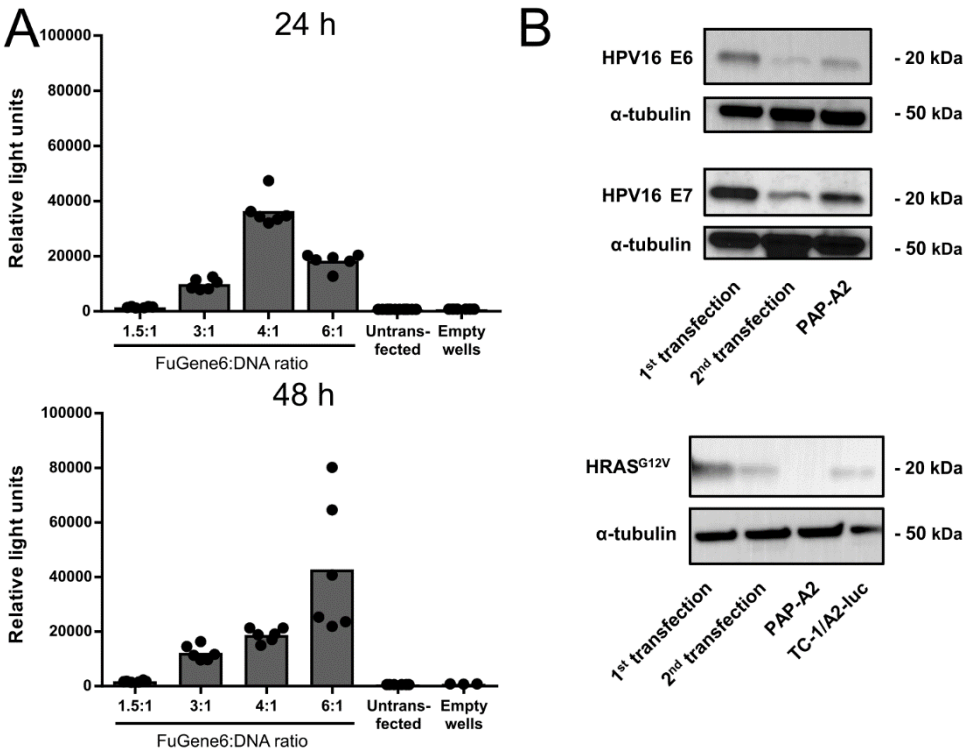

Figure 20. Characterization of $E6^+E7^+$ lung cells transfected with S/MAR-UbC-Hras-CMV-Luc. HPV16 E6 and E7-expressing A2.DR1 lung cells were transfected with the S/MAR-UbC-Hras-CMV-Luc vector in the indicated FuGene6:DNA ratios. (A) Luminescence measurement of transfected $E6^+E7^+$ lung cells after addition of D-luciferin after 24 h (top) and 48 h (bottom) of incubation with transfection reagent in comparison to untransfected $E6^+E7^+$ lung cells and empty wells. (B) Western blots for detection of HPV16 proteins E6 and E7 (top) and $HRAS^{G12V}$ (bottom) in transfected $E6^+E7^+$ lung cells. HPV16 E6 and E7 expression was assessed in two batches of transfected $E6^+E7^+$ lung cells and PAP-A2. Expression of $HRAS^{G12V}$ was assessed in two batches of transfected $E6^+E7^+$ lung cells, PAP-A2 and TC-1/A2-luc, which are known to express $HRAS^{G12V}$.

4.1.2.2 Test of subcutaneous tumorigenicity and reisolation of resulting tumors

The transfected cell pool, hereafter named 'E6/7H-luc' was then injected s.c. into the flank of four mice to test its tumorigenicity. All mice developed tumors (Figure 21A), which stood in contrast to $E6^+E7^+HRAS^{G12V-}$ - lung cells that prior to this work were injected s.c. into A2.DR1 mice by Dr. Sebastian Kruse and did not lead to tumor formation (data not shown). The light emitted from the E6/7H-luc cells was also sufficient to be detected in *in vivo* luminescence measurements (Figure 21B). Subsequent to euthanizing the animals, their tumors were reisolated and one of them (labeled with an asterisk in Figure 21A) was single-cell sorted based on high expression of the HHD molecule on the cells' surface (Figure 21C).

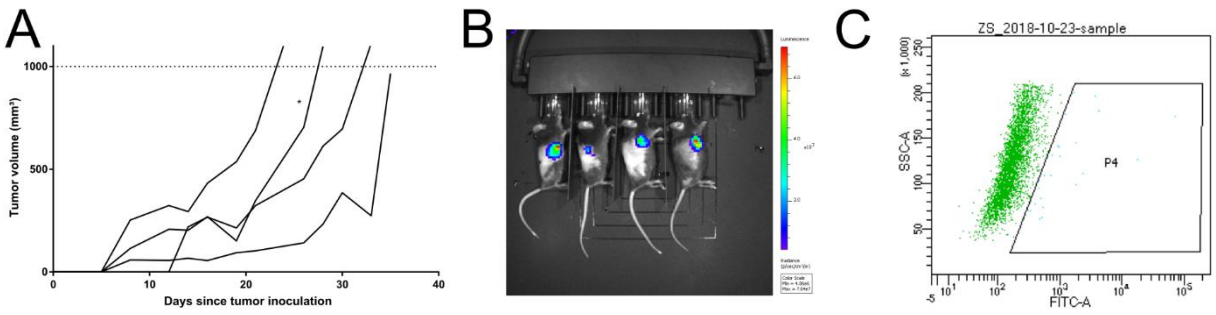

Figure 21. S.c. tumor growth of E6/7H-luc cells in A2.DR1 mice. 5 x 10^6 E6/7H-luc cells were injected s.c. in 100 µl of a 1:2 matrigel:PBS mixture into the flank of four A2.DR1 mice. Subsequently, tumor volumes were measured and luminescence imaging after i.p. injection of 200 µl 15 mg/ml D-luciferin in PBS was performed. Mice were killed upon tumors reaching a volume of 1 cm^3 or upon visible sign of distress. (A) Tumor growth curve of s.c. E6/7H-luc cells over time in four mice. The asterisk indicates the mouse whose tumor was resected for further development of the cell line. (B) Luminescence measurement of mice in A) on day 21 after tumor inoculation. (C) Single cell sorting of isolated tumor cells of the mouse indicated in A) for clones with high HLA-A2/HHD expression as indicated by anti-HLA-A2- FITC staining.

4.1.2.3 Establishment of a first cell line

After single-cell sorting I cultured the cells, which resulted in 13 clonal cell lines. These were then characterized for the properties I deemed to be important for the new tumor model: HHD expression (Figure 22A), luminescence (Figure 22B) and the expression of the proteins E6, E7 and $HRAS^{G12V}$ (Figure 22C). All markers were still detectable in all cell lines, albeit in different levels. The criteria for the desired cell line were that the cells express enough HHD to be able to present HPV16 epitopes to CTLs. However, there should not be too much HHD on the surface to prevent easy detection and elimination by the immune cells and also not too little HHD to prevent NK cell-mediated killing. Second, the cells had to express detectable levels of luciferase. Third, E6 and especially E7 had to be expressed on a sufficient level to ensure epitope presentation on the cell surfaces. Finally, $HRAS^{G12V}$ had to be expressed and therefore detectable. Resulting from these criteria I decided to move forward in the development of the cell line with the clonal lines IH11 (low HHD, high luminescence, high E7), IIG6 (high HHD, low luminescence, high E7) and IVA4 (high HHD, low luminescence, high E7).

These clonal cell lines were then injected s.c. into three mice per cell line. All of the cell lines proved to be tumorigenic and one tumor of each cell line was reisolated (indicated by asterisks in Figure 23). The reisolated cell lines (‘IH11re’, ‘IIG6re’, ‘IVA4re’,) were then tested for their ivag. tumorigenicity by instilling 1 x 10^6 cells per cell line into the vagina of three mice each. Tumor formation was only detected in all three mice for IH11re while one mouse each for the other two cell lines did not develop a tumor (Figure 24A, B).

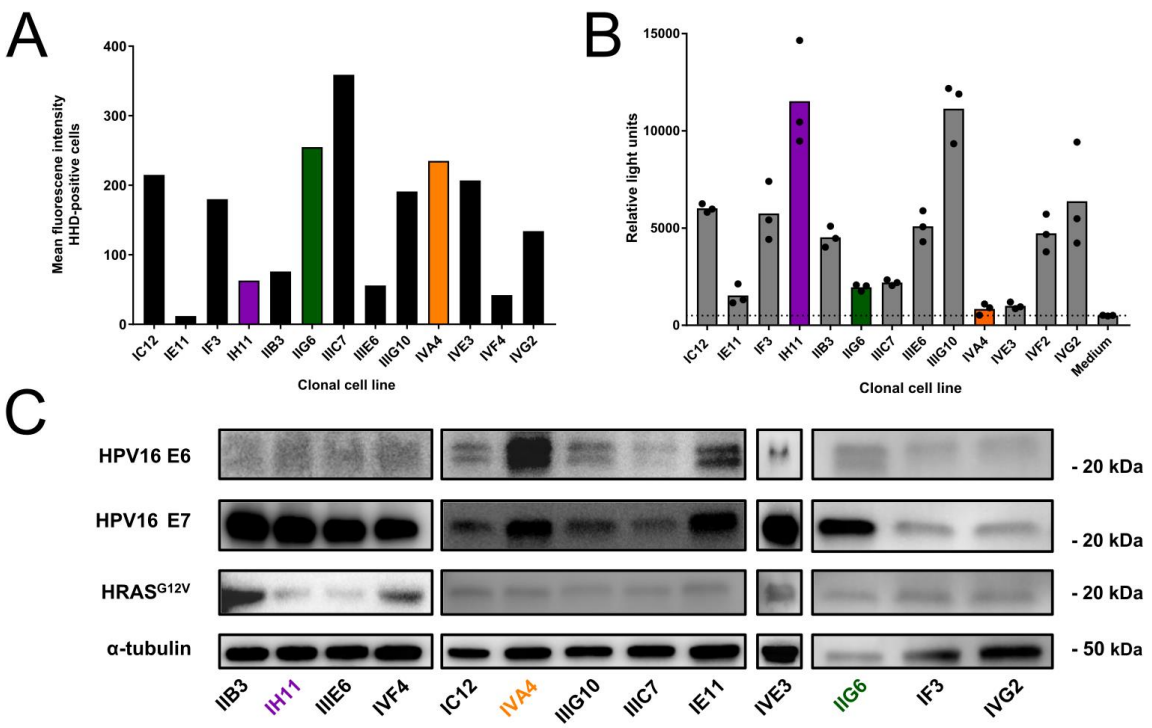

Figure 22. Characterization of E6/7H-luc clonal cell lines. A) Expression of HHD (HLA-A2) on E6/7H-luc clonal cell lines. Shown is the mean fluorescence intensity (MFI) of the respective cells stained with a FITC anti-HLA-A2 antibody minus the MFI of cells stained with a FITC anti-IgG2b antibody (isotype control). B) Luminescence of E6/7H-luc clonal cell lines. 1 x 10^4 cells per cell line were plated in triplicates into a 96 well plate. After addition of D-Luciferin, luminescence was measured over 10 s/well. Shown are the means of triplicate samples. C) Western Blots for detection of HPV16 proteins E6 and E7 and $HRAS^{G12V}$ in E6/7H-luc clonal cell lines. Clones chosen for further analysis are depicted in color (IH11, IVA4, IIG6).

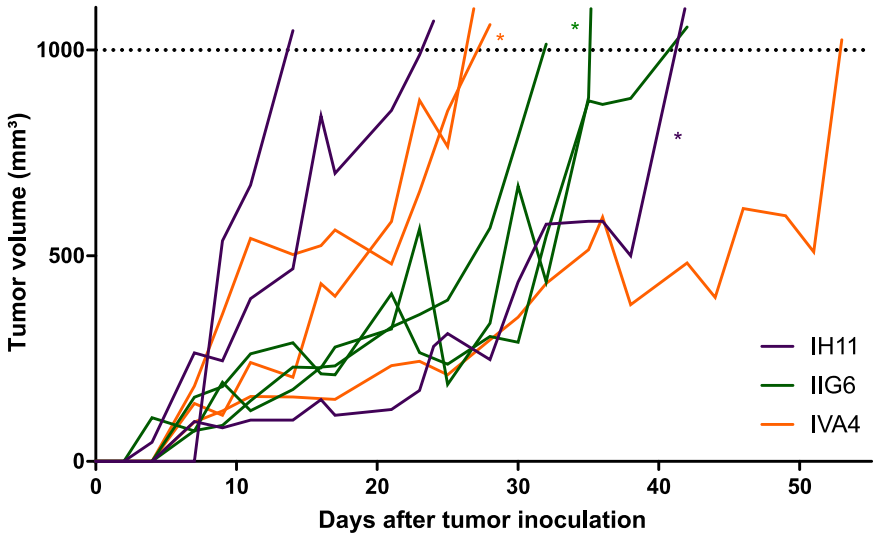

Figure 23. S.c. tumor growth of E6/7H-luc clonal cell lines in A2.DR1 mice. 5 x 10^6 cells of the respective E6/7H-luc cell line were injected s.c. in 100 µl of a 1:2 matrigel:PBS mixture into the flank of three A2.DR1 mice per cell line. Subsequently, the tumor volumes were measured and mice were killed upon tumors reaching a volume of 1 cm^3 or upon visible sign of distress. Asterisks indicate the mice whose tumors were resected for further development of cell lines.

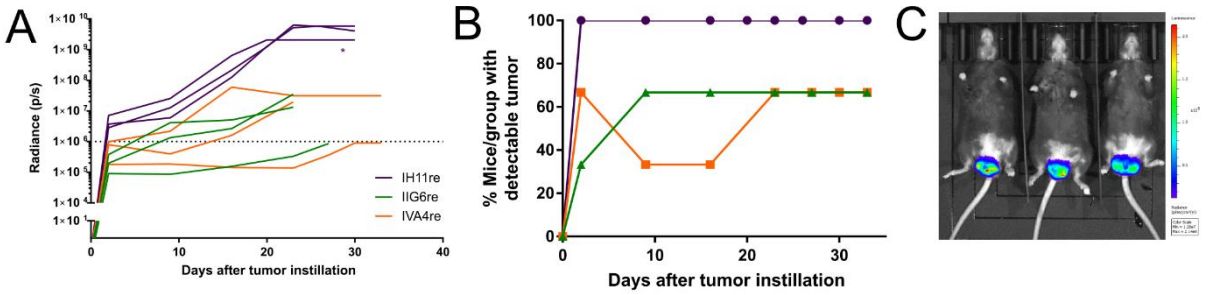

Figure 24. Ivag. tumor growth of reisolated clonal E6/7H-luc tumor cell lines. Three mice per cell line were hormonally synchronized six and five days prior to tumor instillation. Vaginal pretreatment with N-9 was followed 6 h later with ivag. instillation of 1 x 10^6 cells of the respective cell line in 20 µl PBS. Tumor growth was monitored by (bi-)weekly luminescence imaging after i.p. injection of 200 µl 15 mg/ml D-luciferin in PBS. Mice were killed upon visible signs of distress or vaginal bleeding. (A) Tumor growth curves as assessed by luminescence measurements. The asterisk indicates the mouse whose tumor was resected for further development of the cell line. (B) Percentage of mice per group with a detectable tumor as assessed by vaginal luminescence imaging. (C) Exemplary picture of tumor-bearing mice 20 days after instillation of IH11re cells.

As this was the first test of ivag. tumor inoculation, I also checked if the light produced by the luminescent cells could be properly detected, which was the case (Figure 24C). One of the ivag. tumors was reisolated (indicated by an asterisk in Figure 24A), termed 'IH11rere' and used for further development. IH11rere cells were titrated orthotopically to determine the minimal amount of tumor cells needed for the highest possible tumor take in A2.DR1 mice. This is important for ensuring experimental animals are used as efficiently as possible while aiming for tumors to grow slow enough for testing therapeutic interventions. All mice that received 1 x 10^5 – 1 x 10^6 IH11rere cells developed an ivag. tumor, while only three of five mice receiving 5 x 10^4 cells displayed tumor formation (Figure 25A, B). These tumors were found to be correctly located in the vaginal mucosa, as assessed by MRI (Figure 25C). Hence, IH11rere cells were tumorigenic enough to be used for the new tumor model. As the model was intended to be used in therapeutic HPV16 vaccination experiments, the cells have to be susceptible to HPV16-specific CTL killing. However, a comparison of HHD (MHC I) on the surface of E6/7H-luc cells showed that each *in vivo* passage lowered the HHD levels, possibly preventing sufficient presentation of epitopes to $CD8^+$ T cells (Figure 26A).

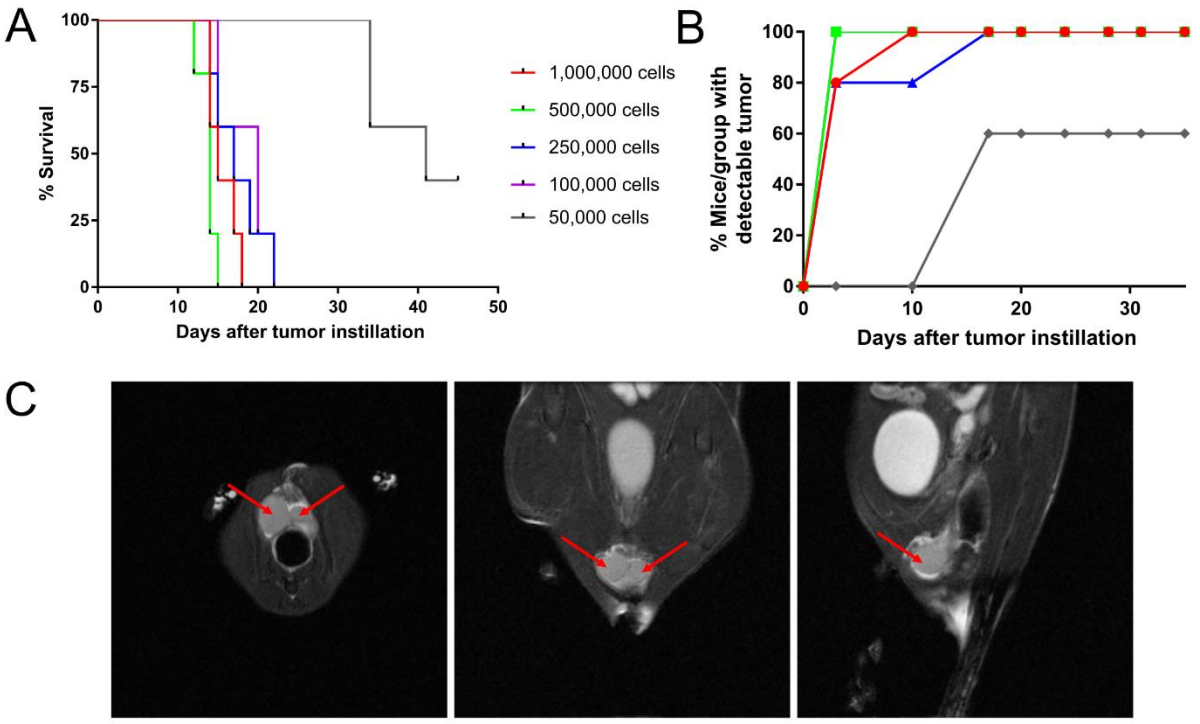

Figure 25. Ivag. titration of the twice reisolated clonal E6/7H-luc tumor cell line IH11rere. Five mice per group were hormonally synchronized six and five days prior to tumor instillation. Vaginal pretreatment with N-9 was followed 6 h later with ivag. instillation of the indicated amount of IH11rere cells in 20 µl PBS. Tumor growth was monitored by (bi-)weekly luminescence imaging after i.p. injection of 200 µl 15 mg/ml D-luciferin in PBS. Mice were killed upon visible signs of distress or vaginal bleeding. (A) Survival curves of individual experimental groups. (B) Percentage of mice per group with a detectable tumor as assessed by vaginal luminescence imaging. (C) Magnetic resonance images (axial, coronal, sagittal) of vaginal tumors (red arrows) of a mouse that had received 50,000 cells ivag. 22 days prior to imaging. Data partly published in Zottnick et al. (2020).

To test if the IH11 and IH11rere cell lines could still be killed by HPV16-specific CTLs, a VITAL-FR cytotoxicity assay was performed. In this assay the specific killing of the target cell line (here: IH11rere and IH11) is calculated by co-culturing HPV16 $E6^+$ and $E7^+$ target cell lines with an $E6^-E7^-$ control target cell line (2277-NS) in addition to specific T cells in different ratios. Resulting ratios of target cells to control target cells are then used to calculate the specific killing depicted in the graphs. The T cells used in this instance were specific for our group's lead epitope HPV16 $E7_{11-19}$ and were derived from a previous mouse vaccination experiment. Unfortunately, not even the positive control of PAP-A2 cells co-cultured with their $HPV16^-$ counterpart were found to be killed although specific killing had been verified for this cell line before (Kruse et al., 2018). Therefore, the findings of this experiment were unusable for assessing if IH11rere or its predecessor cell line IH11 were suited as tumor cell lines.

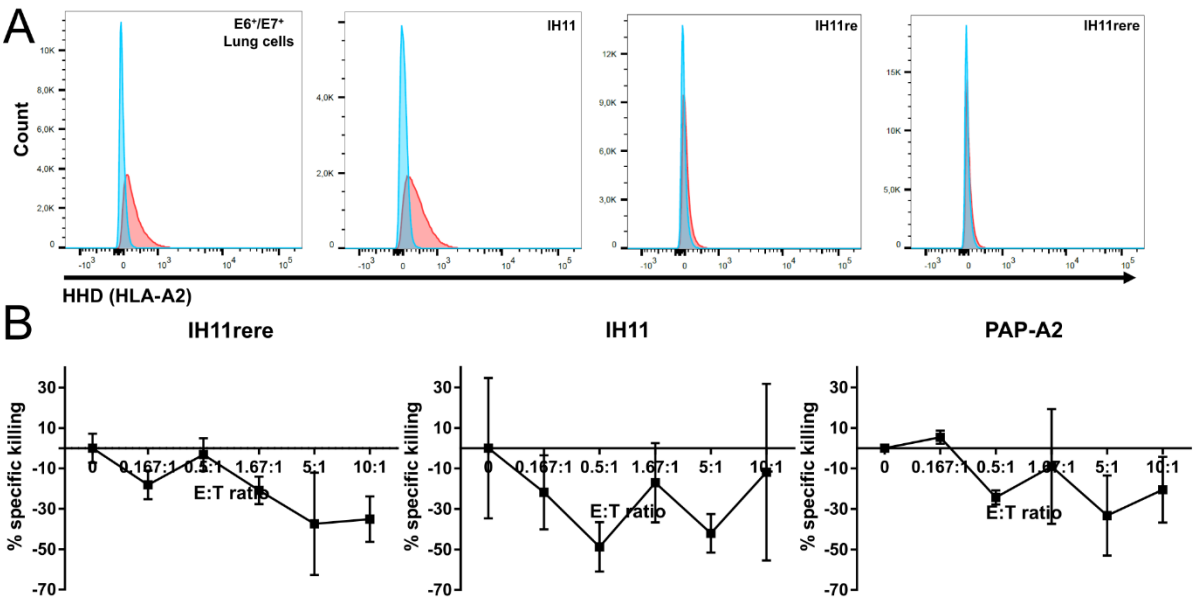

Figure 26. Characterization of E6/7H-luc cells at different stages of cell line development. A) Expression of HHD (HLA-A2) on E6/7H-luc clonal cell lines. Shown are intensity histograms of indicated cell lines stained with either FITC anti-HLA-A2 (red) or FITC anti-IgG2b (isotype control, blue). B) Specific killing of indicated cell lines as assessed by a VITAL-FR cytotoxicity assay. CFSE-labeled specific target cells (T) were co-cultured with Far Red-labeled 2277-NS control target cells, mixed with $E7_{11-19}$-specific T cells (effector, E) in the indicated ratios and analyzed 48 h hours later via flow cytometry. Specific killing was calculated according to Equation 1. Shown are the means of triplicate samples ± SD.

To test the cell's immunogenicity again, I injected them s.c. in twelve mice each, of which half were vaccinated against $E7_{11-19}$. However, there were no differences in outcome observed between vaccinated and unvaccinated animals (Figure 27) although it was expected that vaccinated animals would display a reduction of tumor growth. Thus, IH11 and its derivative IH11rere were unsuitable for my purposes.

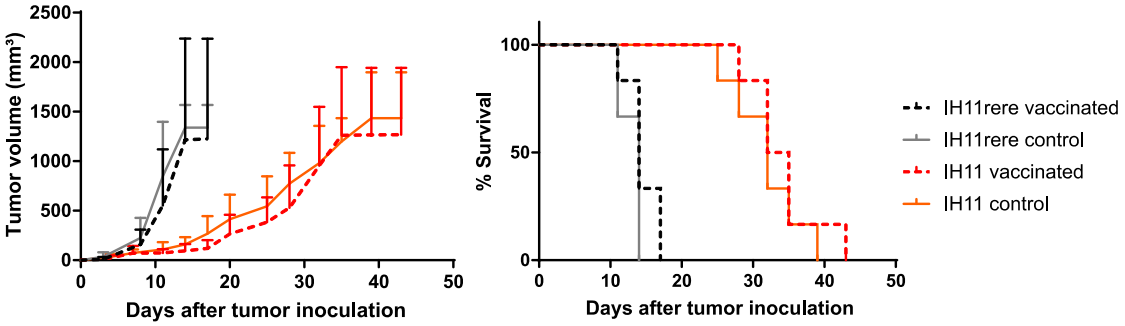

Figure 27. Effect of vaccination with LPP-$E7_{11-19}$ on implanted IH11 and IH11rere tumors. 1.5 x 10^6 cells of the respective cell line were injected s.c.in 100 µl of a 1:2 matrigel:PBS mixture into the flank of six A2.DR1 mice per group. Mice in ‚vaccinated' groups received s.c. vaccinations with 50 nmol LPP-$E7_{11-19}$ + 50 µg poly(I:C) in 100 µl PBS on days 4, 9 and 14 after tumor inoculation into the contralateral flank. Control mice were left untreated. Subsequently, the tumor volumes were measured and mice were killed upon tumors reaching a volume of 1 cm^3 or upon visible signs of distress. Tumor growth curves with tumor volume means/group + SD (left) and survival curves of mice (right) are displayed.

4.1.2.4 Establishment of a second cell line

As IH11rere could not be killed by $E7_{11-19}$-specific T cells, I went back to the other two clonal cell lines IIG6 and IVA4 and assessed their immunogenicity in both a VITAL-FR cytotoxicity assay (Figure 28A) as well as in an s.c. tumor vaccination experiment (Figure 28B) as done for IH11.

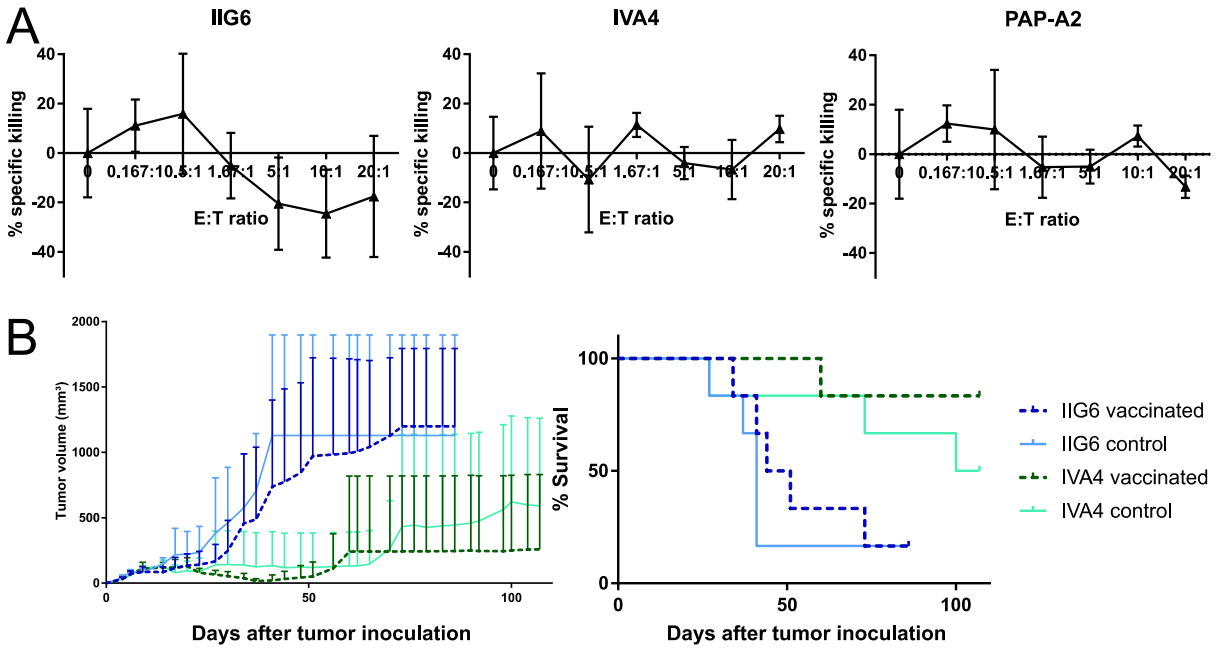

Figure 28. Effect of vaccination-induced T cells on IIG6 and IVA4. A) Specific killing of indicated cell lines as assessed by a VITAL-FR cytotoxicity assay. CFSE-labeled specific target cells (T) were co-cultured with Far Red-labeled 2277-NS control target cells, mixed with $E7_{11-19}$-specific T cells (effector, E) in the indicated ratios and analyzed 48 h hours later via flow cytometry. Specific killing was calculated according to Equation 1. Shown are the means of triplicate samples ± SD. B) *In vivo* effect of vaccination with LPP-$E7_{11-19}$ on IIG6 and IVA4 tumors. 1.5 x 10^6 cells of the respective cell line were injected s.c. in 100 µl of a 1:2 matrigel:PBS mixture into the flank of six A2.DR1 mice per group. Mice in ‚vaccinated' groups received s.c. vaccinations with 50 nmol LPP-$E7_{11-19}$ + 50 µg poly(I:C) in 100 µl PBS on days 4, 9 and 14 after tumor inoculation into the contralateral flank. Control mice were left untreated. Subsequently, the tumor volumes were measured and mice were killed upon tumors reaching a volume of 1 cm^3 or upon visible signs of distress. Tumor growth curves with tumor volume means/group + SD (left) and survival curves of mice (right) are displayed.

Again, the cell lines were not specifically killed and the positive control did not work in the VITAL-FR cytotoxicity assay either. However, after these experiments it was discovered that the LPP-$E7_{11-19}$ vaccination batch used for the experiments in Figures 26 - 28 did not contain the correct construct and was therefore useless for inducing an anti-$E7_{11-19}$ CTL response. After obtaining $E7_{11-19}$-specific T cells from a working vaccination batch, I repeated the VITAL-FR cytotoxicity assays with the original IH11 (Figure 29A) cell line, as well as with IIG6 (Figure 29B). Now the positive control showed that PAP-A2 cells were killed by the employed CTLs.

Both of the tested cell lines could be killed when they were pulsed with $E7_{11-19}$ prior to addition of T cells, therefore they apparently expressed enough HHD on their surfaces for T cell-mediated killing. Although IH11 was again not killed by the T cells, specific killing could be observed for IIG6 cells with increasing amounts of added $E7_{11-19}$-specific T cells. Therefore, I decided to further develop IIG6 for generation of the novel tumor cell line. Before continuing with *in vivo* testing of IIG6, however, I first characterized the cells extensively. The cells were sufficiently luminescent (Figure 30A) compared to their mother cell line, $E6^+E7^+$ lung cells. Although IIG6 did not emit as much light as luciferase-transfected HeLa cells, the cells were still suited for the tumor model as they just have to be detectable *in vivo*. IIG6 cells also expressed much less HHD than PAP-A2 cells (Figure 30B). However, as I had shown before that the cell line can be killed in an $E7_{11-19}$-specific T cell-mediated fashion, the MHC I level was not of concern.

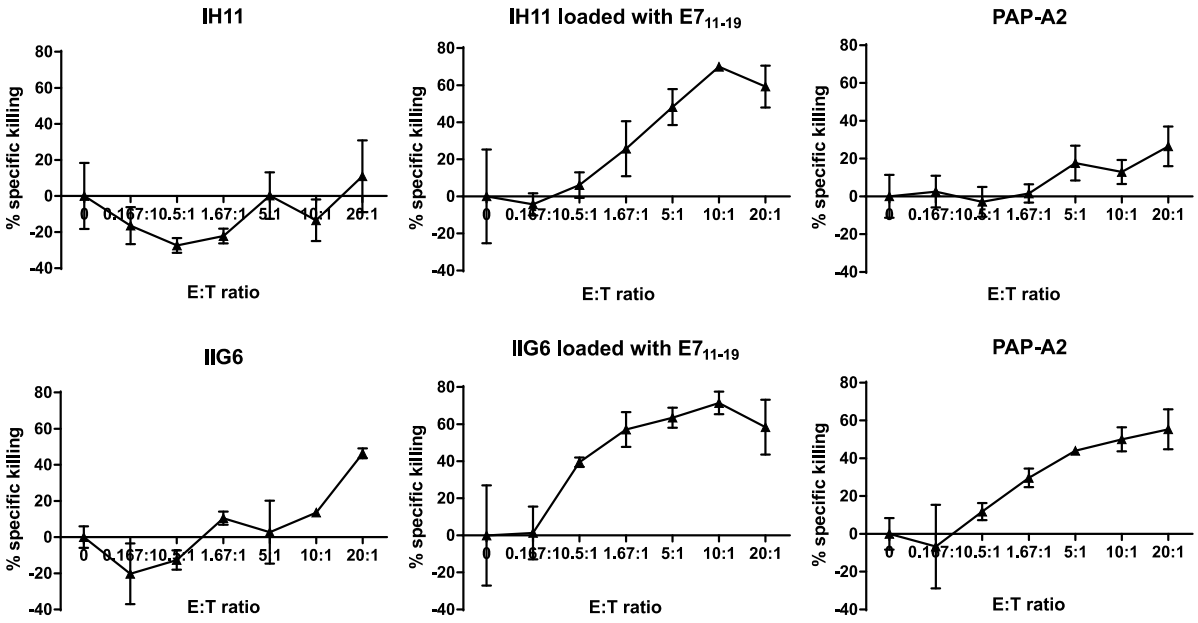

Figure 29. $E7_{11-19}$-specific killing of IH11, IIG6 and PAP-A2 cell lines in VITAL-FR cytotoxicity assays. CFSE-labeled specific target cells (T) were co-cultured with Far Red-labeled 2277-NS control target cells, mixed with $E7_{11-19}$-specific T cells (effector, E) in the indicated ratios and analyzed 48 h hours later via flow cytometry. Specific killing was calculated according to Equation 1. Shown are the means of triplicate samples ± SD. Left panels show specific killing of unpulsed, middle panels of $E7_{11-19}$-pulsed IH11 (top) or IIG6 (bottom) target cells. The right panels show specific killing of positive control cell line PAP-A2 in the respective experiment.

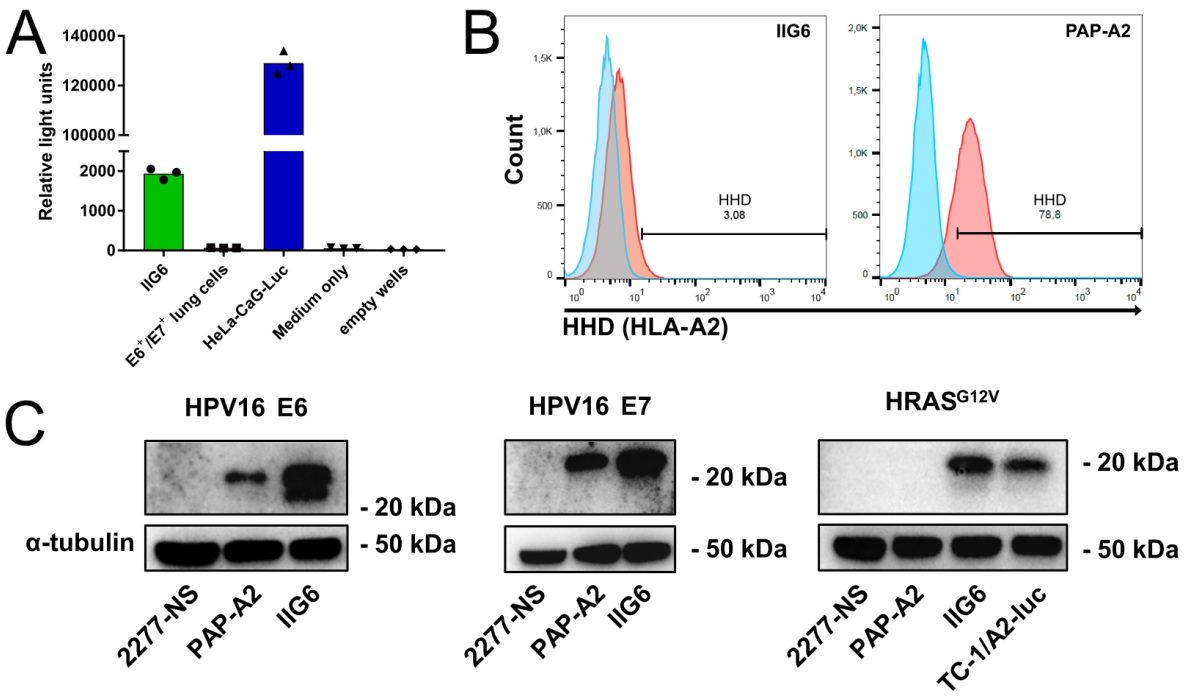

Figure 30. Characterization of the IIG6 clonal cell line. A) Luminescence of indicated cell lines. 1 x 10^4 cells per cell line were plated in triplicates into a 96 well plate. After addition of D-Luciferin, luminescence was measured over 10 s/well. Shown are the means of triplicate samples. (B) Expression of HHD (HLA-A2) on IIG6 and PAP-A2 cells. Shown are intensity histograms of indicated cell lines stained with either FITC anti-HLA-A2 (red) or FITC anti-IgG2b (isotype control, blue). (C) Western blots for detection of HPV16 proteins E6 and E7 and $HRAS^{G12V}$ in indicated cell lines.

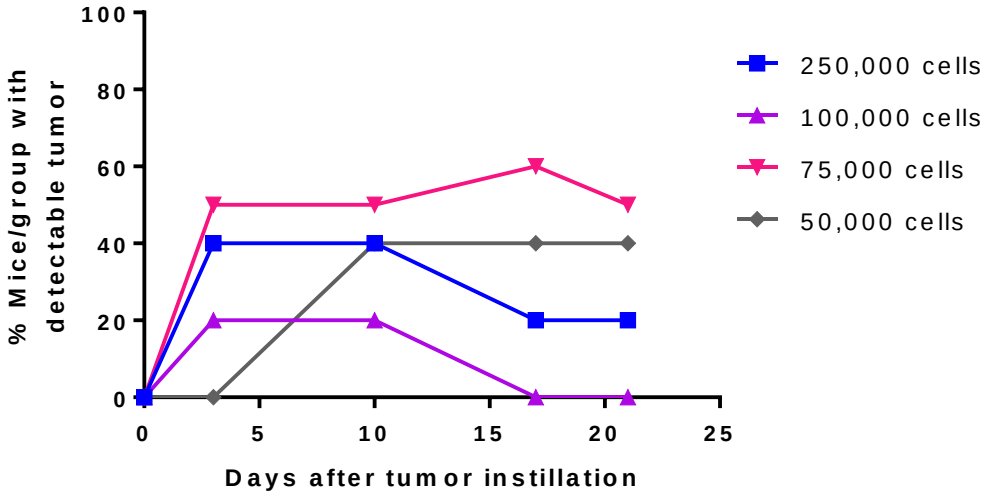

Figure 31. Ivag. titration of the IIG6 clonal tumor cell line. Five mice per cell line (n=10 for 75,000 cells group) were hormonally synchronized six and five days prior to tumor instillation. Vaginal pretreatment with N-9 was followed 6 h later with ivag. instillation of the indicated amount of IIG6 cells in 20 µl PBS. Tumor growth was monitored by (bi-)weekly luminescence imaging after i.p. injection of 200 µl 15 mg/ml D-luciferin in PBS. Mice were killed upon visible signs of distress or vaginal bleeding. Percentage of mice per group with a detectable tumor as assessed by vaginal luminescence is shown.

Lastly, the cells were additionally examined for their expression of HPV16 E6 and E7 in comparison to 2277-NS and PAP-A2 and for $HRAS^{G12V}$ in comparison to 2277-NS, PAP-A2 and TC1/A2-luc (Figure 30C). All necessary proteins were expressed. In the end, IIG6 cells were titrated orthotopically as IH11rere had been before. Unfortunately, tumor take turned out to be only 50 % in one group at maximum (Figure 31). This was not considered enough for a working tumor model because a tumor take rate of 50 % would require an unethical amount of experimental animals for tumor experiments. Therefore, the formed tumors were reisolated and taken into culture as *in vivo* passages can increase tumorigenicity. This is probably due to the tumors developing immune evasion mechanisms.

4.1.2.5 Establishment of the final cell line

Three cell lines resulted from the isolation of the tumors as stated above. These cell lines, named 'IIG6re769', 'IIG6re772' and 'IIG6re787' were again checked if they were immunogenic enough to be killed by $E7_{11-19}$-specific CTLs (Figure 32).

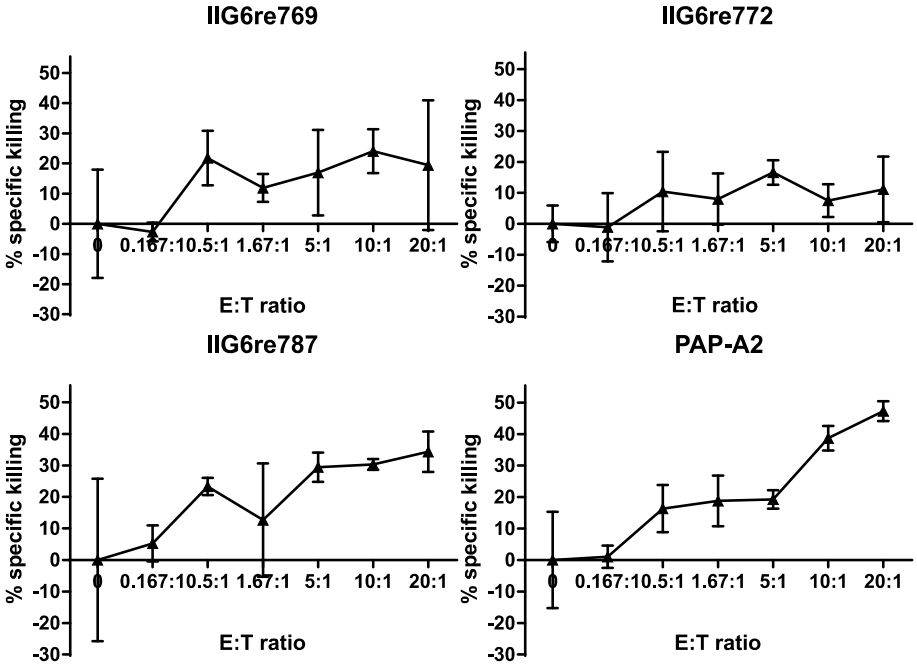

Figure 32. $E7_{11-19}$-specific killing of reisolated IIG6 cell lines in VITAL-FR cytotoxicity assays. CFSE-labeled specific target cells (T) were co-cultured with Far Red-labeled 2277-NS control target cells, mixed with $E7_{11-19}$-specific T cells (effector, E) in the indicated ratios and analyzed 48 h hours later via flow cytometry. Specific killing was calculated according to Equation 1. Shown are the means of triplicate samples ± SD. PAP-A2 served as positive control.

This was found to be the case and based on their specific killing curve, I chose the cell lines IIG6re769 and IIG6re787 to continue with. As IIG6 had displayed low tumorigenicity before, I tested the two reisolated cell lines for their ivag. tumorigenicity in a small group of mice, respectively. All of the five mice per group developed tumors upon vaginal cell implantation and had to be euthanized due to the tumors (Figure 33A, B). Under consideration of the specific killing curve derived from the VITAL-FR assay, I chose the IIG6re787 cell line as the final tumor cell line and renamed it to 'E6/7-lucA2'.

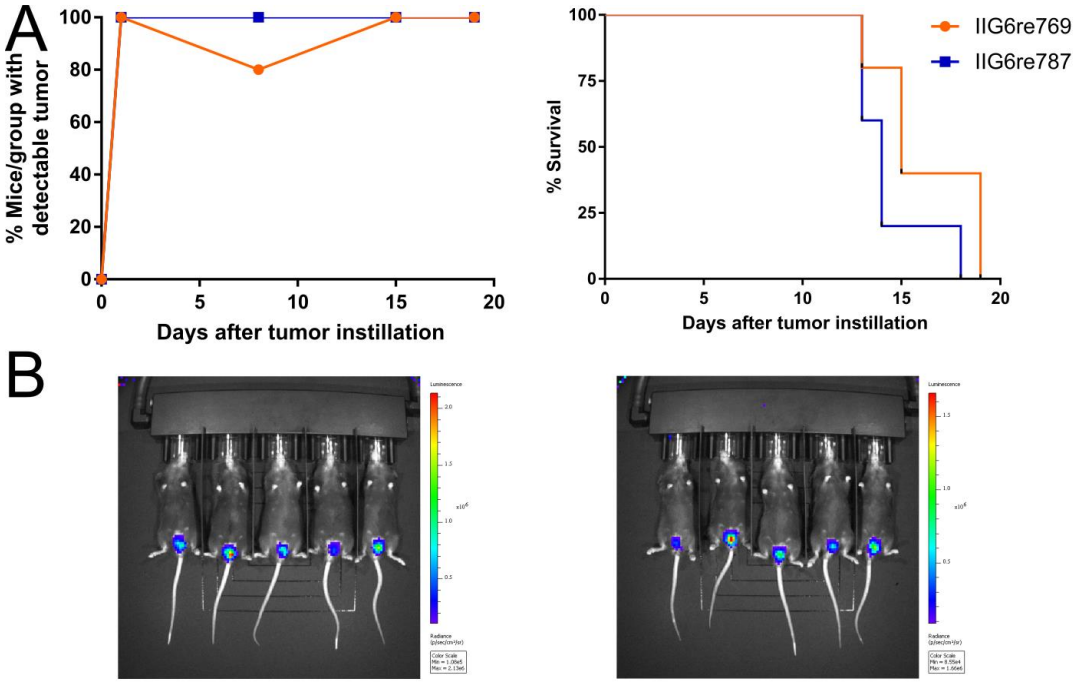

Figure 33. Tumorigenicity of reisolated IIG6 cell lines IIG6re769 and IIG6re787. Five mice per cell line were hormonally synchronized six and five days prior to tumor instillation. Vaginal pretreatment with N-9 was followed 6 h later with ivag. instillation of 1 x 10^6 cells of the respective cell line in 20 µl PBS. Tumor growth was monitored by (bi-)weekly luminescence imaging after i.p. injection of 200 µl 15 mg/ml D-luciferin in PBS. Mice were killed upon visible signs of distress or vaginal bleeding. (A) Percentage of mice per group with a detectable tumor as assessed by vaginal luminescence (left) and group survival rates over time (right) are shown. (B) Exemplary picture of tumor-bearing mice 1 day after instillation of IIG6re769 (left) and IIG6re787 cells (right).

This cell line was then characterized again. I first checked for the expression of all relevant proteins. E6/7-lucA2 cells still expressed HPV16 E6 and E7 and $HRAS^{G12V}$ (Figure 34A). HPV16 E6 and E7 are larger proteins in E6/7-lucA2 and PAP-A2 than in TC-1/A2-luc and human CaSki cells as they are strep- and FLAG-tagged (see Appendix Figure 2 and Kruse et al. (2018)). To assess if the HPV oncoproteins are functionally active, I analyzed the E7 downstream protein $p16^{INK4a}$, which us also used in standard pathology to assess the HPV status of lesions (Burd, 2016). It was clearly overexpressed in E6/7-lucA2, as well as in TC-1/A2-luc

(luminescent TC-1 cells expressing the chimeric MHC molecule AAD) cells, but not in equally HPV16 $E6^+E7^+$ PAP-A2 cells (Figure 34B). This shows that the E7 protein in E6/7-lucA2 and TC-1/A2-luc apparently has the same function as seen in human keratinocytes (Moody & Laimins, 2010). Additionally, the overexpression of $p16^{INK4a}$ indicates the cell lines' dependence on E7's functions for survival as the overexpression was not detected in PAP-A2 sarcoma-based cells, which survive without HPV16 $E6^+E7^+$.

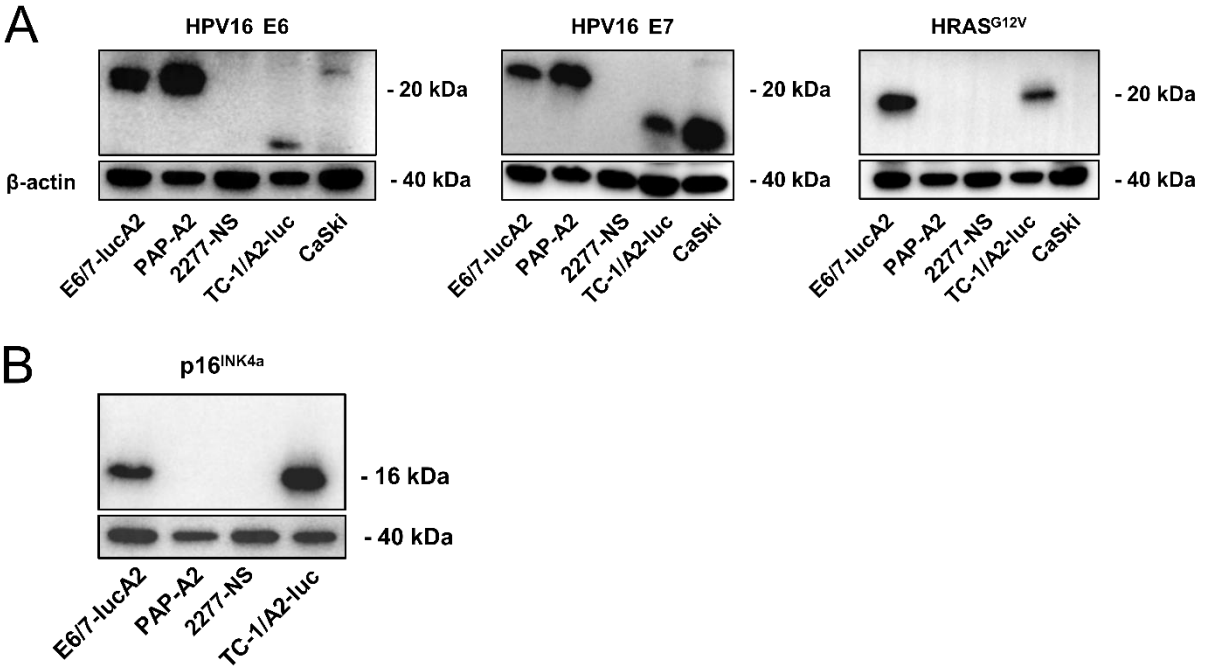

Figure 34. Characterization of the E6/7-lucA2 clonal cell line by Western blot. (A) Analysis of introduced proteins E6, E7 and $HRAS^{G12V}$. (B) Analysis of HPV downstream target protein $p16^{INK4a}$ in indicated cell lines.

Furthermore, E6/7-lucA2 cells were shown to be luminescent (Figure 35A) and to express low levels of HHD (HLA-A2) on their cell surface (Figure 35B) in comparison to other HPV16 $E6^+E7^+$ cells such as PAP-A2 or the human CaSki cell line. The cells displayed a doubling time of roughly 24 – 36 h (Figure 35C) as examined by live cell imaging. Finally, our group's targeted immunopeptidomics pipeline was applied by Jonas Förster and showed that E6/7-lucA2 cells truly present the HPV16 epitope $E7_{11-19}$ (YMLDLQPET) on their surface HHD molecules (Figure 35D). It is also very likely that they present the HPV16 $E7_{7-15}$ (TLHEYMLDL) epitope on their surface although the normalized spectral contrast angles (dotp) were below the threshold of 0.85. Finally, I orthotopically titrated the E6/7-lucA2 cell line in A2.DR1 mice (Figure 36). All ten mice instilled ivag. with 250,000 cells developed a tumor and had to be euthanized due to it. Therefore, this amount of cells will be used for future

experiments utilizing ivag. E6/7-lucA2-derived tumors. With this final step, the vaginal, HPV16 E6 and E7-dependent A2.DR1 tumor model E6/7-lucA2 was established, and thus the first two aims of my PhD project reached.

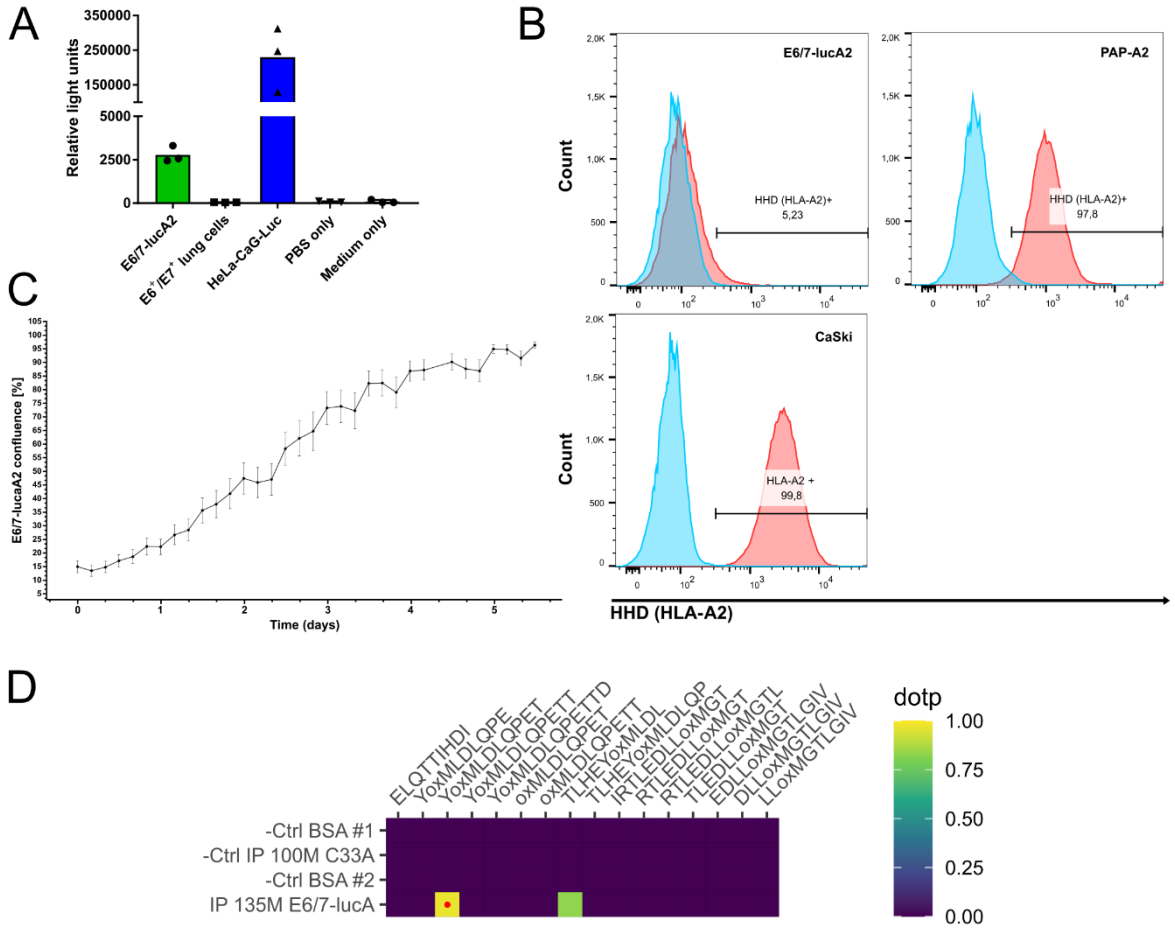

Figure 35. Characterization of the E6/7-lucA2 clonal cell line by luminescence measurement, flow cytometry, live cell imaging and mass spectrometry. A) Luminescence of indicated cell lines. 1 x 10^4 cells per cell line were plated in triplicates into a 96 well plate. After addition of D-Luciferin, luminescence was measured over 10 s/well. Shown are the means of triplicate samples. (B) Expression of HHD on E6/7-lucA2 and PAP-A2 and HLA-A2 on CaSki cells. Shown are intensity histograms of indicated cell lines stained with either FITC anti-HLA-A2 (red) or FITC anti-IgG2b (isotype control, blue). (C) Growing curve of E6/7-lucA2 cells as assessed by live cell imaging. 1 x 10^4 cells were plated in triplicates into a 96 well plate and examined with an Incucyte® live cell microscope. Analysis was performed by Christoph Schifflers. (D) Mass spectrometry-based detection of HPV16 peptides presented on HHD molecules on E6/7-lucA2 cells. Shown are normalized spectral contrast angles (dotp) of different HPV16 peptides checked for in BSA and the C33A cell line controls as well as the E6/7-lucA2 cell line. A dotp ≥ 0.85 was used as a cut-off for detection validation. MS sample preparation and analysis was performed by Jonas Förster with help of Rebecca Köhler.

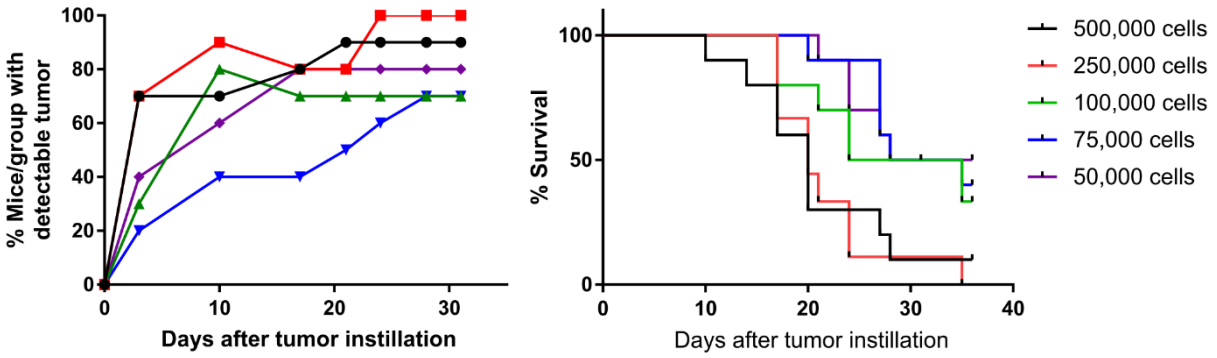

Figure 36. Ivag. titration of E6/7-lucA2. Ten mice per group were hormonally synchronized six and five days prior to tumor instillation. Vaginal pretreatment with N-9 was followed 6 h later with ivag. instillation of the indicated amounts of E6/7-lucA2 cells in 20 µl PBS. Tumor growth was monitored by (bi-)weekly luminescence imaging after i.p. injection of 200 µl 15 mg/ml D-luciferin in PBS. Mice were killed upon visible signs of distress or vaginal bleeding. Percentage of mice per group with a detectable tumor by checking for vaginal luminescence (left) and group survival rates over time (right) are shown.

4.2 Examination of vaccination approaches to induce HPV16-specific T cells systemically and locally in the mucosa

The third aim of my PhD was the examination of methods to induce and increase levels of HPV16-specific T cells in the mucosa of the murine GT. To achieve this goal I tested various methods by either directly vaccinating mice ivag. or by vaccinating via 'classical' routes for induction of systemic immunity and then influence the trafficking of specific CTLs to the mucosa. For all the following experiments, mice were vaccinated and in the end euthanized to remove their GTs and/or spleens. The organs were mechanically and enzymatically dissociated and analyzed for their surface markers and produced cytokines. Splenocytes were used as a proxy indicator for the systemic T cell response while GT cells were examined for the local immune response. The $CD8^+$ T cells were checked for their subsets of T_{RM} ($CD69^+CD103^+$), T_{EM} ($CD44^+CD62L^-$) and T_{CM} ($CD44^+CD62L^+$), as well as for their specificity by restimulation with cognate ($E7_{11-19}$) or non-cognate peptide ($Surv_{96-104}$) and subsequent analysis of IFNγ and TNFα production.

First, the GT dissociation protocol and antibody panel for flow cytometric analysis as established by Alessa Henneberg (Voß, 2020) had to be tested in an *ex vivo* application. Six animals per group were therefore vaccinated with our gold standard vaccination LPP-$E7_{11-19}$ + poly(I:C), poly(I:C) only or were left untreated. While the levels of $CD8^+$ T cells were slightly higher in splenocytes of treated groups than the untreated one, there was no difference in GT $CD8^+$ levels (Figure 37A).

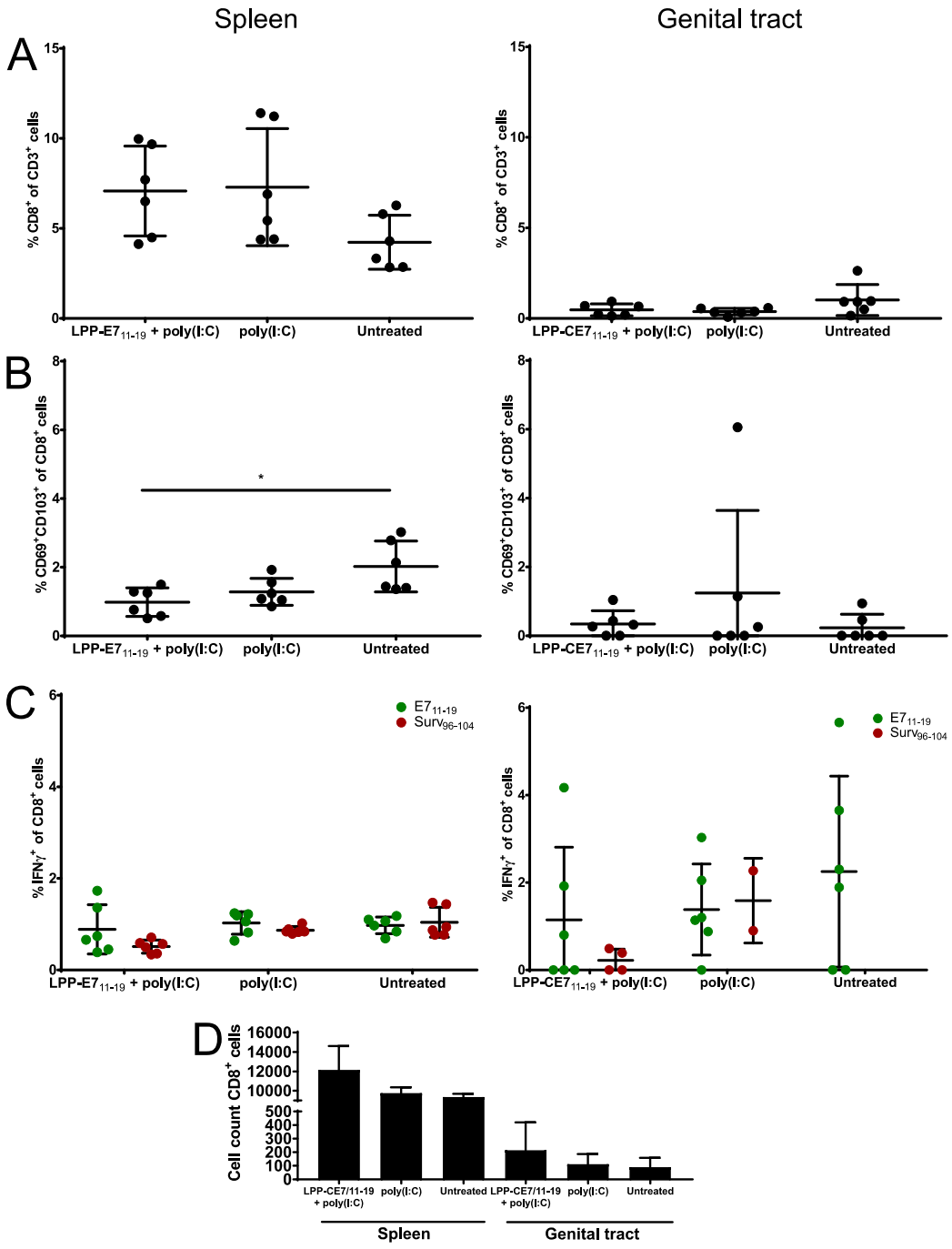

Figure 37. S.c. vaccination with LPP-E7$_{11-19}$ and validation of a genital lymphocyte flow cytometry staining panel. Six mice per group were hormonally synchronized six and five days prior to the first vaccination. S.c. vaccination was performed on days 0, 7 and 14 with 50 nmol LPP-E7$_{11-19}$ + 50 µg poly(I:C) in 100 µl PBS or 50 µg poly(I:C) in 100 µl PBS, respectively. The third group was left untreated. After sacrifice on day 21, spleens and GTs were removed, dissociated and cells analyzed by flow cytometry. Results for splenocytes are displayed on the left, for GT cells on the right. (A) Percentages of CD8$^+$ of CD3$^+$ cells. (B) Percentages of CD69$^+$ CD103$^+$ of CD8$^+$ cells. (C) Percentages of IFNγ$^+$ of CD8$^+$ cells after 5 h restimulation of cells with either cognate peptide E7$_{11-19}$ (green) or non-cognate peptide Surv$_{96-104}$ (red). (D) Total amount of CD8$^+$ of CD3$^+$ cells in the respective tissues. Statistical analysis of experimental groups for A – C was performed with Kruskal-Wallis tests followed by Dunn's multiple comparison and in C within an experimental group with Wilcoxon matched-pairs signed rank tests. *p≤0.05

A significant difference could be observed in splenic $CD8^+$ cells expressing the T_{RM} markers CD69 and CD103, however no significance was detected in the GT where T_{RM} are expected to be enriched. Specific T cells, i.e. IFNγ-producing ones after restimulation with $E7_{11-19}$, were only found in the GTs but not among the splenocytes (Figure 37C). This was probably due to improper permeabilization of splenocytes prior to intracellular staining. Therefore, I took the cells into culture and restimulated them again one week later whereupon their specificity became detectable (data not shown). As can be seen in Figure 37C, there were no cells left from the GTs of untreated mice for stimulation with non-cognate peptide. In later experiments, I adjusted the amount of GT cells per condition according to the available cells so that at least $E7_{11-19}$ and $Surv_{96-104}$-stimulation were possible. The examination of total $CD8^+$ T cell numbers showed a big discrepancy between spleen and GT (Figure 37D). As there were not many GT $CD8^+$ T cells to begin with, the percentages were not reliable. This improved in later experiments with more experience and improved GT dissociation protocols.

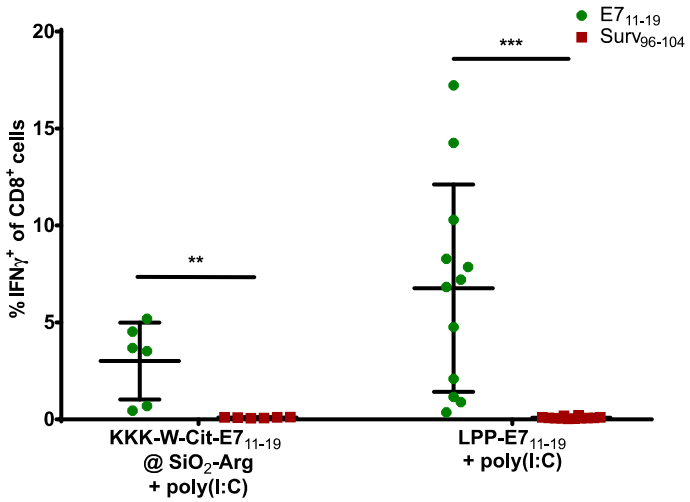

Figure 38. Comparison of two vaccine carriers. Six and twelve mice per group were vaccinated s.c. on days 0, 7 and 14 with KKK-W-Cit-$E7_{11-19}$ (25 nmol) @SiO_2-Arg + 50 µg poly(I:C) or 50 nmol LPP-$E7_{11-19}$ + 50 µg poly(I:C) in 100 µl of PBS. After sacrifice on day 21, spleens were removed, dissociated and cells analyzed by flow cytometry. Shown are percentages of $IFN\gamma^+$ of $CD8^+$ cells after 5 h restimulation of cells with either cognate peptide $E7_{11-19}$ or non-cognate peptide $Surv_{96-104}$. Statistical analysis within an experimental group was performed with Wilcoxon matched-pairs signed rank test. **$p \leq 0.01$, ***$p \leq 0.001$

For use in later vaginal vaccination experiments, I tested two vaccination compounds in an s.c. setting first. Two of those compounds were argynilated SiNP, linked to $E7_{11-19}$ via the linker KKK-W-Citrullin and LPP-$E7_{11-19}$. A direct comparison showed that LPP-$E7_{11-19}$ provided a higher percentage of $E7_{11-19}$-specific T cells in the spleen after the systemic vaccination (Figure

38). Additionally, I tested whether the oxidation status of the methionine in $E7_{11-19}$ (Y**M**LDLQPET) influenced the immune response as described in Weiskopf et al. (2010).

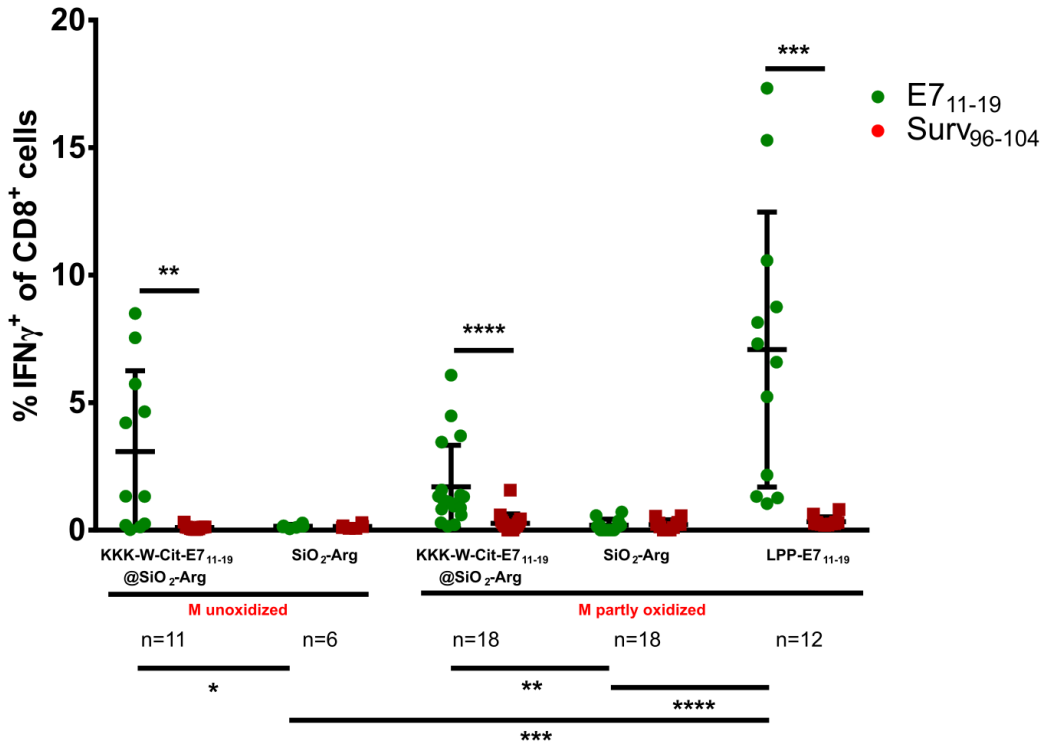

Figure 39. Analysis of the influence of oxidized methionine present in $E7_{11-19}$. Eleven and six mice per group were vaccinated s.c. on days 0, 7 and 14 with KKK-W-Cit-$E7_{11-19}$ (25 nmol) @SiO_2-Arg + 50 µg poly(I:C) or SiO_2-Arg + 50 µg poly(I:C) in 100 µl of 5% aqueous glucose solution. After sacrifice on day 21, spleens were removed, dissociated and cells analyzed by flow cytometry. Shown are percentages of $IFN\gamma^+$ of $CD8^+$ cells after 5 h restimulation of cells with either cognate peptide $E7_{11-19}$ or non-cognate peptide $Surv_{96-104}$. Results are compared to results of experiments conducted by Lia Roth and me (three rightmost data sets). Statistical analysis within an experimental group was performed with Wilcoxon matched-pairs signed rank test (indicated atop). Analysis between groups was performed with Kruskal-Wallis test followed by Dunn's multiple comparison (indicated below). *p≤0.05, **p≤0.01, ***p≤0.001, ****p≤0.0001.

The tested SiNP were either linked to unoxidized $E7_{11-19}$ (Figure 39, left) or linked to $E7_{11-19}$ that contained approximately 10 % of oxidized methionine (Figure 39, right). Although the vaccination with unoxidized methionine in $E7_{11-19}$ worked well compared to empty SiNP I was not able to detect a significant improvement to the performance of SiNP with oxidized $E7_{11-19}$ as tested by Lia Roth and me (Figure 39).

4.2.1 Vaccination for vaginal T cell induction

After establishing the efficacy of the two different compounds for anti-HPV16 E7 vaccination, I tested how to best establish a specific mucosal $CD8^+$ T cell response in the murine GT. Based on reports in literature, one idea was to first establish a systemic T cell response by vaccinating

s.c. one or two times and then vaccinate one or two times ivag. to induce migration of vaccination-induced $CD8^+$ T cells to the vagina. This approach was compared to vaccinating ivag. three times without a prior s.c. vaccination. There were significantly more $CD8^+$ T cells found in the spleen of mice vaccinated two times s.c. and then ivag.. This difference was also seen in GT cells, although it was not as significant as in the spleens (Figure 40A). The $CD8^+$ T cells in the GT displayed a slightly higher percentage of T_{RM} markers than in the spleen in all groups although the level was still under 1 % (Figure 40B). Although there were similar levels of $CD8^+$ T_{EM} found in both tissues (Figure 40C), there were very few T_{CM} in the GT compared to the spleen (Figure 40D) in all groups. Unfortunately, no specific $CD8^+$ T cells could be found in the spleens of any of the experimental groups. However, there were more $E7_{11-19}$-specific $CD8^+$ T cells detected in GTs of mice that had been vaccinated two times s.c. with a final ivag. boost compared to the other groups (Figure 40E). It was clear to see here that just vaccinating ivag. with LPP-$E7_{11-19}$ did not induce any vaginal immune response whatsoever. This could be due to LPP-$E7_{11-19}$ not being able to enter the vaginal epithelium on its own, to get processed and finally to establish an immune response. Therefore, I tested if other vaccine carriers might be more successful in establishing mucosal immunity upon exclusively ivag. vaccination. For this approach, I used liposomes that carry cell-penetrating peptides (CPP) on their surface (Uhl et al., 2021). So far, these liposomes had only been used for oral delivery of pharmaceutics but were tested here for the first time to examine their capability to transport vaccines through the vaginal mucosa. The liposomes were therefore filled with $E7_{11-19}$ or LPP-$E7_{11-19}$ and compared to empty liposomes or just LPP-$E7_{11-19}$ in connection with CPPs. One experimental group was also exploratively vaccinated ivag. with SiNP carrying $E7_{11-19}$.

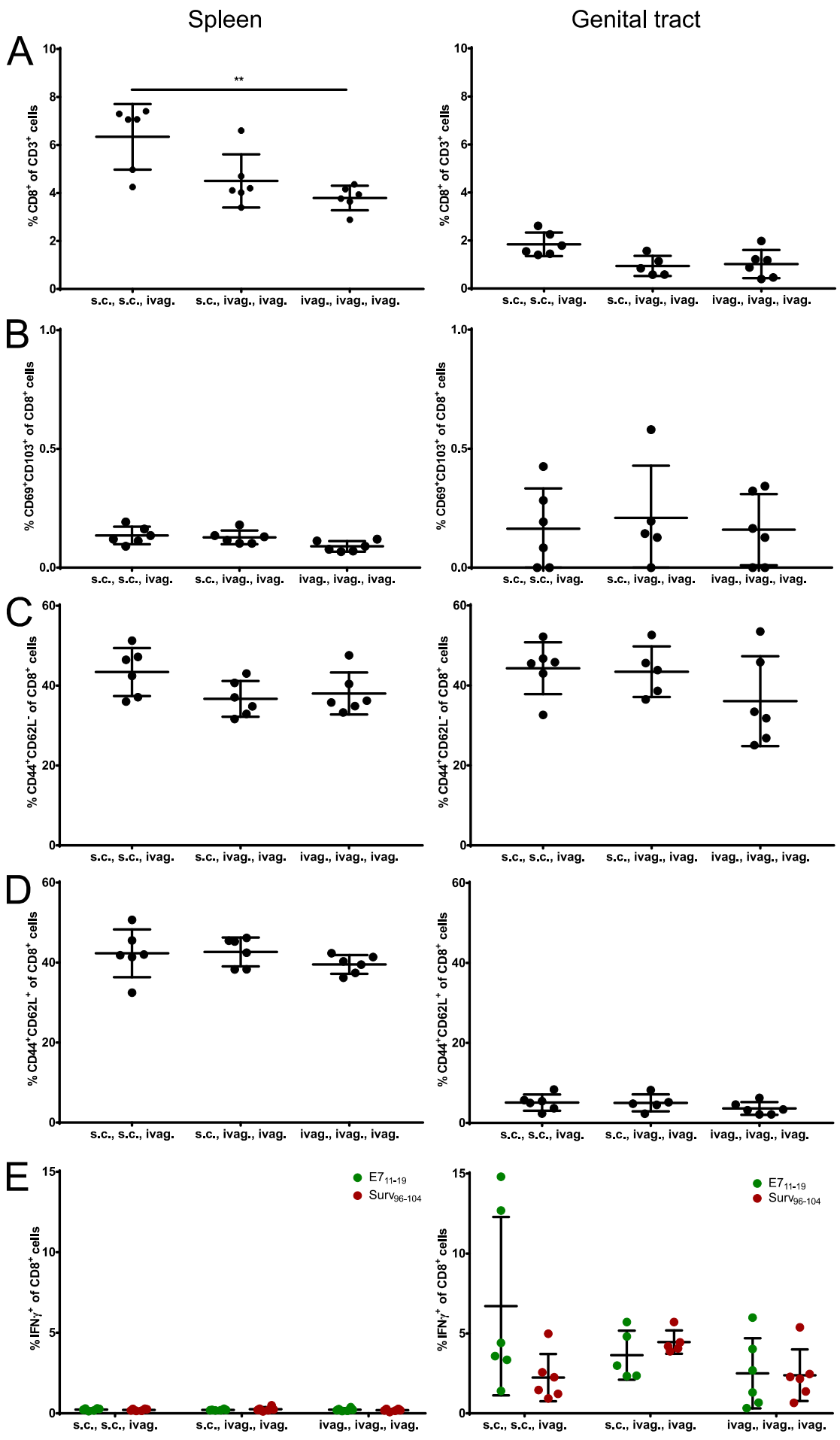
Spleen
Genital tract
A
B
C
D
E
% CD8+ of CD3+ cells
% CD69+CD103+ of CD8+ cells
% CD44+CD62L- of CD8+ cells
% CD44+CD62L+ of CD8+ cells
% IFNγ+ of CD8+ cells
**
s.c., s.c., ivag.
s.c., ivag., ivag.
ivag., ivag., ivag.
E7 11-19
Surv 96-104

Figure 40. Effect of different vaccination routes on induction of mucosal immunity against $E7_{11-19}$. Six mice per group were hormonally synchronized six and five days prior to the first vaccination. Vaccinations were performed on days 0, 7 and 14 via the indicated routes for each time point (s.c. or ivag.). Both routes of vaccination were performed with 50 nmol LPP-$E7_{11-19}$ + 50 µg poly(I:C), which was resuspended in either 100 µl PBS (s.c.) or 20 µl PBS (ivag.). Ivag. vaccinations were preceded by treatment with N-9 6 h earlier. After sacrifice on day 21, spleens and GTs were removed, dissociated and cells analyzed by flow cytometry. Results for splenocytes are displayed on the left, for GT cells on the right. (A) Percentages of $CD8^+$ of $CD3^+$ cells. (B) Percentages of $CD69^+$ $CD103^+$ of $CD8^+$ cells. (C) Percentages of $CD44^+$ $CD62L^-$ of $CD8^+$ cells (D) Percentages of $CD44^+$ $CD62L^+$ of $CD8^+$ cells (E) Percentages of $IFN\gamma^+$ of $CD8^+$ cells after 5 h restimulation of cells with either cognate peptide $E7_{11-19}$ or non-cognate peptide $Surv_{96-104}$. Statistical analysis of experimental groups for A – E was performed with Kruskal-Wallis tests followed by Dunn's multiple comparison and in E within an experimental group with Wilcoxon matched-pairs signed rank tests. **$p \leq 0.01$

The vaginal vaccination did not induce an obvious difference in $CD8^+$ T cell levels of the spleen or GT with any of the tested vaccine carriers (Figure 41A). When analyzing CD69 and CD103 expression, I found much higher percentages of $CD8^+$ T_{RM} in the GTs upon all ivag. vaccination approaches and only low levels of T_{RM} in the spleens of mice (Figure 41B). However, the T_{RM} in GTs may have been artifacts from the flow cytometric analysis as the total number of $CD8^+$ T cells was low and therefore the percentages of $CD8^+$ subsets might be misleading. As before the exclusive ivag. vaccination did not lead to an increase in specific T cells in the GTs of mice (Figure 41C). Surprisingly, I detected high levels of $E7_{11-19}$ specific $CD8^+$ T cells in splenocytes of ivag. SiNP-vaccinated animals. These T cells must have been primed ivag. and then emigrated from the mucosal tissue. This also fits to the observation that the splenocytes of these mice displayed the significantly lowest levels of T_{RM} markers of all experimental groups (Figure 41B). As this first ivag. vaccination approach with liposomes and SiNP resulted in only low lymphocyte yields for the GT and presented the unexpected result of $E7_{11-19}$-specific T cells in the spleens of SiNP-instilled mice, the experiment was repeated later with an optimized GT dissociation protocol and a dedicated SiNP control group.

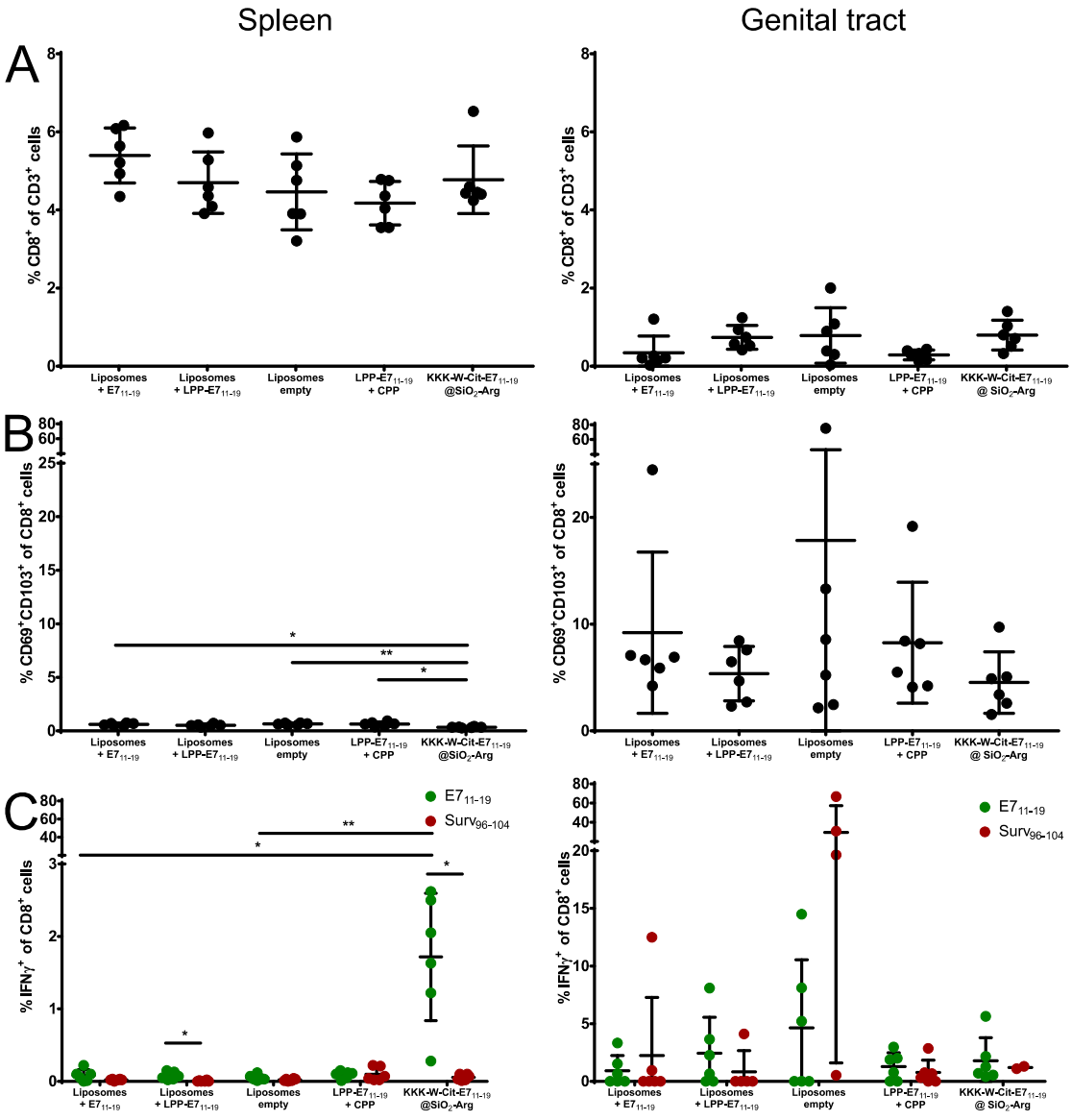

Figure 41. Vaginal vaccination with liposomal formulations and SiNP. Six mice per group were hormonally synchronized six and five days prior to the first vaccination. Ivag. vaccinations were performed on days 0, 7 and 14 with N-9 pretreatment being followed after 6 h by treatment with liposomes containing 50 nmol $E7_{11-19}$ + 50 µg poly(I:C) or 50 nmol LPP-$E7_{11-19}$ + 50 µg poly(I:C), empty liposomes with 50 µg poly(I:C), 50 nmol LPP-$E7_{11-19}$ + 50 µg poly(I:C) + cell-penetrating peptides or KKK-W-Cit-$E7_{11-19}$ (25 nmol) @SiO_2-Arg + 50 µg poly(I:C) in 20 µl PBS or 20 µl of 5% aqueous glucose solution (SiNP). After sacrifice on day 21, spleens and GTs were removed, dissociated and cells analyzed by flow cytometry. Results for splenocytes are displayed on the left, for GT cells on the right. (A) Percentages of $CD8^+$ of $CD3^+$ cells. (B) Percentages of $CD69^+$ $CD103^+$ of $CD8^+$ cells. (C) Percentages of $IFN\gamma^+$ of $CD8^+$ cells after 5 h restimulation of cells with either cognate peptide $E7_{11-19}$ or non-cognate peptide $Surv_{96-104}$. Statistical analysis of experimental groups for A – C was performed with Kruskal-Wallis tests followed by Dunn's multiple comparison and in C within an experimental group with Wilcoxon matched-pairs signed rank tests. *p≤0.05, **p≤0.01

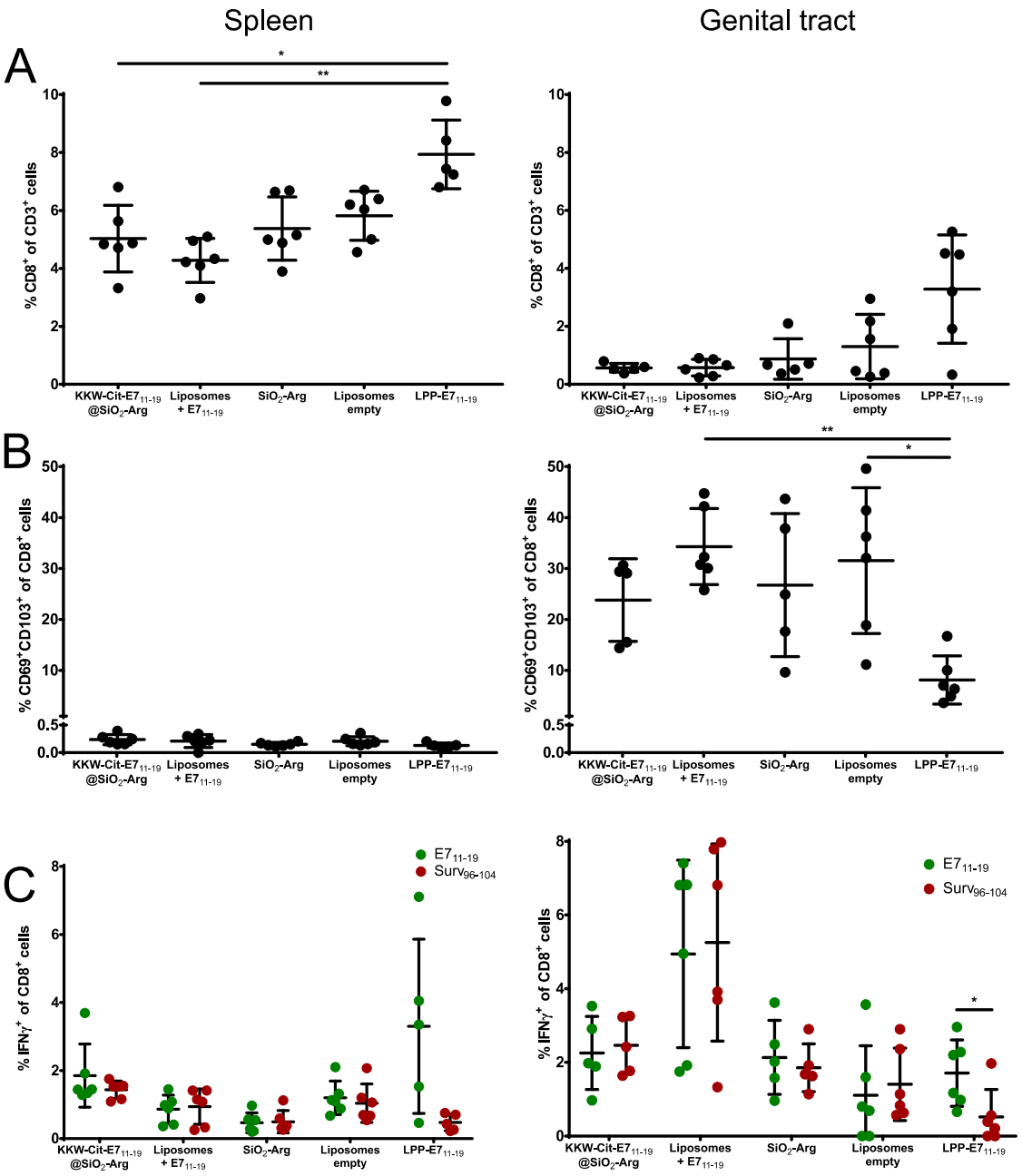

Figure 42. Comparison of vaginal vaccination with liposomal formulations and SiNP. Ivag. vaccinations were performed on days 0, 7 and 14 with N-9 pretreatment being followed after 6 h by treatment with KKK-W-Cit-$E7_{11-19}$ (25 nmol) @SiO_2-Arg + 50 µg poly(I:C), liposomes containing 25 nmol $E7_{11-19}$ + 50 µg poly(I:C), SiO_2-Arg + 50 µg poly(I:C) or empty liposomes + 50 µg poly(I:C) in either 20 µl of 5% aqueous glucose solution (SiNP) or PBS (liposomes). S.c. vaccinations were performed on days 0, 7 and 14 with 25 nmol LPP-$E7_{11-19}$ + 50 µg poly(I:C) in 100 µl PBS. n=6 for all groups. All mice were hormonally synchronized six and five days prior to the first vaccination. After sacrifice on day 21, spleens and GTs were removed, dissociated and cells analyzed by flow cytometry. Results for splenocytes are displayed on the left, for GT cells on the right. (A) Percentages of $CD8^+$ of $CD3^+$ cells. (B) Percentages of $CD69^+$ $CD103^+$ of $CD8^+$ cells. (C) Percentages of $IFN\gamma^+$ of $CD8^+$ cells after 5 h restimulation of cells with either cognate peptide $E7_{11-19}$ or non-cognate peptide $Surv_{96-104}$. Statistical analysis of experimental groups for A – C was performed with Kruskal-Wallis tests followed by Dunn's multiple comparison and in C within an experimental group with Wilcoxon matched-pairs signed rank tests. *$p \leq 0.05$, **$p \leq 0.01$

For an intraexperimental positive control, one group of mice was vaccinated only s.c. with LPP-$E7_{11-19}$. As expected, the s.c. immunized mice displayed the highest levels of $CD8^+$ T cells in their spleen and also in the GT (Figure 42A). While no significant difference of $CD8^+$ T_{RM} was found in splenocytes, the GT cells displayed higher levels of $CD69^+CD103^+$ T cells. The lowest percentage of T_{RM} in the GT was detected for the s.c. vaccinated group. Animals instilled ivag. with liposomes had more T_{RM} in their GTs than those instilled with SiNP. Again, the ivag. vaccination did not elicit $E7_{11-19}$-specific T cells in the GTs while s.c. vaccinated mice also had specific T cells in their GT additional to their spleen (Figure 42C). These cells had most likely migrated into the mucosa from the blood stream. Unfortunately, the clear induction of systemic immunity through ivag. SiNP vaccination could not be replicated apart from one mouse with 2 % $CD8^+$ $IFN\gamma^+$ T cells over background (restimulation with the non-cognate peptide). In conclusion, the ivag. vaccination route does not induce a specific local immunity to the epitope of interest when liposomes, LPP or SiNP are used as vehicles. The examination of other carrier systems might result in a working ivag. vaccination approach.

4.2.2 Prime and pull approach

Another interesting approach to increase the amount of mucosal, $E7_{11-19}$-specific T cells is systemic vaccination followed by a vaginal stimulus for the T cells to migrate into the mucosa. First described in Shin and Iwasaki (2012), specific T cells can be primed by a systemic vaccination and then be pulled towards the target tissue via application of an immunomodulating pull, i.e. the induction of a local inflammatory state. Shin and Iwasaki used the chemokines CXCL9 and CXCL10 for this purpose, but also the topical application of TLR agonists that activate the innate immune response (Soong et al., 2014) or local irradiation (Klug et al., 2013) are thinkable. The chemokines CXCL9 and CXCL10 are usually produced by infected tissues upon IFNγ-signaling and induce a chemotactic migration of $CXCR3^+$ T cells into the tissue (Mueller et al., 2013; Laidlaw et al., 2016).

Vaginal applications or tumor instillations are mostly preceded by vaginal application of the spermicide N-9 some hours prior to treatment, which disrupts the mucosa (Roberts et al., 2007). This facilitates the uptake of treatment compounds or tumor cells. As I did not find any evidence in literature whether an N-9 pretreatment is necessary to successfully pull T cells towards the murine genital mucosa, I tested it by vaccinating mice s.c. three times and then locally treating

them with CXCL9 and CXCL10. The chemokine application was either preceded by an N-9 treatment or not (Figure 43).

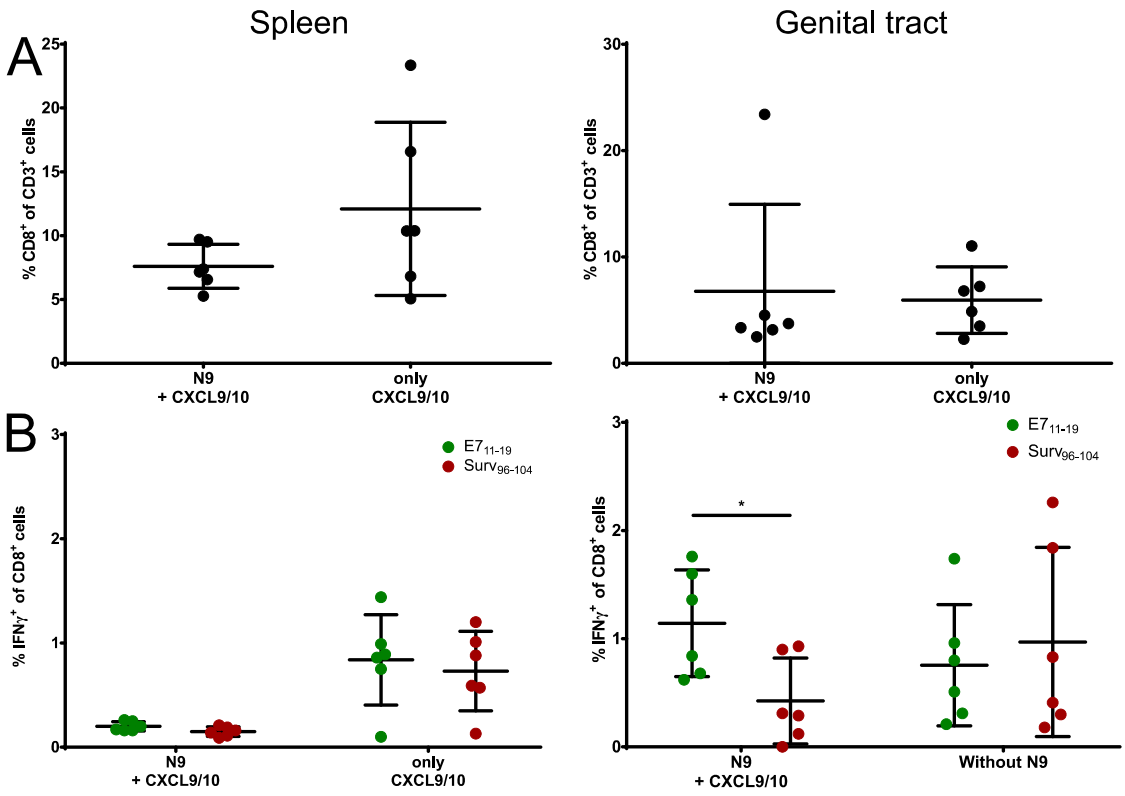

Figure 43. Necessity of N-9 for successful pulling of T cells. Six mice per group were hormonally synchronized six and five days prior to the first vaccination. S.c. vaccination was performed on days 0, 7 and 14 with 50 nmol LPP-$E7_{11-19}$ + 50 µg poly(I:C) in 100 µl PBS. On day 19, mice were either treated with N-9 or not and received 3 µg CXCL9 and 3 µg CXCL10 in 20 µl PBS ivag. 6 h afterwards. After sacrifice on day 20, spleens and GTs were removed, dissociated and cells analyzed by flow cytometry. Results for splenocytes are displayed on the left, for GT cells on the right. (A) Percentages of $CD8^+$ of $CD3^+$ cells. (B) Percentages of $IFN\gamma^+$ of $CD8^+$ cells after 5 h restimulation of cells with either cognate peptide $E7_{11-19}$ or non-cognate peptide $Surv_{96-104}$. Statistical analysis of experimental groups for A + B was performed with Kruskal-Wallis tests followed by Dunn's multiple comparison and in B within an experimental group with Wilcoxon matched-pairs signed rank tests. *$p \leq 0.05$

Interestingly, the level of $CD8^+$ splenocytes was higher when no N-9 was used ivag. However, it does not seem that T cells in N-9-treated mice traveled to the GT as the cells obtained from the GT did not display an elevated level of $CD8^+$ T cells except in one mouse (Figure 43A). When examining the $E7_{11-19}$-specific T cells a significant percentage was found in the GTs of N-9 pretreated mice but not of untreated ones. These T cells were also not an artifact of a very high splenic rate of $E7_{11-19}$-specific T cells as no big difference was observed in splenocytes (Figure 43B). Therefore, I applied N-9 to the mucosa in all subsequent experiments 6 h before ivag. treatment with the immunomodulatory substance.

The final goal of this series of experiments was the comparison of TLR7 agonists resiquimod and imiquimod (TLR7) with CXCL9 and CXCL10 for their capacity to induce T cell trafficking into the vaginal mucosa. To find out which amount of the TLR agonists was needed I titrated both substances by vaccinating mice s.c. with LPP-$E7_{11-19}$ and afterwards using the TLR agonist as an ivag. pulling agent. Resiquimod was titrated in a range from 1 – 20 µg. Although there was a significant difference in splenic $CD8^+$ T cell levels, this was not observed in the GTs. Interestingly though, the experimental group with the lowest level of $CD8^+$ T cells among splenocytes displayed the highest levels of $CD8^+$ cells in their GTs (Figure 44A). It was confirmed that the resiquimod treatment did have an effect on $CD8^+$ T cells because they expressed the surface marker CD69 in both spleen and GT in correlation to the amount of applied TLR agonist (Figure 44B). This had been described before in literature (Craft et al., 2014). When checking for pulled, $E7_{11-19}$-specific $CD8^+$ T cells I did not detect a significant difference between the experimental groups (Figure 44C). The biggest observed difference between $E7_{11-19}$ and $Surv_{96-104}$-stimulated cells was detected in GTs treated with 2.5 µg of resiquimod. Therefore, this amount of TLR agonist was used for later experiments. It has to be noted that no specific T cell response could be found when analyzing the splenocytes.

As done for resiquimod, I also titrated the amount of imiquimod. Resiquimod is known to be more potent than imiquimod, which is why the amount used for imiquimod application was in a higher range of 2.5 µg – 50 µg. After ivag. treatment of imiquimod there were nearly no differences in $CD8^+$ T cell levels in the spleen or the genital tract observed (Figure 45A). Additionally, no significant differences between IFNγ-producing T cells after $E7_{11-19}$ and $Surv_{96-104}$ stimulation was detected in spleen or GT, respectively (Figure 45B). When GTs were treated with 25 µg of imiquimod, the difference between $E7_{11-19}$ and $Surv_{96-104}$-restimulated T cells was the largest, which is why 25 µg of imiquimod were used in the following experiments.

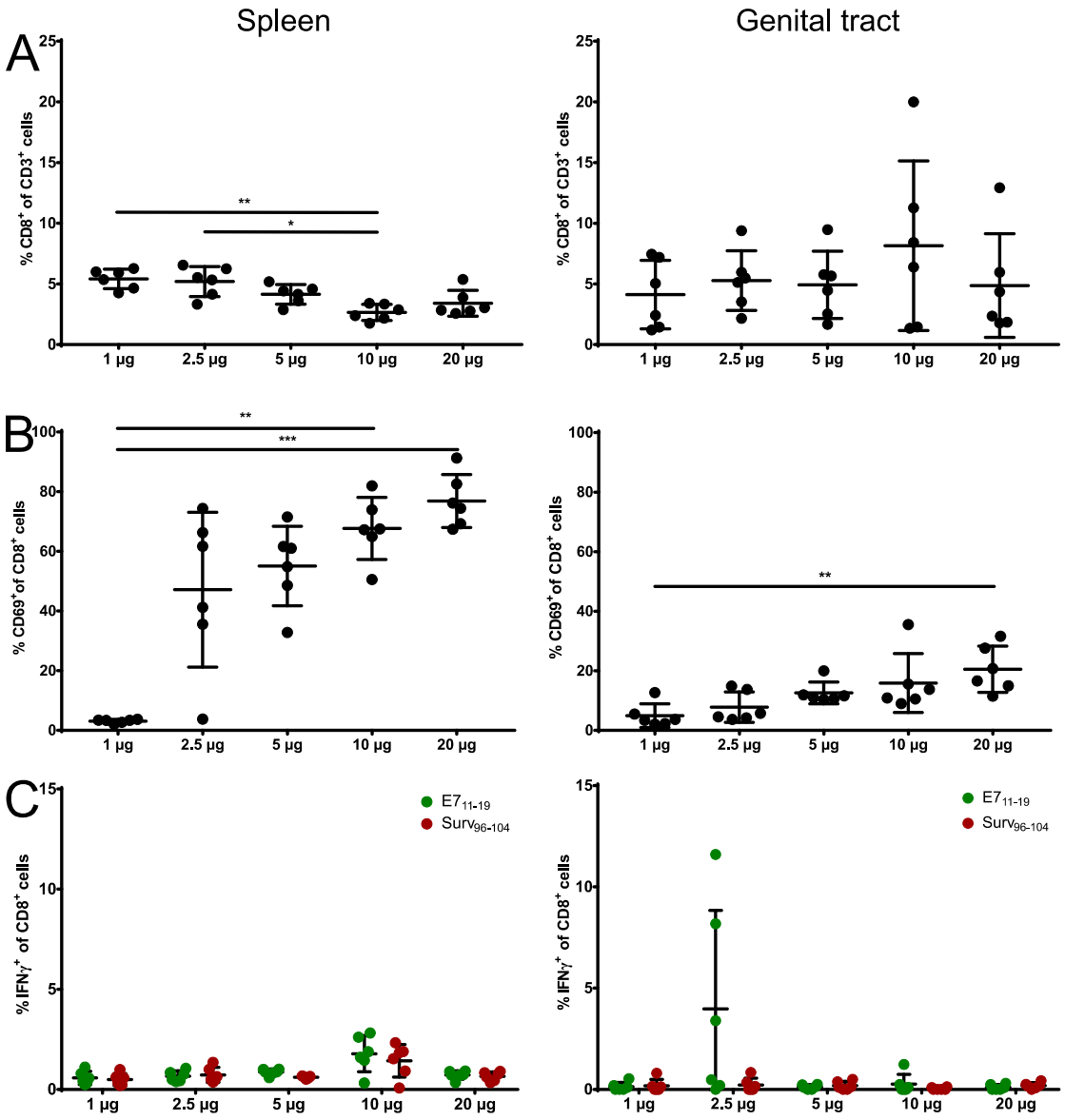

Figure 44. Titration of resiquimod to pull T cells into the genital mucosa. Six mice per group were hormonally synchronized six and five days prior to the first vaccination. S.c. vaccination was performed on days 0, 7 and 14 with 50 nmol LPP-$E7_{11-19}$ + 50 µg poly(I:C) in 100 µl PBS. On day 19, mice were treated with N-9 and received the indicated amounts of resiquimod in 20 µl PBS ivag. 6 h afterwards. After sacrifice on day 20, spleens and GTs were removed, dissociated and cells analyzed by flow cytometry. Results for splenocytes are displayed on the left, for GT cells on the right. (A) Percentages of $CD8^+$ of $CD3^+$ cells. (B) Percentages of $CD69^+$ $CD103^+$ of $CD8^+$ cells. (C) Percentages of $IFN\gamma^+$ of $CD8^+$ cells after 5 h restimulation of cells with either cognate peptide $E7_{11-19}$ or non-cognate peptide $Surv_{96-104}$. Statistical analysis of experimental groups for A – C was performed with Kruskal-Wallis tests followed by Dunn's multiple comparison and in C within an experimental group with Wilcoxon matched-pairs signed rank tests. *p≤0.05, **p≤0.01, ***p≤0.001

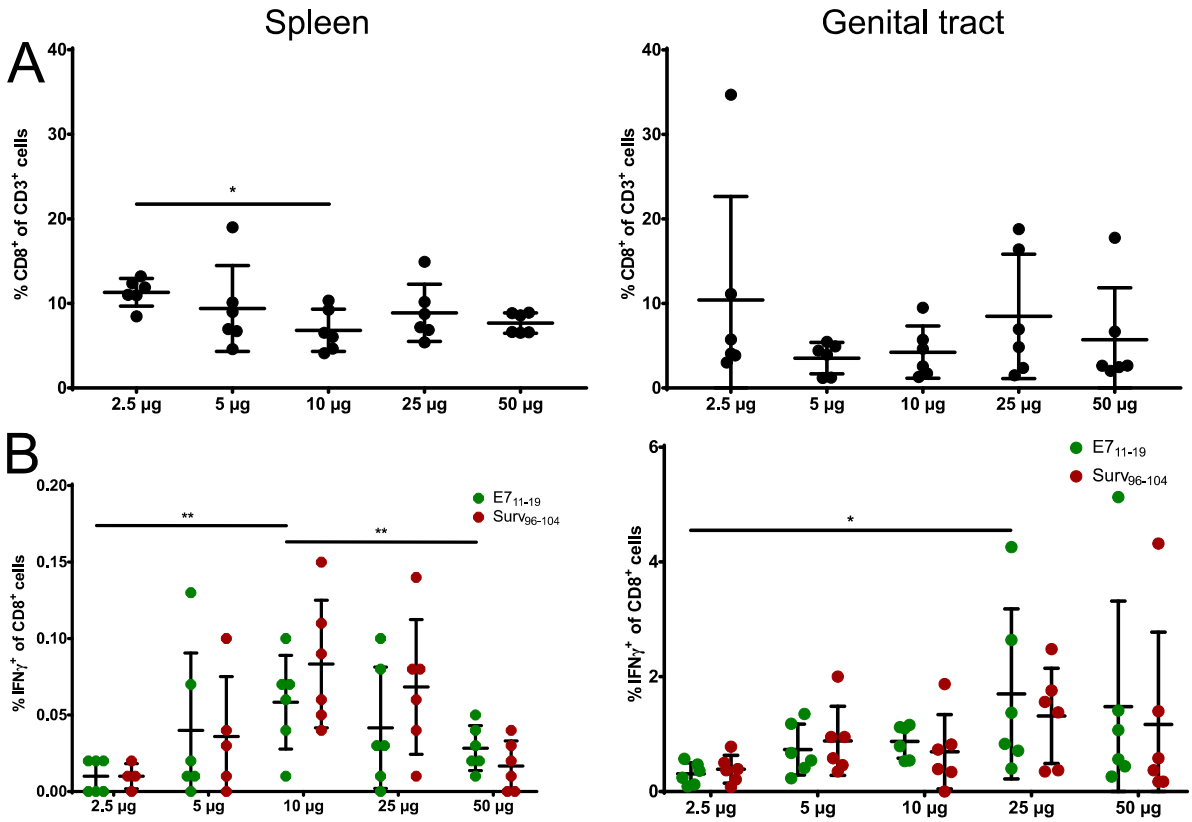

Figure 45. Titration of imiquimod to pull T cells into the genital mucosa. Six mice per group were hormonally synchronized six and five days prior to the first vaccination. S.c. vaccination was performed on days 0, 7 and 14 with 50 nmol LPP-$E7_{11-19}$ + 50 µg poly(I:C) in 100 µl PBS. On day 19, mice were treated with N-9 and received the indicated amounts of imiquimod in 20 µl PBS ivag. 6 h afterwards. After sacrifice on day 20, spleens and GTs were removed, dissociated and cells analyzed by flow cytometry. Results for splenocytes are displayed on the left, for GT cells on the right. (A) Percentages of $CD8^+$ of $CD3^+$ cells. (B) Percentages of $IFN\gamma^+$ of $CD8^+$ cells after 5 h restimulation of cells with either cognate peptide $E7_{11-19}$ or non-cognate peptide $Surv_{96-104}$. Statistical analysis for A + B was performed with Kruskal-Wallis tests followed by Dunn's multiple comparison in B within an experimental group with Wilcoxon matched-pairs signed rank tests. *$p \leq 0.05$, **$p \leq 0.01$.

After the preliminary experiments were concluded, I used the established TLR agonist amounts to compare different methods of pulling T cells into the vaginal mucosa (Figure 46). Six mice per group were again vaccinated s.c. three times with LPP-$E7_{11-19}$. Afterwards the animals were treated with N-9 and either CXCL9 and CXCL10, resiquimod, imiquimod or PBS were later topically applied to the genital mucosa. Unfortunately, it turned out that the mice of the control group treated ivag. with PBS showed the highest level of $E7_{11-19}$-specific T cells in their GTs (Figure 46F). It was expected that PBS treatment would not induce a migration of T cells into the mucosa. Therefore, the most probable explanation was that the detergent N-9 alone was able to pull the previously activated T cells by the induction of a genital inflammation. Therefore, I repeated the same experiment but omitted the N-9 treatment. It was clear to see

that the percentage of $CD8^+$ T cells in the spleens was higher when the mice were not treated with N-9 and thus the cells probably remained in the blood circulation. Vice versa, GTs of mice treated with N-9 possessed elevated levels of $CD8^+$ T cells compared to untreated mice (Figure 46A). As seen before, the treatment with resiquimod did induce significant overexpression of CD69 on $CD8^+$ T cells both in splenic as well as in GT $CD8^+$ T cells. Interestingly, this time also imiquimod caused a rise in $CD8^+CD69^+$ T cells in GTs after N-9 treatment. In general, the CD69 levels in GTs were enhanced in all N-9-pretreated mice, which may result from the activation of T cells and subsequent expression of the activation marker CD69 (Figure 46B). Comparing the percentages of $CD8^+CD69^+CD103^+$ T cells, there was no significant difference detected within the tissues. However, there was a clear increase in T cells with T_{RM} surface markers in the spleen (Figure 46C). This might have also been due to increase of CD69 on the cell surface resulting in a flow cytometric artifact where these cells fall into the $CD69^+CD103^+$ gating of the splenocytes analysis. $CD8^+$ T cells displaying a T_{EM} phenotype were found abundantly in the spleens of both, N-9-pretreated and untreated mice while the levels were much lower in GTs (Figure 46D). As expected, no T_{CM} were found in the GTs. However, it is intriguing that the level of splenic T_{CM} was elevated in mice treated with N-9, compared to the N-9-untreated animals (Figure 46E). Finally, as mentioned above, most $E7_{11-19}$-specific T cells were found in the GTs of N-9-pretreated mice. When the N-9 treatment was omitted, no significant difference between $E7_{11-19}$ and $Surv_{96-104}$-restimulated GT cells was detected anymore (Figure 46F). There was, however also a discrepancy in efficacy of the s.c. vaccination between the two experiments. While there were significant levels of $E7_{11-19}$-specific T cells in the spleens of N-9 treated mice, there was only a very small induction of an immune response in the experiment without N-9 treatment. This might also have influenced the amount of specific $CD8^+$ T cells in the GTs of the respective mice. Therefore, I plotted the levels of $E7_{11-19}$-specific $CD8^+$ T cells in the GTs in correlation to those in the spleen of mice seen in Figure 46 (Figure 47). It is very clear to see for N-9-pretreated mice that the two animals with the highest levels of splenic specific $CD8^+$ T cells also display the highest levels of specific T cells in their GTs. This can also be observed for the groups treated with CXCL9 and CXCL10 and resiquimod. It therefore seems that N-9 had only minor effects, if any, on the T cell trafficking. Mice untreated with N-9 also showed more genital specific $CD8^+$ T cells when they already had high levels in their blood (Figure 47).

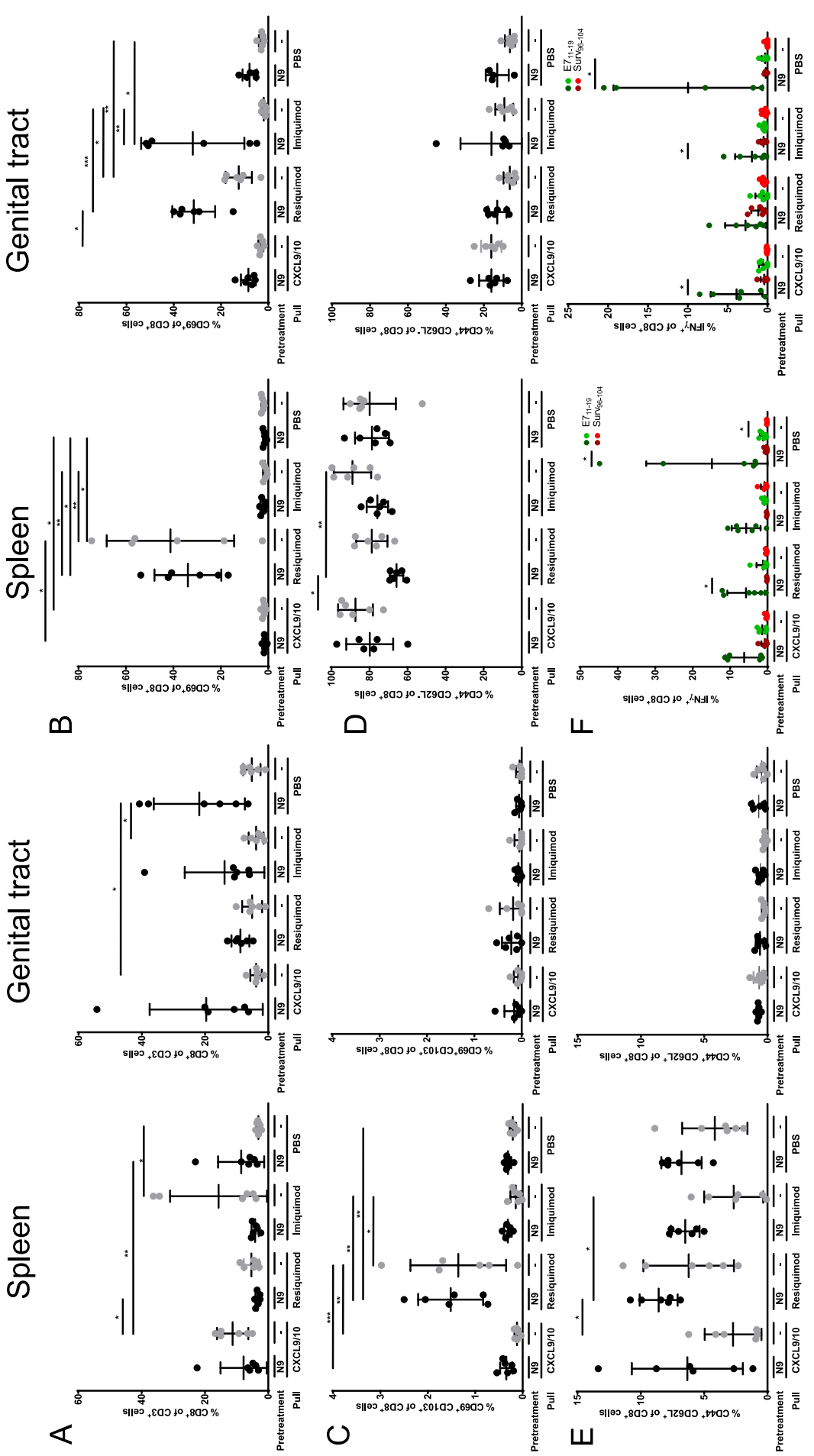
Spleen
Genital tract
Spleen
Genital tract
A
B
C
D
E
F
% CD8+ of CD3+ cells
% CD69+ of CD8+ cells
% CD69+ CD103+ of CD8+ cells
% CD44+ CD62L- of CD8+ cells
% CD44+ CD62L+ of CD8+ cells
% IFNγ+ of CD8+ cells
E7 11-19
Surv 96-104
Pretreatment
Pull
N9
CXCL9/10
Resiquimod
Imiquimod
PBS

Figure 46. Comparison of immunomodulatory compounds for pulling T cells into the genital mucosa. Six mice per group were hormonally synchronized six and five days prior to the first vaccination. S.c. vaccination was performed on days 0, 7 and 14 with 50 nmol LPP-$E7_{11-19}$ + 50 µg poly(I:C) in 100 µl PBS. On day 19, mice were either treated with N-9 or not and received 3 µg CXCL9 and 3 µg CXCL10, 2.5 µg Resiquimod or 25 µg Imiquimod in 20 µl PBS or PBS only ivag. 6 h afterwards. After sacrifice on day 20, spleens and GTs were removed, dissociated and cells analyzed by flow cytometry. Results for splenocytes are displayed on the left, for GT cells on the right. (A) Percentages of $CD8^+$ of $CD3^+$ cells. (B) Percentages of $CD69^+$ of $CD8^+$ cells. (C) Percentages of $CD69^+$ $CD103^+$ of $CD8^+$ cells. (D) Percentages of $CD44^+$ $CD62L^-$ of $CD8^+$ cells (E) Percentages of $CD44^+$ $CD62L^+$ of $CD8^+$ cells (F) Percentages of $IFN\gamma^+$ of $CD8^+$ cells after 5 h restimulation of cells with either cognate peptide $E7_{11-19}$ or non-cognate peptide $Surv_{96-104}$. Statistical analysis for A - F was performed with Kruskal-Wallis tests followed by Dunn's multiple comparison and with Wilcoxon matched-pairs signed rank tests (F).

In conclusion it can be assumed that N-9, as well as the other immunomodulatory substances including the published CXCL9 and CXCL10 chemokines, do not have or only have a small effect on pulling the T cells. The level of systemic specific T cells seems to be a more important factor for T cell migration to the genital mucosa.

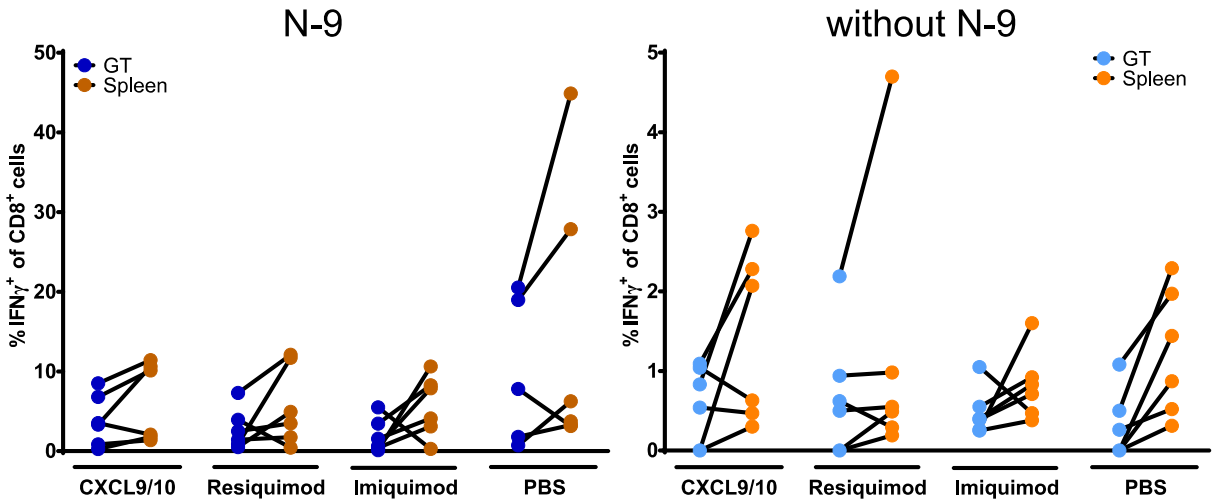

Figure 47. Percentages of $IFN\gamma^+$ of $CD8^+$ cells in GTs and spleens of mice treated ivag. with immunomodulatory substances. Shown are the percentages of $IFN\gamma^+$ of $CD8^+$ cells after 5 h restimulation of cells with cognate peptide $E7_{11-19}$ in the respective tissue as seen in Figure 46F for N-9-pretreated (left) and not pretreated animals (right). The values of the GT and spleen of each single mouse are connected by a line.

5 Discussion

HPV16 is one of the main causes for oropharyngeal and anogenital cancers. In 2018 690,000 cancer cases attributed to HPV infection were recorded worldwide (de Martel et al., 2020). Most of these cases were cervical cancers, which are almost exclusively caused by HPV and are the fourth most common cancers found in women. Of 570,000 women with cervical cancer, 311,000 died from the disease in 2018 (Arbyn et al., 2020). The economic loss attributed to HPV-related cancers in the US amounts to about 150,000 years of potential life loss and $ 3.8 billion 'present value of future lost productivity'. Therefore, these cancers are also a considerable economic burden (Priyadarshini et al., 2021). While rates of cervical cancer are progressively declining in well-developed countries, they are still one of the most prevalent cancers and one of the leading causes of cancer-related deaths for women in less-developed countries. This is especially due to insufficient access to prevention measures and lack of sexual education (Hu & Ma, 2018; Hull et al., 2020). Common and widely used therapies for HPV-related cancers and especially cervical cancers are surgery, chemotherapy and radiotherapy. However, these can result in infertility, higher incidence of miscarriage as well as irradiation-induced off-target damages to surrounding tissues (Cohen et al., 2019). Thankfully, there are so far three different prophylactic HPV vaccines on the market that prevent infections with the most oncogenic HPV types such as HPV16 or HPV18 (Cheng et al., 2020). In 2020, 85 % of high-income countries had the HPV vaccination introduced to their national immunization schedules while only 25 % of less-developed countries had so far introduced the vaccines. However, despite their proven efficacy, the vaccination rates in countries where the vaccines are easily accessible are often equally low as in low-income countries (World Health Organization, 2017; Bruni et al., 2021; Dorji et al., 2021). Low vaccination rates in turn mean that although there will be fewer HPV-associated malignancies in the future, there will still be a substantial amount of mucosal lesions and cancers to make a new efficient treatment option with fewer side effects a desirable goal for research. The possibly best option for this purpose is the development of a therapeutic vaccine. Therefore, the focus of our research group is on the development of a therapeutic vaccine against HPV16-mediated disease.

HPV with its oncoproteins E6 and E7 is a prime candidate for an anti-cancer vaccine. The expression of the two proteins is necessary for the sustained growth of the tumors. If their expression is lost by the infected cells, they either go into apoptosis or senescence (Pal &

Kundu, 2019). Additionally, E6 and E7 are only expressed in HPV-infected cells and thus serve as neoantigens and markers for infection. This makes them ideal targets for an immunotherapeutic vaccine stimulating a $CD8^+$ T cell response (Lee et al., 2016; Chabeda et al., 2018). In the past, many different approaches to therapeutic HPV vaccination have already been tested (reviewed in Chabeda et al. (2018)). However, even though there have been many successful studies where immunity to HPV oncoproteins could be induced in mice and led to regression in preclinical tumor models such as TC-1, the therapies failed to properly translate into clinical trials. How can this discrepancy be explained?

First and foremost is the difference between mice and humans. The most commonly used laboratory animal is *mus musculus*, the laboratory mouse. Mice and humans are separated by about 70 million years of evolution in different ecological niches since their last common ancestor. Still, only 300 genes are truly unique to only one of the two species. Despite the high levels of genetic conservation, there are still some major differences in the immune systems. These differences include the ratios of leukocyte populations in blood, differential expression and function of TLRs and PRRs, Ig isotypes, as well as T cell development, signaling and regulation (Mestas & Hughes, 2004). Another problem is the lack of accurate modeling of disease onset and progression. In the case of HPV, for example, the viruses are species-restricted and do not infect rodents (Christensen et al., 2017). Therefore, mice are more suited to gain focused glimpses into modeled diseases but not for examination of the whole picture (Mak et al., 2014). The translation success between mice and humans is unpredictable and can range from 0 – 100 % (Leenaars et al., 2019).

The second reason for poor translatability between the two species in therapeutic vaccination approaches are the MHC molecules. Therapeutic vaccines are targeted for induction of $CD8^+$ T cell-mediated immune responses. The epitopes needed for induction of such $CD8^+$ T cell responses vary in their immunogenicity, i.e. they induce different levels of immune responses. As murine MHCs bind different epitopes than HLAs, the immunogenic effect of minimal epitope vaccine formulations can hardly be translated. The best example for this is HPV16 $E7_{49\text{-}57}$, a highly immunodominant H-$2D^b$-restricted epitope (Feltkamp et al., 1993) used in many preclinical studies. This epitope is presented on the surface of the E6 and E7-expressing TC-1 tumor model, which is often used to test preclinical therapeutic vaccines against HPV16 (Lin et al., 1996). Due to the immunodominance of $E7_{49\text{-}57}$, TC-1 tumors are readily eradicated

by a $CD8^+$ T cell response in mice. If the human epitope used in a subsequent clinical trial is not as immunogenic as the murine epitope, the clinical response is not as strong as seen in C57BL/6 mice. Moreover, it has to be considered that a human individual can express up to 6 different MHC I molecules on their cells' surfaces (Murphy & Weaver, 2017) while inbred mice mostly express only one or two different molecules. The presentation of many different epitopes on different MHC molecules leads to less total presentation of one specific epitope and consequently to a subdued immune response in comparison to animals possessing only one MHC I variant.

Third, many vaccination studies with transplantable HPV16 tumor models have been conducted with s.c. TC-1 tumors. It has been reported that mucosal tissue, where HPV-mediated tumors mostly reside, is only accessible to T cells upon local inflammation. Otherwise the mucosae are exempt from T cell circulation (Shin & Iwasaki, 2013). Therefore, HPV-specific T cells may be very successful in clearing a tumor they easily detect in the subcutis, but they might struggle to reach a mucosally located tumor in patients. One possibility to facilitate T cell migration to a mucosal tumor is an inflammatory cytokine release in the mucosa, but induction of the necessary inflammatory state might be prevented by HPV-infected cells (Steinbach & Riemer, 2017). The mucosal tumor environment is also likely to influence the differential expression of proteins compared to the subcutis (Killion et al., 1998), rendering previously efficacious vaccination methods useless when applied to the mucosal setting. Other factors such as adjuvants working differently in mice and humans due to differences of TLRs (Mestas & Hughes, 2004; Apostolico et al., 2016) can also negatively affect the translational value of preclinical mouse experiments.

Hence, we are working in our group on developing a therapeutic HPV16 vaccine based on epitopes truly presented by HLA molecules on HPV16-derived tumors. Our lead epitope is HPV16 $E7_{11\text{-}19}$, which is presented on cervical cancers and which induces stable anti-tumor $CD8^+$ T cell responses in the HLA-A2-restricted epitope-presenting MHC-humanized A2.DR1 mouse model (Riemer et al., 2010; Keskin et al., 2011; Kruse et al., 2018).

In this PhD project I first worked on the establishment of an HPV16 E6 and E7-dependent vaginal tumor model in A2.DR1 mice to overcome the disparity of mucosal and s.c. tumor environments. The MHC-humanized mouse model A2.DR1 allows for the study of HLA-A2-

restricted epitopes instead of H-2-restricted epitopes. Not only does this directly benefit individuals carrying HLA-A2 on their cells (e.g. about 50 % of Europeans) but it also excludes the immunodominant H-2D^b epitope E7$_{49-57}$ and therefore an extremely potent and possibly misleading murine CD8$^+$ T cell response. The T cells of these MHC-humanized mice are trained in the thymus on HHD and HLA-DR1 instead of H-2 molecules in absence of the murine MHCs, leading to the recognition of HLA-restricted epitopes on human MHC molecules. HHD additionally has a murine instead of a human α_3 domain to improve interaction with murine CD8 co-receptors on T cells (Pascolo et al., 1997). Even though these mice are used to study HLA-restricted immune responses, the responses are still embedded in an otherwise murine system. This means that the innate immune system and also the antigen processing works differently than in human cells (Pascolo, 2005), which mitigates the translational aspects of the A2.DR1 mouse model. Additionally, the murine T cells also seem to be affected by the genetic alterations as A2.DR1 possess a lower fraction of CD8$^+$ T cells of CD3$^+$ cells than their mother strain C57BL/6 (observation by Sebastian Dr. Kruse). If these limitations are kept in mind, the mouse strain offers a more accurate picture of a human epitope-specific T cell response than mice expressing murine MHCs.

The presented vaginal tumor model located in the murine cervicovaginal mucosa resembles the clinical situation of HPV cancer patients more closely than s.c. tumor models surrounded by adipose and connective tissues. Although HPV16 can also cause vaginal cancer, cervical cancers are much more common and make up the majority of HPV-related cancers. Unfortunately, the murine cervix is quite small and therefore hard to transplant with tumor cells. Human cervical cancers most often develop from an HPV infection at the transition zone where columnar epithelium of the uterus meets stratified epithelium of the vagina (McBride, 2022). Conveniently, the mouse epithelial transition zone is not only limited to the murine cervix but also covers a large part of the cervicovaginal tract (Böttinger et al., 2020). Therefore, the transplanted tumors in the vaginal mucosa can be considered to be located in a similar environment as tumors of cervical cancer patients. Another difference is that the tumors established in this work are enclosed by mucosal epithelial cells instead of arising from the vaginal epithelium, which might affect the anti-tumor response. Tumor models where the tumors develop from genetically altered murine mucosal cells also exist (reviewed in Santos et al. (2017)) although so far these do not exist in MHC-humanized mice. Additionally, as the

introduced oncogenes are present throughout the life of the animal, they are limited by the possible development of T cell tolerance to the expressed HPV proteins (Trimble & Frazer, 2009).

The dependence of the tumor cells of my newly established tumor model E6/7-lucA2 on E6 and E7 not only ensures the continuous expression of these vaccination target proteins but also increases the translational value of the model. If expression of E6 and E7 was lost, the tumor cells would become senescent or apoptotic. This is not the case in HPV-independent cell lines such as PAP-A2 where for example E7 does not seem to fulfill its biological function (Figure 34). The dependence of E6/7-lucA2 on the HPV oncoproteins guarantees that the established tumors present the epitopes of interest at all times during experiments. This eliminates the possibility of loss of epitope on the tumor cells, which could lead to false-positive failure of therapeutic vaccinations against HPV16 peptides. On the other hand, the likelihood of tumor cells evading the immune response is increased if E6 and E7 are active. The proteins for example interfere with immune signaling pathways, leading to reduced antigen presentation on MHCs or suppressed expression of inflammatory-associated genes (Zhou et al., 2019). This immune evasion can hamper therapeutic vaccination efforts but renders the model more comparable to the human situation.

To overcome the problem of T cells not entering the genital mucosa I tested different methods for facilitation of T cell trafficking into the vaginal tissue. It has been shown before that $CD103^+$ tumor infiltrating lymphocytes (TILs) and therefore T cells with tissue residency markers play a vital role in cervical cancer control, as for example $CD103^+$ TILs showed a prognostic benefit for cervical cancer patients (Komdeur et al., 2017). The induction of mucosal T cells, or even better T_{RM}, might therefore be crucial for an efficacious cancer vaccination approach (Lange et al., 2021).

In summary, I set out to narrow the gap between human and mouse studies by establishing an HPV16 E6 and E7-dependent tumor model in the vaginal mucosa of MHC-humanized mice and by examining how to induce a T cell response in the GT.

5.1 Generation of an HPV16-dependent tumor cell line for A2.DR1 mice

For the establishment of the novel cell line I aimed for an HPV16 $E6^{+}E7^{+}$ tumorigenic cell line for use in an orthotopic tumor model. The easiest solution was the further development of the already existing PAP-A2 cell line.

Thus, in a first approach, PAP-A2 cells needed additional expression of firefly luciferase for allowing intracorporeal tumor tracking. The cells are based on the MCA-induced A2.DR1 sarcoma cell line 2277-NS (Quandt, 2014), which was transduced with HPV16 E6 and E7 in our lab (Kruse et al., 2018). Due to its sarcoma origin, the PAP-A2 cell line was already tumorigenic in itself, which made transfection with $HRAS^{G12V}$ for tumorigenic transformation unnecessary. Additionally, this cell line is already immortal independently of HPV16 E6 and E7, increasing the likelihood of undetected loss of the vaccination target proteins. Although the newly generated PAP-A2-luc cell line proved to be tumorigenic, its development was abandoned due to the cells not being killed by HPV16-specific T cells.

In a next step, I took non-tumorigenic A2.DR1 cells of origin into my focus. The most genuine possible transplantable cell line would have been derived from A2.DR1 cervicovaginal keratinocytes, as basal keratinocytes are the cells infected in human cervical cancers (Gheit, 2019). As the GT comprises a manifold of different cells, I first tried to isolate mouse epidermal keratinocytes from newborn mice where the separation of dermis from epidermis is easier than for adult mice (Li et al., 2017). Unfortunately, these cells turned out to be very hard to culture and even harder to transfect or transduce, which is why I abandoned this approach. The widely used transplantable HPV16 tumor model TC-1 consists of transformed C57BL/6 lung cells that model epithelial cells expressing HPV proteins (Lin et al., 1996). Consequently, I chose A2.DR1 lung cells for the development of the E6 and E7-dependent syngeneic tumor cell line, analogous to the TC-1 cell line. TC-1 consists of C57BL/6 lung cells that were immortalized with HPV16 E6 and E7 and became tumorigenic through transduction with $HRAS^{G12V}$ (Lin et al., 1996). TC-1/A2-luc cells used in this work as a control cell line are a luminescent version of TC-1 cells, which additionally express the AAD molecule, another HLA-A2 analog for MHC I, on their surface (Peng et al., 2006). As TC-1 cells are derived from another mouse strain and express a different set of MHC molecules they are not suited to be used in A2.DR1

mice, which is why I replicated their generation with syngeneic lung cells. However, they provided a good control cell line to check for expression of the desired proteins (HPV16 E6 and E7, $HRAS^{G12V}$).

The lungs are lined by pseudostratified epithelial cells, i.e. the nuclei of the single line of cells are not on the same level and therefore appear to be multilayered, as well as being lined by respiratory mucosa (Kia'i & Bajaj, 2021). Being epithelial cells, the lung cells resemble cells of the genital mucosa more closely than sarcoma-derived cells such as 2277-NS and PAP-A2. Additionally, the lungs display a large surface area (Knust et al., 2009), which promises high cell yields upon dissociation. When Lin et al. (1996) developed the TC-1 cell line they checked the cells for expression of cytokeratin to ensure the epithelial origin of cells. This has not yet been done for the lung cells used here, which might be a limitation for the cell lines' usefulness in translational purposes in addition to their non-cervicovaginal origin. However, the respective experiments for verification of epithelial origin are in progress in our group.

In contrast to PAP-A2, one can expect much less mutational burden that could enhance off-target immunogenic effects for the lung cell-derived line. In other studies, MCA-derived mouse sarcomas, such as 2277-NS or PAP-A2, harbored roughly 80 times more mutations than cells transformed with irradiation or $KRAS^{G12D}/p53^{-/-}$ mutations (Lee et al., 2019). The A2.DR1 lung cells had been transduced with HPV16 E6 and E7 prior to my work. Along with the transfection of the telomerase hTERT and the simian virus 40 (SV40) early region genes, the transformation with E6 and E7 belongs to the most common methods of cell immortalization (Yeager & Reddel, 1999) as described before in 1.3.3. Conveniently, the two immortalizing oncoproteins are also the targets of our therapeutic vaccination efforts. In previous experiments in our group, the E6 and E7-transduced syngeneic lung cells had not induced tumor growth when injected s.c. into A2.DR1 mice and were therefore not pursued further as a possible tumor cell line. However, the two HPV proteins need help of a synergizing activated oncoprotein such as $HRAS^{G12V}$ to establish tumorigenicity of the cell line (Lin et al., 1996; Eiben et al., 2002; Schreiber et al., 2004), which was my starting point. In addition to ensuring tumorigenicity, firefly luciferase for enabling intracorporeal tumor tracking again had to be introduced.

Each introduction of new genes into cells also increases the possibility of introducing neoepitopes, which might enhance the cells' immunogenicity and therefore promote

vaccination-independent tumor clearance. There are immunogenic MHC I epitopes of firefly luciferase origin known for the murine H-2K^{d} and H-2D^{b} molecules (Limberis et al., 2009). Literature research did not lead me to any HLA-A2-restricted luciferase epitopes but *in silico* prediction with NetMHC 4.0 (Andreatta & Nielsen, 2016) resulted in six possible strong and 25 possible weak binding 8mer, 9mer and 10mer peptides. By the same prediction approach, the transfection and subsequent expression of HRAS^{G12V} in these cells may lead to the additional presentation of one strong and seven weak binding epitopes on the cell surfaces. Obviously, the blasticidin resistance gene was also expressed as seen in the cells' resistance to 1 µg/ml blasticidin in media. Epitope prediction resulted for the resistance gene in one strong and two weak binders according to NetMHC 4.0. However, as no tumor rejection was seen in the first test of tumorigenicity of E6/7H-luc cells, obviously none of the introduced genes resulted in actual HLA-presentation of strongly immunogenic neoepitopes.

Another important point for the prospective tumor model cell line was the continuous expression of all necessary proteins. As tumors are heterogeneous entities (Fisher et al., 2013), especially the single-cell sorted clonal cell lines had to be checked again for the proteins. The different stages of cell line development were also assessed repeatedly *in vivo* for their tumorigenic potential. They all led to tumor formation, which is in line with published observations that *in vivo* passaging makes cell lines more tumorigenic (Sanford et al., 1959; Woodruff & Hodson, 1985).

During the establishment of the cell line I found that HPV16 E6 was consistently expressed less than E7 in all clonal cell lines. This is probably due to the vector used for the transduction of both, PAP-A2 and the lung cells (Appendix Figure 2). There, E6 and E7 are connected via a P2A sequence. This 19 amino acid-long sequence is widely used in biotechnology and helps in translation of both genes connected via P2A (Ryan et al., 1991). However, E6 is located after E7 on the vector, which most probably decreases the level of expressed E6 as generally seen for genes found in later positions on vectors (Liu et al., 2017).

Although all of the clonal cell lines expressed the target protein E7, I did not detect any specific killing of the E6/7H-luc cells (E6/7-lucA2 predecessor cells) in several VITAL-FR cytotoxicity assays or s.c. vaccination experiments. Although this could have been because of the cells' low presentation of target epitope, it turned out that the batch of LPP-E7$_{11-19}$ used for eliciting

specific CTLs was faulty. Once I used T cells resulting from a functional vaccine batch, the cytotoxicity assay worked as intended - although it turned out that the then preferred clone IH11 could not be specifically killed. IH11 cells were however specifically killed when they were artificially loaded with $E7_{11-19}$, which indicates that they express enough HHD on their surface but produce or present not enough endogenous E7.

The final tumor cell line E6/7-lucA2, obtained from a reisolation after an *in vivo* passage of the clone IIG6, was both tumorigenic in most mice implanted with the cells as well as amenable to peptide-specific killing by vaccination-induced T cells. Without this characteristic, novel vaccination approaches cannot be verified with the tumor model, thus rendering it indispensable for our purposes. However, immunogenicity levels correlate directly with MHC I expression in murine transplantable tumor models (Lechner et al., 2013). Analyzing the HHD level of the different cell lines, I saw a decline with each *in vivo* passage (Figure 26), which fits to the fact that MHC I downregulation is a general tumor evasion mechanism (Taylor & Balko, 2022). It is known that HPV-derived tumors downregulate the surface abundance of MHC I due to E7's effects on signaling pathways (Doorbar et al., 2015). Therefore the low MHC I levels as seen for example in IH11rere are true to the situation in the clinics.

To finalize the characterization of the newly generated cell line, a member of our group analyzed the E6/7-lucA2 HPV16 epitome by mass spectrometry-based immunopeptidomics and confirmed the presentation of $E7_{11-19}$ on the cell surfaces, which corroborates my VITAL-FR cytotoxicity data. Another epitope, $E7_{7-15}$ was found to be likely presented on the cells, which might be an interesting vaccination target for the established cell line as well. This epitope has also been shown to be a target of HPV16-specific T cells on PAP-A2 cells (Kruse et al., 2018). Although the murine antigen processing machinery works slightly differently and may produce other peptides than the human one (Street et al., 2002), they both result in the presentation of $E7_{11-19}$ as evidenced in E6/7-lucA2, PAP-A2 and human $HPV16^+$ cell lines and $HPV16^+$ tumor samples (Riemer et al., 2010; Keskin et al., 2011; Kruse et al., 2018). This means this epitope is highly suitable as a target of therapeutic vaccination approaches in A2.DR1 mice as well as in $HLA\text{-}A2^+$ patients.

In contrast to PAP-A2, E6/7-lucA2 cells are dependent on the expression of the HPV16 proteins E6 and E7, which immortalize the cells. When checking the expression of HPV16 E7

downstream protein $p16^{INK4a}$, which is used as a standard marker to assess a lesion's HPV status (Munger et al., 2013; Burd, 2016), I saw that E6/7-lucA2 as well as TC-1/A2-luc but not PAP-A2 overexpress the protein. This suggests an active role of E7 in the signaling of both E6/E7-immortalized murine lung cell lines in contrast to PAP-A2 cells. Therefore, it is reasonable to assume that E6/7-lucA2 cells truly depend on the expression of the HPV16 proteins for their maintenance.

Although E6/7-lucA2 have been generated very similarly to TC-1-luc cells (Lin et al., 1996; Decrausaz, Goncalves, et al., 2011) they have the major advantage of presenting HLA-A2-restricted epitopes to $CD8^+$ T cells, facilitating the translation to the human setting. Even though TC-1 cells have been transduced with AAD molecules equally presenting HLA-A2-epitopes, the resulting TC-1/A2 cells also still present H-$2D^b$-restricted epitopes, most prominently the immunodominant $E7_{49-56}$ epitope (Feltkamp et al., 1993). This skews the observed immune responses towards the murine epitope and its amino acid sequence has to be artificially altered when using TC-1/A2 to assess anti-HLA-A2 epitope responses in vaccination studies (Peng et al., 2006). The only drawback of E6/7-lucA2 cells compared to TC-1-luc cells are the increased numbers of cells needed for ivag. tumor formation. While C57BL/6 mice require only 12,500 TC-1-luc cells for stable ivag. tumor formation (Decrausaz, Goncalves, et al., 2011), A2.DR1 mice have to be instilled with 250,000 cells, indicating less tumorigenic potential or a more potent anti-tumor response in the MHC-humanized mice. However, as TC-1-luc-bearing mice had to be killed after 15 – 35 days post tumor instillation (Decrausaz, Goncalves, et al., 2011) and E6/7-lucA2 bearing mice after 17 – 35 days, the disparity in required cell numbers is just a technical aspect to be considered for experimental planning.

Other transplantable HPV^+ tumor cell lines also mostly present H-2-restricted epitopes and can just be used for studying vaccines in context of a murine epitope-restricted $CD8^+$ T cell response. Additionally, some of them are limited to the expression of only HPV E7 such as AT-84 cells in C3H mice (Paolini et al., 2014) or EL4-E7/C2 cells in C57BL/6 mice (Tindle et al., 1995; Fernando et al., 1998). In contrast to transplantable cell lines, some HPV^+ tumor models are generated by genetic modification and/or induction of HPV protein expression in mucosal cells such as tonsillar epithelial cells or cervicovaginal cells (Hoover et al., 2007; Mermod et al., 2018; Böttinger et al., 2020). Despite offering the advantage of modeling natural disease progression,

which cannot be provided by the transplantable cell line E6/7-lucA2, these induced tumor models are elaborate to set up and can also only be treated with vaccines against murine epitopes.

Another limitation for E6/7-lucA2 cells is the exclusive expression of E6 and E7. Although these HPV16 proteins are considered to be the major drivers of oncogenesis (Pal & Kundu, 2019), other HPV proteins might also provide immunogenic HLA-A2-restricted epitopes that can be used as vaccination targets. As E2 and E5 have been shown to be major targets of the intratumoral $CD8^+$ immune response in HNSCC patients (Eberhardt et al., 2021), these proteins also seem to be good targets for immunotherapy.

In summary, as planned, the new A2.DR1-syngeneic E6/7-lucA2 cell line is HPV16 E6 and E7-dependent, tumorigenic, as well as luminescent. It can be used for ivag. tumor modeling as established in this work, as well as for generating an HPV-driven HNSCC tumor model in A2.DR1 mice (ongoing work in another project in the group). Additionally, the cell line can be used as an E6 and E7-dependent s.c. tumor model. E6/7-lucA2 tumors can be used in *in vivo* vaccination studies or other immunotherapeutic or combination approaches.

5.2 Orthotopic tumor model

The murine ivag. tumor model was first established by the Nardelli-Haefliger group in 2011 with TC-1-luc cells (Decrausaz, Goncalves, et al., 2011) and served as the template for my work. The orthotopic, i.e. mucosal location provides different conditions for the tumors than for example in the subcutis: Most importantly, the tumors are located in the stratified epithelium of the murine vagina, making them accessible to only few pAPCs (Zhou et al., 2018). Incorporating this challenge into modeling of HPV^+ tumors in mice improves the translatability of preclinical studies to the clinical setting.

There have also been other vaginal and cervical murine HPV tumor models. These immunologically murine models are described in 1.4.1. For many of these models the HPV oncoproteins are expressed from birth in the respective mouse tissues which can lead to tolerance of these proteins by the immune system and therefore loss of immunogenicity (Trimble & Frazer, 2009). Other models, such as AMES-16, which is described in Henkle et al. (2021) and depends on *in vivo* electroporation with different genes, are much more elaborate to set up than a transplantable tumor model. The major difference of my work to other models are obviously the MHC-humanized A2.DR1 mice. In contrast to C57BL/6 mice commonly used in

HPV research, A2.DR1 cells present HLA- instead of H-2-restricted epitopes on their surface. So far, there have only been a handful of MHC-humanized mice used in HPV research. Apart from our own work (Kruse et al., 2018) there exist to the best of my knowledge only TC-1/A2 cells and *in vivo* immortalized cells in AAD mice (Peng et al., 2006; Peng et al., 2022). As TC-1/A2 still express the murine MHC molecules, they present the immunodominant epitope HPV16 $E7_{49-57}$, which needs to be artificially altered to allow the examination of an HLA-A2-restricted immune response. This is also true for AAD mice, which also express all H-2 molecules in addition to HLA-A2 epitope-presenting AAD proteins (Newberg et al., 1996; Kruse, 2019) and thus are not as suitable as A2.DR1 mice for therapeutic vaccination development studies. For focused assessment of HLA-restricted epitopes, it is necessary to use a fully humanized mouse model. However, it still has to be kept in mind that A2.DR1 mice can only be used for the examination of HLA-A2-restricted epitope vaccines and do not allow for research on other HLA alleles.

The first step of orthotopic tumor instillation is the synchronization of the mice' estrus cycle to a diestrus-like state. First, this is done to equal the parameter of the animals' cycle stage (Domingos-Pereira et al., 2013) and second to ensure the best possible level of tumor cell uptake into the mucosa. The diestrus enables for example the easy uptake of bacteria (Islam et al., 2016) or chemotherapeutics (Mahjabeen et al., 2018). The progesterone treatment also enhances the Langerhans cell counts in the cervicovaginal mucosa (Zhao et al., 2003), which is important for the induction of an immune response after ivag. vaccination as described later in 5.3. Hormones also change the integrity of the vaginal epithelium, induce neutrophil invasion and influence plasma cells in the mucosa (McDermott et al., 1980; Li et al., 2018). Importantly, the vaginal epithelium thins in diestrus and becomes covered with living cells (Long & Evans, 1922). As described by others (Roberts et al., 2007), I treated the mice 6 h before tumor instillation with N-9 to disrupt their vaginal mucosa. This N-9 pretreatment is not as precise as an s.c. tumor cell injection because one cannot know how many wounds the N-9 causes and where they are located. Evidence for this interexperimental variability can be found for example in Figure 36: in the first part of the experiment, only 17 of 25 mice grew tumors in their mucosa while all but one animal developed a tumor in the second part. Although all animals receiving 50,000 in the second experiment developed a tumor, I chose 250,000 cells for further use of the tumor model to account for the variability. It is reasonable to assume that handling differences

and unintended PBS/tumor cell efflux from the murine vagina during the experiment are causing differences in experiments.

The successfully established tumor model with E6/7-lucA2 cells in the vaginal mucosa of A2.DR1 mice will provide a more clinically relevant *in vivo* model compared to s.c. tumors by mirroring the environment that limits access to immune cells.

5.3 Vaccination and T cell trafficking

Concurrently to establishing the vaginal tumor model for A2.DR1 mice with the new syngeneic and HPV oncoprotein-dependent cell line E6/7-lucA2 I examined methods to influence T cell trafficking.

There have been many studies on the induction of a vaginal T cell response against HPV. These include reports about ivag. vaccination (Echchannaoui et al., 2008; Choi et al., 2016; Sun et al., 2016; Li et al., 2020) as well as systemic vaccination followed by pulling the induced T cells into the mucosa via a local vaccination boost (Çuburu et al., 2019) or via vaginal application of immunomodulators (Domingos-Pereira et al., 2013; Soong et al., 2014). Consulting the preexisting literature, I set out to examine ways of inducing a robust anti-HPV16 $CD8^+$ T cell response in the genital mucosa of A2.DR1 mice, which is strong enough to induce orthotopic tumor regression. To this end, I studied novel vaccine compounds as well as synergistic treatments to enhance HPV-specific T cell levels. For this, I also tested already published methods for treatment of other sexually transmitted infections such as the prime and pull method, which was first used for HSV treatment (Shin & Iwasaki, 2012). In my experiments, I quantified the anti-HPV16 response by assessing the $CD8^+$ T cell memory response of vaccine-induced T cells upon restimulation with the target epitope $E7_{11\text{-}19}$ by ICS.

First I tested the newly established protocols for GT dissociation and subsequent flow cytometric antibody staining of genital T cells (Voß, 2020) in systemically immunized mice. The chosen vaccination compound was LPP-$E7_{11\text{-}19}$, an amphiphilic peptide construct incorporating our lead epitope HPV16 $E7_{11\text{-}19}$, which is presented on HLA-$A2^+$ human cervical cancer cells (Riemer et al., 2010; Keskin et al., 2011; Blatnik et al., 2018). Vaccination against $E7_{11\text{-}19}$ has been shown before to induce regression of s.c. HPV16 $E7^+$ tumors in A2.DR1 mice (Kruse et al., 2018) and clinical trials against the epitope by vaccination (NCT02865135; NCI Drug Dictionary ID 785825) and TCR-engineered T cell therapy (NCT02858310; Nagarsheth

et al. (2021)) are currently ongoing. The amphiphilic peptide construct consists of (1,2-distearoyl-3-sn-phosphatidylethanolamine)-PEG-maleimide coupled N-terminally to YMLDLQPET ($E7_{11-19}$) via a cysteine residue. Based on the work of Liu et al. (2014) the amphiphilic peptide uses the mechanism of 'albumin hitchhiking' i.e. binding to albumin for accumulation in lymph nodes instead of systemic dissemination of the compound. Dr. Sebastian Kruse tested the lipopeptides with the HPV16 peptides $E7_{7–15}$, $E7_{11–19}$, $E7_{82–90}$ and $E6_{25–33}$. LPP-$E7_{11-19}$ was herein able to therapeutically clear 50 % of mice of their s.c. PAP-A2 tumors (Kruse et al., 2018).

To test if other vaccine formulations may be more effective, I additionally tested argynilated silica nanoparticles (SiNPs) linked to $E7_{11–19}$ via a KKK-W-citrullin linker that are produced in a collaboration with our group and the company Silvacx (manuscript in preparation). The SiNPs are taken up by DCs and the epitope is cleaved from the linker via cathepsin B and other cysteine proteases. In an s.c. head-to-head comparison, LPP-$E7_{11-19}$ turned out to be more potent in inducing a specific $CD8^+$ T cell response than SiNP in A2.DR1 mice. The mean percentage of $CD8^+IFN\gamma^+$ T cells found here was at about 6 %, which fits to previous observations in our group (Kruse et al., 2018). One reason for the different efficacies might be that the lipopeptides in the LPP vaccination are directly targeted towards the lymph nodes (Liu et al., 2014) where the immune response is established, which might increase the methods' efficacy. Another reason might have been the oxidation status of the methionine contained in the epitope linked to the SiNP. Methionine can oxidize and thereby becomes methionine sulfoxide. This common post-translational modification can help among others in prevention of oxidative stress mediated by reactive oxygen species (ROS). Oxidation of methionine mostly leads to protein inactivation through conformational changes (Drazic & Winter, 2014). The question was now if the conformational changes are also induced in peptides, which might lead to a decrease in antigen presentation and/or recognition. Weiskopf et al. (2010) tested the immunogenicity of an HLA-A2-restricted T cell epitope from CMV where they intentionally oxidized the methionine. It turned out that the oxidation impaired binding of the epitope to the TCR and therefore decreased the antigenicity. This is why I tested if SiNP synthesized in a way that prevents methionine oxidation of $E7_{11-19}$ are more immunogenic than those containing about 10 % of oxidized methionine (Figure 39). Although both conditions of SiNP caused lower percentages of specific T cells than LPP-$E7_{11-19,}$ the specific T cell levels did not differ

significantly among the two SiNP conditions. However, the mean of $E7_{11-19}$-restimulated $CD8^+IFN\gamma^+$ T cells of mice vaccinated with SiNPs carrying the epitope with unoxidized methionine was approximately 30 times higher than the mean of the same cells restimulated with $Surv_{96-104}$, while this difference was only six times in mice vaccinated with oxidized methionine. This indicates that oxidation status might indeed play a role for the T cell-mediated immune response. One also has to keep in mind that in my experiment only 10 % of the methionine was oxidized in the oxidized SiNP formulation, whilst Weiskopf et al. (2010) compared completely oxidized with completely unoxidized methionine. The effect might have therefore been more pronounced than in my experiment. As not necessarily the quantity but rather the quality of the T cell response counts for tumor vaccination (Buhrman & Slansky, 2013) I still considered SiNPs as vaccine candidates for further experiments.

After having tested the two compounds s.c. I went on to examine the effects of ivag. vaccinations. For this I either vaccinated two times s.c. and one time ivag., one time s.c. and two times ivag. or three times ivag. with LPP-$E7_{11-19}$ (Figure 40). Surprisingly, there were no specific T cells detected in the spleen although at least two mice of the first group displayed epitope specificity in their genital $CD8^+$ T cell pool. Of course, it is possible that all epitope-specific T cells in these animals could have migrated into the GTs, however one would assume there are still some detected in the blood circulation. Especially so as not all mice displayed a clear genital $CD8^+IFN\gamma^+$ T cell response. Additionally, only a fraction of effector T cells is supposed to migrate into the mucosa and not all of them (Shin & Iwasaki, 2013). It would be interesting to explore if vaccinating three times s.c. before an ivag. boost leads to an increase in systemic epitope-specific T cells as well as in the GT.

For establishing an ivag. immune response via ivag. vaccination only I tested liposomes with CPP on their surface as potential carriers for LPP-$E7_{11-19}$ or peptide only with the adjuvant poly(I:C) (Figure 41). These liposomes have so far been used to deliver drugs across the intestinal mucosal barrier. The CPP on the surface can penetrate cell membranes and deliver the liposome cargo into cells (Uhl et al., 2021). One explorative group of ivag. instilled SiNP with $E7_{11-19}$ was also included. Interestingly, the liposomes carrying LPP-$E7_{11-19,}$ as well as the ivag. vaccination with SiNP caused a significant level of $E7_{11-19}$-specific $CD8^+$ T cells in splenocytes. The SiNP-induced level of $E7_{11-19}$-specific $CD8^+$ T cells in the spleen was nearly on par with the magnitude observed after s.c. SiNP vaccinations (Figure 38, Figure 39). This

observation also fits to SiNP-vaccinated mice possessing the significantly lowest percentage of T_{RM} in their spleens. The lack of homing molecules probably enabled the cells to emigrate from the cervicovaginal tract. In agreement with reports from Wang et al. (2015) the $CD8^+$ T cells must have been primed in the vaginal type II mucosa and then, instead of becoming resident there, emigrated into circulation. For this, their expression of the homing marker CD103 has to be low, which fits to the observations in the spleen. The T cells in the GT also display only low levels of T_{RM} markers. When consulting literature the emigration of cells from the mucosa after ivag. priming is not described very well. Ballou et al. (2012) hypothesized that systemic immunity after ivag. immunization might be due to transport of vaccinated antigens to the local, in this case iliac, lymph nodes. This is also corroborated by studies showing transport of ivag. instilled horseradish peroxidase tracer to the iliac lymph nodes (Parr & Parr, 1990), transport of exogenous lymphocytes from the vagina to lymph nodes (Ibata et al., 1997) and transport of T and B cells from the vagina to iliac lymph nodes (King et al., 1998). Most of the available literature, however, describes migration into the vaginal mucosa instead of this retrograde migration.

The ivag. immunization experiment showed clearly that the induction of vaginal immunity via ivag. instillation of liposomes did not work as expected. One reason might be that the liposomes were developed to deliver pharmaceuticals via the intestinal mucosa, which does not necessarily imply a similar effect for the vaginal mucosa. Primarily, the two forms of mucosae differ in their composition. The intestine for example possesses so-called Peyer's patches acting as special inductive sites for immune responses where a plethora of immune cells resides. Additionally, the intestine contains microfold (M) cells, specialized epithelial cells that take up antigen from the lumen and release it on their basal site to lymphocytes (Murphy & Weaver, 2017). In contrast to the intestine, the cervicovaginal tract does not contain M cells. However, at least in the human GT there are lymphoid aggregates with organizational similarities to Peyer's patches, although their biological functions are still mostly unclear (Zhou et al., 2018). Such lymphoid aggregates have also been found in the genital mucosa of mice immunized against HSV-2 (Gillgrass et al., 2005) even though literature about their function in mice is scarce, too. However, these aggregates might act as inductive sites for an HPV-specific mucosal T cell response.

Another important point is that the liposomes used in this experiment deliver their cargo into the cells. Before, this cargo had been pharmaceuticals. However, if the cargo consists of peptides as in this experiment the intracellular release into epithelial cells will prevent the peptides to reach epithelial Langerhans cells or DCs. This is a likely explanation why the ivag. vaccinations did not work. Nevertheless, the liposomes could still be used for oral vaccination approaches, as the M cells would deliver the antigen to their associated lymphocytes and DCs (Lavelle & Ward, 2022).

Resulting from these experiments I deemed the exclusively ivag. vaccination approaches not promising for the establishment of a genital $CD8^+$ T cell response to HPV16 epitopes. Nevertheless, it is possible to achieve mucosal priming of $CD8^+$ T cells through ivag. vaccinations (Wang et al., 2015). This has also been shown in successful ivag. vaccination studies by Çuburu et al. (2012). The increased abundance of DCs and Langerhans cells in the diestrus stage of the mice (Ensign et al., 2014) can also support the induction of a T cell response in the genital mucosa. However, many studies underline the difficulty of inducing a vaginal immune response by only vaccinating ivag. (Black et al., 2000; Russell, 2002; Decrausaz, Goncalves, et al., 2011; Wright, 2011; Buffa et al., 2012).

Therefore, I went on to examine the induction of immune responses by induction of a systemic T cells response with subsequent ‘pulling’ of T cells via chemokines and immunomodulators as described in Shin and Iwasaki (2012). Based on the results shown in Figure 43, N-9 was applied prior to application of the immunomodulators.

The final goal was to compare the published chemokine pulling method of CXCL9/CXCL10 usage (Shin & Iwasaki, 2012) to mucosal application of TLR agonists imiquimod and resiquimod. TLR agonists bind their respective TLR on the cell surface, which leads to rapid induction of an inflammatory immune response and thereby to induction of an IFN response. IFNs in turn induce the release of chemokines attracting T cells (Kanzler et al., 2007; Shin & Iwasaki, 2013). TLR7 and TLR8, which are discussed in the following, both recognize RNA molecules (Barrat, 2018).

The TLR7 agonist imiquimod has been reported before to be suitable for inducing T cell migration towards the topical application site (Soong et al., 2014; Bernstein et al., 2019; Çuburu et al., 2019). Many reports use imiquimod in the form of the Aldara® cream, which contains

5 % imiquimod (used for example in Çuburu et al. (2019)). However, many authors omit the information of how much imiquimod they used in total. Following my experiment, I settled on a dose of 25 µg imiquimod for further use.

The TLR7 and 8 agonist resiquimod (R848) is an up to 100 times more potent imidazoquinoline than its predecessor imiquimod (Dockrell & Kinghorn, 2001; Dowling, 2018). It is important to note that mice express only a non-functional form of TLR8 due to missing five amino acids compared to human TLR8 (Liu et al., 2010; Kugelberg, 2014). It might still act as a regulator of TLR7 signaling, though (Barrat, 2018). Therefore, the effect elicited by resiquimod in mouse experiments is induced predominantly or rather only by TLR7 activation. Once resiquimod was applied to LPP-$E7_{11-19}$-vaccinated mice, I detected expression of CD69 in both $CD8^+$ cells in spleen and GT. This effect had been shown before by Craft et al. (2014). For further experiments I used 2.5 µg of resiquimod even though others have reported usage of higher amounts such as 20 µg of resiquimod as an adjuvant (Buffa et al., 2012).

In the final experiment (Figure 46), I compared the effect of vaginal application of the CXCL9 and CXCL10 chemokines vs. resiquimod vs. imiquimod vs. PBS on the induction of T cell migration towards the mucosa. The two chemokines attract $CXCR3^+$ T cells into the mucosal tissue (Nakanishi et al., 2009; Metzemaekers et al., 2018)(see 1.2.1.5). Surprisingly, PBS seemed to induce the highest levels of $E7_{11-19}$-specific T cells in the murine GTs. The most logical explanation was that the N-9 pretreatment itself attracted the T cells by inducing a local inflammation (Fichorova et al., 2001; Ensign et al., 2012), which in turn induced a release of IFNs, followed by chemokine production and T cell migration. Therefore, I repeated the experiment without the N-9 treatment. The original authors of the prime & pull method, Shin and Iwasaki (2012) did not use N-9, either. Apparently, they deemed it unnecessary after the preceding medroxyprogesterone acetate treatment (personal communication with Haina Shin). As stated above, this hormone treatment thins the vaginal epithelium (Long & Evans, 1922) and allows easier uptake of compounds.

Unfortunately, the levels of $E7_{11-19}$-specific T cells in the spleens differed strongly between the two experimental parts: while the induction of an anti-$E7_{11-19}$ response worked very well in the experiment with N-9-treated mice, the vaccination-induced effect was much more subdued in the experiment with N-9-untreated mice. As the vaginal treatments were performed after the

vaccination regimen had been finished, they cannot have influenced vaccination success per se. Focusing on the specific T cell levels in the GTs without N-9 treatment one can only observe some slightly enhanced T cell levels for chemokine and resiquimod-treated mice although the difference seems negligible. Upon comparison of $E7_{11-19}$-specific T cell levels in the spleen and GT of each animal one can see that the mice with the highest $CD8^+IFN\gamma^+$ T cell levels mostly also had the highest levels in their spleens (Figure 47). Therefore, it can be concluded that in my experiments, the applied immunomodulators did have none or only a marginal influence on T cell migration and the far more important parameter was the magnitude of the systemic T cell response.

Clearly, the prime and pull method did not work as intended with A2.DR1 mice although I replicated the experimental layout described by Shin and Iwasaki (2012). At least I expected the chemokines to attract more specific T cells into the mucosa than PBS. As can be seen in the Shin and Iwasaki publication, vaccinated mice treated with PBS already had about ten times more specific T cells in their GTs than naïve mice (Suppl. Figure 2 of Shin and Iwasaki (2012)). This means that already many cells migrated to the vagina through the initial immunization process and maybe also through mechanical stress induced by instillation of PBS. Injuries to the epithelial barrier can result in recruitment of immune cells through chemokine and cytokine signaling (Larsen et al., 2020). The question is if a more gentle approach of instilling the PBS would have resulted in less mucosal T cell infiltration. Another idea would be to add CXCL11 to the chemokine mixture. This chemokine is also known to induce trafficking of $CXCR3^+$ T cells (Groom & Luster, 2011). Apart from the chemokines, the TLR agonists did not induce lymphocyte migration to the vaginal mucosa either. Imiquimod is a TLR7 agonist while resiquimod also serves as a TLR7 agonist in mice and additionally as a TLR 8 agonist in humans (Schön & Schön, 2008). Both are supposed to trigger at least a TLR7-mediated chemokine release in mice for attraction of activated, specific T cells. Although murine TLR8 is not functional, resiquimod can still bind TLR7 and is described as being 100 times more potent than imiquimod (Vinod et al., 2020). It might be that the amounts I used of the TLR agonists were not high enough to induce an immunomodulatory effect. After all, Fraillery et al. (2009) as well as Decrausaz, Domingos-Pereira, et al. (2011) used 75 µg of imiquimod per mouse while Soong et al. (2014) used 400 µg for their T cell pull. However, it is unclear if more of the TLR agonists would have changed anything as I saw by the expression of CD69 on the T cells

of resiquimod-treated mice that there was an effect elicited. An important question, which should also be examined, is whether A2.DR1 mice actually upregulate CXCR3 enough for chemokine sensing as other mice do. CXCR3 is the chemokine receptor upregulated by T cells upon their activation that leads them towards an inflammatory site in a chemotactic fashion (Halle et al., 2017; Kuo et al., 2018). Furthermore, the lack of CD103 expression on the specific T cells was a problem in the experiments. CD103 is the marker used for tissue-residency and its absence on the cells correlates to $CD69^+$ T cells being found in the spleen of resiquimod-treated mice, as they must have migrated there from the GT. Therefore, the induction of higher levels of CD103 on the T cell surfaces might be crucial to specific T cells remaining in the vaginal epithelium. For example, I saw in Figure 41 that CD103 was upregulated upon ivag. vaccination although no $E7_{11-19}$-specific immune response was induced.

Summarizing the T cell trafficking results, it seems likely that the epitope-specific T cells I found in the GT were s.c. vaccination-induced T cells that migrated into the vaginal mucosa even without a pull. Although it is stressed in literature that T cells only enter the vagina upon local inflammatory signaling (e.g. Shin and Iwasaki (2013)) I have observed that this does not seem to be a major obstacle if the induced systemic T cell response is strong enough. Indeed, Su et al. (2016) suggest that systemic vaccination (s.c., i.m., intradermal, i.p. and transcutaneous) leads to the diffusion of the vaccine to regional lymph nodes, which are the iliac lymph nodes for my experiments. The pAPCs located there prime lymphocytes, which then migrate to the mucosal tissue. As my s.c. vaccinations are injected into the posterior flank of the mice, the LPP might diffuse to the iliac lymph node. A possible solution was suggested by Mestecky et al. (2005) who hypothesized that rectal immunizations are more effective for the induction of a vaginal immune response than ivag. vaccinations. The rectum possesses, as part of the intestinal tract, many immune inductive sites and lies anatomically close to the vagina. Therefore, they share the same lymphatic drainage system, which might distribute rectally induced T cells with mucosal markers into the GT. Another possibility is the induction of a vaginal immune response by i.n. vaccination, which can even protect from ivag. tumors (Decrausaz, Domingos-Pereira, et al., 2011; Sierra et al., 2020).

When examining ways to induce a vaginal HPV16-specific $CD8^+$ T cell response, I saw that the most promising approaches are either the induction of a high level of specific T cells systemically as seen in the prime and pull experiments or the usage of an additional ivag.

vaccination to attract the T cells into the vaginal mucosa. The future goal will be to verify promising approaches with the orthotopic tumor model. This was unfortunately not possible in the scope of this PhD project due to COVID-19 pandemic-caused mouse colony reductions and subsequent animal shortages.

6 Summary and Outlook

Herein I described the successful establishment of a novel, A2.DR1-syngeneic HPV16 E6 and E7-dependent tumor cell line. This cell line was then used to develop an orthotopic tumor model in the vaginal mucosa of the mice with the aim of providing a suitable animal model to test therapeutic HPV16 vaccination approaches in addition to other treatment options.

Additionally, I tested different methods for establishing vaginal $CD8^+$ T cell immunity to the HLA-A2:01-restricted HPV16 epitope $E7_{11-19}$. Among those were vaginal vaccinations or the induction of a systemic vaccination-specific T cell response followed by ivag. treatments intended to attract the T cells into the mucosa.

While an ivag. boost after s.c. vaccinations resulted in $E7_{11-19}$-specific T cells in the GT, the sole ivag. vaccinations with LPP, liposomes or SiNP did not lead to vaginal immunity against $E7_{11-19}$. The application of N-9, imiquimod, resiquimod and CXCL9/CXCL10 did not induce a migration towards the vaginal mucosa, either. The most important factor for vaginal immunity as found in this work have been the levels of systemic $E7_{11-19}$-specific T cells.

Regarding the contradictory literature and my own results concerning the induction of epitope-specific mucosal $CD8^+$ T cell immunity, more research will be necessary to determine a reliable method that works in most or all animal models and subsequently in the clinics. The resulting insights into the mucosal immune system and workings of immunotherapy at this location will not only benefit HPV patients but can also be transferred to other mucosal diseases such as sexually transmitted infections.

The newly established MHC-humanized orthotopic HPV tumor model will pave the way for examination of vaccination-induced anti-HPV16 immune responses in a clinically relevant model. It will help to improve the reliability of preclinical data and allow a more efficient development of immunotherapeutic approaches to HPV16 therapeutic vaccination. An interesting approach to examine will be the assessment of effects by low-dose irradiation on the migratory behavior of T cells. Low-dose irradiation has so far been shown to induce differentiation of macrophages that can recruit T cells for immunotherapeutic killing of tumors (Klug et al., 2013). Another method to be tested in the novel tumor model will be immune checkpoint blockade, which might enhance the anti-tumor effect of other approaches.

Furthermore, the tumor model will allow a stricter examination of novel therapeutic HPV16 vaccination compounds. These should ideally include HLA II-restricted CD4 epitopes as $CD4^+$ T cells recruit $CD8^+$ T cells to the mucosa (Laidlaw et al., 2016).

In conclusion, although a reliable method to induce HPV-specific T cell trafficking to the vaginal mucosa of MHC-humanized A2.DR1 mice could not yet be established, I have developed an orthotopic HPV16 E6 and E7-dependent tumor model, which will serve to improve research on therapeutic HPV vaccination efforts.

7 References

Aaij, C., & Borst, P. (1972). The gel electrophoresis of DNA. *Biochim Biophys Acta, 269*(2), 192-200.

affymetrix eBioscience. Mouse Haplotype Table. Retrieved from https://tools.thermofisher.com/content/sfs/brochures/Mouse_Haplotype_Table.pdf on 18.03.2022.

Aggarwal, C., Cohen, R. B., Morrow, M. P., Kraynyak, K. A., Sylvester, A. J., Knoblock, D. M., Bauml, J. M., Weinstein, G. S., Lin, A., Boyer, J., Sakata, L., Tan, S., Anton, A., Dickerson, K., Mangrolia, D., Vang, R., Dallas, M., Oyola, S., Duff, S., Esser, M., Kumar, R., Weiner, D., Csiki, I., & Bagarazzi, M. L. (2019). Immunotherapy Targeting HPV16/18 Generates Potent Immune Responses in HPV-Associated Head and Neck Cancer. *Clin Cancer Res, 25*(1), 110-124.

Ahmed, R., & Akondy, R. S. (2011). Insights into human CD8(+) T-cell memory using the yellow fever and smallpox vaccines. *Immunology and Cell Biology, 89*(3), 340-345.

Ai, W., Li, H., Song, N., Li, L., & Chen, H. (2013). Optimal method to stimulate cytokine production and its use in immunotoxicity assessment. *Int J Environ Res Public Health, 10*(9), 3834-3842.

Ajayi, A. F., & Akhigbe, R. E. (2020). Staging of the estrous cycle and induction of estrus in experimental rodents: an update. *Fertil Res Pract, 6*, 5.

Alberts, B., Johnson, A., Lewis, J., Raff, M., Roberts, K., & Walter, P. (2002). Epidermis and its renewal by stem cells. In *Molecular Biology of the Cell. 4th edition*: Garland Science.

Alcover, A., Alarcon, B., & Di Bartolo, V. (2018). Cell Biology of T Cell Receptor Expression and Regulation. *Annu Rev Immunol, 36*, 103-125.

Altmann, D. M., Douek, D. C., Frater, A. J., Hetherington, C. M., Inoko, H., & Elliott, J. I. (1995). The T cell response of HLA-DR transgenic mice to human myelin basic protein and other antigens in the presence and absence of human CD4. *J Exp Med, 181*(3), 867-875.

Amsen, D., van Gisbergen, K., Hombrink, P., & van Lier, R. A. W. (2018). Tissue-resident memory T cells at the center of immunity to solid tumors. *Nat Immunol, 19*(6), 538-546.

Andreatta, M., & Nielsen, M. (2016). Gapped sequence alignment using artificial neural networks: application to the MHC class I system. *Bioinformatics, 32*(4), 511-517.

Aoki, M., Aoki, H., Ramanathan, R., Hait, N. C., & Takabe, K. (2016). Sphingosine-1-Phosphate Signaling in Immune Cells and Inflammation: Roles and Therapeutic Potential. *Mediators Inflamm, 2016*, 8606878.

Apostolico, J. d. S., Lunardelli, V. A., Coirada, F. C., Boscardin, S. B., & Rosa, D. S. (2016). Adjuvants: Classification, Modus Operandi, and Licensing. *J Immunol Res, 2016*, 1459394.

Araldi, R. P., Sant'Ana, T. A., Modolo, D. G., de Melo, T. C., Spadacci-Morena, D. D., de Cassia Stocco, R., Cerutti, J. M., & de Souza, E. B. (2018). The human papillomavirus (HPV)-related cancer biology: An overview. *Biomed Pharmacother, 106*, 1537-1556.

References

Arbyn, M., Weiderpass, E., Bruni, L., de Sanjosé, S., Saraiya, M., Ferlay, J., & Bray, F. (2020). Estimates of incidence and mortality of cervical cancer in 2018: a worldwide analysis. *Lancet Glob Health, 8*(2), e191-e203.

Bagarazzi, M. L., Yan, J., Morrow, M. P., Shen, X., Parker, R. L., Lee, J. C., Giffear, M., Pankhong, P., Khan, A. S., Broderick, K. E., Knott, C., Lin, F., Boyer, J. D., Draghia-Akli, R., White, C. J., Kim, J. J., Weiner, D. B., & Sardesai, N. Y. (2012). Immunotherapy against HPV16/18 generates potent TH1 and cytotoxic cellular immune responses. *Sci Transl Med, 4*(155), 155ra138.

Baldwin, P. J., van der Burg, S. H., Boswell, C. M., Offringa, R., Hickling, J. K., Dobson, J., Roberts, J. S. C., Latimer, J. A., Moseley, R. P., Coleman, N., Stanley, M. A., & Sterling, J. C. (2003). Vaccinia-expressed human papillomavirus 16 and 18 E6 and E7 as a therapeutic vaccination for vulval and vaginal Intraepithelial neoplasia. *Clin Cancer Res, 9*(14), 5205-5213.

Ballou, B., Andreko, S. K., Osuna-Highley, E., McRaven, M., Catalone, T., Bruchez, M. P., Hope, T. J., & Labib, M. E. (2012). Nanoparticle transport from mouse vagina to adjacent lymph nodes. *PLoS One, 7*(12), e51995.

Barrat, F. J. (2018). TLR8: No gain, no pain. *Journal of Experimental Medicine, 215*(12), 2964-2966.

Barrios, K., & Celis, E. (2012). TriVax-HPV: an improved peptide-based therapeutic vaccination strategy against human papillomavirus-induced cancers. *Cancer Immunol Immunother, 61*(8), 1307-1317.

Bassani-Sternberg, M., Braunlein, E., Klar, R., Engleitner, T., Sinitcyn, P., Audehm, S., Straub, M., Weber, J., Slotta-Huspenina, J., Specht, K., Martignoni, M. E., Werner, A., Hein, R., D, H. B., Peschel, C., Rad, R., Cox, J., Mann, M., & Krackhardt, A. M. (2016). Direct identification of clinically relevant neoepitopes presented on native human melanoma tissue by mass spectrometry. *Nat Commun, 7*, 13404.

Bernstein, D. I., Cardin, R. D., Bravo, F. J., Awasthi, S., Lu, P., Pullum, D. A., Dixon, D. A., Iwasaki, A., & Friedman, H. M. (2019). Successful application of prime and pull strategy for a therapeutic HSV vaccine. *npj Vaccines, 4*, 33.

Bevan, M. J. (2004). Helping the CD8(+) T-cell response. *Nat Rev Immunol, 4*(8), 595-602.

Bhuyan, P. K., Dallas, M., Kraynyak, K., Herring, T., Morrow, M., Boyer, J., Duff, S., Kim, J., & Weiner, D. B. (2021). Durability of response to VGX-3100 treatment of HPV16/18 positive cervical HSIL. *Hum Vaccin Immunother, 17*(5), 1288-1293.

Bialkowski, L., van Weijnen, A., Van der Jeught, K., Renmans, D., Daszkiewicz, L., Heirman, C., Stange, G., Breckpot, K., Aerts, J. L., & Thielemans, K. (2016). Intralymphatic mRNA vaccine induces CD8 T-cell responses that inhibit the growth of mucosally located tumours. *Sci Rep, 6*, 22509.

BioRender.com. (2022). Retrieved from https://biorender.com/ on 28.04.2022.

Bjorkman, P. J., Saper, M. A., Samraoui, B., Bennett, W. S., Strominger, J. L., & Wiley, D. C. (1987). Structure of the human class I histocompatibility antigen, HLA-A2. *Nature, 329*(6139), 506-512.

References

Black, C. A., Rohan, L. C., Cost, M., Watkins, S. C., Draviam, R., Alber, S., & Edwards, R. P. (2000). Vaginal mucosa serves as an inductive site for tolerance. *J Immunol, 165*(9), 5077-5083.

Blass, E., & Ott, P. A. (2021). Advances in the development of personalized neoantigen-based therapeutic cancer vaccines. *Nat Rev Clin Oncol, 18*(4), 215-229.

Blatnik, R., Mohan, N., Bonsack, M., Falkenby, L. G., Hoppe, S., Josef, K., Steinbach, A., Becker, S., Nadler, W. M., Rucevic, M., Larsen, M. R., Salek, M., & Riemer, A. B. (2018). A targeted LC-MS strategy for low-abundant HLA class I-presented peptide detection identifies novel human papillomavirus T-cell epitopes. *Proteomics*, e1700390.

Böttinger, P., Schreiber, K., Hyjek, E., Krausz, T., Spiotto, M. T., Steiner, M., Idel, C., Booras, H., Beck-Engeser, G., Riederer, J., Willimsky, G., Wolf, S. P., Karrison, T., Jensen, E., Weichselbaum, R. R., Nakamura, Y., Yew, P. Y., Lambert, P. F., Kurita, T., Kiyotani, K., Leisegang, M., & Schreiber, H. (2020). Cooperation of genes in HPV16 E6/E7-dependent cervicovaginal carcinogenesis trackable by endoscopy and independent of exogenous estrogens or carcinogens. *Carcinogenesis, 41*(11), 1605-1615.

Bozza, M., Green, E. W., Espinet, E., De Roia, A., Klein, C., Vogel, V., Offringa, R., Williams, J. A., Sprick, M., & Harbottle, R. P. (2020). Novel Non-integrating DNA Nano-S/MAR Vectors Restore Gene Function in Isogenic Patient-Derived Pancreatic Tumor Models. *Mol Ther Methods Clin Dev, 17*, 957-968.

Brotherton, J. M. L. (2019). Impact of HPV vaccination: Achievements and future challenges. *Papillomavirus Res, 7*, 138-140.

Bruni, L., Saura-Lazaro, A., Montoliu, A., Brotons, M., Alemany, L., Diallo, M. S., Afsar, O. Z., LaMontagne, D. S., Mosina, L., Contreras, M., Velandia-Gonzalez, M., Pastore, R., Gacic-Dobo, M., & Bloem, P. (2021). HPV vaccination introduction worldwide and WHO and UNICEF estimates of national HPV immunization coverage 2010-2019. *Prev Med, 144*, 106399.

Buffa, V., Klein, K., Fischetti, L., & Shattock, R. J. (2012). Evaluation of TLR agonists as potential mucosal adjuvants for HIV gp140 and tetanus toxoid in mice. *PLoS One, 7*(12), e50529.

Buhrman, J. D., & Slansky, J. E. (2013). Improving T cell responses to modified peptides in tumor vaccines. *Immunol Res, 55*(1-3), 34-47.

Burd, E. M. (2016). Human Papillomavirus Laboratory Testing: the Changing Paradigm. *Clin Microbiol Rev, 29*(2), 291-319.

Caligioni, C. S. (2009). Assessing reproductive status/stages in mice. *Curr Protoc Neurosci, Appendix 4*, Appendix 4I.

Carbone, F. R. (2015). Tissue-Resident Memory T Cells and Fixed Immune Surveillance in Nonlymphoid Organs. *J Immunol, 195*(1), 17-22.

Chabeda, A., Yanez, R. J. R., Lamprecht, R., Meyers, A. E., Rybicki, E. P., & Hitzeroth, I. I. (2018). Therapeutic vaccines for high-risk HPV-associated diseases. *Papillomavirus Res, 5*, 46-58.

Chatila, T., Silverman, L., Miller, R., & Geha, R. (1989). Mechanisms of T cell activation by the calcium ionophore ionomycin. *J Immunol, 143*(4), 1283-1289.

References

Cheng, L., Wang, Y., & Du, J. (2020). Human Papillomavirus Vaccines: An Updated Review. *Vaccines, 8*(3).

Chesson, H. W., Dunne, E. F., Hariri, S., & Markowitz, L. E. (2014). The estimated lifetime probability of acquiring human papillomavirus in the United States. *Sex Transm Dis, 41*(11), 660-664.

Choi, Y. W., Kang, M. C., Seo, Y. B., Namkoong, H., Park, Y., Choi, D. H., Suh, Y. S., Lee, S. W., Sung, Y. C., & Jin, H. T. (2016). Intravaginal Administration of Fc-Fused IL7 Suppresses the Cervicovaginal Tumor by Recruiting HPV DNA Vaccine-Induced CD8 T Cells. *Clin Cancer Res, 22*(23), 5898-5908.

Chong, C., Marino, F., Pak, H., Racle, J., Daniel, R. T., Muller, M., Gfeller, D., Coukos, G., & Bassani-Sternberg, M. (2018). High-throughput and Sensitive Immunopeptidomics Platform Reveals Profound Interferongamma-Mediated Remodeling of the Human Leukocyte Antigen (HLA) Ligandome. *Mol Cell Proteomics, 17*(3), 533-548.

Christensen, N. D., Budgeon, L. R., Cladel, N. M., & Hu, J. (2017). Recent advances in preclinical model systems for papillomaviruses. *Virus Res, 231*, 108-118.

Chumduri, C., & Turco, M. Y. (2021). Organoids of the female reproductive tract. *J Mol Med, 99*(4), 531-553.

Cohen, P. A., Jhingran, A., Oaknin, A., & Denny, L. (2019). Cervical cancer. *The Lancet, 393*(10167), 169-182.

Conway, M. J., & Meyers, C. (2009). Replication and assembly of human papillomaviruses. *J Dent Res, 88*(4), 307-317.

Cosgrove, D., Gray, D., Dierich, A., Kaufman, J., Lemeur, M., Benoist, C., & Mathis, D. (1991). Mice lacking MHC class II molecules. *Cell, 66*(5), 1051-1066.

Craft, N., Birnbaum, R., Quanquin, N., Erfe, M. C. B., Quant, C., Haskell, J., Bruhn, K. W., & Wilkins, P. P. (2014). Topical Resiquimod Protects against Visceral Infection with Leishmania infantum chagasi in Mice. *Clinical and Vaccine Immunology, 21*(9), 1314-1322.

Çuburu, N., Graham, B. S., Buck, C. B., Kines, R. C., Pang, Y. Y., Day, P. M., Lowy, D. R., & Schiller, J. T. (2012). Intravaginal immunization with HPV vectors induces tissue-resident CD8+ T cell responses. *J Clin Invest, 122*(12), 4606-4620.

Çuburu, N., Kim, R., Guittard, G. C., Thompson, C. D., Day, P. M., Hamm, D. E., Pang, Y.-Y. S., Graham, B. S., Lowy, D. R., & Schiller, J. T. (2019). A Prime-Pull-Amplify Vaccination Strategy To Maximize Induction of Circulating and Genital-Resident Intraepithelial CD8+ Memory T Cells. *J Immunol*.

Çuburu, N., Wang, K., Goodman, K. N., Pang, Y. Y., Thompson, C. D., Lowy, D. R., Cohen, J. I., & Schiller, J. T. (2015). Topical herpes simplex virus 2 (HSV-2) vaccination with human papillomavirus vectors expressing gB/gD ectodomains induces genital-tissue-resident memory CD8+ T cells and reduces genital disease and viral shedding after HSV-2 challenge. *J Virol, 89*(1), 83-96.

Cunha, G. R., Sinclair, A., Ricke, W. A., Robboy, S. J., Cao, M., & Baskin, L. S. (2019). Reproductive tract biology: Of mice and men. *Differentiation, 110*, 49-63.

References

Davidson, E. J., Faulkner, R. L., Sehr, P., Pawlita, M., Smyth, L. J., Burt, D. J., Tomlinson, A. E., Hickling, J., Kitchener, H. C., & Stern, P. L. (2004). Effect of TA-CIN (HPV 16 L2E6E7) booster immunisation in vulval intraepithelial neoplasia patients previously vaccinated with TA-HPV (vaccinia virus encoding HPV 16/18 E6E7). *Vaccine, 22*(21-22), 2722-2729.

Day, P. M., & Schelhaas, M. (2014). Concepts of papillomavirus entry into host cells. *Curr Opin Virol, 4*, 24-31.

De Gregorio, P. R., Salva, S., Tomas, M. S. J., & Nader-Macias, M. E. F. (2018). Effects of exogenous sex hormones on mouse estrous cycle, vaginal microbiota and immune cells. *Scandinavian Journal of Laboratory Animal Science, 44*(3), 1-14.

de Jong, A., O'Neill, T., Khan, A. Y., Kwappenberg, K. M. C., Chisholm, S. E., Whittle, N. R., Dobson, J. A., Jack, L. C., Roberts, J. S., Offringa, R., van der Burg, S. H., & Hickling, J. K. (2002). Enhancement of human papillomavirus (HPV) type 16 E6 and E7-specific T-cell immunity in healthy volunteers through vaccination with TA-CIN, an HPV16 L2E7E6 fusion protein vaccine. *Vaccine, 20*(29-30), 3456-3464.

de Martel, C., Georges, D., Bray, F., Ferlay, J., & Clifford, G. M. (2020). Global burden of cancer attributable to infections in 2018: a worldwide incidence analysis. *Lancet Glob Health, 8*(2), e180-e190.

de Sanjosé, S., Brotons, M., & Pavon, M. A. (2018). The natural history of human papillomavirus infection. *Best Pract Res Clin Obstet Gynaecol, 47*, 2-13.

de Villiers, E. M. (2013). Cross-roads in the classification of papillomaviruses. *Virology, 445*(1-2), 2-10.

Decrausaz, L., Domingos-Pereira, S., Duc, M., Bobst, M., Romero, P., Schiller, J. T., Jichlinski, P., & Nardelli-Haefliger, D. (2011). Parenteral is more efficient than mucosal immunization to induce regression of human papillomavirus-associated genital tumors. *Int J Cancer, 129*(3), 762-772.

Decrausaz, L., Goncalves, A. R., Domingos-Pereira, S., Pythoud, C., Stehle, J. C., Schiller, J., Jichlinski, P., & Nardelli-Haefliger, D. (2011). A novel mucosal orthotopic murine model of human papillomavirus-associated genital cancers. *Int J Cancer, 128*(9), 2105-2113.

Decrausaz, L., Revaz, V., Bobst, M., Corthesy, B., Romero, P., & Nardelli-Haefliger, D. (2010). Induction of human papillomavirus oncogene-specific CD8 T-cell effector responses in the genital mucosa of vaccinated mice. *Int J Cancer, 126*(10), 2469-2478.

Dockrell, D. H., & Kinghorn, G. R. (2001). Imiquimod and resiquimod as novel immunomodulators. *J Antimicrob Chemother, 48*(6), 751-755.

Domingos-Pereira, S., Decrausaz, L., Derre, L., Bobst, M., Romero, P., Schiller, J. T., Jichlinski, P., & Nardelli-Haefliger, D. (2013). Intravaginal TLR agonists increase local vaccine-specific CD8 T cells and human papillomavirus-associated genital-tumor regression in mice. *Mucosal Immunol, 6*(2), 393-404.

Doorbar, J. (2013). The E4 protein; structure, function and patterns of expression. *Virology, 445*(1-2), 80-98.

Doorbar, J. (2016). Model systems of human papillomavirus-associated disease. *J Pathol, 238*(2), 166-179.

Doorbar, J., Egawa, N., Griffin, H., Kranjec, C., & Murakami, I. (2015). Human papillomavirus molecular biology and disease association. *Rev Med Virol, 25 Suppl 1*, 2-23.

Dorji, T., Nopsopon, T., Tamang, S. T., & Pongpirul, K. (2021). Human papillomavirus vaccination uptake in low-and middle-income countries: a meta-analysis. *EClinicalMedicine, 34*, 100836.

Dowling, D. J. (2018). Recent advances in the discovery and delivery of TLR7/8 agonists as vaccine adjuvants. *ImmunoHorizons, 2*(6), 185-197.

Drazic, A., & Winter, J. (2014). The physiological role of reversible methionine oxidation. *Biochim Biophys Acta, 1844*(8), 1367-1382.

Duranti, S., Pietragalla, A., Daniele, G., Nero, C., Ciccarone, F., Scambia, G., & Lorusso, D. (2021). Role of Immune Checkpoint Inhibitors in Cervical Cancer: From Preclinical to Clinical Data. *Cancers, 13*(9).

Eberhardt, C. S., Kissick, H. T., Patel, M. R., Cardenas, M. A., Prokhnevska, N., Obeng, R. C., Nasti, T. H., Griffith, C. C., Im, S. J., Wang, X., Shin, D. M., Carrington, M., Chen, Z. G., Sidney, J., Sette, A., Saba, N. F., Wieland, A., & Ahmed, R. (2021). Functional HPV-specific PD-1(+) stem-like CD8 T cells in head and neck cancer. *Nature, 597*(7875), 279-284.

Echchannaoui, H., Bianchi, M., Baud, D., Bobst, M., Stehle, J. C., & Nardelli-Haefliger, D. (2008). Intravaginal immunization of mice with recombinant Salmonella enterica serovar Typhimurium expressing human papillomavirus type 16 antigens as a potential route of vaccination against cervical cancer. *Infect Immun, 76*(5), 1940-1951.

Egawa, N., Egawa, K., Griffin, H., & Doorbar, J. (2015). Human Papillomaviruses; Epithelial Tropisms, and the Development of Neoplasia. *Viruses, 7*(7), 3863-3890.

Eiben, G. L., Velders, M. P., Schreiber, H., Cassetti, M. C., Pullen, J. K., Smith, L. R., & Kast, W. M. (2002). Establishment of an HLA-A*0201 human papillomavirus type 16 tumor model to determine the efficacy of vaccination strategies in HLA-A*0201 transgenic mice. *Cancer Res, 62*(20), 5792-5799.

Ensign, L. M., Cone, R., & Hanes, J. (2014). Nanoparticle-based drug delivery to the vagina: a review. *J Control Release, 190*, 500-514.

Ensign, L. M., Tang, B. C., Wang, Y. Y., Tse, T. A., Hoen, T., Cone, R., & Hanes, J. (2012). Mucus-penetrating nanoparticles for vaginal drug delivery protect against herpes simplex virus. *Sci Transl Med, 4*(138), 138ra179.

Falcaro, M., Castanon, A., Ndlela, B., Checchi, M., Soldan, K., Lopez-Bernal, J., Elliss-Brookes, L., & Sasieni, P. (2021). The effects of the national HPV vaccination programme in England, UK, on cervical cancer and grade 3 cervical intraepithelial neoplasia incidence: a register-based observational study. *Lancet, 398*(10316), 2084-2092.

Falk, K., Rötzschke, O., Stevanović, S., Jung, G., & Rammensee, H. G. (1991). Allele-Specific Motifs Revealed by Sequencing of Self-Peptides Eluted from MHC Molecules. *Nature, 351*(6324), 290-296.

Feltkamp, M. C., Smits, H. L., Vierboom, M. P., Minnaar, R. P., de Jongh, B. M., Drijfhout, J. W., ter Schegget, J., Melief, C. J., & Kast, W. M. (1993). Vaccination with cytotoxic T lymphocyte epitope-containing peptide protects against a tumor induced by human papillomavirus type 16-transformed cells. *Eur J Immunol, 23*(9), 2242-2249.

Fernando, G. J. P., Stewart, T. J., Tindle, R. W., & Frazer, I. H. (1998). Th2-type CD4(+) cells neither enhance nor suppress antitumor CTL activity in a mouse tumor model. *J Immunol, 161*(5), 2421-2427.

Fichorova, R. N., Tucker, L. D., & Anderson, D. J. (2001). The molecular basis of nonoxynol-9-induced vaginal inflammation and its possible relevance to human immunodeficiency virus type 1 transmission. *J Infect Dis, 184*(4), 418-428.

Fisher, R., Pusztai, L., & Swanton, C. (2013). Cancer heterogeneity: implications for targeted therapeutics. *Br J Cancer, 108*(3), 479-485.

Fraillery, D., Zosso, N., & Nardelli-Haefliger, D. (2009). Rectal and vaginal immunization of mice with human papillomavirus L1 virus-like particles. *Vaccine, 27*(17), 2326-2334.

Frazer, I. H., & Chandra, J. (2019). Immunotherapy for HPV associated cancer. *Papillomavirus Res, 8*, 100176.

Gates, B. J., & DeLuca, M. (1975). The production of oxyluciferin during the firefly luciferase light reaction. *Arch Biochem Biophys, 169*(2), 616-621.

Gheit, T. (2019). Mucosal and Cutaneous Human Papillomavirus Infections and Cancer Biology. *Front Oncol, 9*, 355.

Gibbs, J. B., Ellis, R. W., & Scolnick, E. M. (1984). Autophosphorylation of V-Ha-Ras-P21 Is Modulated by Amino-Acid Residue-12. *Proc Natl Acad Sci U S A, 81*(9), 2674-2678.

Gillgrass, A. E., Tang, V. A., Towarnicki, K. M., Rosenthal, K. L., & Kaushic, C. (2005). Protection against genital herpes infection in mice immunized under different hormonal conditions correlates with induction of vagina-associated lymphoid tissue. *J Virol, 79*(5), 3117-3126.

Gonzalez-Galarza, F. F., McCabe, A., Santos, E., Jones, J., Takeshita, L., Ortega-Rivera, N. D., Cid-Pavon, G. M. D., Ramsbottom, K., Ghattaoraya, G., Alfirevic, A., Middleton, D., & Jones, A. R. (2020). Allele frequency net database (AFND) 2020 update: gold-standard data classification, open access genotype data and new query tools. *Nucleic Acids Res, 48*(D1), D783-D788.

Gopinath, S., Lu, P., & Iwasaki, A. (2020). Cutting Edge: The Use of Topical Aminoglycosides as an Effective Pull in "Prime and Pull" Vaccine Strategy. *J Immunol*.

Gottgens, E. L., Ostheimer, C., Span, P. N., Bussink, J., & Hammond, E. M. (2019). HPV, hypoxia and radiation response in head and neck cancer. *Br J Radiol, 92*(1093), 20180047.

Gourley, T. S., Wherry, E. J., Masopust, D., & Ahmed, R. (2004). Generation and maintenance of immunological memory. *Semin Immunol, 16*(5), 323-333.

Graham, S. V. (2017). The human papillomavirus replication cycle, and its links to cancer progression: a comprehensive review. *Clin Sci (Lond), 131*(17), 2201-2221.

Griep, A. E., Herber, R., Jeon, S., Lohse, J. K., Dubielzig, R. R., & Lambert, P. F. (1993). Tumorigenicity by human papillomavirus type 16 E6 and E7 in transgenic mice correlates with alterations in epithelial cell growth and differentiation. *J Virol, 67*(3), 1373-1384.

Groom, J. R., & Luster, A. D. (2011). CXCR3 in T cell function. *Exp Cell Res, 317*(5), 620-631.

Gruber, C. J., Tschugguel, W., Schneeberger, C., & Huber, J. C. (2002). Production and actions of estrogens. *N Engl J Med, 346*(5), 340-352.

Grunwitz, C., Salomon, N., Vascotto, F., Selmi, A., Bukur, T., Diken, M., Kreiter, S., Türeci, Ö., & Sahin, U. (2019). HPV16 RNA-LPX vaccine mediates complete regression of aggressively growing HPV-positive mouse tumors and establishes protective T cell memory. *Oncoimmunology, 8*(9), e1629259.

Gulley, J. L. (2013). Therapeutic vaccines: the ultimate personalized therapy? *Hum Vaccin Immunother, 9*(1), 219-221.

Gunn, G. R., Zubair, A., Peters, C., Pan, Z. K., Wu, T. C., & Paterson, Y. (2001). Two Listeria monocytogenes vaccine vectors that express different molecular forms of human papilloma virus-16 (HPV-16) E7 induce qualitatively different T cell immunity that correlates with their ability to induce regression of established tumors immortalized by HPV-16. *J Immunol, 167*(11), 6471-6479.

Halbert, C. L., Demers, G. W., & Galloway, D. A. (1991). The E7 Gene of Human Papillomavirus Type-16 Is Sufficient for Immortalization of Human Epithelial-Cells. *J Virol, 65*(1), 473-478.

Halle, S., Halle, O., & Förster, R. (2017). Mechanisms and Dynamics of T Cell-Mediated Cytotoxicity In Vivo. *Trends Immunol, 38*(6), 432-443.

Hammer, G. E., Kanaseki, T., & Shastri, N. (2007). The final touches make perfect the peptide-MHC class I repertoire. *Immunity, 26*(4), 397-406.

Hasan, Y., Spiotto, M. T., Furtado, L. V., Tergas, A. I., Lee, N. K., Brooks, R. A., McCall, A. R., Golden, D. W., Jolly, S., Fleming, G. F., Morrow, M. P., Skolnik, J., Esser, M., Kumar, R., & Weichselbaum, R. R. (2018). A phase 1/2A trial of synthetic DNA vaccine immunotherapy targeting HPV-16 and-18 after chemoradiation for cervical cancer. *J Clin Oncol, 36*(15).

Henkle, T. R., Lam, B., Kung, Y. J., Lin, J., Tseng, S. H., Ferrall, L., Xing, D., Hung, C. F., & Wu, T. C. (2021). Development of a Novel Mouse Model of Spontaneous High-Risk HPVE6/E7-Expressing Carcinoma in the Cervicovaginal Tract. *Cancer Res, 81*(17), 4560-4569.

Hickman, D. L., Johnson, J., Vemulapalli, T. H., Crisler, J. R., & Shepherd, R. (2017). Commonly Used Animal Models. In *Principles of Animal Research* (pp. 117-175).

Hoover, A. C., Spanos, W. C., Harris, G. F., Anderson, M. E., Klingelhutz, A. J., & Lee, J. H. (2007). The role of human papillomavirus 16 E6 in anchorage-independent and invasive growth of mouse tonsil epithelium. *Arch Otolaryngol Head Neck Surg, 133*(5), 495-502.

Hu, Z., & Ma, D. (2018). The precision prevention and therapy of HPV-related cervical cancer: new concepts and clinical implications. *Cancer Med, 7*(10), 5217-5236.

Hull, R., Mbele, M., Makhafola, T., Hicks, C., Wang, S. M., Reis, R. M., Mehrotra, R., Mkhize-Kwitshana, Z., Kibiki, G., Bates, D. O., & Dlamini, Z. (2020). Cervical cancer in low and middle-income countries. *Oncology Letters, 20*(3), 2058-2074.

Hunter, M. C., Teijeira, A., & Halin, C. (2016). T Cell Trafficking through Lymphatic Vessels. *Front Immunol, 7*, 613.

Ibata, B., Parr, E. L., King, N. J. C., & Parr, M. B. (1997). Migration of foreign lymphocytes from the mouse vagina into the cervicovaginal mucosa and to the iliac lymph nodes. *Biology of Reproduction, 56*(2), 537-543.

Islam, E. A., Shaik-Dasthagirisaheb, Y., Kaushic, C., Wetzler, L. M., & Gray-Owen, S. D. (2016). The reproductive cycle is a pathogenic determinant during gonococcal pelvic inflammatory disease in mice. *Mucosal Immunol, 9*(4), 1051-1064.

Issa, A., Sebro, K., Kwok, A., Janisch, F., Grossmann, N. C., Lee, E., Lucky, M., Oliveira, P., Lau, M., Parnham, A., Sangar, V., & Fankhauser, C. D. (2021). Treatment Options and Outcomes for Men with Penile Intraepithelial Neoplasia: A Systematic Review. *Eur Urol Focus*.

Iwasaki, A. (2010). Antiviral immune responses in the genital tract: clues for vaccines. *Nat Rev Immunol, 10*(10), 699-711.

Iyer, V., & Poddar, S. S. (2008). Update on nonoxynol-9 as vaginal spermicide. *Eur J Contracept Reprod Health Care, 13*(4), 339-350.

Jahan-Tigh, R. R., Ryan, C., Obermoser, G., & Schwarzenberger, K. (2012). Flow cytometry. *J Invest Dermatol, 132*(10), 1-6.

Jameson, S. C., & Masopust, D. (2018). Understanding Subset Diversity in T Cell Memory. *Immunity, 48*(2), 214-226.

Jardetzky, T. S., Brown, J. H., Gorga, J. C., Stern, L. J., Urban, R. G., Chi, Y. I., Stauffacher, C., Strominger, J. L., & Wiley, D. C. (1994). Three-dimensional structure of a human class II histocompatibility molecule complexed with superantigen. *Nature, 368*(6473), 711-718.

Jenner, E. (1798). *An inquiry into the causes and effects of the variolae vaccinae, a disease discovered in some of the western counties of England, particularly Gloucestershire, and known by the name of the cow pox*.

Ji, H., Chang, E. Y., Lin, K. Y., Kurman, R. J., Pardoll, D. M., & Wu, T. C. (1998). Antigen-specific immunotherapy for murine lung metastatic tumors expressing human papillomavirus type 16 E7 oncoprotein. *Int J Cancer, 78*(1), 41-45.

Jiang, S., & Dong, C. (2013). A complex issue on CD4(+) T-cell subsets. *Immunol Rev, 252*(1), 5-11.

Jin, B. Y., Campbell, T. E., Draper, L. M., Stevanović, S., Weissbrich, B., Yu, Z., Restifo, N. P., Rosenberg, S. A., Trimble, C. L., & Hinrichs, C. S. (2018). Engineered T cells targeting E7 mediate regression of human papillomavirus cancers in a murine model. *JCI Insight, 3*(8).

Joffre, O. P., Segura, E., Savina, A., & Amigorena, S. (2012). Cross-presentation by dendritic cells. *Nat Rev Immunol, 12*(8), 557-569.

Johansson, E. L., Wassen, L., Holmgren, J., Jertborn, M., & Rudin, A. (2001). Nasal and vaginal vaccinations have differential effects on antibody responses in vaginal and cervical secretions in humans. *Infect Immun, 69*(12), 7481-7486.

Johnson, D. E., Burtness, B., Leemans, C. R., Lui, V. W. Y., Bauman, J. E., & Grandis, J. R. (2020). Head and neck squamous cell carcinoma. *Nat Rev Dis Primers, 6*(1), 92.

Kanzler, H., Barrat, F. J., Hessel, E. M., & Coffman, R. L. (2007). Therapeutic targeting of innate immunity with Toll-like receptor agonists and antagonists. *Nat Med, 13*(5), 552-559.

Karamanou, M., Agapitos, E., Kousoulis, A., & Androutsos, G. (2010). From the humble wart to HPV: a fascinating story throughout centuries. *Oncology Reviews, 4*(3), 133-135.

Karkada, M., Quinton, T., Blackman, R., & Mansour, M. (2013). Tumor inhibition by DepoVax-based cancer vaccine is accompanied by reduced regulatory/suppressor cell proliferation and tumor infiltration. *ISRN Oncology, 2013*.

Kawana, K., Adachi, K., Kojima, S., Taguchi, A., Tomio, K., Yamashita, A., Nishida, H., Nagasaka, K., Arimoto, T., Yokoyama, T., Wada-Hiraike, O., Oda, K., Sewaki, T., Osuga, Y., & Fujii, T. (2014). Oral vaccination against HPV E7 for treatment of cervical intraepithelial neoplasia grade 3 (CIN3) elicits E7-specific mucosal immunity in the cervix of CIN3 patients. *Vaccine, 32*(47), 6233-6239.

Kenter, G. G., Welters, M. J., Valentijn, A. R., Lowik, M. J., Berends-van der Meer, D. M., Vloon, A. P., Essahsah, F., Fathers, L. M., Offringa, R., Drijfhout, J. W., Wafelman, A. R., Oostendorp, J., Fleuren, G. J., van der Burg, S. H., & Melief, C. J. (2009). Vaccination against HPV-16 oncoproteins for vulvar intraepithelial neoplasia. *N Engl J Med, 361*(19), 1838-1847.

Keskin, D. B., Reinhold, B., Lee, S. Y., Zhang, G., Lank, S., O'Connor, D. H., Berkowitz, R. S., Brusic, V., Kim, S. J., & Reinherz, E. L. (2011). Direct identification of an HPV-16 tumor antigen from cervical cancer biopsy specimens. *Front Immunol, 2*, 75.

Kia'i, N., & Bajaj, T. (2021). Histology, respiratory epithelium. In *StatPearls*: StatPearls Publishing.

Killion, J. J., Radinsky, R., & Fidler, I. J. (1998). Orthotopic models are necessary to predict therapy of transplantable tumors in mice. *Cancer Metastasis Rev, 17*(3), 279-284.

Kim, T. K., & Eberwine, J. H. (2010). Mammalian cell transfection: the present and the future. *Anal Bioanal Chem, 397*(8), 3173-3178.

King, N. J., Parr, E. L., & Parr, M. B. (1998). Migration of lymphoid cells from vaginal epithelium to iliac lymph nodes in relation to vaginal infection by herpes simplex virus type 2. *J Immunol, 160*(3), 1173-1180.

Kirnbauer, R., Booy, F., Cheng, N., Lowy, D. R., & Schiller, J. T. (1992). Papillomavirus L1 Major Capsid Protein Self-Assembles into Virus-Like Particles That Are Highly Immunogenic. *Proc Natl Acad Sci U S A, 89*(24), 12180-12184.

Kjaer, S. K., Dehlendorff, C., Belmonte, F., & Baandrup, L. (2021). Real-World Effectiveness of Human Papillomavirus Vaccination Against Cervical Cancer. *J Natl Cancer Inst, 113*(10), 1329-1335.

Klug, F., Prakash, H., Huber, P. E., Seibel, T., Bender, N., Halama, N., Pfirschke, C., Voss, R. H., Timke, C., Umansky, L., Klapproth, K., Schakel, K., Garbi, N., Jager, D., Weitz, J., Schmitz-Winnenthal, H., Hammerling, G. J., & Beckhove, P. (2013). Low-dose irradiation programs macrophage differentiation to an iNOS(+)/M1 phenotype that orchestrates effective T cell immunotherapy. *Cancer Cell, 24*(5), 589-602.

Knust, J., Ochs, M., Gundersen, H. J., & Nyengaard, J. R. (2009). Stereological estimates of alveolar number and size and capillary length and surface area in mice lungs. *Anat Rec (Hoboken), 292*(1), 113-122.

Koller, B. H., Marrack, P., Kappler, J. W., & Smithies, O. (1990). Normal Development of Mice Deficient in β2M, MHC Class I Proteins, and CD8+ T Cells. *Science, 248*(4960), 1227-1230.

Koller, B. H., & Smithies, O. (1989). Inactivating the beta 2-microglobulin locus in mouse embryonic stem cells by homologous recombination. *Proc Natl Acad Sci U S A, 86*(22), 8932-8935.

Komdeur, F. L., Prins, T. M., van de Wall, S., Plat, A., Wisman, G. B. A., Hollema, H., Daemen, T., Church, D. N., de Bruyn, M., & Nijman, H. W. (2017). CD103+ tumor-infiltrating lymphocytes are tumor-reactive intraepithelial CD8+ T cells associated with prognostic benefit and therapy response in cervical cancer. *Oncoimmunology, 6*(9), e1338230.

Kozlowski, P. A., Cu-Uvin, S., Neutra, M. R., & Flanigan, T. P. (1997). Comparison of the oral, rectal, and vaginal immunization routes for induction of antibodies in rectal and genital tract secretions of women. *Infect Immun, 65*(4), 1387-1394.

Kruse, S. (2019). *Therapeutic vaccination against HPV-positive tumors in a MHC-humanized mouse model.* Ruperto-Carola University of Heidelberg, PhD thesis.

Kruse, S., Büchler, M., Uhl, P., Sauter, M., Scherer, P., Lan, T. C. T., Zottnick, S., Klevenz, A., Yang, R., Rösl, F., Mier, W., & Riemer, A. B. (2018). Therapeutic vaccination using minimal HPV16 epitopes in a novel MHC-humanized murine HPV tumor model. *Oncoimmunology, 8*(1), e1524694.

Kugelberg, E. (2014). Innate immunity: Making mice more human the TLR8 way. *Nat Rev Immunol, 14*(1), 6.

Kuo, P. T., Zeng, Z., Salim, N., Mattarollo, S., Wells, J. W., & Leggatt, G. R. (2018). The Role of CXCR3 and Its Chemokine Ligands in Skin Disease and Cancer. *Front Med 5*, 271.

Laemmli, U. K. (1970). Cleavage of structural proteins during the assembly of the head of bacteriophage T4. *Nature, 227*(5259), 680-685.

Laidlaw, B. J., Craft, J. E., & Kaech, S. M. (2016). The multifaceted role of CD4(+) T cells in CD8(+) T cell memory. *Nat Rev Immunol, 16*(2), 102-111.

Lange, J., Rivera-Ballesteros, O., & Buggert, M. (2021). Human mucosal tissue-resident memory T cells in health and disease. *Mucosal Immunol*.

Larsen, S. B., Cowley, C. J., & Fuchs, E. (2020). Epithelial cells: liaisons of immunity. *Curr Opin Immunol, 62*, 45-53.

Lavelle, E. C., & Ward, R. W. (2022). Mucosal vaccines - fortifying the frontiers. *Nat Rev Immunol, 22*(4), 236-250.

Lawrance, S. K., Karlsson, L., Price, J., Quaranta, V., Ron, Y., Sprent, J., & Peterson, P. A. (1989). Transgenic HLA-DR alpha faithfully reconstitutes IE-controlled immune functions and induces cross-tolerance to E alpha in E alpha 0 mutant mice. *Cell, 58*(3), 583-594.

Lechner, M., Liu, J., Masterson, L., & Fenton, T. R. (2022). HPV-associated oropharyngeal cancer: epidemiology, molecular biology and clinical management. *Nat Rev Clin Oncol*.

Lechner, M. G., Karimi, S. S., Barry-Holson, K., Angell, T. E., Murphy, K. A., Church, C. H., Ohlfest, J. R., Hu, P. S., & Epstein, A. L. (2013). Immunogenicity of Murine Solid Tumor Models as a Defining Feature of In Vivo Behavior and Response to Immunotherapy. *J Immunother, 36*(9), 477-489.

Lee, C. L., Mowery, Y. M., Daniel, A. R., Zhang, D., Sibley, A. B., Delaney, J. R., Wisdom, A. J., Qin, X., Wang, X., Caraballo, I., Gresham, J., Luo, L., Van Mater, D., Owzar, K., & Kirsch, D. G. (2019). Mutational landscape in genetically engineered, carcinogen-induced, and radiation-induced mouse sarcoma. *JCI Insight, 4*(13).

Lee, S. J., Yang, A., Wu, T. C., & Hung, C. F. (2016). Immunotherapy for human papillomavirus-associated disease and cervical cancer: review of clinical and translational research. *J Gynecol Oncol, 27*(5), e51.

Leenaars, C. H. C., Kouwenaar, C., Stafleu, F. R., Bleich, A., Ritskes-Hoitinga, M., De Vries, R. B. M., & Meijboom, F. L. B. (2019). Animal to human translation: a systematic scoping review of reported concordance rates. *J Transl Med, 17*(1), 223.

Lei, J., Ploner, A., Elfstrom, K. M., Wang, J., Roth, A., Fang, F., Sundstrom, K., Dillner, J., & Sparen, P. (2020). HPV Vaccination and the Risk of Invasive Cervical Cancer. *N Engl J Med, 383*(14), 1340-1348.

Lheureux, S., Butler, M. O., Clarke, B., Cristea, M. C., Martin, L. P., Tonkin, K., Fleming, G. F., Tinker, A. V., Hirte, H. W., Tsoref, D., Mackay, H., Dhani, N. C., Ghatage, P., Weberpals, J., Welch, S., Pham, N. A., Motta, V., Sotov, V., Wang, L., Karakasis, K., Udagani, S., Kamel-Reid, S., Streicher, H. Z., Shaw, P., & Oza, A. M. (2018). Association of Ipilimumab With Safety and Antitumor Activity in Women With Metastatic or Recurrent Human Papillomavirus-Related Cervical Carcinoma. *JAMA Oncol, 4*(7), e173776.

Li, F., Adase, C. A., & Zhang, L. J. (2017). Isolation and Culture of Primary Mouse Keratinocytes from Neonatal and Adult Mouse Skin. *J Vis Exp*(125).

Li, L. L., Wang, H. R., Zhou, Z. Y., Luo, J., Wang, X. L., Xiao, X. Q., Zhou, Y. B., & Zeng, Y. (2016). C3-Luc Cells Are an Excellent Model for Evaluation of Cellular Immunity following HPV16L1 Vaccination. *PLoS One, 11*(2), e0149748.

Li, S., Herrera, G. G., Tam, K. K., Lizarraga, J. S., Beedle, M. T., & Winuthayanon, W. (2018). Estrogen Action in the Epithelial Cells of the Mouse Vagina Regulates Neutrophil Infiltration and Vaginal Tissue Integrity. *Sci Rep, 8*(1), 11247.

Li, S., Zhu, W., Ye, C., Sun, W., Xie, H., Yang, X., Zhang, Q., & Ma, Y. (2020). Local mucosal immunization of self-assembled nanofibers elicits robust antitumor effects in an orthotopic model of mouse genital tumors. *Nanoscale, 12*(5), 3076-3089.

Limberis, M. P., Bell, C. L., & Wilson, J. M. (2009). Identification of the murine firefly luciferase-specific CD8 T-cell epitopes. *Gene Ther, 16*(3), 441-447.

Lin, K. Y., Guarnieri, F. G., Staveley-O'Carroll, K. F., Levitsky, H. I., August, J. T., Pardoll, D. M., & Wu, T. C. (1996). Treatment of established tumors with a novel vaccine that enhances major histocompatibility class II presentation of tumor antigen. *Cancer Res, 56*(1), 21-26.

Lippincott-Schwartz, J., Yuan, L., Tipper, C., Amherdt, M., Orci, L., & Klausner, R. D. (1991). Brefeldin A's effects on endosomes, lysosomes, and the TGN suggest a general mechanism for regulating organelle structure and membrane traffic. *Cell, 67*(3), 601-616.

Liu, H., Moynihan, K. D., Zheng, Y., Szeto, G. L., Li, A. V., Huang, B., Van Egeren, D. S., Park, C., & Irvine, D. J. (2014). Structure-based programming of lymph-node targeting in molecular vaccines. *Nature, 507*(7493), 519-522.

Liu, J., Xu, C. F., Hsu, L. C., Luo, Y. P., Xiang, R., & Chuang, T. H. (2010). A five-amino-acid motif in the undefined region of the TLR8 ectodomain is required for species-specific ligand recognition. *Molecular Immunology, 47*(5), 1083-1090.

Liu, Z., Chen, O., Wall, J. B. J., Zheng, M., Zhou, Y., Wang, L., Ruth Vaseghi, H., Qian, L., & Liu, J. (2017). Systematic comparison of 2A peptides for cloning multi-genes in a polycistronic vector. *Sci Rep, 7*(1), 2193.

Loenen, W. A., Dryden, D. T., Raleigh, E. A., Wilson, G. G., & Murray, N. E. (2014). Highlights of the DNA cutters: a short history of the restriction enzymes. *Nucleic Acids Res, 42*(1), 3-19.

Long, J. A., & Evans, H. M. (1922). *The oestrous cycle in the rat and its associated phenomena* (Vol. 6): University of California Press.

Lopez, J. A., Susanto, O., Jenkins, M. R., Lukoyanova, N., Sutton, V. R., Law, R. H., Johnston, A., Bird, C. H., Bird, P. I., Whisstock, J. C., Trapani, J. A., Saibil, H. R., & Voskoboinik, I. (2013). Perforin forms transient pores on the target cell plasma membrane to facilitate rapid access of granzymes during killer cell attack. *Blood, 121*(14), 2659-2668.

Lowry, O., Rosebrough, N., Farr, A. L., & Randall, R. (1951). Protein Measurement with the Folin Phenol Reagent. *J Biol Chem, 193*(1), 265-275.

Lowy, D. R., Solomon, D., Hildesheim, A., Schiller, J. T., & Schiffman, M. (2008). Human papillomavirus infection and the primary and secondary prevention of cervical cancer. *Cancer, 113*(7 Suppl), 1980-1993.

Maciag, P. C., Radulovic, S., & Rothman, J. (2009). The first clinical use of a live-attenuated Listeria monocytogenes vaccine: A Phase I safety study of Lm-LLO-E7 in patients with advanced carcinoma of the cervix. *Vaccine, 27*(30), 3975-3983.

MacLean, B., Tomazela, D. M., Shulman, N., Chambers, M., Finney, G. L., Frewen, B., Kern, R., Tabb, D. L., Liebler, D. C., & MacCoss, M. J. (2010). Skyline: an open source document editor for creating and analyzing targeted proteomics experiments. *Bioinformatics, 26*(7), 966-968.

Madsen, L., Labrecque, N., Engberg, J., Dierich, A., Svejgaard, A., Benoist, C., Mathis, D., & Fugger, L. (1999). Mice lacking all conventional MHC class II genes. *Proc Natl Acad Sci U S A, 96*(18), 10338-10343.

Mahjabeen, S., Hatipoglu, M. K., Benbrook, D. M., Kosanke, S. D., Garcia-Contreras, D., & Garcia-Contreras, L. (2018). Influence of the estrus cycle of the mouse on the disposition of SHetA2 after vaginal administration. *Eur J Pharm Biopharm, 130*, 272-280.

Mak, I. W., Evaniew, N., & Ghert, M. (2014). Lost in translation: animal models and clinical trials in cancer treatment. *Am J Transl Res, 6*(2), 114-118.

Mami-Chouaib, F., Blanc, C., Corgnac, S., Hans, S., Malenica, I., Granier, C., Tihy, I., & Tartour, E. (2018). Resident memory T cells, critical components in tumor immunology. *J Immunother Cancer, 6*(1), 87.

Manns, J. M. (2011). SDS-Polyacrylamide Gel Electrophoresis (SDS-PAGE) of Proteins. *Curr Protoc Microbiol, 22*(1).

Masters, J. R. (2002). HeLa cells 50 years on: the good, the bad and the ugly. *Nat Rev Cancer, 2*(4), 315-319.

Matlashewski, G., Schneider, J., Banks, L., Jones, N., Murray, A., & Crawford, L. (1987). Human Papillomavirus Type-16 DNA Cooperates with Activated Ras in Transforming Primary-Cells. *Embo Journal, 6*(6), 1741-1746.

McBride, A. A. (2022). Human papillomaviruses: diversity, infection and host interactions. *Nat Rev Microbiol, 20*(2), 95-108.

McDermott, M., Clark, D., & Bienenstock, J. (1980). Evidence for a common mucosal immunologic system. II. Influence of the estrous cycle on B immunoblast migration into genital and intestinal tissues. *J Immunol, 124*(6), 2536-2539.

Mebius, R. E., & Kraal, G. (2005). Structure and function of the spleen. *Nat Rev Immunol, 5*(8), 606-616.

Medzhitov, R. (2001). Toll-like receptors and innate immunity. *Nat Rev Immunol, 1*(2), 135-145.

Mermod, M., Hiou-Feige, A., Bovay, E., Roh, V., Sponarova, J., Bongiovanni, M., Vermeer, D. W., Lee, J. H., Petrova, T. V., Rivals, J. P., Monnier, Y., Tolstonog, G. V., & Simon, C. (2018). Mouse model of postsurgical primary tumor recurrence and regional lymph node metastasis progression in HPV-related head and neck cancer. *Int J Cancer, 142*(12), 2518-2528.

Messa, L., & Loregian, A. (2022). HPV-induced cancers: preclinical therapeutic advancements. *Expert Opin Investig Drugs, 31*(1), 79-93.

Mestas, J., & Hughes, C. C. (2004). Of mice and not men: differences between mouse and human immunology. *J Immunol, 172*(5), 2731-2738.

Mestecky, J., Moldoveanu, Z., & Russell, M. W. (2005). Immunologic uniqueness of the genital tract: challenge for vaccine development. *Am J Reprod Immunol, 53*(5), 208-214.

Metzemaekers, M., Vanheule, V., Janssens, R., Struyf, S., & Proost, P. (2018). Overview of the Mechanisms that May Contribute to the Non-Redundant Activities of Interferon-Inducible CXC Chemokine Receptor 3 Ligands. *Front Immunol, 8*.

Miao, L., Zhang, Y., & Huang, L. (2021). mRNA vaccine for cancer immunotherapy. *Mol Cancer, 20*(1), 41.

Miltenyi Biotec. (2021). Tumor Dissociation Kit mouse protocol. Retrieved from https://www.miltenyibiotec.com/upload/assets/IM0001973.PDF on 04.03.2022.

Moody, C. A., & Laimins, L. A. (2010). Human papillomavirus oncoproteins: pathways to transformation. *Nat Rev Cancer, 10*(8), 550-560.

Moore, A. R., Rosenberg, S. C., McCormick, F., & Malek, S. (2020). RAS-targeted therapies: is the undruggable drugged? *Nat Rev Drug Discov, 19*(8), 533-552.

Mueller, S. N., Gebhardt, T., Carbone, F. R., & Heath, W. R. (2013). Memory T cell subsets, migration patterns, and tissue residence. *Annu Rev Immunol, 31*, 137-161.

Mueller, S. N., & Mackay, L. K. (2016). Tissue-resident memory T cells: local specialists in immune defence. *Nat Rev Immunol, 16*(2), 79-89.

Munger, K., Gwin, T. K., & McLaughlin-Drubin, M. E. (2013). p16 in HPV-associated cancers. *Oncotarget, 4*(11), 1864-1865.

Murphy, K., & Weaver, C. (2017). *Janeway's immunobiology 9th edition*: Garland science.

Nagarsheth, N. B., Norberg, S. M., Sinkoe, A. L., Adhikary, S., Meyer, T. J., Lack, J. B., Warner, A. C., Schweitzer, C., Doran, S. L., Korrapati, S., Stevanović, S., Trimble, C. L., Kanakry, J. A., Bagheri, M. H., Ferraro, E., Astrow, S. H., Bot, A., Faquin, W. C., Stroncek, D., Gkitsas, N., Highfill, S., & Hinrichs, C. S. (2021). TCR-engineered T cells targeting E7 for patients with metastatic HPV-associated epithelial cancers. *Nat Med, 27*(3), 419-425.

Nagy, V., & Watzele, M. (2006). FuGENE® 6 Transfection Reagent: minimizing reagent-dependent side effects as analyzed by gene-expression profiling and cytotoxicity assays. *Nature Methods, 3*(5), iii-v.

Nakanishi, Y., Lu, B., Gerard, C., & Iwasaki, A. (2009). CD8(+) T lymphocyte mobilization to virus-infected tissue requires CD4(+) T-cell help. *Nature, 462*(7272), 510-513.

Netea, M. G., Schlitzer, A., Placek, K., Joosten, L. A. B., & Schultze, J. L. (2019). Innate and Adaptive Immune Memory: an Evolutionary Continuum in the Host's Response to Pathogens. *Cell Host Microbe, 25*(1), 13-26.

Newberg, M. H., Smith, D. H., Haertel, S. B., Vining, D. R., Lacy, E., & Engelhard, V. H. (1996). Importance of MHC class 1 alpha2 and alpha3 domains in the recognition of self and non-self MHC molecules. *J Immunol, 156*(7), 2473-2480.

Nizard, M., Roussel, H., & Tartour, E. (2016). Resident Memory T Cells as Surrogate Markers of the Efficacy of Cancer Vaccines. *Clin Cancer Res, 22*(3), 530-532.

Omilusik, K. D., & Goldrath, A. W. (2017). The origins of memory T cells. *Nature, 552*(7685).

Pajot, A., Michel, M. L., Fazilleau, N., Pancre, V., Auriault, C., Ojcius, D. M., Lemonnier, F. A., & Lone, Y. C. (2004). A mouse model of human adaptive immune functions: HLA-A2.1-/HLA-DR1-transgenic H-2 class I-/class II-knockout mice. *Eur J Immunol, 34*(11), 3060-3069.

Pal, A., & Kundu, R. (2019). Human Papillomavirus E6 and E7: The Cervical Cancer Hallmarks and Targets for Therapy. *Front Microbiol, 10*, 3116.

Paolini, F., Massa, S., Manni, I., Franconi, R., & Venuti, A. (2014). Immunotherapy in new pre-clinical models of HPV-associated oral cancers. *Hum Vaccines Immunother, 9*(3), 534-543.

Papanicolaou, G. N., & Traut, H. F. (1941). The diagnostic value of vaginal smears in carcinoma of the uterus. *Am J Obstet Gynecol, 42*(2), 193-206.

Pardoll, D. M. (2012). The blockade of immune checkpoints in cancer immunotherapy. *Nat Rev Cancer, 12*(4), 252-264.

Park, C. O., & Kupper, T. S. (2015). The emerging role of resident memory T cells in protective immunity and inflammatory disease. *Nat Med, 21*(7), 688-697.

Parr, M. B., & Parr, E. L. (1990). Antigen recognition in the female reproductive tract: I. Uptake of intraluminal protein tracers in the mouse vagina. *J Reprod Immunol, 17*(2), 101-114.

Pascolo, S. (2005). HLA class I transgenic mice: development, utilisation and improvement. *Expert Opin Biol Ther, 5*(7), 919-938.

Pascolo, S., Bervas, N., Ure, J. M., Smith, A. G., Lemonnier, F. A., & Perarnau, B. (1997). HLA-A2.1-restricted education and cytolytic activity of CD8(+) T lymphocytes from beta2 microglobulin (beta2m) HLA-A2.1 monochain transgenic H-2Db beta2m double knockout mice. *J Exp Med, 185*(12), 2043-2051.

Pattillo, R. A., Hussa, R. O., Story, M. T., Ruckert, A. C., Shalaby, M. R., & Mattingly, R. F. (1977). Tumor antigen and human chorionic gonadotropin in CaSki cells: a new epidermoid cervical cancer cell line. *Science, 196*(4297), 1456-1458.

Peacock, A. C., & Dingman, C. W. (1968). Molecular weight estimation and separation of ribonucleic acid by electrophoresis in agarose-acrylamide composite gels. *Biochemistry, 7*(2), 668-674.

Peng, S., Tan, M., Li, Y. D., Cheng, M. A., Farmer, E., Ferrall, L., Gaillard, S., Roden, R. B. S., Hung, C. F., & Wu, T. C. (2021). PD-1 blockade synergizes with intratumoral vaccination of a therapeutic HPV protein vaccine and elicits regression of tumor in a preclinical model. *Cancer Immunol Immunother, 70*(4), 1049-1062.

Peng, S., Trimble, C., He, L., Tsai, Y. C., Lin, C. T., Boyd, D. A., Pardoll, D., Hung, C. F., & Wu, T. C. (2006). Characterization of HLA-A2-restricted HPV-16 E7-specific CD8(+) T-cell immune responses induced by DNA vaccines in HLA-A2 transgenic mice. *Gene Ther, 13*(1), 67-77.

Peng, S., Xing, D., Ferrall, L., Tsai, Y., Roden, R., Hung, C., & Wu, T. (2022). Development of a Spontaneous HPV16 E6/E7-Expressing Head and Neck Squamous Cell Carcinoma in HLA-A2 Transgenic Mice. *mbio, 13*(1), e03252-03221.

Peterson, A. C., Russell, J. D., Bailey, D. J., Westphall, M. S., & Coon, J. J. (2012). Parallel reaction monitoring for high resolution and high mass accuracy quantitative, targeted proteomics. *Mol Cell Proteomics, 11*(11), 1475-1488.

Plummer, M., Schiffman, M., Castle, P. E., Maucort-Boulch, D., Wheeler, C. M., & Group, A. (2007). A 2-year prospective study of human papillomavirus persistence among women with a cytological diagnosis of atypical squamous cells of undetermined significance or low-grade squamous intraepithelial lesion. *J Infect Dis, 195*(11), 1582-1589.

Pohlmann, R., Kruger, S., Hasilik, A., & von Figura, K. (1984). Effect of monensin on intracellular transport and receptor-mediated endocytosis of lysosomal enzymes. *Biochem J, 217*(3), 649-658.

Postow, M. A., Callahan, M. K., & Wolchok, J. D. (2015). Immune Checkpoint Blockade in Cancer Therapy. *J Clin Oncol, 33*(17), 1974-1982.

Priyadarshini, M., Prabhu, V. S., Snedecor, S. J., Corman, S., Kuter, B. J., Nwankwo, C., Chirovsky, D., & Myers, E. (2021). Economic Value of Lost Productivity Attributable to Human Papillomavirus Cancer Mortality in the United States. *Front Public Health, 8*, 624092.

Purcell, A. W., Ramarathinam, S. H., & Ternette, N. (2019). Mass spectrometry-based identification of MHC-bound peptides for immunopeptidomics. *Nat Protoc, 14*(6), 1687-1707.

Quandt, J. (2014). *Common mutations in the tumor suppressor p53 & the oncogene Kras as targets for long peptide anti-cancer vaccination.* Ruperto-Carola University of Heidelberg, PhD thesis.

Rafael, T. S., Rotman, J., Brouwer, O. R., van der Poel, H. G., Mom, C. H., Kenter, G. G., de Gruijl, T. D., & Jordanova, E. S. (2022). Immunotherapeutic Approaches for the Treatment of HPV-Associated (Pre-)Cancer of the Cervix, Vulva and Penis. *J Clin Med, 11*(4).

RC Team. (2013). R: A language and environment for statistical computing.

Rieck, T., Feig, M., & Siedler, A. (2021). Impfquoten von Kinderschutzimpfungen in Deutschland – aktuelle Ergebnisse aus der RKI-Impfsurveillance. *Epidemiologisches Bulletin*(49), 6-29.

Riemer, A. B., Keskin, D. B., Zhang, G., Handley, M., Anderson, K. S., Brusic, V., Reinhold, B., & Reinherz, E. L. (2010). A conserved E7-derived cytotoxic T lymphocyte epitope expressed on human papillomavirus 16-transformed HLA-A2+ epithelial cancers. *J Biol Chem, 285*(38), 29608-29622.

Roberts, J. N., Buck, C. B., Thompson, C. D., Kines, R., Bernardo, M., Choyke, P. L., Lowy, D. R., & Schiller, J. T. (2007). Genital transmission of HPV in a mouse model is potentiated by nonoxynol-9 and inhibited by carrageenan. *Nat Med, 13*(7), 857-861.

Roberts, J. R., Siekas, L. L., & Kaz, A. M. (2017). Anal intraepithelial neoplasia: A review of diagnosis and management. *World J Gastrointest Oncol, 9*(2), 50-61.

Rock, K. L., Reits, E., & Neefjes, J. (2016). Present Yourself! By MHC Class I and MHC Class II Molecules. *Trends Immunol, 37*(11), 724-737.

Roden, R. B. S., & Stern, P. L. (2018). Opportunities and challenges for human papillomavirus vaccination in cancer. *Nat Rev Cancer, 18*(4), 240-254.

Rosales, R., Lopez-Contreras, M., Rosales, C., Magallanes-Molina, J. R., Gonzalez-Vergara, R., Arroyo-Cazarez, J. M., Ricardez-Arenas, A., Del Follo-Valencia, A., Padilla-Arriaga, S., Guerrero, M. V., Pirez, M. A., Arellano-Fiore, C., & Villarreal, F. (2014). Regression of human papillomavirus intraepithelial lesions is induced by MVA E2 therapeutic vaccine. *Hum Gene Ther, 25*(12), 1035-1049.

Rudensky, Y., Preston-Hurlburt, P., Hong, S. C., Barlow, A., & Janeway, C. A., Jr. (1991). Sequence analysis of peptides bound to MHC class II molecules. *Nature, 353*(6345), 622-627.

Russell, M. W. (2002). Immunization for protection of the reproductive tract: a review. *Am J Reprod Immunol, 47*(5), 265-268.

Ryan, M. D., King, A. M. Q., & Thomas, G. P. (1991). Cleavage of Foot-and-Mouth-Disease Virus Polyprotein Is Mediated by Residues Located within a 19 Amino-Acid-Sequence. *J Gen Virol, 72*, 2727-2732.

Salomon, N., Selmi, A., Grunwitz, C., Kong, A., Stanganello, E., Neumaier, J., Petschenka, J., Diken, M., Kreiter, S., Türeci, Ö., Sahin, U., & Vascotto, F. (2021). Local radiotherapy and E7 RNA-LPX vaccination show enhanced therapeutic efficacy in preclinical models of HPV16(+) cancer. *Cancer Immunol Immunother*.

Sanclemente, G., & Gill, D. K. (2002). Human papillomavirus molecular biology and pathogenesis. *J Eur Acad Dermatol Venereol, 16*(3), 231-240.

Sanford, K. K., Merwin, R. M., Hobbs, G. L., & Earle, W. R. (1959). Influence of animal passage on a line of tissue-culture cells. *J Natl Cancer Inst, 23*, 1061-1077.

Sanger, F., Nicklen, S., & Coulson, A. R. (1977). DNA sequencing with chain-terminating inhibitors. *Proc Natl Acad Sci U S A, 74*(12), 5463-5467.

Santos, C., Vilanova, M., Medeiros, R., & Gil da Costa, R. M. (2017). HPV-transgenic mouse models: Tools for studying the cancer-associated immune response. *Virus Res, 235*, 49-57.

Scarth, J. A., Patterson, M. R., Morgan, E. L., & Macdonald, A. (2021). The human papillomavirus oncoproteins: a review of the host pathways targeted on the road to transformation. *J Gen Virol, 102*(3).

Schenkel, J. M., & Masopust, D. (2014). Tissue-resident memory T cells. *Immunity, 41*(6), 886-897.

Schiffman, M., Doorbar, J., Wentzensen, N., de Sanjose, S., Fakhry, C., Monk, B. J., Stanley, M. A., & Franceschi, S. (2016). Carcinogenic human papillomavirus infection. *Nat Rev Dis Primers, 2*, 16086.

Schiller, J., & Lowy, D. (2018). Explanations for the high potency of HPV prophylactic vaccines. *Vaccine, 36*(32 Pt A), 4768-4773.

Schiller, J. T., & Lowy, D. R. (2012). Understanding and learning from the success of prophylactic human papillomavirus vaccines. *Nat Rev Microbiol, 10*(10), 681-692.

Schindler, A. E., Campagnoli, C., Druckmann, R., Huber, J., Pasqualini, J. R., Schweppe, K. W., & Thijssen, J. H. (2008). Classification and pharmacology of progestins. *Maturitas, 61*(1-2), 171-180.

Schön, M. P., & Schön, M. (2008). TLR7 and TLR8 as targets in cancer therapy. *Oncogene, 27*(2), 190-199.

Schreiber, K., Cannon, R. E., Karrison, T., Beck-Engeser, G., Huo, D. Z., Tennant, R. W., Jensen, H., Kast, W. M., Krausz, T., Meredith, S. C., Chen, L. P., & Schreiber, H. (2004). Strong synergy between mutant ras and HPV16 E6/E7 in the development of primary tumors. *Oncogene, 23*(22), 3972-3979.

Shin, H., & Iwasaki, A. (2012). A vaccine strategy that protects against genital herpes by establishing local memory T cells. *Nature, 491*(7424), 463-467.

Shin, H., & Iwasaki, A. (2013). Tissue-resident memory T cells. *Immunol Rev, 255*(1), 165-181.

Sierra, G., Dorta-Estremera, S., Hegde, V. L., Nookala, S. M. K., Yanamandra, A. V., & Sastry, K. J. (2020). Intranasal Therapeutic Peptide Vaccine Promotes Efficient Induction and Trafficking of Cytotoxic T Cell Response for the Clearance of HPV Vaginal Tumors. *Vaccines (Basel), 8*(2).

Sigrist, C. (2018). Vaccine Immunology. In *Plotkin's Vaccines* (pp. 16-34.e17): Elsevier.

Smalley Rumfield, C., Pellom, S. T., Morillon Ii, Y. M., Schlom, J., & Jochems, C. (2020). Immunomodulation to enhance the efficacy of an HPV therapeutic vaccine. *J Immunother Cancer, 8*(1).

Smalley Rumfield, C., Roller, N., Pellom, S. T., Schlom, J., & Jochems, C. (2020). Therapeutic Vaccines for HPV-Associated Malignancies. *Immunotargets Ther, 9*, 167-200.

Soong, R. S., Song, L., Trieu, J., Knoff, J., He, L., Tsai, Y. C., Huh, W., Chang, Y. N., Cheng, W. F., Roden, R. B., Wu, T. C., Trimble, C. L., & Hung, C. F. (2014). Toll-like receptor agonist imiquimod facilitates antigen-specific CD8+ T-cell accumulation in the genital tract leading to tumor control through IFNgamma. *Clin Cancer Res, 20*(21), 5456-5467.

Stanke, J., Hoffmann, C., Erben, U., von Keyserling, H., Stevanović, S., Cichon, G., Schneider, A., & Kaufmann, A. M. (2010). A flow cytometry-based assay to assess minute frequencies of CD8+ T cells by their cytolytic function. *J Immunol Methods, 360*(1-2), 56-65.

Stanley, M. (2003). Chapter 17: Genital human papillomavirus infections--current and prospective therapies. *J Natl Cancer Inst Monogr*(31), 117-124.

Steinbach, A., & Riemer, A. B. (2017). Immune evasion mechanisms of human papillomavirus: An update. *Int J Cancer, 142*(2), 224-229.

Stevanović, S., Helman, S. R., Wunderlich, J. R., Langhan, M. M., Doran, S. L., Kwong, M. L. M., Somerville, R. P. T., Klebanoff, C. A., Kammula, U. S., Sherry, R. M., Yang, J. C., Rosenberg, S. A., & Hinrichs, C. S. (2019). A Phase II Study of Tumor-infiltrating Lymphocyte Therapy for Human Papillomavirus-associated Epithelial Cancers. *Clin Cancer Res, 25*(5), 1486-1493.

Street, M. D., Doan, T., Herd, K. A., & Tindle, R. W. (2002). Limitations of HLA-transgenic mice in presentation of HLA-restricted cytotoxic T-cell epitopes from endogenously processed human papillomavirus type 16 E7 protein. *Immunology, 106*(4), 526-536.

Su, F., Patel, G. B., Hu, S. H., & Chen, W. X. (2016). Induction of mucosal immunity through systemic immunization: Phantom or reality? *Hum Vaccines Immunother, 12*(4), 1070-1079.

Sun, Y., Peng, S., Qiu, J., Miao, J., Yang, B., Jeang, J., Hung, C. F., & Wu, T. C. (2015). Intravaginal HPV DNA vaccination with electroporation induces local CD8+ T-cell immune responses and antitumor effects against cervicovaginal tumors. *Gene Ther, 22*(7), 528-535.

Sun, Y. Y., Peng, S., Han, L., Qiu, J., Song, L., Tsai, Y., Yang, B., Roden, R. B., Trimble, C. L., Hung, C. F., & Wu, T. C. (2016). Local HPV Recombinant Vaccinia Boost Following Priming with an HPV DNA Vaccine Enhances Local HPV-Specific CD8+ T-cell-Mediated Tumor Control in the Genital Tract. *Clin Cancer Res, 22*(3), 657-669.

Szymonowicz, K. A., & Chen, J. (2020). Biological and clinical aspects of HPV-related cancers. *Cancer Biol Med, 17*(4), 864-878.

Tan, H. X., Wheatley, A. K., Esterbauer, R., Jegaskanda, S., Glass, J. J., Masopust, D., De Rose, R., & Kent, S. J. (2017). Induction of vaginal-resident HIV-specific CD8 T cells with mucosal prime-boost immunization. *Mucosal Immunol*.

Tan, X., Sande, J. L., Pufnock, J. S., Blattman, J. N., & Greenberg, P. D. (2011). Retinoic acid as a vaccine adjuvant enhances CD8+ T cell response and mucosal protection from viral challenge. *J Virol, 85*(16), 8316-8327.

Taylor, B. C., & Balko, J. M. (2022). Mechanisms of MHC-I Downregulation and Role in Immunotherapy Response. *Front Immunol, 13*, 844866.

Tindle, R. W., Croft, S., Herd, K., Malcolm, K., Geczy, A. F., Stewart, T., & Fernando, G. J. (1995). A vaccine conjugate of 'ISCAR' immunocarrier and peptide epitopes of the E7 cervical cancer-associated protein of human papillomavirus type 16 elicits specific Th1- and Th2-type responses in immunized mice in the absence of oil-based adjuvants. *Clin Exp Immunol, 101*(2), 265-271.

Toh, Z. Q., Russell, F. M., Garland, S. M., Mulholland, E. K., Patton, G., & Licciardi, P. V. (2021). Human papillomavirus vaccination after COVID-19. *JNCI Cancer Spectrum, 5*(2), pkab011.

Tregoning, J. S., Buffa, V., Oszmiana, A., Klein, K., Walters, A. A., & Shattock, R. J. (2013). A "prime-pull" vaccine strategy has a modest effect on local and systemic antibody responses to HIV gp140 in mice. *PLoS One, 8*(11), e80559.

Trimble, C. L., & Frazer, I. H. (2009). Development of therapeutic HPV vaccines. *Lancet Oncol, 10*(10), 975-980.

Trimble, C. L., Morrow, M. P., Kraynyak, K. A., Shen, X., Dallas, M., Yan, J., Edwards, L., Parker, R. L., Denny, L., Giffear, M., Brown, A. S., Marcozzi-Pierce, K., Shah, D., Slager, A. M., Sylvester, A. J., Khan, A., Broderick, K. E., Juba, R. J., Herring, T. A., Boyer, J., Lee, J., Sardesai, N. Y., Weiner, D. B., & Bagarazzi, M. L. (2015). Safety, efficacy, and immunogenicity of VGX-3100, a therapeutic synthetic DNA vaccine targeting human papillomavirus 16 and 18 E6 and E7 proteins for cervical intraepithelial neoplasia 2/3: a randomised, double-blind, placebo-controlled phase 2b trial. *Lancet, 386*(10008), 2078-2088.

Uhl, P., Grundmann, C., Sauter, M., Storck, P., Tursch, A., Özbek, S., Leotta, K., Roth, R., Witzigmann, D., Kulkarni, J. A., Fidelj, V., Kleist, C., Cullis, P. R., Fricker, G., & Mier, W. (2019). Coating of PLA-nanoparticles with cyclic, arginine-rich cell penetrating peptides enables oral delivery of liraglutide. *Nanomedicine, 24*, 102132.

Uhl, P., Sauter, M., Hertlein, T., Witzigmann, D., Laffleur, F., Hofhaus, G., Fidelj, V., Tursch, A., Özbek, S., Hopke, E., Haberkorn, U., Bernkop-Schnurch, A., Ohlsen, K., Fricker, G., & Mier, W. (2021). Overcoming the Mucosal Barrier: Tetraether Lipid-Stabilized Liposomal Nanocarriers Decorated with Cell-Penetrating Peptides Enable Oral Delivery of Vancomycin. *Adv Ther, 4*(4).

van Poelgeest, M. I., Welters, M. J., van Esch, E. M., Stynenbosch, L. F., Kerpershoek, G., van Persijn van Meerten, E. L., van den Hende, M., Lowik, M. J., Berends-van der Meer, D. M., Fathers, L. M., Valentijn, A. R., Oostendorp, J., Fleuren, G. J., Melief, C. J., Kenter, G. G., & van der Burg, S. H. (2013). HPV16 synthetic long peptide (HPV16-SLP) vaccination therapy of patients with advanced or recurrent HPV16-induced gynecological carcinoma, a phase II trial. *J Transl Med, 11*, 88.

VanBenschoten, H. M., & Woodrow, K. A. (2021). Vaginal Delivery of Vaccines. *Adv Drug Deliv Rev*, 113956.

Vinod, N., Hwang, D., Azam, S. H., Van Swearingen, A. E. D., Wayne, E., Fussell, S. C., Sokolsky-Papkov, M., Pecot, C. V., & Kabanov, A. V. (2020). High-capacity poly(2-oxazoline) formulation of TLR 7/8 agonist extends survival in a chemo-insensitive, metastatic model of lung adenocarcinoma. *Sci Adv, 6*(25), eaba5542.

Vogel, K. G. (1978). Effects of hyaluronidase, trypsin, and EDTA on surface composition and topography during detachment of cells in culture. *Exp Cell Res, 113*(2), 345-357.

Voß, A. L. (2020). *Establishment of orthotopic HPV16-positive tumors in MHC-humanized mice for therapeutic vaccine design.* Eberhard Karls University of Tübingen, Master's thesis.

Waldman, A. D., Fritz, J. M., & Lenardo, M. J. (2020). A guide to cancer immunotherapy: from T cell basic science to clinical practice. *Nat Rev Immunol, 20*(11), 651-668.

Wan, B., Qin, L., Ma, W., & Wang, H. (2022). Construction and immune effect of an HPV16/18/58 trivalent therapeutic adenovirus vector vaccine. *Infect Agent Cancer, 17*(1), 5.

Wang, Y., Sui, Y., Kato, S., Hogg, A. E., Steel, J. C., Morris, J. C., & Berzofsky, J. A. (2015). Vaginal type-II mucosa is an inductive site for primary CD8(+) T-cell mucosal immunity. *Nat Commun, 6*, 6100.

Waring, M. J. (1965). Complex Formation between Ethidium Bromide and Nucleic Acids. *Journal of Molecular Biology, 13*(1), 269-&.

Weiskopf, D., Schwanninger, A., Weinberger, B., Almanzar, G., Parson, W., Buus, S., Lindner, H., & Grubeck-Loebenstein, B. (2010). Oxidative stress can alter the antigenicity of immunodominant peptides. *J Leukoc Biol, 87*(1), 165-172.

Westrich, J. A., Warren, C. J., & Pyeon, D. (2017). Evasion of host immune defenses by human papillomavirus. *Virus Res, 231*, 21-33.

Wickham, H., Averick, M., Bryan, J., Chang, W., McGowan, L. D. A., François, R., Grolemund, G., Hayes, A., Henry, L., & Hester, J. (2019). Welcome to the Tidyverse. *J Open Source Softw, 4*(43), 1686.

Wieczorek, M., Abualrous, E. T., Sticht, J., Alvaro-Benito, M., Stolzenberg, S., Noe, F., & Freund, C. (2017). Major Histocompatibility Complex (MHC) Class I and MHC Class II Proteins: Conformational Plasticity in Antigen Presentation. *Front Immunol, 8*, 292.

Wira, C. R., Rodriguez-Garcia, M., Patel, M. V., Biswas, N., & Fahey, J. V. (2015). Endocrine regulation of the mucosal immune system in the female reproductive tract. *Mucosal Immunol*, 2141-2156.

Wobser, M., Keikavoussi, P., Kunzmann, V., Weininger, M., Andersen, M. H., & Becker, J. C. (2006). Complete remission of liver metastasis of pancreatic cancer under vaccination with a HLA-A2 restricted peptide derived from the universal tumor antigen survivin. *Cancer Immunol Immunother, 55*(10), 1294-1298.

Wong, S. P., Argyros, O., Coutelle, C., & Harbottle, R. P. (2011). Non-viral S/MAR vectors replicate episomally in vivo when provided with a selective advantage. *Gene Ther, 18*(1), 82-87.

Woodruff, M. F., & Hodson, B. A. (1985). The effect of passage in vitro and in vivo on the properties of murine fibrosarcomas I. Tumorigenicity and immunogenicity. *Br J Cancer, 51*(2), 161-169.

World Health Organization. (2017). Human papillomavirus vaccines: WHO position paper, May 2017-Recommendations. *Vaccine, 35*(43), 5753-5755.

Wright, P. F. (2011). Inductive/effector mechanisms for humoral immunity at mucosal sites. *Am J Reprod Immunol, 65*(3), 248-252.

Yeager, T. R., & Reddel, R. R. (1999). Constructing immortalized human cell lines. *Curr Opin Biotechnol, 10*(5), 465-469.

Yuan, X. M., Xie, F. P., Lu, Z. B., Wen, T. X., Zhuang, Y. J., Jones, A. C., & Zhang, Z. (1995). The establishment of two cell lines from a mouse uterine cervical carcinoma (U14) and their metastatic phenotype changes. *Clin Exp Metastasis, 13*(6), 463-473.

Zhao, X., Deak, E., Soderberg, K., Linehan, M., Spezzano, D., Zhu, J., Knipe, D. M., & Iwasaki, A. (2003). Vaginal submucosal dendritic cells, but not Langerhans cells, induce protective Th1 responses to herpes simplex virus-2. *J Exp Med, 197*(2), 153-162.

Zhou, C., Tuong, Z. K., & Frazer, I. H. (2019). Papillomavirus Immune Evasion Strategies Target the Infected Cell and the Local Immune System. *Front Oncol, 9*, 682.

Zhou, J. Z., Way, S. S., & Chen, K. (2018). Immunology of the Uterine and Vaginal Mucosae. *Trends Immunol, 39*(4), 302-314.

Zottnick, S., Voß, A. L., & Riemer, A. B. (2020). Inducing Immunity Where It Matters: Orthotopic HPV Tumor Models and Therapeutic Vaccinations. *Front Immunol, 11*.

8 Appendix

Appendix Figure 1. Vector map of S/MAR-UbC-Hras-CMV-Luc plasmid.

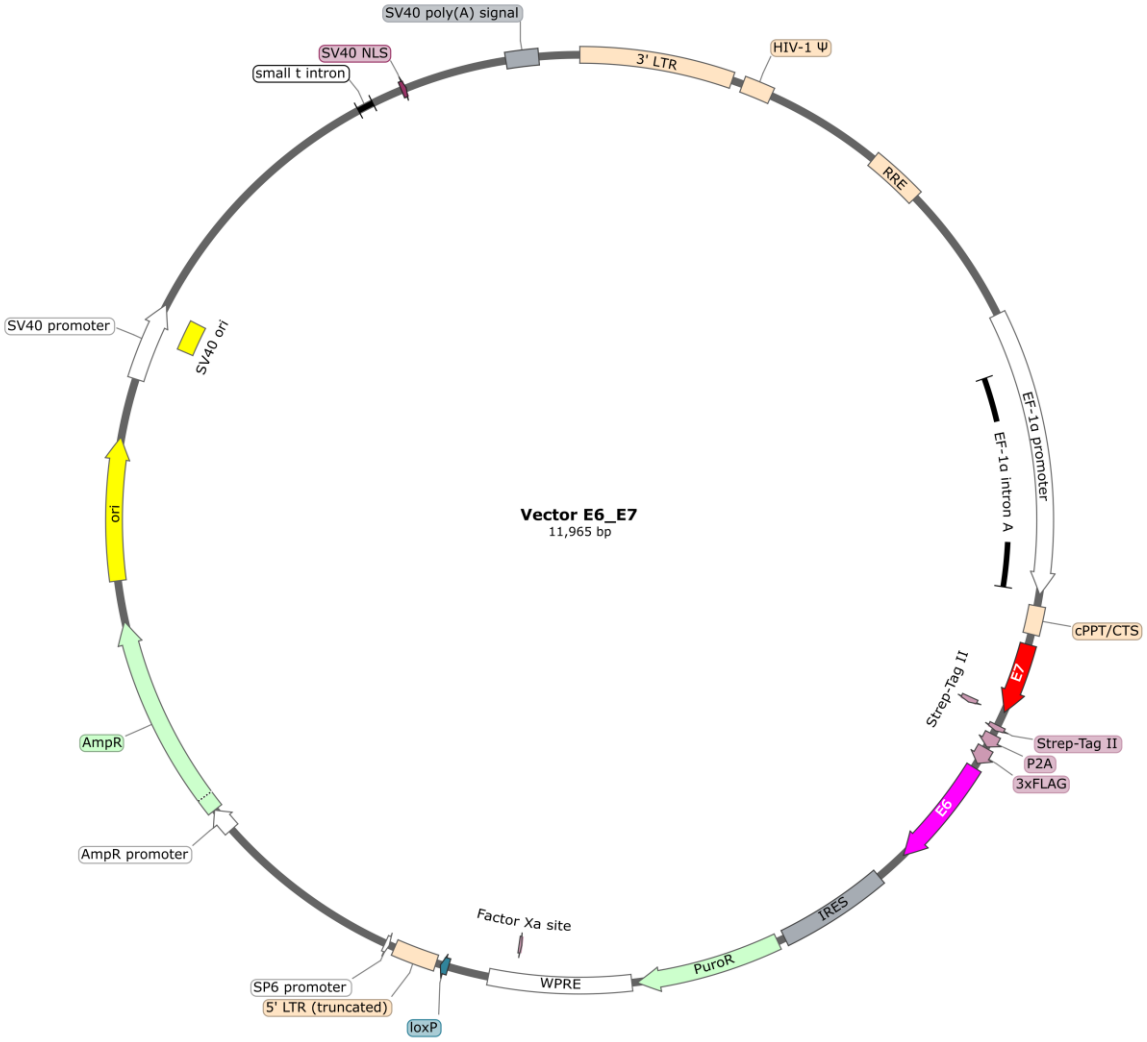

Appendix Figure 2. Vector map of lentiviral plasmid for E6 and E7.